Renormalization of three-quark operators for baryon distribution amplitudes

DISSERTATION ZUR ERLANGUNG DES DOKTORGRADES
DER NATURWISSENSCHAFTEN (DR. RER. NAT.) DER
FAKULTÄT FÜR PHYSIK DER UNIVERSITÄT REGENSBURG

vorgelegt von

Michael Gruber

aus Roding

im Jahr 2017

Promotionsgesuch eingereicht am: 13.05.2016
Die Arbeit wurde angeleitet von: Prof. Dr. Andreas Schäfer

Prüfungsausschuss:

Vorsitzender:	Prof. Dr. Christoph Strunk
1. Gutachter:	Prof. Dr. Andreas Schäfer
2. Gutachter:	Prof. Dr. Vladimir Braun
weiterer Prüfer:	Prof. Dr. Jaroslav Fabian

Abstract

In this thesis we design and study three-quark operators that are essential for the calculation of baryon distribution amplitudes. These nonperturbative objects grant insight into the internal structure of hadrons, but their renormalization patterns are nontrivial and need to be treated with care. With the application to lattice simulations in mind we discuss two renormalization schemes, $\overline{\text{MS}}$ and RI′/SMOM, and connect them by calculating conversion factors. Armed with this knowledge we are able to extract phenomenologically relevant results from an accompanying lattice analysis.

Contents

Chapter 1

Introduction

The goal of high energy physics is to study matter in terms of elementary particles and to understand the interactions which bind them. The Standard Model of particle physics unifies theories that describe three of the fundamental interactions, namely the electromagnetic, weak, and strong forces. This model describes all ordinary matter using only a handful of fundamental particles: 6 quarks, 6 leptons, the force-carrying gauge bosons, and the recently experimentally confirmed Higgs boson [1, 2], which gives intrinsic mass to elementary particles via spontaneous symmetry breaking [3, 4] (Nobel Prize in Physics 2013). The mass of composite objects such as hadrons is another topic. In nucleons, i.e., protons and neutrons, the sum of the individual masses of the valence constituents (3 quarks) contributes only 1% of the total mass. The majority of the remaining mass is generated dynamically by virtue of the strong interaction. This highlights that hadrons must have a rich internal structure worth studying and that the physics of the strong force will play the leading role in its understanding. The accepted theory for the strong force is called quantum chromodynamics (QCD), a non-Abelian gauge theory that describes the interaction of quarks and gluons. Developed in the 1970s (see, e.g., [5–9]), this theory has been highly successful over the years in describing a wide range of high energy physics phenomena. So successful, in fact, that modern-day accelerator experiments can now use high-precision theoretical QCD calculations as the firmly established background over which searches for physics beyond the Standard Model can be conducted.

Experimentally it has been known that baryons are not point-like since the proton form factor (FF) was first measured [10] (Nobel Prize in Physics 1961). Ever since then, FFs have played an important role in studying the internal structure of hadrons. Form factors can be measured by probing a hadron with a virtual photon, usually in a scattering process with a lepton, e.g., for a nucleon form factor: $e^- N \to e^- N$. These FFs can be decomposed into three major contributions [11]. Schematically for the scattering amplitude we have

(the leptonic side is not shown; double lines stand for nucleons, arrow lines for quarks, wavy lines for photons, curly lines for gluons, and elliptical blobs represent nonperturbative objects):

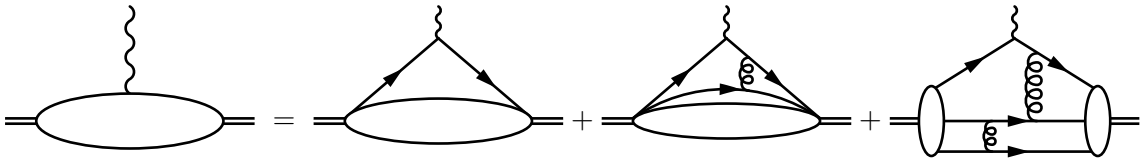

The first two are soft contributions, which are purely nonperturbative and cannot be reduced any further. Unlike these, the third function factorizes [12], i.e., it can be written as a convolution of a hard scattering kernel amidst two distribution amplitudes (DAs) [13], thereby achieving a separation of short- and long-distance physics. The hard scattering kernel describes how the extra momentum incurred from the scattering is distributed among the quarks by gluons and it can be calculated in perturbation theory [14–16]. In this picture we treat the hadron as a bundle of valence partons moving collinearly at small transverse separations. Distribution amplitudes are nonperturbative objects that represent the probability of finding the hadron in such a Fock state, with each parton carrying a certain fraction of the hadron's total momentum. The information encoded in DAs is complementary to conventional parton distribution functions (PDFs), which can be measured by fits to, e.g., deep inelastic scattering or Drell–Yan cross section data [17]. PDFs give the total probability to find a parton with the given momentum, regardless of Fock state, and are described by the DGLAP equations [18–20].

The factorizable contributions of DAs to FFs become dominant in the limit of very high momentum transfer. At moderate energies which are easily accessible in accelerators, however, soft contributions are most relevant. Given their nature they cannot be directly factorized into DAs. Still, a connection between FFs and DAs can be established also in this regime via light-cone sum rules. This method relates both objects to matrix elements containing a hadronic and an electromagnetic current using perturbation theory, dispersion integrals, and quark-hadron-duality. The DAs appearing in this expansion for the soft contributions are the same ones that were used in the description of the hard contribution given above. In general, DAs have the beautiful feature that they are universal, i.e., they only depend on the particle but not on the process under consideration. Once determined, they can be used to describe a multitude of other events involving the same hadron species.

Applications of distribution amplitudes are manifold. A standard mesonic example is the pion DA involved in the theoretical description of the process $\gamma\gamma^* \to \pi^0$ studied, e.g., at B-factories (cf. BaBar puzzle [21–23]). In the baryonic sector the nucleon DA is both the simplest and the most important one, and has therefore received the most attention.

The link between nucleon form factors and nucleon distribution amplitudes [24, 25] allows one to translate from present experimental observations to interesting nonperturbative information on nucleon structure. It will continue to be essential also alongside future experimental programs, e.g., precision nucleon form factor measurements planned for the Jefferson Lab 12 GeV upgrade [26]. The connection between DAs and FFs is also very interesting for the study of nucleon resonances such as $N^*(1535)$ [27, 28].

A natural extension of the study of nucleons is provided by the field of hyperon physics, i.e., nucleon-like baryons containing strange quarks. Compared to nucleons, current experimental data on the FFs of hyperons are scarce [29] since the unstable nature of these particles makes it more difficult to study them. In the future, additional possibilities to measure their form factors should emerge, e.g., using hyperons produced in antiproton-proton collisions for $\overline{\mathrm{P}}$ANDA at FAIR [30].

On the side of DAs, early attempts at generalizing the concept of DAs from nucleons to hyperons have been made in [31, 32], but these did not attempt to provide a consistent framework in which the DAs of nucleons and hyperons can be treated collectively. A unified description of the baryon octet is required to enable the study of the effects of SU(3) breaking on DAs; such a parametrization has been achieved recently [33, 34].

SU(3) symmetry and its breaking relate to several nontrivial aspects of hyperon physics. The strangeness-changing radiative decay $\Sigma^+ \to p\gamma$ is particularly noteworthy. Experiments [35, 36] determined the so-called asymmetry parameter of this process to be relatively large as well as negative. This came as a surprise since it had been predicted to vanish in the exact SU(3) limit (cf. Hara's theorem [37]), and the large magnitude contradicts the usual expectation of mild SU(3) breaking effects. Interestingly, we will find in our final results that symmetry breaking actually has major impact on the shape of hyperon DAs.

From the theoretical side, access to DAs is often gained in terms of their moments, i.e., integrals over DAs weighted by powers of light-cone momentum fractions. There are two main paths to these moments of DAs. One is to calculate the normalizations and low moments via standard QCD sum rules [38, 39]. Another way to access the moments is to calculate them from first principles using lattice QCD. These calculations are very computer time intensive and require the development of advanced algorithms and the power of supercomputers. The usual lattice approach to DAs involves the nonperturbative evaluation of hadronic two-point matrix elements of local operators. Such lattice studies of the pion [40–44] and nucleon [45–48] DAs have a long history. In our recent article [49] we have universalized the lattice method for baryon DAs to include the full SU(3) octet, i.e., we treat not only nucleons but also hyperons, which have not been previously explored in lattice QCD. In this thesis, several theoretical challenges that needed to be overcome for a successful lattice calculation of SU(3) baryon DAs are addressed.

A core issue is the topic of renormalization, which is a technique required to get physically meaningful results. In general, the renormalization of moments of baryon DAs is nontrivial since they can mix under renormalization. This is especially true when taking into account the full SU(3) octet instead of just the nucleon, as doing so increases the number of independent nonperturbative parameters that can take part in the mixing. To better control the mixing under renormalization one can select operators in a suitable basis. With a lattice calculation in mind it is essential to select operator multiplets that transform under irreducible representations of the spinorial hypercubic group $\overline{\mathrm{H}(4)}$, which is the correct symmetry group for fermions on a 4-dimensional hypercubic lattice. This method has been developed in [50–52] for the case of the nucleon DA. One of our goals will be to improve this technique and make it suitable for a simultaneous treatment of nucleon and hyperon DAs by further refining the choice of operators. We will achieve this by taking into account not only the transformation behavior under $\overline{\mathrm{H}(4)}$ but also that of SU(3) particle multiplets.

Another matter which we will discuss are so-called renormalization schemes. In order to embed our results into the context of other studies and to assure comparability it is preferable to present them in the widely used $\overline{\mathrm{MS}}$ ("MS-bar") scheme. However, this is a perturbative prescription that is not well suited for a direct implementation on the lattice. To overcome this gap we will establish a two-step procedure. First, lattice data will be renormalized nonperturbatively using a RI′/SMOM scheme. This prescription can be used both in nonperturbative and in perturbative calculations and is therefore suited as an intermediate scheme. As a second step we will perform a calculation in continuum perturbation theory to determine the conversion factors from RI′/SMOM to $\overline{\mathrm{MS}}$.

The outline of the text is as follows: In the next chapter we will provide the foundations on which the rest of the work is built. We will cover two major areas: quantum chromodynamics, the theory describing the physics of the strong interaction, and group theory, which offers mathematical insights into the concepts of symmetry. Chapter 3 then constitutes the main part, where we will examine the central quantities, namely baryon distribution amplitudes. After giving the relevant definitions we will discuss how to measure them and construct suitable operators for this task. The renormalization behavior of these operators will be treated in detail. In particular, we shall introduce two renormalization schemes — a perturbative and a nonperturbative one — which can be combined to obtain useful renormalized data from lattice simulations. In chapter 4 we will proceed from theory to practical applications and describe a framework for measurements of DAs on the lattice. From such an analysis of lattice data we will obtain numerical results for the DAs of the baryon octet and then discuss and illustrate the physical implications of our observations. Finally, chapter 5 provides a short summary.

Chapter 2

Foundations

2.1. Quantum chromodynamics

Quantum chromodynamics is the theory of the strong interaction sector of the Standard Model of particle physics. Introductions to QCD can be found in most standard textbooks on quantum field theory, such as [53, 54]. It is a non-Abelian gauge theory with the gauge group SU(3) formulated in terms of two kinds of fundamental fields. The fermionic fields are called quarks and the bosonic fields are called gluons. We work in the Lagrangian formulation of the theory, where the central object is the Lagrangian density[1,2]

$$\begin{aligned}\mathscr{L} &= \sum_f \left[\bar{f}^a_\alpha \left(i(\gamma^\mu)_{\alpha\beta} D^{ab}_\mu - m_f (\mathbb{1}_4)_{\alpha\beta}\delta^{ab}\right) f^b_\beta\right] - \frac{1}{4} F^{\mu\nu,A} F^A_{\mu\nu} \\ &= \sum_f \left[\bar{f}(i\not{D} - m_f) f\right] - \frac{1}{4} F^{\mu\nu,A} F^A_{\mu\nu}\,, \end{aligned} \tag{2.1}$$

which contains the fields, their derivatives, and some parameters (coupling and masses).

In the first line we have written out all indices explicitly (with the implied summation convention for all indices appearing twice), while in the second line we cast the QCD Lagrangian into the familiar form where contracted color indices in the fundamental representation (a, b) as well as Dirac indices (α, β) are omitted and Feynman slash notation $(\not{D} = \gamma^\mu D_\mu)$ is used to denote the scalar product between a four-vector and the gamma matrices, which are discussed in appendix A.3. Furthermore, the Lagrangian is a local object, and we have suppressed the position dependence of all its components in our notation.

[1] We will henceforth — in a commonly accepted abuse of nomenclature — simply refer to it as a Lagrangian.
[2] A perturbative approach to QCD will require additional terms in the Lagrangian, for the full expression see eq. (2.11).

Table 2.1.: The six quark flavors f, their masses m_f (from [58]) as well as their quantum numbers: electric charge Q, spin S, isotopic spin T, isospin z-component T_3, strangeness S' (cf. section 2.2.1), charmness C', bottomness B', and topness T'. All masses are in the $\overline{\text{MS}}$ scheme, but due to the wide range of values, two different definitions are used. The u, d, and s masses are current quark masses given at the scale $\mu = 2\,\text{GeV}$, while the c, b, and t masses are running quark masses given at the scale $\mu = m_c$, $\mu = m_b$, and $\mu = m_t$, respectively. See also the review "Quark masses" in [58].

flavor	f	m_f	Q	S	T	T_3	S'	C'	B'	T'
up	u	$2.2^{+0.6}_{-0.4}$ MeV	$+\frac{2}{3}$	$\frac{1}{2}$	$\frac{1}{2}$	$+\frac{1}{2}$	0	0	0	0
down	d	$4.7^{+0.5}_{-0.4}$ MeV	$-\frac{1}{3}$	$\frac{1}{2}$	$\frac{1}{2}$	$-\frac{1}{2}$	0	0	0	0
strange	s	96^{+8}_{-4} MeV	$-\frac{1}{3}$	$\frac{1}{2}$	0	0	-1	0	0	0
charm	c	$1.27^{+0.03}_{-0.03}$ GeV	$+\frac{2}{3}$	$\frac{1}{2}$	0	0	0	$+1$	0	0
bottom	b	$4.18^{+0.04}_{-0.03}$ GeV	$-\frac{1}{3}$	$\frac{1}{2}$	0	0	0	0	-1	0
top	t	$160^{+4.8}_{-4.3}$ GeV	$+\frac{2}{3}$	$\frac{1}{2}$	0	0	0	0	0	$+1$

The first term of the Lagrangian (2.1) contains the quark and antiquark fields, f and $\bar{f}$. The number of different types of quarks (called flavors) is not fixed by the theory. Experiments have detected six quark flavors (named up, down, strange, charm, bottom, and top [55, 56]), whose properties are collected in table 2.1. The possible existence of yet undiscovered seventh and eighth flavors is excluded by current experimental data with high confidence [57]. We use the same symbol both for the quark field itself as well as for flavor labels, e.g., we have up quark fields u with mass m_u. These fields are coupled to the gluon fields A^A_μ via a gauge-covariant derivative

$$D^{ab}_\mu = \delta^{ab}\partial_\mu - ig\big(t^A\big)^{ab} A^A_\mu \,, \tag{2.2}$$

where g parametrizes the strength of the coupling and t^A are the generating matrices for the fundamental representation of SU(3), see appendix A.2.

The second term in eq. (2.1) is the standard Yang–Mills Lagrangian [59], which encodes the purely gluonic contributions. The gluon field strength tensor $F^A_{\mu\nu}$ can be defined by the commutator of two covariant derivatives,

$$t^A F^A_{\mu\nu} = \frac{i}{g}\big[D_\mu, D_\nu\big] \,. \tag{2.3}$$

An explicit calculation yields its presentation in terms of gluon fields:

$$F^A_{\mu\nu} = \partial_\mu A^A_\nu - \partial_\nu A^A_\mu + g f^{ABC} A^B_\mu A^C_\nu \,, \tag{2.4}$$

where f^{ABC} are the totally antisymmetric structure constants of SU(3). (Their definition and their values can be found in appendix A.2.)

While the first two terms in eq. (2.4) are analogous to the form of the photon field strength tensor in quantum electrodynamics (QED), the last term has no counterpart in the Abelian gauge theory. This term gives rise to the three- and four-gluon vertices that characterize QCD as a non-Abelian gauge theory. The strength of both of these gluonic self-interaction vertices is governed by the same parameter g that determines the coupling of quarks to gluons, meaning that the whole theory has only a single dimensionless coupling constant.

In principle, yet another term should be included in the Lagrangian, namely

$$-\frac{\theta}{32\pi^2}\varepsilon^{\mu\nu\rho\sigma}F^A_{\mu\nu}F^A_{\rho\sigma}\,, \qquad 0 \leq \theta < 2\pi\,, \tag{2.5}$$

which is required for a description of the topological structure of the QCD vacuum [60]. While the other terms in the Lagrangian respect *CP* symmetry (invariance under simultaneous charge conjugation and parity transformation), this so-called theta term would break it (because the Levi-Civita pseudotensor $\varepsilon^{\mu\nu\rho\sigma}$ acquires an extra minus sign under *CP* transformation). *CP* violation is observed in weakly decaying particles [61] (Nobel Prize in Physics 1980) and is a necessary ingredient for the matter-antimatter asymmetry in Big Bang baryogenesis (cf. Sakharov conditions [62]). Yet, there is no experimental evidence for any amount of *CP* violation originating from the strong interaction sector of the Standard Model. Measurements of the neutron electric dipole moment constrain the vacuum angle θ to be extremely small [63]. The absence of strong *CP* violation with no known reason can be seen as a fine-tuning problem (known as the strong *CP* problem [64]). Since *CP* violation is not relevant for the topic of this thesis, we will not concern ourselves with this any further and simply exclude the term by setting $\theta = 0$.

Both terms in the Lagrangian (2.1) are individually gauge invariant under local (i.e., position-dependent) gauge transformations,

$$f(x) \to U(x)f(x)\,, \tag{2.6a}$$

$$\bar{f}(x) \to \bar{f}(x)U^\dagger(x)\,, \tag{2.6b}$$

$$t^A A^A_\mu(x) \to U(x)t^A A^A_\mu(x)U^\dagger(x) - \frac{i}{g}[\partial_\mu U](x)U^\dagger(x)\,, \tag{2.6c}$$

with any SU(3)-valued function $U(x)$. This establishes SU(3), the special unitary group of degree 3, as the gauge group of QCD. For more information on SU(3) see section 2.2.1. For infinitesimal transformations it is justified to expand the exponential parametrization of SU(3) given by $U(x) = \exp\bigl(-i\epsilon t^A\theta^A(x)\bigr)$, cf. eq. (2.64), and linearize in the infinitesimal

real number ϵ, writing the local gauge transformation with eight real parameters $\theta^A(x)$:

$$f(x) \to f(x) - i\epsilon\theta^A(x)t^A f(x)\,, \tag{2.7a}$$

$$\bar{f}(x) \to \bar{f}(x) + i\epsilon\theta^A(x)\bar{f}(x)t^A\,, \tag{2.7b}$$

$$A^A_\mu(x) \to A^A_\mu(x) + \epsilon f^{ABC}\theta^B(x)A^C_\mu(x) - \frac{\epsilon}{g}\big[\partial_\mu\theta^A\big](x)\,. \tag{2.7c}$$

In the functional approach to quantum field theory one formally defines vacuum expectation values via the Feynman path integral, similarly to the path integral formulation of quantum mechanics (which itself is a generalization of the classical principle of stationary action). For an operator $\mathcal{O}$, which is a time-ordered product of fields, we have

$$\langle 0|\mathcal{O}|0\rangle = \frac{\int \mathcal{D}q\mathcal{D}\bar{q}\mathcal{D}A\, e^{iS[q,\bar{q},A]}\mathcal{O}[q,\bar{q},A]}{\int \mathcal{D}q\mathcal{D}\bar{q}\mathcal{D}A\, e^{iS[q,\bar{q},A]}}\,, \tag{2.8}$$

where an action S is defined as a position integral over the Lagrangian,

$$S = \int d^4x\, \mathscr{L}(x)\,, \tag{2.9}$$

and the functional integration measures prefixed with $\mathcal{D}$ symbolize integrating each component of the fields at each spacetime position over all values, see also eq. (2.28) later on. The expression is normalized so that $\langle 0|0\rangle = 1$.

Since the Lagrangian (2.1) is fully gauge invariant, the action takes the same value for all field configurations that are related by a local SU(3) gauge transformation (as defined in eq. (2.7)). This amounts to an overcounting of infinitely many equivalent field configurations for every single unique physical state since the functional integration runs over each and every field configuration. As a result, the path integral is divergent and it is not possible to evaluate it in its present form.

The solution is to impose a gauge-fixing condition and factor out the integration over all physically equivalent field configurations, ensuring that there is only a single contribution from each physically distinct orbit of configurations. This is usually accomplished by the Faddeev–Popov method [65], which involves some clever manipulation of the path integral that will not be repeated here. After some algebra, one finds that the vacuum expectation value of $\mathcal{O}$ can be calculated via

$$\langle 0|\mathcal{O}|0\rangle = \frac{\int \mathcal{D}q\mathcal{D}\bar{q}\mathcal{D}A\mathcal{D}\eta\mathcal{D}\bar{\eta}\, e^{iS[q,\bar{q},A,\eta,\bar{\eta}]}\mathcal{O}[q,\bar{q},A]}{\int \mathcal{D}q\mathcal{D}\bar{q}\mathcal{D}A\mathcal{D}\eta\mathcal{D}\bar{\eta}\, e^{iS[q,\bar{q},A,\eta,\bar{\eta}]}}\,, \tag{2.10}$$

using a modified Lagrangian

$$\mathscr{L} = \sum_f \big[\bar{f}(i\not{D} - m_f)f\big] - \frac{1}{4}F^{\mu\nu,A}F^A_{\mu\nu} - \frac{1}{2\xi}\big(\partial^\mu A^A_\mu\big)\big(\partial^\nu A^A_\nu\big) - \bar{\eta}^A\partial^\mu D^{AB}_\mu\eta^B\,. \tag{2.11}$$

The first new term (called gauge-fixing term) establishes a family of linear covariant gauges with a gauge parameter ξ.[3] This is a generalization of the classical Lorenz gauge condition for the electromagnetic four-potential ($\partial^\mu A_\mu = 0$). For operators which are gauge invariant, the vacuum expectation values cannot depend on the gauge parameter. In such cases one may therefore decide to perform any calculation only for one particular value of ξ that suits ones purpose. Popular choices are Feynman gauge ($\xi = 1$, used in perturbative calculations because it makes the gluon propagator, eq. (2.16b), take its most simple form) and Landau gauge ($\xi \to 0$, can be implemented in lattice simulations, see eq. (2.32)).

The other new term (called gauge-compensating term) contains new massless fields, η^A and $\bar{\eta}^A$. They are Graßmann-valued (i.e., anticommuting) complex scalar (spin 0) fields and as such they violate the spin-statistics theorem [66]. Therefore, these aptly named ghost fields cannot correspond to physical particles. However, their inclusion in the Lagrangian actually cancels other unphysical contributions stemming from the (longitudinal) gluonic sector, allowing for a diagrammatic (perturbative) treatment of QCD. The ghost fields couple to gluons via

$$\begin{aligned} D_\mu^{AB} &= \delta^{AB}\partial_\mu - ig\big(t^C\big)^{AB} A_\mu^C \\ &= \delta^{AB}\partial_\mu - g f^{ABC} A_\mu^C \,, \end{aligned} \tag{2.12}$$

i.e., they carry color indices in the adjoint representation of SU(3). Every diagram containing an internal gluon loop (coupled to the rest of the diagram only via three-gluon vertices) has to be accompanied by an analogous diagram containing an internal ghost loop (coupled via ghost-gluon vertices) in order to get a correct physical result. The requirement for a proper treatment of ghost fields is specific to non-Abelian gauge theories. For Abelian gauge groups these fields would completely decouple from the gauge bosons since the adjoint representation is trivial in such cases.

Due to the newly added terms, the full Lagrangian (2.11) is no longer SU(3) gauge invariant. Yet, the action still enjoys another type of symmetry, namely BRST invariance [67, 68], corresponding to the transformation (with an infinitesimal Graßmann number ϵ):

$$f(x) \to f(x) - i\epsilon\eta^A(x) t^A f(x) \,, \tag{2.13a}$$

$$\bar{f}(x) \to \bar{f}(x) + i\epsilon\eta^A(x) \bar{f}(x) t^A \,, \tag{2.13b}$$

$$A_\mu^A(x) \to A_\mu^A(x) + \epsilon f^{ABC}\eta^B(x) A_\mu^C(x) - \frac{\epsilon}{g}\big[\partial_\mu \eta^A\big](x) \,, \tag{2.13c}$$

$$\eta^A(x) \to \eta^A(x) + \frac{\epsilon}{2} f^{ABC}\eta^B(x)\eta^C(x) \,, \tag{2.13d}$$

$$\bar{\eta}^A(x) \to \bar{\eta}^A(x) + \frac{\epsilon}{g\xi}\big[\partial^\mu A_\mu^A\big](x) \,. \tag{2.13e}$$

[3] There are many other methods for the gauge fixing (such as the Coulomb, axial and light-cone gauges) which will not be discussed here.

BRST symmetry is a generalization of non-Abelian gauge symmetry. Comparing the effect of the BRST transformation on the quark and gluon fields, eqs. (2.13a–c), to a gauge transformation, eqs. (2.7), it becomes clear that for the physical fields the BRST transformation acts exactly like a gauge transformation, but now with the eight ghost fields $\eta^A(x)$ playing a role analogous to the parameters $\theta^A(x)$. Therefore, any gauge-invariant operator is automatically BRST invariant. In general, the BRST formalism is a mathematical approach to the quantization of gauge field theories, and BRST-quantizable theories are guaranteed to have some very useful properties. Without going into further detail we simply state that the BRST symmetry of QCD ensures both unitarity and renormalizability of the theory to all orders.

The QCD Lagrangian is just a single, concise, seemingly simple formula that should tell us everything there is to know about the strong interaction. Yet, solving QCD completely turns out to be an extremely hard (or rather, impossible) task. In practice, most calculations in quantum chromodynamics have to be done using some simplifications, models, numerical approximations, etc. In the following sections we will introduce two such methods, namely perturbative QCD in section 2.1.1 and lattice QCD in section 2.1.2. For our study of baryon distribution amplitudes both methods are relevant and need to be combined to obtain the final results. Lattice QCD is used to calculate the raw data and to renormalize them in a RI′/SMOM scheme, while perturbative QCD is used to convert to a $\overline{\text{MS}}$ renormalization scheme.

2.1.1. Perturbative QCD

To tackle the QCD path integral we will need some approach to reduce the complexity of the problem. One such approach is QCD perturbation theory, wherein we treat the interacting (g-dependent) part of the action as a perturbation to the free (g-independent) part. In this section we will present only a brief discussion of some basic principles of perturbative QCD. For an extensive treatment of perturbative methods in QCD, their justification, the many processes they can be applied to, and their connection to experiments see [69].

Let us now decompose the action S into the free part S_{free} and the interacting part S_{int} by defining

$$S = S_{\text{free}} + S_{\text{int}}\,, \qquad \text{with } S_{\text{free}} = \lim_{g\to 0} S\,, \tag{2.14}$$

and let us, as a starting point, study the free theory without any interactions. First, we need to identify the free propagators, the knowledge of which will turn out to be essential for perturbative QCD. We define the propagators as Green's functions of the differential

operators appearing in field bilinears in the free action, i.e., as solutions of[4]

$$\delta^{ab}(i\not{\partial}_x - m_f \mathbb{1}_4)_{\alpha\beta} S^{bc}_{f,\beta\gamma}(x-y) = i\delta^4(x-y)\delta^{ac}(\mathbb{1}_4)_{\alpha\gamma}\,, \tag{2.15a}$$

$$\delta^{AB}\big(g^{\mu\nu}(\partial_x)^2 - (1-\xi^{-1})\partial_x^\mu\partial_x^\nu\big) D^{BC}_{\nu\rho}(x-y) = i\delta^4(x-y)\delta^{AC} g^\mu_\rho\,, \tag{2.15b}$$

$$-\delta^{AB}(\partial_x)^2 G^{BC}(x-y) = i\delta^4(x-y)\delta^{AC}\,. \tag{2.15c}$$

The best approach to these differential equations is a Fourier transformation to momentum space. Solutions are the so-called Feynman propagators for the quark, gluon, and ghost fields,

$$S^{ab}_{f,\alpha\beta}(x-y) = i\delta^{ab}\int \frac{d^4p}{(2\pi)^4}\frac{(\not{p}+m_f\mathbb{1}_4)_{\alpha\beta}}{p^2-m_f^2+i\epsilon}e^{-ip\cdot(x-y)}\,, \tag{2.16a}$$

$$D^{AB}_{\mu\nu}(x-y) = -i\delta^{AB}\int \frac{d^4p}{(2\pi)^4}\frac{1}{p^2+i\epsilon}\left(g_{\mu\nu} - (1-\xi)\frac{p_\mu p_\nu}{p^2+i\epsilon}\right)e^{-ip\cdot(x-y)}\,, \tag{2.16b}$$

$$G^{AB}(x-y) = i\delta^{AB}\int \frac{d^4p}{(2\pi)^4}\frac{1}{p^2+i\epsilon}e^{-ip\cdot(x-y)}\,, \tag{2.16c}$$

where an infinitesimal positive number ϵ appears in the denominator, specifying a prescription to slightly shift the poles of the integrand away from the integration region. Often the $i\epsilon$ will not be written down explicitly.

We define a generating functional

$$\mathscr{Z}[J] = \frac{\int \mathcal{D}q\mathcal{D}\bar{q}\mathcal{D}A\mathcal{D}\eta\mathcal{D}\bar{\eta}\, e^{iS_{\text{free}}-iJ}}{\int \mathcal{D}q\mathcal{D}\bar{q}\mathcal{D}A\mathcal{D}\eta\mathcal{D}\bar{\eta}\, e^{iS_{\text{free}}}}\,, \tag{2.17}$$

where J contains source terms ($\boldsymbol{f}$, $\mathcal{A}$, $\boldsymbol{\eta}$) for each field type (f, A, η):

$$\begin{aligned} J = i\int d^4x \Bigg(&\sum_f [\bar{\boldsymbol{f}}^a_\alpha(x) f^a_\alpha(x)] + \sum_f [\bar{f}^a_\alpha(x)\boldsymbol{f}^a_\alpha(x)] \\ &+ \mathcal{A}^{\mu,A}(x)A^A_\mu(x) + \bar{\boldsymbol{\eta}}^A(x)\eta^A(x) + \bar{\eta}^A(x)\boldsymbol{\eta}^A(x)\Bigg)\,. \end{aligned} \tag{2.18}$$

This allows us to obtain vacuum expectation values (cf. eq. (2.10)) by first applying functional derivatives (with respect to the source fields) to the generating functional and setting all source terms to zero afterward. For example,

$$\langle 0|\,\mathrm{T}\, A^A_\mu(x)A^B_\nu(y)|0\rangle = \frac{\delta}{\delta\mathcal{A}^{\mu,A}(x)}\frac{\delta}{\delta\mathcal{A}^{\nu,B}(y)}\mathscr{Z}[J]\Big|_{J=0}\,. \tag{2.19}$$

The beauty of the generating functional formalism is that once we know the full form of $\mathscr{Z}[J]$, we have basically solved the whole system. Any vacuum expectation value in the

[4] Without the gauge-fixing term in the full Lagrangian (2.11) we would be unable to define the free gluon propagator, as eq. (2.15b) would have no solution.

free theory can then be calculated by the derivative method described above. To calculate the generating functional, eq. (2.17), we perform the following transformation inside the numerator integral:

$$f^a_\alpha(x) \to f^a_\alpha(x) + \int d^4y\, S^{ab}_{f,\alpha\beta}(x-y) \boldsymbol{f}^b_\beta(y)\,, \tag{2.20a}$$

$$\bar{f}^a_\alpha(x) \to \bar{f}^a_\alpha(x) + \int d^4y\, \bar{\boldsymbol{f}}^b_\beta(y) S^{ba}_{f,\beta\alpha}(y-x)\,, \tag{2.20b}$$

$$A^A_\mu(x) \to A^A_\mu(x) + \int d^4y\, D^{AB}_{\mu\nu}(x-y) \mathcal{A}^{\nu,B}(y)\,, \tag{2.20c}$$

$$\eta^A(x) \to \eta^A(x) + \int d^4y\, G^{AB}(x-y) \boldsymbol{\eta}^B(y)\,, \tag{2.20d}$$

$$\bar{\eta}^A(x) \to \bar{\eta}^A(x) + \int d^4y\, \bar{\boldsymbol{\eta}}^B(y) G^{BA}(y-x)\,. \tag{2.20e}$$

Since this is simply a shift in all integration variables, the path integral measures remain unchanged. Performing further simplifications of the expression by using the defining equations (2.15) shows that this transformation amounts to completing the squares in those multi-dimensional Gaußian integrals. Thereby, the fields and their source terms are separated in the exponent such that the integral involving the free action drops out completely, leaving us with the result:

$$\begin{aligned}\mathscr{Z}[J] = \exp \int d^4x d^4y \Bigg(\sum_f [\bar{\boldsymbol{f}}^a_\alpha(x) S^{ab}_{f,\alpha\beta}(x-y) \boldsymbol{f}^b_\beta(y)] + \frac{1}{2} \mathcal{A}^{\mu,A}(x) D^{AB}_{\mu\nu}(x-y) \mathcal{A}^{\nu,B}(y) \\ + \bar{\boldsymbol{\eta}}^A(x) G^{AB}(x-y) \boldsymbol{\eta}^B(y) \Bigg)\,.\end{aligned} \tag{2.21}$$

It is now straightforward to evaluate the vacuum expectation values that involve just two fields,

$$\langle 0|\, \mathrm{T}\, f^a_\alpha(x) \bar{f}^b_\beta(y) |0\rangle = S^{ab}_{f,\alpha\beta}(x-y)\,, \tag{2.22a}$$

$$\langle 0|\, \mathrm{T}\, A^A_\mu(x) A^B_\nu(y) |0\rangle = D^{AB}_{\mu\nu}(x-y)\,, \tag{2.22b}$$

$$\langle 0|\, \mathrm{T}\, \eta^A(x) \bar{\eta}^B(y) |0\rangle = G^{AB}(x-y)\,, \tag{2.22c}$$

confirming that the two-point functions are — as should be expected — given by the propagators.

What about products involving more than two fields? In principle one could now evaluate all of them explicitly using the derivative method. This possibly tedious process is eased greatly by Wick's theorem [70], which states that the vacuum expectation value of a time-ordered product of any number of fields is given by the sum over all possible contractions of two fields. Each contraction (indicated by a line connecting the two fields) results in a propagator. Products which cannot be fully contracted (such as those involving

an odd number of fields of any type) give zero.[5] The whole procedure is probably best illustrated by an example:

$$\begin{aligned}
&\langle 0|\,\mathrm{T}\, f^{a_1}_{\alpha_1}(x_1)\bar{f}^{b_1}_{\beta_1}(y_1)f^{a_2}_{\alpha_2}(x_2)\bar{f}^{b_2}_{\beta_2}(y_2)|0\rangle = \\
&\quad = \overbrace{f^{a_1}_{\alpha_1}(x_1)\bar{f}^{b_1}_{\beta_1}(y_1)}\overbrace{f^{a_2}_{\alpha_2}(x_2)\bar{f}^{b_2}_{\beta_2}(y_2)} + \overbrace{f^{a_1}_{\alpha_1}(x_1)\bar{f}^{b_1}_{\beta_1}(y_1)f^{a_2}_{\alpha_2}(x_2)\bar{f}^{b_2}_{\beta_2}(y_2)} \\
&\quad = S^{a_1b_1}_{f,\alpha_1\beta_1}(x_1-y_1)S^{a_2b_2}_{f,\alpha_2\beta_2}(x_2-y_2) - S^{a_1b_2}_{f,\alpha_1\beta_2}(x_1-y_2)S^{a_2b_1}_{f,\alpha_2\beta_1}(x_2-y_1)\,. \qquad (2.23)
\end{aligned}$$

(The negative sign of the second term in the third line is due to fermion anticommutativity.)

Having an understanding of how to treat the free theory we now move on to incorporating the full interacting action as well. Using eq. (2.14) we can rewrite the exponential function in the path integral as[6]

$$e^{iS} = e^{i(S_\mathrm{free}+S_\mathrm{int})} = e^{iS_\mathrm{free}}e^{iS_\mathrm{int}} = e^{iS_\mathrm{free}}\left(1 + iS_\mathrm{int} + \frac{1}{2!}(iS_\mathrm{int})^2 + \cdots\right). \qquad (2.24)$$

The idea behind perturbation theory is to treat this as an expansion in the gauge coupling g and to truncate the series at a certain order, e.g., neglect all terms starting from $\mathcal{O}(g^3)$. If g is small enough (see below), results obtained using the truncated series should provide a reasonable approximation of the true values.

By means of this expansion a calculation in perturbation theory can be carried out by evaluating vacuum expectation values just like in the free theory, with the only difference being the extra powers of S_int, which translate to additional fields in the product. This is not a problem in principle, as we know how to handle arbitrarily many fields. In practice however, we are forced to stop at some order as calculations can quickly become unfeasable. The perturbative calculations in this work are all done at next-to-leading order (NLO), i.e., including all terms of $\mathcal{O}(g^2)$.

Now let us finally turn to the question whether g can be considered small, and with it whether perturbation theory is a valid approach at all. For this discussion let us define the strong coupling

$$\alpha_s = \frac{g^2}{4\pi}\,. \qquad (2.25)$$

This definition is similar to the fine structure constant $\alpha = e^2/(4\pi\varepsilon_0)$, which governs the strength of the electromagnetic interaction. The (renormalized) coupling α_s is not a constant, instead it is a function of the renormalization scale μ. For any physical process

[5] According to Wick's theorem they result in terms involving normal-ordered operators. Such normal-ordered products always have vanishing vacuum expectation values.

[6] The second step is allowed because the anticommuting fields appear in the action only as bilinear combinations, meaning that individual terms of the action commute with each other.

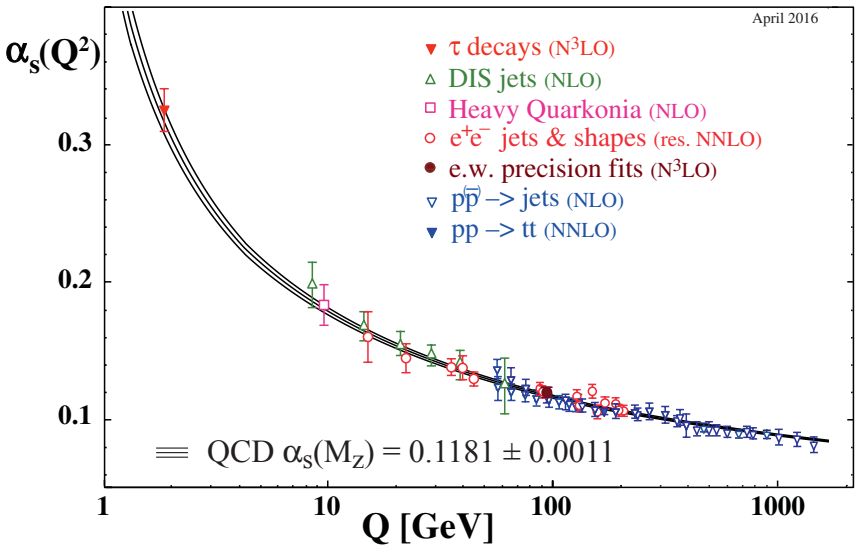

Figure 2.1.: Summary of measurements of α_s as a function of the energy scale Q. The world average value is customarily quoted at a scale equal to the mass of the neutral gauge boson of the weak interaction (Z boson), $m_Z \approx 91.19\,\text{GeV}$. (Figure taken from [58]; used with permission.)

the coupling is dependent on the energy scale Q at which this process is measured,[7] with the value $\alpha_s(\mu^2 = Q^2)$ being a measure for the strength of the interaction. The running of α_s (i.e., its scale dependence) is given by the QCD beta function

$$\beta(\alpha_s) = \mu^2 \frac{d\alpha_s}{d\mu^2} = -\left(11 - \frac{2}{3}n_f\right)\frac{\alpha_s^2}{4\pi} + \mathcal{O}(\alpha_s^3)\,, \tag{2.26}$$

where n_f is the number of flavors that can be considered light at the given scale (i.e., the number of flavors for which $m_f < \mu$). The calculation of the beta function (which is currently known to five-loop accuracy [71], i.e., eq. (2.26) is known including all terms of $\mathcal{O}(\alpha_s^6)$) and the determination of α_s itself (which is averaged from many different experiments as well as lattice studies to obtain an overall uncertainty of less than 1%) are among the main achievements of high-precision QCD. The results are summarized in fig. 2.1, see review 9.4 in [58] for more information.

The leading contribution to the QCD beta function (2.26) is negative (as long as $n_f \leq 16$, which is true in the real world), which indicates that this gauge theory has an interesting property called asymptotic freedom (discovered in 1973 [6, 7], awarded with the Nobel Prize in Physics 2004). As the energy scale becomes larger (corresponding to shorter distances), the coupling strength is ever decreasing such that for asymptotically large

[7] E.g., consider a high-energy scattering event with a large space-like momentum transfer vector q. The relevant energy scale of this process would be $Q = \sqrt{-q^2}$.

energies the quarks can be treated as almost free particles. On the other hand, the coupling actually starts to diverge when the energy scale becomes small. By solving the one-loop beta function (a first order differential equation) we find the one-loop approximation

$$\alpha_s(\mu^2) = \frac{4\pi}{\left(11 - \frac{2}{3}n_f\right)\ln\left(\frac{\mu^2}{\Lambda^2_{\mathrm{QCD}}}\right)}\,, \tag{2.27}$$

with $\mu = \Lambda_{\mathrm{QCD}}$ marking the point of divergence. This process of dimensional transmutation — i.e., a new scale (dimensionful quantity) appearing due to the renormalization group behavior in a theory with a dimensionless coupling — happens even in massless QCD where the Lagrangian is fully scale invariant, meaning that the conformal invariance of the classical theory is broken by quantum corrections. The exact value of the QCD scale Λ_{QCD} depends on various factors, such as the loop order used in the beta function and (starting from three loops) the renormalization scheme, but usually it is of $\mathcal{O}(200\,\mathrm{MeV})$.

At scales $\mu < \Lambda_{\mathrm{QCD}}$ the perturbative approach to QCD is obviously not valid, while at very large scales (such as those given by the momentum transfers reachable in collider experiments) the coupling becomes small and perturbation theory should work very well. For our calculation of hadron distribution amplitudes we work between these two extreme regimes, setting the renormalization scale to a typical hadronic scale $\mu = 2\,\mathrm{GeV} > \Lambda_{\mathrm{QCD}}$ (so that we are working in the same order of magnitude as, e.g., the proton mass $m_p \approx 0.938\,\mathrm{GeV}$), where perturbative calculations are justified.

2.1.2. Lattice QCD

Lattice QCD is a nonperturbative method for QCD calculations from first principles based on discretized Euclidean spacetime and numerical integration. Invented in the 1970s [72], lattice QCD is now a well-established tool in particle physics, harnessing the power of high-performance computing to provide data for a wide range of QCD observables. The method has enjoyed a lot of success in producing results that are in agreement with experiments, e.g., by calculating the hadronic spectrum [73], but it can also be applied to quantities that cannot be determined directly in experiments, such as the moments of distribution amplitudes that we consider in this work. In the following we will give a brief overview regarding some concepts of lattice QCD; for more information see textbooks such as [74].

The definition of the path integral is somewhat heuristic and in the present form it is not immediately suited for direct numerical computation. For example, the integration measure

$$\mathcal{D}q = \prod_{b,\beta,f}\prod_{x} d\left[f^b_\beta(x)\right] \tag{2.28}$$

is a product encompassing all field components and all locations. While the former is well

defined (there are only 3 values for the color index b, 4 Dirac components β, and 6 quark flavors f), the latter is an uncountably infinite formal product over all points x of the continuous 4-dimensional space.

We can start to regularize this infinity by discretizing the spacetime continuum as a hypercubic lattice of discrete spacetime points, with all neighboring lattice sites separated by a lattice spacing a. This procedure reduces the product in eq. (2.28) to a countably infinite one. Furthermore, if we were to give up the notion of infinitely extending physical space and instead are content with examining only a bounded hypercuboidic "box" of spacetime, we are left with a finite number of integration variables. Working with a finite volume is often justified, as we are usually not interested in the behavior of QCD at very long distances. Interesting strong interaction physics processes can take place on length scales of the proton radius, i.e., shorter than a femtometer. Still, it is desirable to have reasonably large lattice volumes to limit the influence of finite size effects. In this study we will work with spatial extents of at least 2.7 fm.

Many different numerical methods can be applied to the evaluation of multi-dimensional integrals, but often the computational effort grows exponentially with the dimensionality of the integration. Even though our number of variables is now finite, it is still very large (even for small lattices), making such approaches unfeasable. A class of methods that is suited for these higher-dimensional integrals are the so-called Monte Carlo methods, which try to approximate the integral by sampling the integrand at many points that are selected randomly according to some probability distribution. To be more specific, modern lattice ensembles are generated using the Hybrid Monte Carlo algorithm [75]. This is an importance sampling technique, meaning that each field configuration is assigned a weight factor to judge the relevance of its contribution to the integral, ensuring that the most important regions of the integration domain are sampled more often and that little computer time is spent sampling configurations that have not much impact on the result.

This brings us to another important property of lattice QCD, namely the use of Euclidean spacetime. In the Minkowski path integral in eq. (2.8) the action enters as a complex phase factor, making the integrand highly oscillatory. This undesirable behavior can be circumvented by a change to Euclidean spacetime with a positive-definite metric, which is accomplished by replacing the time coordinate $x^0 \to -ix_4$, cf. also appendix A.4. By virtue of transforming the action from Minkowski space (M) to Euclidean space (E), the complex phase factor becomes a real weight factor,

$$e^{iS_M} \to e^{-S_E}\,, \tag{2.29}$$

assuming a meaning very similar to the Boltzmann factor $e^{-\beta E}$ in the canonical partition function of statistical physics. It is this interpretation as a probability distribution that

allows the importance sampling method described above to be applied to the calculation.[8] The Minkowski correlation functions of interest can be obtained as the analytic continuation of the corresponding Euclidean functions [76, 77].

Let us now take a closer look at the lattice QCD action. Naively one would start with the continuum action, restrict the fields to the lattice sites, replace the integral by a sum, and replace derivatives by difference quotients. This procedure, however, destroys gauge invariance. Instead one starts by defining a new action for a Euclidean field theory on the lattice that tends to the correct gauge-invariant continuum action in the limit of vanishing lattice spacing a. This approach is not unique. There exists a multitude of different lattice actions, each with its own set of advantages and disadvantages. To be instructive we only present one simple case (called the Wilson action [72]) that provided the starting point for many modern lattice actions:

$$\begin{aligned} S = a^4 \sum_x \sum_f \bar{f}(x) \Bigg(\sum_\mu \gamma_\mu \frac{U(x,\mu) f(x+\hat{\mu}) - U(x-\hat{\mu},\mu)^\dagger f(x-\hat{\mu})}{2a} + m_f f(x) \Bigg) \\ + \frac{2}{g^2} \sum_x \sum_{\mu<\nu} \mathrm{Re}\,\mathrm{tr}\big\{ \mathbb{1}_3 - U(x,\mu) U(x+\hat{\mu},\nu) U(x+\hat{\nu},\mu)^\dagger U(x,\nu)^\dagger \big\} \,. \end{aligned} \tag{2.30}$$

The derivative acting on the fermions has indeed been implemented as a type of difference quotient.[9] In contrast, the realization of the gauge fields has changed drastically. Instead of algebra-valued fields $t^A A_\mu^A(x)$ one now has group-valued fields $U(x,\mu) \mathrel{\hat{=}} \exp\big(igat^A A_\mu^A(x)\big)$.[10] Their behavior under SU(3) gauge transformations $\tilde{U}(x)$,

$$U(x,\mu) \to \tilde{U}(x) U(x,\mu) \tilde{U}(x+\hat{\mu})^\dagger + \mathcal{O}(a) \,, \tag{2.31}$$

ensures gauge invariance for the fermionic part of the action by operating as a gauge transporter. This geometric aspect of $U(x,\mu)$ as an oriented variable linking the sites x and $x+\hat{\mu}$ motivates its name, link variable.

The gluonic part of the action has to be constructed from gauge-invariant objects containing link variables only. It is easy to see that this can be accomplished by taking the trace of any closed loop of links. (Taking the real part effectively averages each loop with

[8] Actually, the situation is not that simple. Due to their Graßmannian nature the fermion field variables in the lattice QCD partition function have to be integrated out first, resulting in a so-called fermion determinant. A probabilistic interpretation is only straightforward if this determinant is guaranteed to be real and non-negative. Whether or not this is the case depends on the specific choice of lattice action. For more information see [74].

[9] $\hat{\mu}$ is defined as a vector of length a, pointing in μ-direction. Thus the lattice sites $x+\hat{\mu}$ and $x-\hat{\mu}$ are nearest neighbors of the site x.

[10] This is not just a change of notation. In the lattice formulation the new fields $U(x,\mu)$ are now the fundamental degrees of freedom. Hence, in a lattice path integral one has an integration measure $\mathcal{D}U$, not $\mathcal{D}A$.

another loop running in the opposite direction.) For the Wilson gauge action one takes the sum over all of the shortest possible loops (squares consisting of just 4 link variables), called plaquettes.[11] An explicit calculation can be performed to show that this form correctly reproduces a gauge-invariant Euclidean continuum QCD action in the limit $a \to 0$.

Lattice studies are not restricted to simulating QCD with all its parameters at the physical values. In fact, simulations are usually done with light quark masses larger than the physical ones since the computational cost increases as the mass parameters become smaller. To connect these simulations to the real world one can use chiral perturbation theory (ChPT) [79], as described in section 4.5.

Now for a few words on gauge fixing in lattice QCD. Unlike continuum perturbation theory (where it is imperative to have a gauge-fixing term in order to make the path integral manageable), lattice QCD can be performed without gauge fixing because the lattice acts as an automatic regulator for the path integral. Therefore, gauge-independent observables can be calculated without further complications. In our case the situation is not that simple, as the lattice renormalization factors for the distribution amplitudes will have to be calculated from gauge-dependent vertices, meaning that these lattices will have to be gauge fixed as well. For our application we require a gauge that can be implemented in perturbative QCD as well as in lattice simulations. Regrettably, the perturbative physicist's favorite gauge — Feynman gauge — is not well suited for lattice use, see [80]. Even though lattice implementations of Feynman gauge are being developed, not all problems are yet under control [81]. We therefore settle for the use of Landau gauge. Its lattice implementation is well established, but in exchange the perturbative side of our calculation will become a bit harder because more complicated integrals will have to be evaluated.

The lattice analog of the continuum Landau gauge condition $\partial^\mu A^A_\mu = 0$ is not implemented via a gauge-fixing term in the Lagrangian, but as a numerical extremalization problem.[12] To begin with, one generates a gauge configuration $U(x, \mu)$ without restrictions. Then one tries to maximize

$$\sum_x \sum_\mu \operatorname{Re} \operatorname{tr}\{\tilde{U}(x) U(x, \mu) \tilde{U}(x + \hat{\mu})^\dagger\} \tag{2.32}$$

as a functional of SU(3) matrices $\tilde{U}(x)$. Such a procedure as well as the details of the accompanying algorithms used to search for the global maximum are, e.g., presented in [84]. In the end, one uses the resulting $\tilde{U}(x)$ to gauge transform the link variables $U(x, \mu)$, which will then fulfill the Landau gauge condition up to corrections of $\mathcal{O}(a^2)$ [85].

[11] Improved lattice actions will also incorporate other kinds of loops, such as larger rectangles [78].

[12] A nonperturbative implementation of a gauge-fixed BRST-invariant Lagrangian (analogous to eq. (2.11), which is used in perturbation theory) is not straightforward. Associated topics such as Gribov copies [82] and the Neuberger 0/0 problem [83] will not be discussed here.

2.1.3. Regularization

Calculations in quantum field theory often yield divergent results that need to be regularized, i.e., made finite. One approach to this is putting the theory on a lattice as discussed above. In this section we will instead look at it from the perspective of perturbative QCD and perform an example computation while illustrating the need for regularization and the general principles of such perturbative calculations as we proceed.

Let us try to determine the one-loop correction to the fermion propagator. For simplicity we will perform this exercise in massless Feynman-gauge QCD, so that (in momentum space) the propagation of quarks and gluons at tree level is governed by these simple expressions:

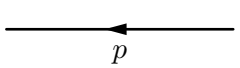

$$\hat{=} \quad S^{ab}_{\alpha\beta}(p) = i\delta^{ab}\frac{\not{p}_{\alpha\beta}}{p^2}\,, \tag{2.33a}$$

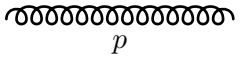

$$\hat{=} \quad D^{AB}_{\mu\nu}(p) = -i\delta^{AB}\frac{g_{\mu\nu}}{p^2}\,. \tag{2.33b}$$

And for the interaction vertex we have:

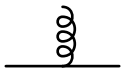

$$\hat{=} \quad ig\big(t^A\big)^{ab}(\gamma^\mu)_{\alpha\beta}\,. \tag{2.33c}$$

The first order radiative correction to the fermion propagator is due to the emission and reabsorption of a single gluon:

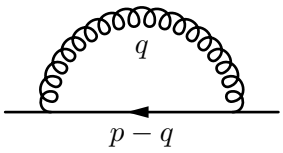

We have to calculate the corresponding fermion self-energy,

$$\begin{aligned}\Sigma^{ab}_{\alpha\beta}(p) &= \int\frac{d^4q}{(2\pi)^4}\,ig\big(t^A\big)^{aa'}(\gamma^\mu)_{\alpha\alpha'}\times S^{a'b'}_{\alpha'\beta'}(p-q)\times ig\big(t^B\big)^{b'b}(\gamma^\nu)_{\beta'\beta}\times D^{AB}_{\mu\nu}(q)\\ &= -\frac{4}{3}g^2\delta^{ab}(\gamma^\mu\gamma_\nu\gamma_\mu)_{\alpha\beta}\int\frac{d^4q}{(2\pi)^4}\frac{(p-q)^\nu}{q^2(p-q)^2}\,,\end{aligned} \tag{2.34}$$

where the integration variable q is the momentum of the virtual gluon. By analyzing the integral in the region of very large q we find that it behaves like

$$\int\frac{d^4q}{(2\pi)^4}\frac{q^\nu}{q^4}\,, \tag{2.35}$$

meaning that the integral is divergent there because the integrand does not fall off fast enough. To be able to evaluate the integral we need to make it finite by introducing

some form of regulator. To this end, various prescriptions are available, e.g., Pauli–Villars regularization or a simple momentum cutoff. For the perturbative calculations done in this work we use only one procedure, namely dimensional regularization [86, 87].

The integrand q^ν/q^4 leads to an ultraviolet (UV) divergence in the 4-dimensional integration. However, if we were to perform this integration in a spacetime with a different number of dimensions, then this divergence need not necessarily appear. If the number of dimensions becomes small enough, then the UV divergence will indeed disappear. This motivates dimensional regularization, where we calculate the integral using d-dimensional integration (for an arbitrary, in general noninteger, number d). This elegant procedure will make it easy to identify the divergences and the associated renormalization scheme (the $\overline{\text{MS}}$ scheme, see section 2.1.4) is straightforward to implement. Dimensional regularization also has many advantages compared to other regularization prescriptions. Compared to Pauli–Villars, it does not require auxiliary massive fields, and unlike a momentum cutoff it keeps Lorentz invariance intact. Furthermore, dimensional regularization can also regularize infrared divergences (i.e., those stemming from the region of very small momenta) without the need for a fictitious gluon mass.

Knowing that the integration converges in some region of d, we can continue the result from there and find it to be a meromorphic function of d with an isolated singularity for $d \to 4$. It is convenient to parametrize the dimension as $d = 4 - 2\epsilon$, with ϵ acting as the regulator. The Laurent expansion around $\epsilon = 0$ of a full result at n-loop order may then exhibit poles up to the type $1/\epsilon^n$, allowing us to disentangle the finite and divergent parts of the integral at the physical dimension. It is the responsibility of the renormalization scheme to cancel these poles, so that a finite result can be obtained after removing the regulator by taking the limit $\epsilon \to 0$.

For the integral in eq. (2.34), dimensional regularization amounts to the replacement

$$\int \frac{d^4q}{(2\pi)^4} \frac{(p-q)^\nu}{q^2(p-q)^2} \to \mu^{2\epsilon} \int \frac{d^dq}{(2\pi)^d} \frac{(p-q)^\nu}{q^2(p-q)^2} \,. \tag{2.36}$$

To keep the dimension of the whole expression unchanged we introduce a new energy scale μ, raised to the appropriate power to absorb the change in dimension. This scale of dimensional regularization is, for the time being, an arbitrary constant that will later be identified with the renormalization scale (see below).

Even though the way in which the scale is introduced in dimensional regularization may seem somewhat unintuitive, the fact that such a scale parameter does appear at all should not come as a surprise. Other methods for regularizing the UV divergences of QCD introduce a scale as well, but may have a more immediately evident interpretation for the parameter, such as the maximal momentum in cutoff regularization or the inverse lattice spacing in the lattice regularization.

We still have not provided an answer to the question of how to actually obtain results for the dimensionally regularized loop integrals such as the one in eq. (2.36). The general strategy for this consists of two parts. First, one examines the Lorentz structure of the numerator and performs a tensor decomposition, i.e., one writes down a sum of all Lorentz tensors (with the same number of open indices as in the numerator) that can be constructed from the available structures such as four-vectors of external momenta or (starting from two open indices) the metric tensor. Each tensor in this decomposition is accompanied by a (currently unknown) prefactor of its own. These prefactors have to be Lorentz scalars and may therefore only depend on Lorentz-invariant quantities, e.g., on four-momenta squared. Having performed the tensor decomposition, the problem can now be reformulated in a way that requires only the determination of scalar integrals [88].

In our example we have only one open Lorentz index, ν, and one external momentum, p. From this we can deduce that the tensor decomposition consists of only one term. The result has to be proportional to the four-vector p^ν with a p^2-dependent prefactor:

$$\mu^{2\epsilon} \int \frac{d^d q}{(2\pi)^d} \frac{(p-q)^\nu}{q^2 (p-q)^2} = I(p^2) p^\nu \,. \tag{2.37}$$

By contracting the open index with p_ν we find

$$I(p^2) = \mu^{2\epsilon} \int \frac{d^d q}{(2\pi)^d} \frac{p \cdot (p-q)}{p^2 q^2 (p-q)^2} = \frac{\mu^{2\epsilon}}{2} \int \frac{d^d q}{(2\pi)^d} \frac{1}{q^2 (p-q)^2} \,, \tag{2.38}$$

thereby reformulating the problem in terms of a scalar integral.

The second step is the calculation of said scalar integrals. In general, one can proceed as follows: Combine the propagator denominators by introducing an auxiliary integration variable α (called a Feynman parameter), complete the square in the new denominator by shifting the momentum integration, apply a Wick rotation to the integration contour and move to d-dimensional Euclidean space ($\int d^d q \to i \int d^d q_E$, $q^2 \to -q_E^2$), perform the momentum integration in d-dimensional spherical coordinates, and finally integrate out the Feynman parameter. In our example:

$$\begin{aligned}
\mu^{2\epsilon} \int \frac{d^d q}{(2\pi)^d} \frac{1}{q^2 (p-q)^2} &= \mu^{2\epsilon} \int \frac{d^d q}{(2\pi)^d} \int_0^1 \frac{d\alpha}{[(1-\alpha) q^2 + \alpha (p-q)^2]^2} \\
&= \mu^{2\epsilon} \int_0^1 d\alpha \int \frac{d^d q}{(2\pi)^d} \frac{1}{[q^2 + \alpha(1-\alpha) p^2]^2} \\
&= i \mu^{2\epsilon} \int_0^1 d\alpha \int \frac{d^d q_E}{(2\pi)^d} \frac{1}{[q_E^2 - \alpha(1-\alpha) p^2]^2} \\
&= i \mu^{2\epsilon} \int_0^1 d\alpha \int \frac{d^{d-1}\Omega}{(2\pi)^d} \int_0^\infty \frac{d|q_E| \, |q_E|^{d-1}}{[|q_E|^2 - \alpha(1-\alpha) p^2]^2}
\end{aligned}$$

$$= \frac{i}{(4\pi)^2} \int_0^1 \frac{d\alpha}{[\alpha(1-\alpha)]^\epsilon} \Gamma(\epsilon) \left(\frac{-p^2}{4\pi\mu^2} \right)^{-\epsilon}$$
$$= \frac{i}{(4\pi)^2} \frac{\Gamma(1-\epsilon)^2}{\Gamma(2-2\epsilon)} \Gamma(\epsilon) \left(\frac{-p^2}{4\pi\mu^2} \right)^{-\epsilon}, \tag{2.39}$$

with the gamma function,

$$\Gamma(z) = \int_0^\infty dt\, t^{z-1} e^{-t}\,, \tag{2.40}$$

and the $(d-1)$-dimensional surface area of the unit sphere in d dimensions,

$$\int d^{d-1}\Omega = \frac{2\pi^{\frac{d}{2}}}{\Gamma(d/2)}\,. \tag{2.41}$$

In general, one may need to compute many different loop integrals, even when working at one-loop order. Fortunately, this tedious task is simplified somewhat thanks to the existence of certain recurrence relations between the scalar integrals. A systematic application of these relations makes it possible to rewrite complicated integrals as linear combinations involving only a small set of fundamental integrals. Such a reduction method is described in [89] and we make use of it in all our calculations.

Let us now try to put it all together and formulate the dimensionally regularized result for the self-energy defined in eq. (2.34). We have to be careful though, because in addition to the integrals other parts of the theory have to be promoted to d dimensions as well. For the Dirac matrices we now have $\gamma^\mu\gamma_\mu = d\mathbb{1}_4$ instead of $4\mathbb{1}_4$, such that

$$\gamma^\mu\gamma_\nu\gamma_\mu = -2(1-\epsilon)\gamma_\nu\,. \tag{2.42}$$

With that we obtain the final result:

$$\Sigma^{ab}_{\alpha\beta}(p) = i\delta^{ab}\frac{\alpha_s}{3\pi}\frac{\Gamma(1-\epsilon)\Gamma(2-\epsilon)}{\Gamma(2-2\epsilon)}\Gamma(\epsilon)\left(\frac{-p^2}{4\pi\mu^2}\right)^{-\epsilon} \not{p}_{\alpha\beta}\,. \tag{2.43}$$

As stated above, this calculation has been performed in Feynman gauge (i.e., for $\xi = 1$) to keep it as short as possible. A calculation using the full gauge-dependent gluon propagator gives the following result for arbitrary ξ:

$$\Sigma^{ab}_{\alpha\beta}(p) = i\delta^{ab}\xi\frac{\alpha_s}{3\pi}\frac{\Gamma(1-\epsilon)\Gamma(2-\epsilon)}{\Gamma(2-2\epsilon)}\Gamma(\epsilon)\left(\frac{-p^2}{4\pi\mu^2}\right)^{-\epsilon} \not{p}_{\alpha\beta}\,. \tag{2.44}$$

We leave it as an exercise for the interested reader to verify this result.

An important quantity in perturbative calculations is the dressed quark propagator, i.e., the tree-level propagator plus the radiative corrections:

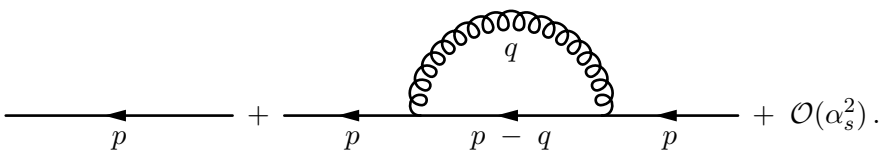

Using the result from the previous calculation we can write in dimensional regularization:

$$\begin{aligned} S^{ab}_{\alpha\beta}(p) &= [S^{\text{free}} + S^{\text{free}}\Sigma S^{\text{free}}]^{ab}_{\alpha\beta}(p) + \mathcal{O}(\alpha_s^2) \\ &= i\delta^{ab}\frac{\not{p}_{\alpha\beta}}{p^2}\left(1 - \xi\frac{\alpha_s}{3\pi}\frac{\Gamma(1-\epsilon)\Gamma(2-\epsilon)}{\Gamma(2-2\epsilon)}\Gamma(\epsilon)\left(\frac{-p^2}{4\pi\mu^2}\right)^{-\epsilon}\right) + \mathcal{O}(\alpha_s^2)\,. \end{aligned} \tag{2.45}$$

Still, this expression is divergent in the limit $\epsilon \to 0$, i.e., when going to the physical dimension $d = 4$. To isolate the divergent contribution we perform a Laurent series expansion around $\epsilon = 0$. We obtain

$$S^{ab}_{\alpha\beta}(p) = i\delta^{ab}\frac{\not{p}_{\alpha\beta}}{p^2}\left(1 - \xi\frac{\alpha_s}{3\pi}\left(\frac{1}{\epsilon} - \gamma + \ln(4\pi) + 1 + \ln\left(\frac{-p^2}{\mu^2}\right)\right)\right) + \mathcal{O}(\epsilon, \alpha_s^2)\,, \tag{2.46}$$

with the Euler–Mascheroni constant γ, which is defined as the negative derivative of the gamma function evaluated at 1:

$$\gamma = -\Gamma'(1) = \lim_{\epsilon\to 0}\left(\frac{1}{\epsilon} - \Gamma(\epsilon)\right) \approx 0.57722\,. \tag{2.47}$$

2.1.4. Renormalization

A way to cure the $1/\epsilon$ divergence evident in eq. (2.46) would be to include, by hand, another term in the Lagrangian. Such a term would need to be designed so as to counterbalance the pole in the perturbative calculation, leading to a theory where the result is finite. A priori it is yet unclear whether this procedure will bring forth a well-defined theory at all. Given that there are both infinitely many divergent Green's functions and infinitely many orders in perturbation theory, it may well be possible that one would have to add an infinite number of different counterterms to the Lagrangian if one wants to make all those Green's functions finite.

A theory where this happens would acquire an infinite number of parameters (the prefactors of those counterterms) and thus might lose its predictive power. Such theories are called nonrenormalizable.[13] Fortunately, QCD is indeed renormalizable [87]: There is only a finite number of structures that are required as counterterms. Aside from their prefactors, they are identical to the operators appearing in the original Lagrangian. The small handful of counterterm structures appearing at the one-loop order is sufficient to enable cancelation of divergences to all orders in perturbation theory. Armed with this

[13] While this shows that renormalizability is obviously a very desirable property, it does not mean that nonrenormalizable theories are worthless. Chiral perturbation theory, for example, is in general nonrenormalizable, but thanks to the power counting theorem [79] the number of counterterms needed at each chiral order is finite and the theory can be used to predict the behavior of observables in the low-energy regime of QCD.

knowledge we can proceed to illustrate the renormalization of QCD in an instructive manner where the counterterms in the Lagrangian arise naturally.

The formulation is based on the fact that the fields and parameters appearing in the QCD Lagrangian are not observable quantities. We can utilize this to rescale the fields in a way that absorbs the divergence into the unrenormalized (bare) fields. Let us define the renormalized quark fields,[14]

$$f^R = \sqrt{Z_q} f\,, \qquad\qquad \bar{f}^R = \sqrt{Z_q}\bar{f}\,, \tag{2.48a–b}$$

with an as yet undetermined quark field renormalization factor Z_q. It is our goal to fix this factor such that Green's functions of the renormalized fields are finite (even after removing the regulator, $\epsilon \to 0$), thanks to the divergent parts of the Z-factor exactly canceling the divergent parts of the bare diagram.

Rewriting the fermionic part of the massless Lagrangian in terms of the renormalized fields we find

$$\sum_f \big[\bar{f} i \not{D} f\big] = \sum_f \big[\bar{f}^R i \not{D} f^R\big] + \big(Z_q^{-1} - 1\big) \sum_f \big[\bar{f}^R i \not{D} f^R\big]\,. \tag{2.49}$$

We have organized the expressions such that the first term mimics the form of the original Lagrangian, but is now built from the renormalized (finite) fields. The divergent parts are contained in the second term, which serves as a counterterm. Having the same structure, this part looks as if it could give rise to another kinetic term. However, the prefactor $Z_q^{-1} - 1$ will be of $\mathcal{O}(\alpha_s)$ in the perturbative expansion (as reflected in (2.54a)), meaning that this term will contribute only to the interaction part of the Lagrangian, effectively leading to a new quark-antiquark counterterm vertex,

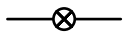

$$\hat{=} \quad i\big(Z_q^{-1} - 1\big)\delta^{ab} \not{p}_{\alpha\beta}\,, \tag{2.50}$$

that has to be taken into account in renormalized perturbation theory.

In a calculation of the renormalized quark propagator to an accuracy of $\mathcal{O}(\alpha_s)$, the counterterm contributes only via a tree diagram (and not inside loops, as such contributions would already be of $\mathcal{O}(\alpha_s^2)$),

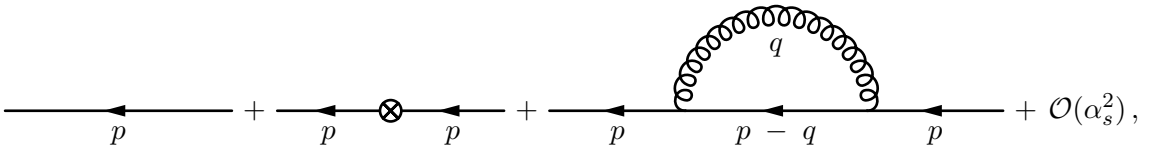

[14] For the sake of our example we focus on just the quark fields. Generally, the gluon and ghost fields and the parameters such as the gauge coupling and the quark masses have to be renormalized as well.

thus leading to

$$\begin{aligned}\left[S^R\right]^{ab}_{\alpha\beta}(p) &= Z_q S^{ab}_{\alpha\beta}(p) = \\ &= i\delta^{ab}\frac{\not{p}_{\alpha\beta}}{p^2}\left(1-\left(Z_q^{-1}-1\right)-\xi\frac{\alpha_s}{3\pi}\left(\frac{1}{\epsilon}-\gamma+\ln(4\pi)+1+\ln\left(\frac{-p^2}{\mu^2}\right)\right)\right)+\mathcal{O}(\alpha_s^2)\,.\end{aligned} \tag{2.51}$$

For the renormalized propagator to be finite, the renormalization factor Z_q will have to be chosen such that it cancels the $1/\epsilon$ pole. And while this condition fixes the divergent part of Z_q, it does not constrain the finite part, meaning that we are left with some freedom of choice.

Prescriptions that set the finite part are called renormalization schemes. In principle, various schemes are feasible, but depending on the situation one scheme may be preferred over others. In the QCD community a number of schemes are in common use and these different schemes are not equivalent. Results obtained in one renormalization scheme can not be directly compared with calculations done in another scheme. A central goal of this work is to determine conversion factors between two of those schemes in order to connect data obtained from lattice QCD simulations to the phenomenological work done in perturbative QCD.

In the following we will introduce several common types of renormalization prescriptions, namely the MS, $\overline{\text{MS}}$, and RI′ schemes, and discuss some of their properties, once again using the quark propagator as an example.

MS scheme

In the minimal subtraction (MS) scheme only the poles themselves are subtracted and no finite parts are defined into the renormalization factor [90]. In our example this leads to the following expressions for the Z-factor and the renormalized quark propagator:

$$Z_q^{\text{MS}} = 1+\xi\frac{\alpha_s}{3\pi}\frac{1}{\epsilon}+\mathcal{O}(\alpha_s^2)\,, \tag{2.52a}$$

$$\left[S^{\text{MS}}\right]^{ab}_{\alpha\beta}(p) = i\delta^{ab}\frac{\not{p}_{\alpha\beta}}{p^2}\left(1-\xi\frac{\alpha_s}{3\pi}\left(-\gamma+\ln(4\pi)+1+\ln\left(\frac{-p^2}{\mu^2}\right)\right)\right)+\mathcal{O}(\alpha_s^2)\,. \tag{2.52b}$$

This is the simplest renormalization scheme, but it is of little practical relevance since it has been superseded by the $\overline{\text{MS}}$ scheme.

$\overline{\text{MS}}$ scheme

As it turns out, a certain combination of terms appearing in the dimensionally regularized quark propagator seen in eq. (2.46), namely

$$\frac{1}{\bar{\epsilon}} = \frac{1}{\epsilon}-\gamma+\ln(4\pi)\,, \tag{2.53}$$

is not specific to this particular calculation. Actually, it universally appears at the one-loop level in dimensional regularization. This fact motivates the definition of the modified minimal subtraction ($\overline{\text{MS}}$) scheme (introduced in [91]), in which we absorb the expression (2.53) into the Z-factor, leading to a more compact form for the renormalized propagator:

$$Z_q^{\overline{\text{MS}}} = 1 + \xi \frac{\alpha_s}{3\pi} \frac{1}{\bar{\epsilon}} + \mathcal{O}(\alpha_s^2)\,, \tag{2.54a}$$

$$\left[S^{\overline{\text{MS}}}\right]^{ab}_{\alpha\beta}(p) = i\delta^{ab} \frac{\not{p}_{\alpha\beta}}{p^2} \left(1 - \xi \frac{\alpha_s}{3\pi} \left(1 + \ln\left(\frac{-p^2}{\mu^2}\right)\right)\right) + \mathcal{O}(\alpha_s^2)\,. \tag{2.54b}$$

The $\overline{\text{MS}}$ scheme is simple and straightforward to implement in perturbative calculations done in dimensional regularization, and it has become by far the most widely used scheme in this scenario.

The biggest drawback of the MS and $\overline{\text{MS}}$ schemes is, however, that this scenario is the only one where they are directly applicable at all. On the one hand, their prescriptions are inherently perturbative, as the poles have to be determined and subtracted order by order in the perturbative expansions. On the other hand, the schemes are intimately linked to the evaluation of integrals in noninteger spacetime dimensions ($d = 4 - 2\epsilon$). These two facts make the $\overline{\text{MS}}$ scheme incompatible with the nonperturbative realization of QCD on an exactly 4-dimensional spacetime that is lattice QCD.

RI′ scheme

The last scheme we discuss is the RI′ scheme, which is also called Rome–Southampton scheme [92]. This scheme belongs to a more general class of momentum subtraction (MOM) schemes and is designed to be regularization invariant (RI). Therefore, it can be used in conjunction with both dimensional regularization and lattice regularization.

The method is centered around imposing nonperturbative renormalization conditions (enforced at a certain renormalization point) upon the Green's functions in a manner that projects onto their free value. For the quark propagator the RI′ renormalization condition reads

$$\lim_{m_q \to 0} \frac{1}{12} \operatorname{tr}\left\{ S^{\text{Born}} \left(S^{\text{RI}'}\right)^{-1} \right\}\Big|_{p^2=-\mu^2} \overset{!}{=} \lim_{m_q \to 0} \frac{1}{12} \operatorname{tr}\left\{ S^{\text{Born}} \left(S^{\text{Born}}\right)^{-1} \right\}\Big|_{p^2=-\mu^2} = 1\,, \tag{2.55}$$

where the trace (as well as the inverse) is to be taken in 4-dimensional Dirac as well as in 3-dimensional color space, and the prefactor $1/12$ ensures its overall normalization. This trace operation acts similar to a scalar product, contracting the open Dirac and color indices and projecting the renormalized two-point function onto its Born, i.e., noninteracting, counterpart.[15] Formulating the renormalization condition in the limit of vanishing quark

[15] In continuum perturbation theory the Born term is simply the tree-level propagator. In lattice QCD the noninteracting case corresponds to a simulation with unit gauge fields.

masses ensures that the renormalization factor in this scheme is mass independent.[16]

This renormalization condition has to be fulfilled only for certain momenta, namely at the so-called renormalization point, which introduces the renormalization scale into the picture. The exact specification of this point is part of the definition of the scheme. In particular, it should be noted that the condition given above is constructed to generate a Lorentz-invariant scheme as long as the renormalization point is also declared in a Lorentz-invariant manner. For an object involving only one momentum variable p it is only natural to define the renormalization at the point where the scale equals the virtuality of this momentum, i.e., at $\mu^2 = -p^2$.[17] If there are multiple independent external momenta (as, e.g., in the case of three-quark operators), there are various choices for the renormalization point. Our renormalization scheme for three-quark operators will be detailed in section 3.5.2.

In the RI′ scheme the Z-factor and renormalized propagator are given by

$$Z_q^{\mathrm{RI}'} = 1 + \xi \frac{\alpha_s}{3\pi}\left(\frac{1}{\epsilon} - \gamma + \ln(4\pi) + 1\right) + \mathcal{O}(\alpha_s^2)\,, \tag{2.56a}$$

$$\left[S^{\mathrm{RI}'}\right]^{ab}_{\alpha\beta}(p) = i\delta^{ab}\frac{\not{p}_{\alpha\beta}}{p^2}\left(1 - \xi\frac{\alpha_s}{3\pi}\ln\left(\frac{-p^2}{\mu^2}\right)\right) + \mathcal{O}(\alpha_s^2)\,. \tag{2.56b}$$

As usual for a MOM scheme, the definition is such that the renormalized propagator is free of $\mathcal{O}(\alpha_s)$ corrections at the renormalization point.

Converting between renormalization schemes

Often one would like to convert results from one renormalization scheme to another, especially to enable comparability between values that have been obtained using different approaches (each using a different renormalization scheme for reasons of necessity, tradition, or convenience). In our case the key quantities are baryon distribution amplitudes, which will be defined and discussed in section 3.2. On the one hand, their normalization constants and shape parameters can be estimated using SVZ sum rules [93]; for such a calculation see [38]. Furthermore, the DAs are often required as input parameters in the description of scattering experiments, e.g., by light-cone sum rules [94]; for such an application see [95]. All these calculations are done in the continuum and naturally use the $\overline{\mathrm{MS}}$ scheme, which is the most relevant scheme in perturbative contexts, and also all amplitudes describing experimental processes are usually only studied in the $\overline{\mathrm{MS}}$ scheme as well. On the other hand, when DAs are determined using lattice QCD (see sections 3.3 and 4.2 for more

[16] In continuum perturbation theory this limit is trivial to implement, as the calculation can just be performed directly at zero quark mass. In lattice QCD, simulations with vanishing mass are not possible and therefore one has to extrapolate to the chiral limit from multiple simulations done at different masses.

[17] The equation refers to Minkowski spacetime. In Euclidean space one would naturally set $\mu^2 = p^2$ instead.

information), the $\overline{\text{MS}}$ scheme cannot be implemented directly. Since lattice QCD can provide valuable complementary data on important nonperturbative parameters, it would be very desirable to have results obtained from lattice QCD expressed in the $\overline{\text{MS}}$ scheme so that they can immediately be compared to (and also used in) perturbative calculations.

The basic idea is as follows: We start from the unrenormalized raw lattice data. After the desired quantities have been extracted in the analysis they are renormalized nonperturbatively (on the lattice) using a suitable intermediate scheme. For a review on nonperturbative renormalization in lattice QCD see [96]. In our case we will select an RI′ scheme as the intermediate scheme. We determine the conversion factor between the RI′ and $\overline{\text{MS}}$ schemes in an accompanying calculation in continuum perturbation theory with dimensional regularization, i.e., in a scenario where both schemes can be implemented. This conversion factor can then be applied to the lattice calculation in order to obtain the final results in the $\overline{\text{MS}}$ scheme. In theory these results are now independent of the choice made for the intermediate scheme, but in practice this is not exactly true owing to the necessary truncation of the perturbative series.

We define the conversion factor as the product of the $\overline{\text{MS}}$ Z-factor and the inverse of the RI′ Z-factor. Even though both of these factors contain regulator-dependent divergences, their product will be finite (and the regulator can be removed) because it facilitates a conversion between two renormalized (and therefore finite) objects. For our familiar example we combine eqs. (2.54a) and (2.56a) to find

$$C_q = Z_q^{\overline{\text{MS}}} \big(Z_q^{\text{RI}'}\big)^{-1} = 1 - \xi \frac{\alpha_s}{3\pi} + \mathcal{O}(\alpha_s^2)\,. \tag{2.57}$$

This conversion factor is known to three-loop accuracy [97].

It is very interesting to note that C_q can also be calculated without explicit knowledge of the RI′ Z-factor and RI′ renormalized propagator. It follows from its definition that this conversion factor (or rather, its inverse) can be obtained by combining the $\overline{\text{MS}}$ renormalized propagator with the RI′ renormalization condition:

$$C_q^{-1} = \frac{1}{12}\,\text{tr}\Big\{ S^{\text{free}} \big(S^{\overline{\text{MS}}}\big)^{-1} \Big\}\Big|_{p^2=-\mu^2}\,. \tag{2.58}$$

In practice, this will actually be the preferred approach, and in section 3.5.3 we will use a similar method to obtain the conversion factors for three-quark operators.

In the calculation of the conversion factor we set both the RI′ renormalization scale and the $\overline{\text{MS}}$ renormalization scale equal to the scale introduced in dimensional regularization. And of course we have to make sure that this scale used in the continuum calculation is equal to the scale used for the nonperturbtive renormalization on the lattice. We will label this common scale μ. The conversion factor (2.57) has an implicit scale dependence per the running of the strong coupling $\alpha_s(\mu)$.

Finding an optimal value for μ is nontrivial. On the one hand, it is advantageous to make μ large enough to stay clear of the nonperturbative regime. While the intermediate RI′ scheme is well able to handle potential nonperturbative effects, the perturbative conversion to the $\overline{\text{MS}}$ scheme is not. Hence, increasing μ improves the convergence behavior of the perturbative expansion (cf. eq. (2.26) and fig. 2.1) and reduces the dependence on the intermediate scheme. On the other hand, making μ too large can enhance lattice artefacts. Ideally we would like to have a window between the QCD scale and the scale generated by the lattice regularization,

$$\Lambda^2_{\text{QCD}} \ll \mu^2 \ll 1/a^2\,, \tag{2.59}$$

to simultaneously limit the size of both nonperturbtive and discretization effects [92]. In reality, the available lattice spacings determine how well such a window can be realized. Taking the spacing of the ensembles used in this work, $a = 0.0857\,\text{fm}$ (cf. table 4.2), and aiming for a well-behaved perturbative behavior by selecting the typical hadronic scale $\mu = 2\,\text{GeV}$ means that

$$\Lambda^2_{\text{QCD}} \ll \mu^2 < 1/a^2\,. \tag{2.60}$$

This is promising as it shows that the method should indeed be applicable in our case, but some lattice artefacts should be expected. However, the study of such discretization errors is not the main objective of this thesis. We content ourselves with the prospect that in the near future several ensembles with smaller lattice spacings (and therefore smaller discretization errors) will be analyzed, allowing one to investigate these effects. Furthermore, some methods designed to tackle the problem of discretization errors in lattice renormalization are being developed. E.g., one can try to subtract the leading lattice artefacts, see [98, 99]. Also, provided one does have access to ensembles at various spacings, there exists a new strategy where one uses information obtained at the finest of these spacings (where the window problem is hopefully well under control) to reduce cutoff effects also in the renormalization factors for the coarser lattices [100]. Currently, however, these techniques have only been applied to various quark-antiquark bilinear operators, not to the three-quark operators involved in the study of baryon distribution amplitudes.

2.2. Group theory

In the previous section we have established QCD as a gauge theory with the underlying symmetry group SU(3). Groups will also play an important role in other parts of this work, mainly for the classification of particles and operators. An understanding of the basics of group theory will be essential to our cause. In the following we will therefore briefly explain some concepts of group theory. The treatment will neither be exhaustive, nor will it be mathematically rigorous (e.g., some of the statements made below are in general only valid for finite groups). Instead, we focus on introducing just the definitions and theorems (without proofs) relevant to us. For more detailed discussions we refer the reader to textbooks on group theory such as [101, 102].

Groups A group is a nonempty set G together with a binary relation $\circ\colon G \times G \to G$. This pair needs to fulfill some additional requirements: The relation has to be associative, $(g_1 \circ g_2) \circ g_3 = g_1 \circ (g_2 \circ g_3)$. There has to be a unique identity element $e \in G$ that leaves all other group elements invariant, $e \circ g = g \circ e = g$. And for each element there has to be a unique inverse element $g^{-1} \in G$ such that $g^{-1} \circ g = g \circ g^{-1} = e$.

Subgroups A nonempty subset $H \subseteq G$ is called a subgroup if it forms a group together with the same binary relation $\circ$ restricted to the subset, i.e., $H \times H \to H$.

Conjugacy classes A conjugacy class C_h is a set consisting of all group elements which are conjugate to $h \in G$, i.e., $C_h \equiv \{\, g \circ h \circ g^{-1} \mid g \in G \,\}$. Most conjugacy classes are not subgroups since the identity element forms a conjugacy class of its own and thus cannot be part of any other class. Two conjugacy classes can be either identical or disjoint, and thus the concept of conjugacy classes provides a standard way of partitioning the group into disjoint sets of (conjugate) elements.

Representations Representation theory is a branch of mathematics with various topics and applications [103]. For physicists, studying group representations is often helpful in order to explore the symmetry properties related to groups. The concept of representations is quite general; for the purpose of this work it is however sufficient to accept a very basic definition of matrix representations. Consider a mapping $R\colon G \to \mathrm{GL}(d, \mathbb{C})$ from a group G to the general linear group $\mathrm{GL}(d, \mathbb{C})$. (After choosing a basis on the vector space $\mathbb{C}^d$ one can identify $\mathrm{GL}(d, \mathbb{C})$ with the regular $d \times d$ matrices built from complex entries.) We will call this mapping a d-dimensional representation of G if it is a group homomorphism, i.e., if $R(g_1 \circ g_2) = R(g_1)R(g_2)$.

Inequivalent irreducible representations Even for a singleton group, $\{e\}$, there are infinitely many representations and it is therefore clear that a lot of the information

provided by the representations is actually redundant. To deal with this redundancy we introduce two new terms. First, we will call two d-dimensional matrix representations equivalent if they can be converted into each other by a change of basis on $\mathbb{C}^d$. Second, we will call a matrix representation reducible if there exists a basis in which the representation matrices of all group elements simultaneously acquire the same block-diagonal form. (Since block-diagonal form is preserved under matrix multiplication it follows that the blocks constitute lower-dimensional representations of the group.) For any finite group the number of inequivalent irreducible representations is limited. To be more specific, the number of conjugacy classes is equal to the number of inequivalent irreducible representations and the sum of the squares of the representations' dimensions has to be equal to the group order, i.e., to the number of group elements.

Unitary representations Every representation is equivalent to a unitary representation, i.e., one that represents all group elements by unitary matrices.[18] We can therefore, without loss of generality, consider only unitary representations $R\colon G \to \mathrm{U}(d)$, which have the nice property $R(g^{-1}) = R(g)^\dagger$.

Characters Given the ambiguity of equivalent representations it is desirable to have objects which are invariant under a change of basis. One such object is the trace, i.e., the sum of the diagonal elements of a matrix. One therefore defines the character of a group element g in a representation R as $\chi^R(g) \equiv \mathrm{tr}(R(g))$. From the cyclic permutation property of the trace operation it follows that $\chi^R(g \circ h \circ g^{-1}) = \chi^R(h)$, and therefore we have exactly one character per conjugacy class per inequivalent representation. This information can be neatly arranged in so-called character tables, see, e.g., tables 2.2 and B.1. While a character table does not define a group, it contains the essential information regarding its representations. In principle, it is possible to construct all irreducible representations from the characters [104].

Products and sums of representations Given two matrix representations R_a and R_b of the same group G one can take the direct (Kronecker) product and the direct sum of the representation matrices.[19] The newly constructed objects $R_a \otimes R_b$ and $R_a \oplus R_b$ are now also representations of G. In most cases the products of irreducible representations will

[18] Such a transformation can be constructed explicitly. Let R be an arbitrary representation, let $S = \sum_{g\in G} R(g)^\dagger R(g)$, and let D be a unitary matrix which diagonalizes S. (This procedure is well defined since S is a positive-definite Hermitian matrix by construction.) Now take the square root $T = D^\dagger \sqrt{DSD^\dagger} D$ of S, then the mapping $g \mapsto TR(g)T^{-1}$ is a unitary representation.

[19] Let A and B be matrices of size $d_A \times d_A$ and $d_B \times d_B$, respectively. We define the direct product $A \otimes B$ as a $d_A d_B \times d_A d_B$ matrix such that the components are given by $(A \otimes B)_{d_B(i-1)+k, d_B(j-1)+l} = A_{ij} B_{kl}$. We define the direct sum $A \oplus B$ as the $(d_A + d_B) \times (d_A + d_B)$ block-diagonal matrix $A \oplus B = \mathrm{diag}(A, B)$. Both operations are associative but noncommutative. Many useful properties such as unitarity carry over from A and B to $A \otimes B$ and $A \oplus B$.

not be irreducible themselves, and sum representations are always reducible by definition. The characters of the product/sum representation are the products/sums of the individual characters, i.e., $\chi^{R_a \otimes R_b}(g) = \chi^{R_a}(g)\chi^{R_b}(g)$ and $\chi^{R_a \oplus R_b}(g) = \chi^{R_a}(g) + \chi^{R_b}(g)$.

Reduction of representations Any (reducible) representation R can always be decomposed into a direct sum of irreducible representations R_i (where the subscript i is used to label all inequivalent irreducible representations). The multiplicity of R_i in R is given by the scalar product of the characters χ^{R_i} and χ^R, such that

$$R \cong \bigoplus_i \left(\frac{1}{|G|} \sum_{g \in G} \chi^{R_i}(g)^* \chi^R(g) \right) R_i \,. \tag{2.61}$$

Transformation according to a representation Take a set of d vectors O_i, $i = 1, \ldots, d$, and a d-dimensional representation R of G. We will say that the O_i transform as a d-dimensional multiplet under the representation R if there exists a basis such that for all $g \in G$ and for all $i \in \{1, \ldots, d\}$

$$g.O_i = [R(g)]_{ji} O_j \,, \tag{2.62}$$

where the left-hand side stands for the action of g on O_i. The definition implicitly depends on the choice of action which will have to be specified.[20]

2.2.1. Special unitary group SU(3)

The special unitary group of degree 3, called SU(3), is of twofold importance for this work. First, it serves as the underlying symmetry group of the non-Abelian gauge theory of strong interactions (SU(3) color symmetry). Second, we can use the same group to classify multiplets of hadrons (SU(3) flavor symmetry). Let us briefly outline the basic properties of SU(3) and then discuss its physical implications.

Often one does not differentiate between SU(3) itself as a group of linear operators and its fundamental representation in terms of unitary 3×3 matrices with determinant 1, i.e., one can think of SU(3) as

$$\mathrm{SU}(3) = \{\, U \in \mathrm{GL}(3, \mathbb{C}) \mid U^\dagger U = \mathbb{1}_3,\ \det U = 1 \,\} \,. \tag{2.63}$$

SU(3) is a continuous group with uncountably many elements. Writing down all elements is impossible, but since SU(3) is a compact connected Lie group we can write down a simple parametrization that can generate any element using only a handful of parameters.

[20] In many cases the standard choice is self-evident, e.g., if G is a linear group and O_i are elements of a suitable vector space, then $g.O_i$ is the application of the linear operator g to the vector O_i.

To illustrate this, let us make use of the following property: Any unitary matrix U (with determinant 1) can be written as $U = \exp(-iH)$ with a (traceless) Hermitian matrix H. The 3×3 traceless Hermitian matrices form an 8-dimensional real vector space. Hence, after selecting eight basis matrices t^A, $A = 1, \ldots, 8$, the fundamental representation of an element of SU(3) can be expressed as

$$U = \exp\left(-i \sum_{A=1}^{8} t^A \theta^A\right), \tag{2.64}$$

parametrized by eight real numbers θ^A. Particle physicists favor a basis called the Gell-Mann matrices, defined and studied in appendix A.2.

SU(3) flavor symmetry

Consider a world with only three quark flavors (up, down, and strange) of equal mass. Since QCD is flavor blind, all quantities which are governed mostly by the strong interaction (e.g., hadron masses) should be invariant under changes of flavor (up to corrections from the electroweak sector). In this world, particles with the same properties would form multiplets corresponding to the irreducible representations of this SU(3) flavor symmetry,[21] which is a generalization of SU(2) isospin symmetry. As the elementary degrees of freedom, the three quarks correspond to the fundamental (triplet) representation, labeled 3,[22] and the three antiquarks correspond to the complex conjugate of the fundamental representation (antitriplet), labeled $\bar{3}$. Composite states such as mesons (one quark and one antiquark) and baryons (three quarks) are related to direct products, which can be reduced to direct sums of irreducible representations. For SU(3) meson and baryon multiplets one finds

$$3 \otimes \bar{3} = 1 \oplus 8\,, \tag{2.65a}$$

$$3 \otimes 3 \otimes 3 = 1 \oplus 8 \oplus 8 \oplus 10\,. \tag{2.65b}$$

In the real world, SU(3) flavor symmetry is broken explicitly by the quark mass differences. (For reference, the numerical values for the quark masses can be found in table 2.1 on page 12.) Since the strange quark mass is more than an order of magnitude larger than the up and down quark masses (which also differ from each other, but are of equal order of magnitude), SU(3) flavor symmetry is broken more badly than isospin symmetry. Even so, this approximate symmetry is useful in practice and enjoys lots of phenomenological success.

[21] For an overview regarding the historical developments and the group-theoretical considerations surrounding the emergence of SU(3) as the correct flavor symmetry and the elimination of other candidate algebras see [105].

[22] We follow the common convention of labeling the irreducible representations of SU(3) by their dimension.

As one can see from the decomposition presented above, baryons are expected to form singlets, octets, or decuplets. In the early 1960s when these concepts were first introduced [106] and quarks had not yet been postulated, there were eight known $J^P = \frac{1}{2}^+$ ground state baryons (p, n, Σ^+, Σ^0, Σ^-, Ξ^0, Ξ^-, and Λ), which fit the description of an SU(3) octet. Furthermore, there were nine $J^P = \frac{3}{2}^+$ baryons (Δ^{++}, Δ^+, Δ^0, Δ^-, Σ^{*+}, Σ^{*0}, Σ^{*-}, Ξ^{*0}, and Ξ^{*-}), possibly an SU(3) decuplet with one member still undiscovered. The prediction of the Ω^- with a mass at 1685 MeV [107] and the subsequent experimental discovery of a new state with the appropriate quantum numbers and a mass of 1686 ± 12 MeV [108] was the first success of SU(3) flavor symmetry and led to the development of the quark model [109, 110].

Let us now take a closer look at how the baryon multiplets are realized. To classify the baryons we use certain quantum numbers of the quarks. Isospin is carried only by up ($T = \frac{1}{2}$, $T_3 = +\frac{1}{2}$) and down ($T = \frac{1}{2}$, $T_3 = -\frac{1}{2}$) quarks, whereas strangeness is carried only by strange quarks ($S' = -1$).[23] T_3 and S' are additive and therefore the corresponding quantum numbers for hadrons can be obtained by adding up the quantum numbers of their constituents, whereas the possible values of the hadron's total isospin T can be obtained by coupling the individual isospins in the standard manner established in quantum mechanics.

The most relevant SU(3) baryon representation is 8 because the hadrons which account for most of the visible matter in the universe, i.e., the nucleons, belong to an octet. Proton and neutron together with 6 hyperons form a $J^P = \frac{1}{2}^+$ octet, which is depicted in fig. 2.2. This also illustrates the fact that SU(3) flavor is a generalization of SU(2) isospin. In the rows of the diagram one can identify isospin submultiplets of constant strangeness: the nucleon iso-doublet ($T = \frac{1}{2}$, $S' = 0$), the Σ iso-triplet ($T = 1$, $S' = -1$), the Ξ iso-doublet ($T = \frac{1}{2}$, $S' = -2$), and the Λ iso-singlet ($T = 0$, $S' = -1$). Taking a look at the measured masses for the baryons [58] allows one to get a quantitative picture of the SU(3) symmetry breaking. The mass differences within one isospin multiplet (this corresponds to changing only the light quark constituents) are much smaller ($\mathcal{O}(1\,\text{MeV})$) than between those multiplets of different strangeness ($\mathcal{O}(100\,\text{MeV})$). This pattern is of course a direct consequence of the quark mass spectrum, cf. table 2.1. It also shows that the breaking of the isospin subgroup is indeed much smaller than the breaking of SU(3) as a whole. When studying the effects of SU(3) symmetry breaking it is therefore a good approximation to always work in the limit of exact isospin symmetry (and we will do so throughout this work). The flavor structure of SU(3) octet baryons will be further discussed in appendix C.1.

[23] The negative sign has historical reasons. Strange particles such as kaons have been discovered [111] and the concept of strangeness has been introduced [112] many years before quarks were proposed [109, 110]. The sign was chosen such that the positively/negatively charged kaons have positive/negative strangeness.

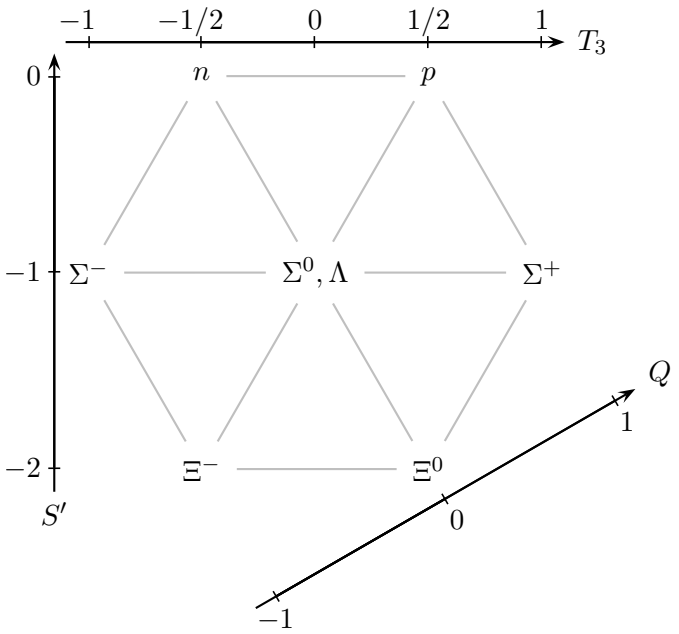

Figure 2.2.: The members of the $J^P = \frac{1}{2}^+$ baryon octet and their quantum numbers T_3 (isospin z-component), S' (strangeness) and Q (electric charge).

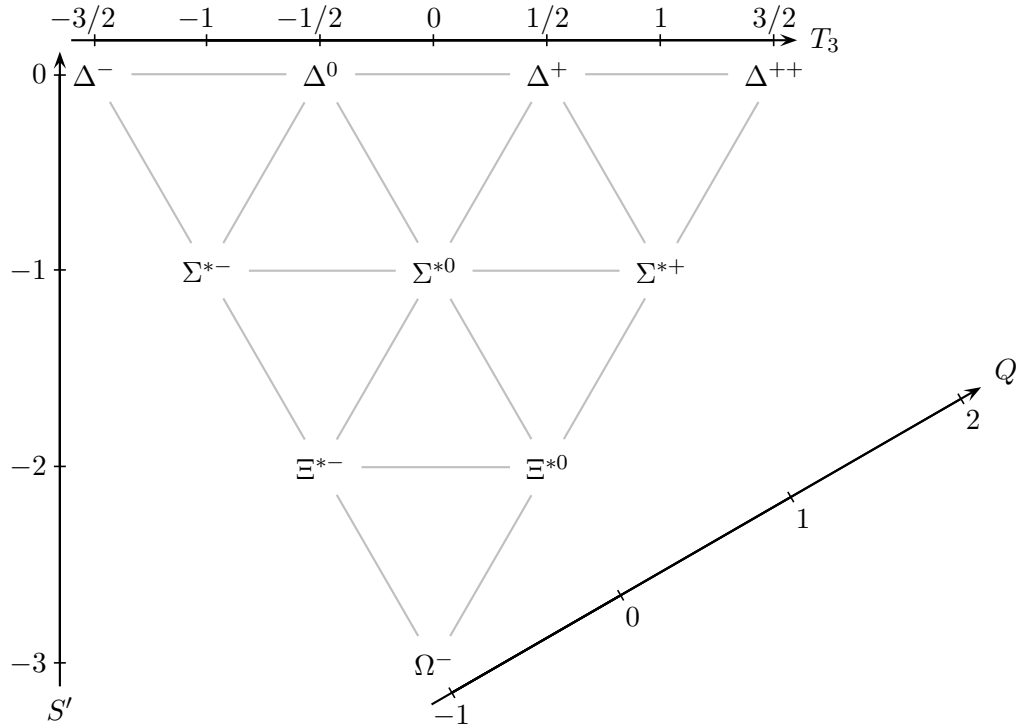

Figure 2.3.: The members of the $J^P = \frac{3}{2}^+$ baryon decuplet and their quantum numbers T_3 (isospin z-component), S' (strangeness) and Q (electric charge).

Moving on to the representation 10, one can arrange ten ground state baryons to form a $J^P = \frac{3}{2}^+$ decuplet. Similar to the above it is made of four isospin submultiplets, namely the $\Delta(1232)$ iso-quartet ($T = \frac{3}{2}$, $S' = 0$), the $\Sigma(1385)$ iso-triplet ($T = 1$, $S' = -1$), the $\Xi(1530)$ iso-doublet ($T = \frac{1}{2}$, $S' = -2$), and the Ω^- iso-singlet ($T = 0$, $S' = -3$). This decuplet is shown in figure 2.3.

These baryon multiplets are not the only ones possible in the respective representations. E.g., the negative parity baryons $N(1520)$, $\Sigma(1580)$, $\Xi(1820)$, and $\Lambda(1520)$ can be thought of as forming another octet with $J^P = \frac{3}{2}^-$. These additional particle multiplets will not be considered in this work, and when talking about the baryon octet and baryon decuplet we will always be referring to the $J^P = \frac{1}{2}^+$ and $J^P = \frac{3}{2}^+$ multiplets described above.

Finally, the representation 1 is of little relevance with respect to SU(3) flavor particle multiplets because no positive parity ground state singlet baryons are observed. This is consistent with the usual symmetry considerations for the wave functions (see also section 3.4.3), since three quark spins cannot be in a totally antisymmetric combination. In contrast, states with nonzero orbital angular momentum can indeed transform as a flavor singlet. Possible singlets are the $J^P = \frac{3}{2}^+$ $\Lambda(1890)$ and the $J^P = \frac{1}{2}^-$ $\Lambda(1405)$.[24] (Any SU(3) flavor-singlet state has quark content uds with $T = 0$ and $S' = -1$.)

SU(3) color symmetry

The quark model interpretation of the hadrons in terms of their constituent quarks is not enough for a consistent description. Consider, e.g., $\Omega^- \mathrel{\hat{=}} sss$. This should be a ground state baryon, with zero orbital angular momentum and all quarks in the same location. The expected total spin in the decuplet is $\frac{3}{2}$, and for that all quark spins would have to be aligned in parallel. Since quarks of the same flavor are involved, this leads to multiple identical fermions occupying the same quantum state. This would be a clear violation of the Pauli exclusion principle, unless there were some other hidden quantum number [113].

Today, this quantum number is called color.[25] Quarks are color triplets [114, 115], transforming according to the fundamental representation of SU(3), while the force-carrying gluons form a color octet [5] (adjoint representation). This is manifest in the Lagrangian formulation of QCD (see chapter 2.1), and unlike its flavor counterpart, SU(3) color is an exact symmetry.

[24] $\Lambda(1405)$ has been a puzzling case for decades. It is the lightest negative parity baryon despite having nonzero strangeness. While many attempts have been made to explain its nature (such as a large pentaquark Fock component, a $N\bar{K}$ bound state, or a hybrid baryon containing a valence gluon) the internal structure of $\Lambda(1405)$ still remains not fully understood, see also the review article "Pole structure of the $\Lambda(1405)$ region" in [58].

[25] The concept of color in QCD is not related to visible colors, but it motivates an analogy to additive color mixing. Consider three primary colors red, green, and blue. A colorless composite state can be formed by combining the three colors: red + green + blue = white.

For composite particles made from quarks (i.e., mesons and baryons) the SU(3) decompositions (2.65) also apply in the color sector, meaning that in principle we might find color-singlet, color-octet and color-decuplet hadrons. However, in all physics experiments ever conducted, no isolated color-charged particles have ever been observed. Even though the fundamental strongly interacting particles of the standard model, quarks and gluons, carry color charge, they only form color-neutral (i.e., singlet) hadrons.

This striking and unique property of QCD has been the subject of many discussions and is called color (or quark) confinement, see [116] for a short review. Any attempt at isolating color charges by separating individual quarks, e.g., through high-energy collisions, does instead lead to the creation of additional color-neutral hadrons by means of quark-antiquark pair production fueled by the potential energy between quarks. Lattice simulations using static sources (where pair production cannot happen; see [117] for a long review) indicate that the potential between a quark and an antiquark increases almost linearly with their distance.

2.2.2. Symmetric group $\mathcal{S}_3$

The symmetric group $\mathcal{S}_n$ is the group formed by all possible permutations of n objects, with the group operation being the composition of permutations. In itself, the theory of symmetric groups is rich enough to fill whole books, such as [118], but in the context of this work we will merely introduce a few properties of $\mathcal{S}_3$. These will be relevant for the symmetry properties of baryons, i.e., hadrons made of three quarks, see sections 3.4.2 and 3.4.3.

In general, given n objects there are $n!$ possible permutations, and thus the group order of $\mathcal{S}_3$ is 6. We can easily write down all the group elements: the identity element which does not change the order of the objects,

$$(123)\,, \tag{2.66a}$$

two cycles of length three,

$$(231)\,, \quad (312)\,, \tag{2.66b}$$

and three transpositions which exchange the positions of two objects,

$$(132)\,, \quad (213)\,, \quad (321)\,. \tag{2.66c}$$

In general, the conjugacy classes of symmetric groups are related to the cycle structure. In the case of $\mathcal{S}_3$ it is straightforward to see that there are three conjugacy classes, formed by the identity element (e), the two cycles (c) and the three transpositions (t).

From the number of conjugacy classes we also learn that there are three inequivalent irreducible representations. The first one is the one-dimensional trivial representation which we will call T^s.[26] There, each group element is represented by the number 1:

$$T^s(123) = 1\,, \tag{2.67a}$$
$$T^s(231) = T^s(312) = 1\,, \tag{2.67b}$$
$$T^s(132) = T^s(213) = T^s(321) = 1\,. \tag{2.67c}$$

The second one, T^a, is the one-dimensional signum representation, in which each group element is represented by the signum of the permutation:[27]

$$T^a(123) = 1\,, \tag{2.68a}$$
$$T^a(231) = T^a(312) = 1\,, \tag{2.68b}$$
$$T^a(132) = T^a(213) = T^a(321) = -1\,. \tag{2.68c}$$

Since the squared dimensions of the inequivalent irreducible representations have to add up to the group order, the third representation, T^m, has to be two-dimensional ($1^2 + 1^2 + 2^2 = 6$). To construct explicit representation matrices for T^m let us utilize the fact that $\mathcal{S}_3$ is isomorphic to the triangular dihedral group. Consider an equilateral triangle formed by three numbered vertices $v_n = e^{-i\frac{2\pi}{3}n}$, $n = 1, 2, 3$ in the complex plane. We canonically identify this with a two-dimensional Euclidean space, i.e., we have

$$v_1 = \frac{1}{2}\begin{pmatrix} -1 \\ -\sqrt{3} \end{pmatrix}, \qquad v_2 = \frac{1}{2}\begin{pmatrix} -1 \\ +\sqrt{3} \end{pmatrix}, \qquad v_3 = \begin{pmatrix} 1 \\ 0 \end{pmatrix}. \tag{2.69a–c}$$

There are some elements of the orthogonal group O(2) which map this triangle onto itself, but with permuted vertices. The six corresponding orthogonal matrices serve as a two-dimensional representation of $\mathcal{S}_3$:

$$T^m(123) = \begin{pmatrix} 1 & 0 \\ 0 & 1 \end{pmatrix},$$
$$T^m(231) = \frac{1}{2}\begin{pmatrix} -1 & \sqrt{3} \\ -\sqrt{3} & -1 \end{pmatrix}, \quad T^m(312) = \frac{1}{2}\begin{pmatrix} -1 & -\sqrt{3} \\ \sqrt{3} & -1 \end{pmatrix},$$
$$T^m(132) = \frac{1}{2}\begin{pmatrix} -1 & \sqrt{3} \\ \sqrt{3} & 1 \end{pmatrix}, \quad T^m(213) = \begin{pmatrix} 1 & 0 \\ 0 & -1 \end{pmatrix}, \quad T^m(321) = \frac{1}{2}\begin{pmatrix} -1 & -\sqrt{3} \\ -\sqrt{3} & 1 \end{pmatrix}. \tag{2.70a–f}$$

[26] The superscripts s, a, and m stand for symmetric, antisymmetric, and mixed, respectively. The reasons for this naming scheme will become clear in section 3.4.2.

[27] Each element can be written as a composition containing only transpositions. The number of transpositions used is not unique, but it is either even or odd. The signum of a permutation is defined as 1 if that number is even and -1 if it is odd.

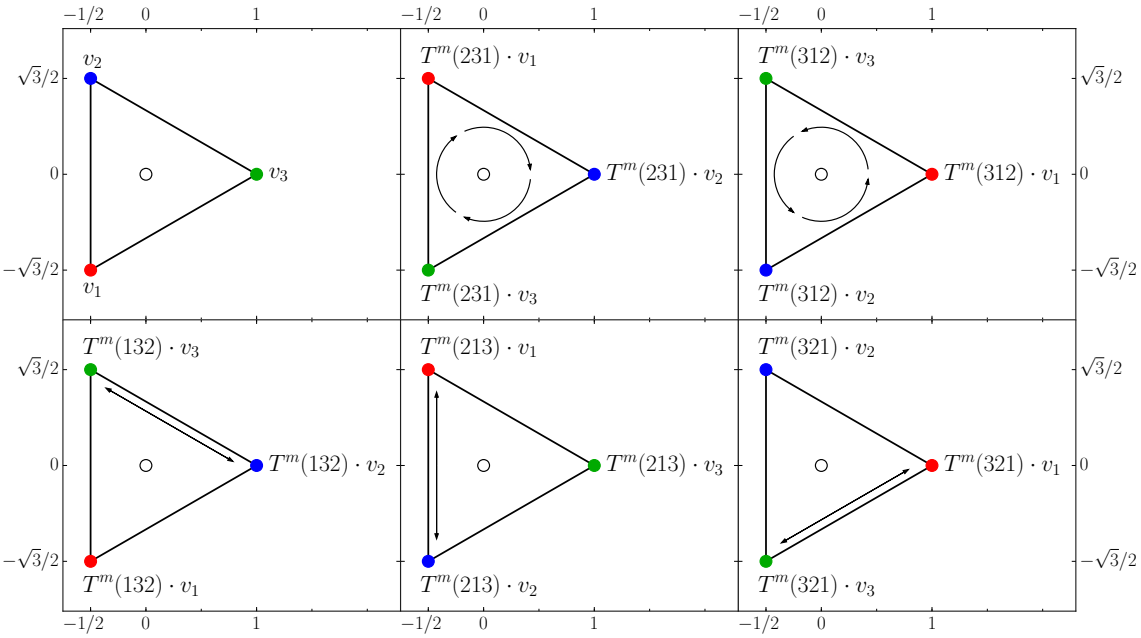

Figure 2.4.: The geometric aspect of the two-dimensional $\mathcal{S}_3$ representation T^m, illustrated using automorphisms of an equilateral triangle.

The correspondence between orthogonal transformations of two-dimensional space and permutations of three objects is illustrated in figure 2.4. From there it is also apparent that cyclic permutations in $\mathcal{S}_3$ correspond to rotation matrices in O(2), while the transpositions are mapped to reflections.

It is straightforward to see that this indeed provides a new irreducible two-dimensional representation (and not just a sum of two one-dimensional representations) by calculating its characters. Now that all irreducible representations of $\mathcal{S}_3$ have been found, we can immediately assemble the full character table, see table 2.2.

Tab. 2.2.: $\mathcal{S}_3$ characters.

	T^s	T^a	T^m
e	1	1	2
c	1	1	−1
t	1	−1	0

2.2.3. Hypercubic groups H(4) and $\overline{\text{H}(4)}$

Properties of H(4)

The hypercubic group H(4) is the symmetry group of a four-dimensional hypercube and, hence, a discrete subgroup of the orthogonal group O(4). It is obvious that this group is significant for lattice gauge theory, because in almost all lattice simulations the four-dimensional spacetime is discretized as a hypercubic lattice [72, 74], breaking O(4) symmetry down to H(4) symmetry.

To count the number of group elements we imagine a hypercube centered around the origin of four-dimensional Euclidean space and determine all transformations that map the cube onto itself. Such a transformation can be performed by either inverting one of the four spatial axes or by a permutation of the four axes (or any combination of these basic operations). This illustrates the fact that the hypercubic group is a semidirect product involving four copies of the group of order two[28] (each axis can either be reversed or not) and the symmetric group on four objects (accounting for all permutations of axes): $\mathrm{H}(4) \cong Z_2^4 \rtimes \mathcal{S}_4$. From these considerations it can be read off that the group order is $|\mathrm{H}(4)| = 2^4 \cdot 4! = 384$.

Given this group order it would be impractical to write down the properties of all elements. Instead, we work with a set of generators, i.e., a small set of elements selected such that all other group elements can be written as products of these. In total we will use 6 generators.[29] We start with the inversion elements I_i ($i = 1, \ldots, 4$) that invert the i-th axis. Each of these generates one of the Z_2 subgroups. To generate the $\mathcal{S}_4$ subgroup we use 2 permutations named γ (a transposition of axes 1 and 3) and t (a cyclic permutation involving axes 2, 3, and 4). These generators satisfy the following relations:

$$\begin{aligned}
&I_i^2 = e\,, && \gamma^2 = e\,, && t^3 = e\,, && (t \circ \gamma)^4 = e\,, \\
&I_i \circ I_j = I_j \circ I_i\,, && \gamma \circ I_1 = I_3 \circ \gamma\,, && \gamma \circ I_2 = I_2 \circ \gamma\,, && \gamma \circ I_4 = I_4 \circ \gamma\,, \\
&t \circ I_1 = I_1 \circ t\,, && t \circ I_2 = I_4 \circ t\,, && t \circ I_3 = I_2 \circ t\,, && t \circ I_4 = I_3 \circ t\,.
\end{aligned} \tag{2.71a–l}$$

The full multiplicative structure of H(4) is encoded therein. All group elements can be written as a product of generators, and products of group elements can be re-expressed as other group elements using the equations above. In this way the whole multiplication table of H(4) could be constructed, but this process would not provide us with much insight.

In [120–122] the conjugacy class structure and representation theory of H(4) has been worked out. There are 20 conjugacy classes and consequently there are also 20 inequivalent irreducible representations of H(4). One can find 4 one-dimensional, 2 two-dim., 4 three-dim., 4 four-dim., 4 six-dim. and 2 eight-dim. representations. (We can check that $4 \cdot 1^2 + 2 \cdot 2^2 + 4 \cdot 3^2 + 4 \cdot 4^2 + 4 \cdot 6^2 + 2 \cdot 8^2 = 384$.)

Of these 20 representations only a four-dimensional one, namely the fundamental representation, is of particular relevance to us. Its explicit construction is straightforward: Consider O(4) and the fundamental representation thereof by 4×4 orthogonal matrices with real entries. Restricting this representation to the subgroup H(4) naturally yields

[28] All groups of order two are equivalent. Labeling the two elements as e and I, the group structure is always given by $e^2 = I^2 = e$ and $e \circ I = I \circ e = I$. We denote this group as Z_2.

[29] This generating set is not minimal. As pointed out in [119], it is possible to generate all of H(4) using only 2 elements, but such a set lacks the straightforward geometrical interpretation and does not generate the related subgroups independently.

a representation thereof by 4×4 orthogonal matrices (now with integer entries). This representation of H(4) turns out to be irreducible and its matrices (see appendix B.2) have the usual geometrical interpretation of exchanging and reversing the four axes.

Construction of $\overline{\mathrm{H}(4)}$, a double cover for H(4)

In four-dimensional Minkowski spacetime, fermions (such as quarks) are described by spinors conforming to spinorial representations of $\mathrm{SL}(2,\mathbb{C})$, the double cover of the (proper orthochronous) Lorentz group. Analogously, for the study of fermions on a hypercubic lattice we should examine the spinorial representations of a double cover of H(4). Let us now construct such a group, which will be called $\overline{\mathrm{H}(4)}$.

In general, a double-covering group G of H is characterized by a 2-to-1 surjective homomorphism $c\colon G \to H$. For every $h \in H$ the preimage $c^{-1}(h)$ consists of exactly 2 elements of G; we call them g and $-g$. As a famous example for such a double cover consider the spin group SU(2) as the double cover of the rotation group SO(3). There is a covering homomorphism $c\colon \mathrm{SU}(2) \to \mathrm{SO}(3),\ U \mapsto O$ with $O_{ij} = \frac{1}{2}\,\mathrm{tr}\{\sigma_i U \sigma_j U^\dagger\}$ (where U and O are in the fundamental representations of SU(2) and SO(3), respectively). For any matrix $U \in \mathrm{SU}(2)$ both $+U$ and $-U$ are mapped to the same rotation matrix in SO(3).

Instead of directly constructing a double cover for the discrete group H(4) we will try to find a double cover for the continuous group O(4) (of which H(4) is a subgroup). First we will need to define our candidate group (which will be a semidirect product $\mathrm{SU}(2)^2 \rtimes Z_2$), and then we will need to show that it does indeed provide a double cover for O(4). After that, finding a double cover for the subgroup H(4) will be trivial.

To create a group structure on the set of tuples[30]

$$\left\{ (U^+, U^-, \pm) \;\middle|\; U^+ \in \mathrm{SU}(2),\ U^- \in \mathrm{SU}(2),\ \pm \in \{+,-\} = Z_2 \right\}, \tag{2.72}$$

we note that there is a natural nontrivial[31] homomorphism from Z_2 to the outer automorphism group of $\mathrm{SU}(2) \times \mathrm{SU}(2)$,

$$\begin{aligned} \varphi : Z_2 &\to \mathrm{Out}(\mathrm{SU}(2) \times \mathrm{SU}(2)), \\ \pm &\mapsto \big((U^+, U^-) \mapsto (U^\pm, U^\mp)\big), \end{aligned} \tag{2.73}$$

which induces the following group operation:

$$\begin{aligned} (U_1^+, U_1^-, \pm_1) \circ (U_2^+, U_2^-, \pm_2) &= \big((U_1^+, U_1^-) \circ \varphi_{\pm_1}(U_2^+, U_2^-), \pm_1 \circ \pm_2\big) \\ &= (U_1^+ U_2^{\pm_1}, U_1^- U_2^{\mp_1}, \pm_1 \circ \pm_2). \end{aligned} \tag{2.74}$$

[30] The group operation on the realization of Z_2 used here is the usual multiplication rule for signs, that is $+ \circ + = - \circ - = +$ and $+ \circ - = - \circ + = -$.

[31] If one considers the trivial homomorphism $\pm \mapsto \big((U^+, U^-) \mapsto (U^+, U^-)\big)$ one will end up with a direct product $\mathrm{SU}(2)^2 \times Z_2$ instead. This is unsuitable for the description of a group of rotations and reflections.

This defines a semidirect product $\mathrm{SU}(2)^2 \rtimes Z_2$, which we will henceforth call $\mathrm{Pin}(4)$.[32] The spin group $\mathrm{SU}(2) \times \mathrm{SU}(2)$ appears as a normal subgroup.[33]

If we manage to construct a double cover $c : \mathrm{Pin}(4) \to \mathrm{O}(4)$, we can define the subgroup $\overline{\mathrm{H}(4)} \subset \mathrm{Pin}(4)$ as the preimage of the subgroup $\mathrm{H}(4) \subset \mathrm{O}(4)$:

$$\begin{array}{ccc} \overline{\mathrm{H}(4)} & \hookrightarrow & \mathrm{Pin}(4) = \mathrm{SU}(2)^2 \rtimes Z_2 \\ \big\downarrow c & & \big\downarrow c \\ Z_2^4 \rtimes \mathcal{S}_4 = \mathrm{H}(4) & \hookrightarrow & \mathrm{O}(4) \end{array}$$

As our mapping for the double cover we define

$$\begin{aligned} c : \mathrm{Pin}(4) = \mathrm{SU}(2)^2 \rtimes Z_2 &\to \mathrm{O}(4)\,, \\ (U^+, U^-, \pm) &\mapsto R\,, \end{aligned} \tag{2.75}$$

where the components of the matrix R are given by

$$R_{\mu\nu} \equiv [R(U^+, U^-, \pm)]_{\mu\nu} = \tfrac{1}{2}\,\mathrm{tr}\big\{\sigma_\mu^+ U^- \sigma_\nu^\mp U^{+\dagger}\big\}\,, \tag{2.76}$$

with a Euclidean four-vector of Pauli matrices $\sigma^\pm = (\pm i\boldsymbol{\sigma}, \mathbb{1}_2)$, cf. appendix A.1.

One can easily see that the two group elements $(+U^+, +U^-, \pm)$ and $(-U^+, -U^-, \pm)$ are always mapped to the same matrix, hinting at a double-covering nature. But before we can really proclaim this mapping a double cover of $\mathrm{O}(4)$ we need to make a few more checks. In particular, we should prove that the expression for $R_{\mu\nu}$ given above always specifies a matrix that is in $\mathrm{O}(4)$ and, most importantly, that the mapping we defined is actually a group homomorphism. This is verified explicitly in appendix B.1.

Properties of $\overline{\mathrm{H}(4)}$

Now that we have established the existence of the covering group $\overline{\mathrm{H}(4)}$, we can focus on its properties. Naturally we have $|\overline{\mathrm{H}(4)}| = 2|\mathrm{H}(4)| = 768$. Again we select 6 generators using the same names as before. The new group has the generating relations $(i \neq j)$

$$\begin{aligned} I_i^2 &= -e\,, & \gamma^2 &= -e\,, & t^3 &= -e\,, & (t\circ\gamma)^4 &= -e\,, \\ I_i \circ I_j &= -I_j \circ I_i\,, & \gamma \circ I_1 &= -I_3 \circ \gamma\,, & \gamma \circ I_2 &= -I_2 \circ \gamma\,, & \gamma \circ I_4 &= -I_4 \circ \gamma\,, \\ t \circ I_1 &= I_1 \circ t\,, & t \circ I_2 &= I_4 \circ t\,, & t \circ I_3 &= I_2 \circ t\,, & t \circ I_4 &= I_3 \circ t\,, \end{aligned} \tag{2.77a–l}$$

[32] The term "pin group" can be derived from reinterpreting spin group as "special pin group." For more information on spin groups and pin groups see [123] and [124], respectively.

[33] It is not surprising to see two copies of SU(2) in the product, keeping in mind the composition of the Dirac four-spinor from two two-component Weyl spinors.

where $-g \equiv g \circ \gamma^2 = \gamma^2 \circ g$. Comparing to eqs. (2.71) one notices that the two sets of equations are almost identical, only differing by some minus signs.

The conjugacy class structure on $\overline{\mathrm{H}(4)}$ is closely related to that of H(4). For every conjugacy class $C_h \subset \mathrm{H}(4)$ the preimage $c^{-1}(C_h)$ can either be a single conjugacy class in $\overline{\mathrm{H}(4)}$, $c^{-1}(C_h) = C_g = C_{-g}$, or it can split into two disjoint conjugacy classes, $c^{-1}(C_h) = C_g \cup C_{-g}$ ($C_g \cap C_{-g} = \emptyset$). The simplest example of such a splitting class is $C_{-e} = \{-e\}$, since, in any group, the identity element e has to form a conjugacy class of its own and cannot be contained in any class other than C_e. Overall, 5 out of the 20 conjugacy classes of H(4) split into pairs of classes when lifted into $\overline{\mathrm{H}(4)}$, therefore bringing the total number of conjugacy classes in $\overline{\mathrm{H}(4)}$ to 25.

The 20 inequivalent irreducible representations of H(4) induce 20 inequivalent irreducible representations of $\overline{\mathrm{H}(4)}$ by virtue of the following mechanism: If $c\colon \overline{\mathrm{H}(4)} \to \mathrm{H}(4)$ is a double cover and $R(h)$ is a representation of the elements $h \in \mathrm{H}(4)$, then $R(c(g))$ is a representation of the elements $g \in \overline{\mathrm{H}(4)}$. In each of these 20 representations, the 6 named generators are represented by the same matrices as in the corresponding H(4) representation, and therefore $-e$, just like e, is represented by an identity matrix. Among these so-called single-valued representations the most important one is the four-dimensional representation arising from the fundamental representation of O(4) (as described above). This representation, labeled "$\Pi_V \cdot [3]$" in [122] and labeled τ_1^4 in [52], determines the transformation behavior of four-vectors under $\overline{\mathrm{H}(4)}$ and is thus relevant for the construction of operators containing derivatives.

The 25 conjugacy classes indicate 25 inequivalent irreducible representations, meaning that we are still missing 5. The remaining ones are not related to the existing representations of H(4). Instead, these are entirely new spinorial representations of $\overline{\mathrm{H}(4)}$, in which $-e$ is always mapped to a negative identity matrix. As first worked out in [119] there are 2 four-dimensional, 1 eight-dimensional, and 2 twelve-dimensional spinorial representations ($2 \cdot 4^2 + 8^2 + 2 \cdot 12^2 = 384$ as expected). We will label them τ_1^4, τ_2^4, τ^8, τ_1^{12}, and τ_2^{12} in accordance with [52]. All spinorial representations play an important role in the classification of three-quark operators performed in section 3.4.1. In particular, τ_1^4 is the representation that governs the transformation properties of quark four-spinors. The representations τ_1^4 and τ_1^4 are connected to each other through the transformation of Dirac matrices:

$$\big[\tau_1^4(g)^\dagger\big]_{\alpha'\alpha} \big(\gamma_\mu\big)_{\alpha'\beta'} \big[\tau_1^4(g)\big]_{\beta\beta'} = \big[\tau_1^4(g)\big]_{\mu'\mu} \big(\gamma_{\mu'}\big)_{\alpha\beta} \qquad \forall\, g \in \overline{\mathrm{H}(4)}\,. \tag{2.78}$$

Explicit matrix forms for all relevant representations are provided in appendix B.2.

Chapter 3

Distribution amplitudes and their renormalization

3.1. Motivation

Our long-term goal is to provide a precise lattice QCD determination of SU(3) octet baryon distribution amplitudes. These nonperturbative functions provide insight into the structure of hadrons in the form of the distribution of light-cone momentum among the hadron's constituents. The relevant definitions are given in section 3.2 below. The preferred way to determine DAs using lattice QCD is via a calculation of their moments, cf. section 3.3.

Lattice QCD cannot determine results with absolute precision, instead they come with several sources of error including the usual statistical uncertainty as well as an uncertainty associated with the renormalization precedure. In [47] one part of the systematic uncertainty due to the renormalization of three-quark operators has been estimated and it can be seen that it contributes, on average, a third of the total error in their results. Therefore, trying to improve the renormalization procedure is certainly a worthwhile goal.

In the previous lattice studies of nucleon DAs [47, 48] the renormalization has been performed using the operators and methods presented in [51, 52, 125]. A central motivation for this thesis was to improve these pre-existing methods. In particular, we will make methodological advancements on multiple fronts: First, the operators used in previous works have been designed with only the nucleon in mind. We will construct operators that are suited for a simultaneous treatment of all SU(3) baryons in section 3.4. Second, the $\overline{\text{MS}}$ scheme that has been used does not make any attempt to take the effects of so-called evanescent operators into account. This could possibly lead to uncontrolled systematic errors not included in the estimate mentioned above. In this work we employ an $\overline{\text{MS}}$ scheme that automatically excludes any contributions from such operators, see section 3.5.1. Third, a MOM scheme with a nonsymmetric momentum configuration was used, which will be

replaced by an SMOM scheme as described in section 3.5.2. These principal improvements will be further complemented by some improvements regarding the implementation, e.g., by using exact analytical results instead of numerical integration in the loop calculations. We have already published first results using this new renormalization procedure [49], but here we will be explaining the method in more detail and we will also present formulas for the renormalization of second moments (cf. appendix D).

3.2. Octet baryon distribution amplitudes

In order to define baryon distribution amplitudes one needs to consider baryon-to-vacuum matrix elements of renormalized three-quark operators at light-like separations [126],

$$\langle 0|\big[f_\alpha(a_1 n) g_\beta(a_2 n) h_\gamma(a_3 n)\big]^{\overline{\text{MS}}}|B(p,\lambda)\rangle\,, \tag{3.1}$$

where $|B(p,\lambda)\rangle$ is the baryon state with momentum p and helicity λ, while α, β, γ are Dirac indices, n is a light-cone four-vector ($n^2 = 0$), the a_i are arbitrary real numbers, and f, g, h are quark fields of given flavor. In our notation for these matrix elements the Wilson lines (which are needed for gauge invariance), the color antisymmetrization (which is needed to form a color singlet), and the dependence on the renormalization scale are not written out explicitly but always implied.

The $J^P = \frac{1}{2}^+$ baryon octet is composed of the eight particles p, n, Σ^+, Σ^0, Σ^-, Ξ^0, Ξ^-, and Λ. In the limit of exact isospin symmetry ($m_u = m_d$) these baryons form multiplets of definite total isospin, see section 2.2.1. For the study of octet baryon DAs it is sufficient to select one representative from each multiplet. In the following we will therefore only consider

$$B \in \{N \equiv p,\ \Sigma \equiv \Sigma^-,\ \Xi \equiv \Xi^0,\ \Lambda\}\,. \tag{3.2}$$

In general, the matrix element (3.1) is expected to be nonzero only if the three quark flavors f, g, h match the valence quark content of the baryon B. The order of the flavors is relevant. Our convention, which will always be implied from here on, is:

$$p: \quad (f,g,h) = (u,u,d)\,, \tag{3.3a}$$

$$\Sigma^-: \quad (f,g,h) = (d,d,s)\,, \tag{3.3b}$$

$$\Xi^0: \quad (f,g,h) = (s,s,u)\,, \tag{3.3c}$$

$$\Lambda: \quad (f,g,h) = (u,d,s)\,. \tag{3.3d}$$

Quantities defined using other flavors or other baryon representatives would not provide any additional information. They can always be related to our definitions via isospin and Fierz transformations. For more detail on our flavor and phase conventions see appendix C.1.

The general Lorentz decomposition [126] of the matrix element (3.1) consists of 24 terms, which are usually written in the form

$$\begin{aligned}\langle 0|f_\alpha(a_1 n)g_\beta(a_2 n)h_\gamma(a_3 n)|B(p,\lambda)\rangle &= \\ &= \sum_{\mathrm{DA}} \big(\Gamma^{\mathrm{DA}}\big)_{\alpha\beta}\big(\tilde{\Gamma}^{\mathrm{DA}} u^B(p,\lambda)\big)_\gamma \int [dx]\, e^{-ip\cdot n\sum_i a_i x_i}\, \mathrm{DA}^B(x_1,x_2,x_3)\,. \end{aligned} \tag{3.4}$$

Here Γ^{DA} and $\tilde{\Gamma}^{\mathrm{DA}}$ are the Dirac structures corresponding to the distribution amplitude $\mathrm{DA}^B(x_1,x_2,x_3)$, see eq. (2.9) of [126], and $u^B(p,\lambda)$ is the Dirac spinor with on-shell momentum p ($p^2 = m_B^2$) and helicity λ. This decomposition can be organized in such a way that all DAs have definite collinear twist.[34] The variables x_1, x_2, x_3 specify the fractions of the light-cone momentum $p\cdot n$ carried by the quark flavors f, g, h, respectively, and the integration measure is defined as

$$\int [dx] \;=\; \int_0^1\!\!\int_0^1\!\!\int_0^1 dx_1 dx_2 dx_3\, \delta(1-x_1-x_2-x_3)\,. \tag{3.5}$$

The factor $\delta(1-x_1-x_2-x_3)$ enforces momentum conservation.

In eq. (3.4) both the matrix element on the left-hand side and the DAs on the right-hand side are quantities which require renormalization and therefore the DAs are scale- and scheme-dependent objects. The dependence on the renormalization scale μ will not be written out unless needed. Since any phenomenological interpretation as well as comparison to other works is done in the $\overline{\mathrm{MS}}$ scheme, it is clear that an accurate lattice study of baryon DAs will have to be accompanied by a conversion to this scheme.

3.2.1. Leading twist distribution amplitudes

Focusing on the DAs of leading twist three, the general decomposition (3.4) is simplified to three terms [130]:[35]

$$\begin{aligned} 4\langle 0|f_\alpha(a_1 n)g_\beta(a_2 n)h_\gamma(a_3 n)|B(p,\lambda)\rangle &= \int [dx]\, e^{-ip\cdot n\sum_i a_i x_i} \\ &\times \big(v^B_{\alpha\beta;\gamma} V^B(x_1,x_2,x_3) + a^B_{\alpha\beta;\gamma} A^B(x_1,x_2,x_3) + t^B_{\alpha\beta;\gamma} T^B(x_1,x_2,x_3) + \cdots\big)\,. \end{aligned} \tag{3.6}$$

[34] In an ordinary operator product expansion [127] the importance of contributions is said to decrease as the mass dimensions of the operators increase. When working with separations that are near the light cone this does not hold. The importance of an operator is now ranked by a new quantity called twist [128], which is described as the difference between dimension and spin. In practice, two variants of twist exist, called geometric twist and collinear twist (see [129] for details). We will not concern ourselves with these differences and henceforth simply refer to it as twist. For baryon operators the leading (i.e., lowest possible) twist is 3.

[35] Our DAs V^N, A^N, and T^N correspond to V_1, A_1, and T_1 in [126].

The Dirac structures corresponding to the three leading twist amplitudes are given by

$$v^B_{\alpha\beta;\gamma} = (\tilde{\not{n}}C)_{\alpha\beta}(\gamma_5 u^B_+(p,\lambda))_\gamma\,, \tag{3.7a}$$
$$a^B_{\alpha\beta;\gamma} = (\tilde{\not{n}}\gamma_5 C)_{\alpha\beta}(u^B_+(p,\lambda))_\gamma\,, \tag{3.7b}$$
$$t^B_{\alpha\beta;\gamma} = (i\sigma_{\perp\tilde{n}}C)_{\alpha\beta}(\gamma^\perp\gamma_5 u^B_+(p,\lambda))_\gamma\,, \tag{3.7c}$$

with the charge conjugation matrix C and the notation

$$\tilde{n}_\mu = p_\mu - \frac{1}{2}\frac{m_B^2}{p\cdot n}n_\mu\,, \qquad u^B_+(p,\lambda) = \frac{1}{2}\frac{\tilde{\not{n}}\not{n}}{\tilde{n}\cdot n}u^B(p,\lambda)\,,$$
$$\sigma_{\perp\tilde{n}}\otimes\gamma^\perp = \sigma^{\mu\rho}\tilde{n}_\rho g^\perp_{\mu\nu}\otimes\gamma^\nu\,, \qquad g^\perp_{\mu\nu} = g_{\mu\nu} - \frac{\tilde{n}_\mu n_\nu + \tilde{n}_\nu n_\mu}{\tilde{n}\cdot n}\,. \tag{3.8a–d}$$

Each of the 24 DAs can be isolated by contracting the decomposition (3.4) with appropriate Dirac structures. For the leading twist DAs such matrix elements read:

$$\langle 0|\big(f^{\uparrow T}(a_1 n)C\not{n}g^\downarrow(a_2 n)\big)\not{n}h^\uparrow(a_3 n)|B(p,\lambda)\rangle =$$
$$= -\tfrac{1}{2}(p\cdot n)\not{n}u^{B\uparrow}(p,\lambda)\int[dx]\,e^{-ip\cdot n\sum_i a_i x_i}\,[V{-}A]^B(x_1,x_2,x_3)\,, \tag{3.9a}$$
$$\langle 0|\big(f^{\uparrow T}(a_1 n)C\gamma^\mu\not{n}g^\uparrow(a_2 n)\big)\gamma_\mu\not{n}h^\downarrow(a_3 n)|B(p,\lambda)\rangle =$$
$$= 2(p\cdot n)\not{n}u^{B\uparrow}(p,\lambda)\int[dx]\,e^{-ip\cdot n\sum_i a_i x_i}\,T^B(x_1,x_2,x_3)\,. \tag{3.9b}$$

The notation in terms of the right- and left-handed components defined as $q^\updownarrow = \frac{1}{2}(\mathbb{1}\pm\gamma_5)q$ and $u^{B\updownarrow}(p,\lambda) = \frac{1}{2}(\mathbb{1}\pm\gamma_5)u^B(p,\lambda)$ makes it apparent that $[V{-}A]^B$ and T^B are related to the $f^\uparrow g^\downarrow h^\uparrow$ and $f^\uparrow g^\uparrow h^\downarrow$ Fock states, respectively.

If $[V{-}A]^B$ is given, then the V^B and A^B components can be reconstructed due to their different symmetry properties under the exchange of the first and the second quark:

$$V^{B\neq\Lambda}(x_2,x_1,x_3) = +V^B(x_1,x_2,x_3)\,, \qquad V^\Lambda(x_2,x_1,x_3) = -V^\Lambda(x_1,x_2,x_3)\,,$$
$$A^{B\neq\Lambda}(x_2,x_1,x_3) = -A^B(x_1,x_2,x_3)\,, \qquad A^\Lambda(x_2,x_1,x_3) = +A^\Lambda(x_1,x_2,x_3)\,,$$
$$T^{B\neq\Lambda}(x_2,x_1,x_3) = +T^B(x_1,x_2,x_3)\,, \qquad T^\Lambda(x_2,x_1,x_3) = -T^\Lambda(x_1,x_2,x_3)\,. \tag{3.10a–f}$$

Using isospin symmetry one can further show that for the nucleon

$$2T^N(x_1,x_3,x_2) = [V{-}A]^N(x_1,x_2,x_3) + [V{-}A]^N(x_3,x_2,x_1)\,, \tag{3.11}$$

such that, to leading twist accuracy, $[V{-}A]^N$ contains all necessary information and is therefore traditionally referred to as *the* leading twist nucleon DA, Φ^N. For other baryons this relation does not hold and consequently the functions T^B are independent from $[V{-}A]^B$.

To explore the consequences of SU(3) flavor symmetry breaking it proves to be convenient to define the following set of DAs:

$$\Phi_\pm^{B\neq\Lambda}(x_1,x_2,x_3) = \tfrac{1}{2}\big([V{-}A]^B(x_1,x_2,x_3) \pm [V{-}A]^B(x_3,x_2,x_1)\big)\,, \tag{3.12a}$$
$$\Pi^{B\neq\Lambda}(x_1,x_2,x_3) = T^B(x_1,x_3,x_2)\,, \tag{3.12b}$$
$$\Phi_+^{\Lambda}(x_1,x_2,x_3) = \sqrt{\tfrac{1}{6}}\big([V{-}A]^\Lambda(x_1,x_2,x_3) + [V{-}A]^\Lambda(x_3,x_2,x_1)\big)\,, \tag{3.12c}$$
$$\Phi_-^{\Lambda}(x_1,x_2,x_3) = -\sqrt{\tfrac{3}{2}}\big([V{-}A]^\Lambda(x_1,x_2,x_3) - [V{-}A]^\Lambda(x_3,x_2,x_1)\big)\,, \tag{3.12d}$$
$$\Pi^{\Lambda}(x_1,x_2,x_3) = \sqrt{6}\,T^\Lambda(x_1,x_3,x_2)\,, \tag{3.12e}$$

where for the nucleon $\Pi^N = \Phi_+^N$ up to isospin breaking. In the limit of SU(3) flavor symmetry, where $m_u = m_d = m_s$ (and in particular at the flavor symmetric point with physical average quark mass, indicated by $\star$), the following relations hold:

$$\Phi_+^\star \equiv \Phi_+^{N\star} = \Phi_+^{\Sigma\star} = \Phi_+^{\Xi\star} = \Phi_+^{\Lambda\star} = \Pi^{N\star} = \Pi^{\Sigma\star} = \Pi^{\Xi\star}\,, \tag{3.13a}$$
$$\Phi_-^\star \equiv \Phi_-^{N\star} = \Phi_-^{\Sigma\star} = \Phi_-^{\Xi\star} = \Phi_-^{\Lambda\star} = \Pi^{\Lambda\star}\,, \tag{3.13b}$$

so that the Π^B (or T^B) amplitudes only need to be considered because flavor symmetry is broken.

In the above we have introduced two different sets of DAs (V^B, A^B, T^B and $\Phi_+^B, \Phi_-^B, \Pi^B$), which both encode the same information. To understand the different physical meaning of these distribution amplitudes it is instructive to work out their relation to light-front wave functions (see, e.g., [38, 131, 132]). Leading twist distribution amplitudes correspond to an approximation for the baryonic Bethe–Salpeter [133] wave function where only the leading three-quark Fock states with vanishing orbital angular momentum are taken into account (i.e., the helicities of the quarks have to sum up to the helicity of the baryon) and the transverse momentum dependence has been integrated out (with a cutoff given by the scale μ):

$$\begin{aligned}
|[B{\neq}\Lambda]^\uparrow\rangle &= \int \frac{[dx]}{8\sqrt{6x_1x_2x_3}} |fgh\rangle \otimes \big\{[V{+}A]^B(x_1,x_2,x_3)|{\downarrow}{\uparrow}{\uparrow}\rangle + [V{-}A]^B(x_1,x_2,x_3)|{\uparrow}{\downarrow}{\uparrow}\rangle \\
&\qquad - 2T^B(x_1,x_2,x_3)|{\uparrow}{\uparrow}{\downarrow}\rangle\big\} \\
&= \int \frac{[dx]}{8\sqrt{3x_1x_2x_3}} |{\uparrow}{\uparrow}{\downarrow}\rangle \otimes \big\{-\sqrt{3}\Phi_+^B(x_1,x_3,x_2)\big(|B_{\rm MS}\rangle - \sqrt{2}|B_{\rm S}\rangle\big)/3 \\
&\qquad - \sqrt{3}\Pi^B(x_1,x_3,x_2)\big(2|B_{\rm MS}\rangle + \sqrt{2}|B_{\rm S}\rangle\big)/3 \\
&\qquad + \Phi_-^B(x_1,x_3,x_2)|B_{\rm MA}\rangle\big\}\,,
\end{aligned} \tag{3.14a}$$

and

$$\begin{aligned}|\Lambda^{\uparrow}\rangle &= \int \frac{[dx]}{4\sqrt{6x_1x_2x_3}}|uds\rangle \otimes \big\{[V{+}A]^{\Lambda}(x_1,x_2,x_3)|{\downarrow}{\uparrow}{\uparrow}\rangle + [V{-}A]^{\Lambda}(x_1,x_2,x_3)|{\uparrow}{\downarrow}{\uparrow}\rangle \\ &\qquad - 2T^{\Lambda}(x_1,x_2,x_3)|{\uparrow}{\uparrow}{\downarrow}\rangle\big\} \\ &= \int \frac{[dx]}{8\sqrt{3x_1x_2x_3}}|{\uparrow}{\uparrow}{\downarrow}\rangle \otimes \big\{-\sqrt{3}\Phi_+^{\Lambda}(x_1,x_3,x_2)|\Lambda_{\rm MS}\rangle \\ &\qquad + \Pi^{\Lambda}(x_1,x_3,x_2)\big(2|\Lambda_{\rm MA}\rangle + \sqrt{2}|\Lambda_{\rm A}\rangle\big)/3 \\ &\qquad + \Phi_-^{\Lambda}(x_1,x_3,x_2)\big(|\Lambda_{\rm MA}\rangle - \sqrt{2}|\Lambda_{\rm A}\rangle\big)/3\big\}\,, \end{aligned} \tag{3.14b}$$

where $|fgh\rangle$ show the quark flavors, which adhere to the ordering convention specified in eqs. (3.3), and $|{\uparrow}{\downarrow}{\uparrow}\rangle$, etc., show quark helicities. In combination, $|fgh\rangle \otimes |{\uparrow}{\downarrow}{\uparrow}\rangle$ specifies a state with quark content $|f^{\uparrow}(x_1)g^{\downarrow}(x_2)h^{\uparrow}(x_3)\rangle$. From this representation it becomes obvious that V^B, A^B, and T^B are convenient DAs if one sorts the quarks with respect to their flavor, while Φ_+^B, Φ_-^B, and Π^B correspond to three distinct flavor structures in a helicity-ordered wave function. $|B_{\rm MS}\rangle$ and $|B_{\rm MA}\rangle$ are the usual mixed-symmetric and mixed-antisymmetric octet flavor wave functions (see tables C.2 and C.3 in appendix C). $|\Lambda_{\rm A}\rangle$ and $|[B{\neq}\Lambda]_{\rm S}\rangle$ are totally antisymmetric and symmetric flavor wave functions (see tables C.1 and C.4). These are usually associated with singlet and decuplet baryons, respectively, and only occur in the octet if SU(3) symmetry is broken. At the flavor symmetric point, $\Phi_+^{\star}$ and $\Phi_-^{\star}$ isolate the mixed-symmetric and mixed-antisymmetric flavor wave functions:

$$|B^{\uparrow}\rangle^{\star} = \int \frac{[dx]}{8\sqrt{3x_1x_2x_3}}|{\uparrow}{\uparrow}{\downarrow}\rangle \otimes \big\{-\sqrt{3}\Phi_+^{\star}(x_1,x_3,x_2)|B_{\rm MS}\rangle + \Phi_-^{\star}(x_1,x_3,x_2)|B_{\rm MA}\rangle\big\}\,. \tag{3.15}$$

Baryon DAs can be expanded in a set of orthogonal polynomials $\mathcal{P}_{nk}$ (of the three variables x_1, x_2, x_3) that describe irreducible representations of the collinear conformal group $\mathrm{SL}(2,\mathbb{R})$ (a conformal partial wave expansion). This procedure has an analogy in quantum mechanics, namely the expansion in spherical harmonics $Y_{lm}(\theta,\varphi)$, which provide a basis for the irreducible representations of the rotation group SO(3). While the quantum mechanical application exploits the spherical symmetry of a potential, the expansion of DAs is based on conformal symmetry [129]. The benefit of such an expansion is that the renormalization group equations guarantee that the coefficients appearing in front of these polynomials have autonomous scale dependence at one loop [126]. The first few polynomials are (see, e.g., [134])[36]

$$\begin{aligned} &\mathcal{P}_{00} = 1\,, && \mathcal{P}_{20} = \tfrac{63}{10}[3(x_1-x_3)^2 - 3x_2(x_1+x_3) + 2x_2^2]\,, \\ &\mathcal{P}_{11} = 7(x_1-2x_2+x_3)\,, && \mathcal{P}_{22} = \tfrac{9}{5}[x_1^2 + 9x_2(x_1+x_3) - 12x_1x_3 - 6x_2^2 + x_3^2]\,, \\ &\mathcal{P}_{10} = 21(x_1-x_3)\,, && \mathcal{P}_{21} = \tfrac{63}{2}(x_1-3x_2+x_3)(x_1-x_3)\,. \end{aligned} \tag{3.16a–f}$$

[36] The polynomials $\mathcal{P}_{nk}$ are orthogonal with respect to $\int [dx]\, 120x_1x_2x_3\, \mathcal{P}_{nk}\mathcal{P}_{n'k'} \propto \delta_{nn'}\delta_{kk'}$.

Note that all $\mathcal{P}_{nk}$ have definite symmetry (being symmetric or antisymmetric) under the exchange of x_1 and x_3. Taking into account the corresponding symmetry of the DAs defined in eqs. (3.12), a generic expansion reads

$$\Phi_+^B = 120x_1x_2x_3\big(\varphi_{00}^B\mathcal{P}_{00} + \varphi_{11}^B\mathcal{P}_{11} + \varphi_{20}^B\mathcal{P}_{20} + \varphi_{22}^B\mathcal{P}_{22} + \cdots\big)\,, \tag{3.17a}$$

$$\Phi_-^B = 120x_1x_2x_3\big(\varphi_{10}^B\mathcal{P}_{10} + \varphi_{21}^B\mathcal{P}_{21} + \cdots\big)\,, \tag{3.17b}$$

$$\Pi^{B\neq\Lambda} = 120x_1x_2x_3\big(\pi_{00}^B\mathcal{P}_{00} + \pi_{11}^B\mathcal{P}_{11} + \pi_{20}^B\mathcal{P}_{20} + \pi_{22}^B\mathcal{P}_{22} + \cdots\big)\,, \tag{3.17c}$$

$$\Pi^{\Lambda} = 120x_1x_2x_3\big(\pi_{10}^\Lambda\mathcal{P}_{10} + \pi_{21}^\Lambda\mathcal{P}_{21} + \cdots\big)\,. \tag{3.17d}$$

In each DA only polynomials of one type appear, either symmetric (Φ_+^B, $\Pi^{B\neq\Lambda}$) or antisymmetric (Φ_-^B, Π^Λ). In this expansion all nonperturbative information is encoded in the set of (scale-dependent) coefficients φ_{nk}^B, π_{nk}^B, which can be related to matrix elements of local operators. These quantities are of phenomenological interest and it is therefore necessary to understand their behavior under renormalization which will be investigated in section 3.5.4.

The leading contributions $120x_1x_2x_3\varphi_{00}^B$ and $120x_1x_2x_3\pi_{00}^{B\neq\Lambda}$ are usually referred to as the asymptotic DAs (see below). The corresponding coefficients φ_{00}^B and $\pi_{00}^{B\neq\Lambda}$ can be thought of as the value of the baryon wave functions at the origin (in position space). In what follows we will use the notation

$$f^B \equiv \int[dx]\,\Phi_+^B(x_1,x_2,x_3) = \varphi_{00}^B\,, \qquad f_T^{B\neq\Lambda} \equiv \int[dx]\,\Pi^B(x_1,x_2,x_3) = \pi_{00}^B\,, \tag{3.18a–b}$$

i.e., f^B and $f_T^{B\neq\Lambda}$ denote the normalization of the DAs Φ_+^B and $\Pi^{B\neq\Lambda}$, respectively. Note that for the nucleon the two couplings coincide, $f_T^N = f^N$. The DAs Φ_-^B and Π^Λ, on the other hand, both have vanishing normalization by construction.

The coefficients of higher order are usually referred to as shape parameters.[37] The one-loop scale evolution of the couplings and shape parameters is given by

$$\varphi_{nk}^B(\mu) = \varphi_{nk}^B(\mu_0)\left(\frac{\alpha_s(\mu)}{\alpha_s(\mu_0)}\right)^{\gamma_{nk}/\beta_0}\,, \qquad \pi_{nk}^B(\mu) = \pi_{nk}^B(\mu_0)\left(\frac{\alpha_s(\mu)}{\alpha_s(\mu_0)}\right)^{\gamma_{nk}/\beta_0}\,, \tag{3.19a–b}$$

where $\beta_0 = 11 - 2n_f/3$ is the first coefficient of the QCD beta function. In this work we restrict ourselves to the contributions of up to second order polynomials and omit all higher terms. The relevant one-loop anomalous dimensions are

$$\gamma_{00} = \frac{2}{3}\,, \qquad \gamma_{11} = \frac{10}{3}\,, \qquad \gamma_{10} = \frac{26}{9}\,,$$
$$\gamma_{20} = \frac{38}{9}\,, \qquad \gamma_{22} = \frac{16}{3}\,, \qquad \gamma_{21} = \frac{46}{9}\,. \tag{3.20a–f}$$

[37] Note that, in contrast to [48], we do not separate the couplings f^B and $f_T^{B\neq\Lambda}$ as overall normalization factors, i.e., our φ_{nk}^N correspond to $f_N\varphi_{nk}^N$ of [48].

Beyond that, the scale dependence of $f^B = \varphi_{00}^B$ and $f_T^{B\neq\Lambda} = \pi_{00}^B$ is known to three-loop order, see refs. [135, 136]. There is a hierarchy in the numerical values of anomalous dimensions, $\gamma_{00} < \gamma_{11} \approx \gamma_{10} < \gamma_{20} \approx \gamma_{22} \approx \gamma_{21} < \cdots$, which implies that in the limit of asymptotically large scales all shape parameters tend to zero at a much faster rate than φ_{00}^B or $\pi_{00}^{B\neq\Lambda}$, thereby justifying the nomenclature of asymptotic DA for $120x_1x_2x_3\varphi_{00}^B$ and $120x_1x_2x_3\pi_{00}^{B\neq\Lambda}$.

3.2.2. Higher twist contributions

The general decomposition (3.4) contains 21 DAs of higher twist, which altogether involve only up to three new normalization constants (just two for N, Σ, and Ξ), for details see refs. [33, 126]. They can be defined as matrix elements of local three-quark twist four operators without derivatives. These twist four couplings are also of interest in a broader context, e.g., in studies of baryon decays in grand unified models [137], and as input parameters for QCD sum rule calculations, see, e.g., refs. [95, 138, 139].

We use the following definitions:[38]

$$\langle 0|\big(f^{\uparrow T}(0)C\gamma^\mu g^\downarrow(0)\big)\gamma_\mu h^\uparrow(0)|[B\neq\Lambda](p,\lambda)\rangle = -\tfrac{1}{2}\lambda_1^B m_B u^{B\downarrow}(p,\lambda)\,, \tag{3.21a}$$

$$\langle 0|\big(f^{\uparrow T}(0)C\sigma^{\mu\nu} g^\uparrow(0)\big)\sigma_{\mu\nu}h^\uparrow(0)|[B\neq\Lambda](p,\lambda)\rangle = \lambda_2^B m_B u^{B\uparrow}(p,\lambda)\,, \tag{3.21b}$$

for the isospin-nonsinglet baryons ($B = N, \Sigma, \Xi$), and

$$\langle 0|\big(u^{\uparrow T}(0)C\gamma^\mu d^\downarrow(0)\big)\gamma_\mu s^\uparrow(0)|\Lambda(p,\lambda)\rangle = \tfrac{1}{2\sqrt{6}}\lambda_1^\Lambda m_\Lambda u^{\Lambda\downarrow}(p,\lambda)\,, \tag{3.22a}$$

$$\langle 0|\big(u^{\uparrow T}(0)Cd^\uparrow(0)\big)s^\downarrow(0)|\Lambda(p,\lambda)\rangle = \tfrac{1}{2\sqrt{6}}\lambda_T^\Lambda m_\Lambda u^{\Lambda\downarrow}(p,\lambda)\,, \tag{3.22b}$$

$$\langle 0|\big(u^{\uparrow T}(0)Cd^\uparrow(0)\big)s^\uparrow(0)|\Lambda(p,\lambda)\rangle = \tfrac{-1}{4\sqrt{6}}\lambda_2^\Lambda m_\Lambda u^{\Lambda\uparrow}(p,\lambda)\,, \tag{3.22c}$$

for the Λ baryon. These definitions are chosen so that the normalization constants of different baryons become equal at the flavor symmetric point, see also [33]:

$$\lambda_1^\star \equiv \lambda_1^{N\star} = \lambda_1^{\Sigma\star} = \lambda_1^{\Xi\star} = \lambda_1^{\Lambda\star} = \lambda_T^{\Lambda\star}\,, \tag{3.23a}$$

$$\lambda_2^\star \equiv \lambda_2^{N\star} = \lambda_2^{\Sigma\star} = \lambda_2^{\Xi\star} = \lambda_2^{\Lambda\star}\,, \tag{3.23b}$$

The one-loop evolution for all twist four normalization constants is the same:

$$\lambda_{1,2,T}^B(\mu) = \lambda_{1,2,T}^B(\mu_0)\left(\frac{\alpha_s(\mu)}{\alpha_s(\mu_0)}\right)^{-2/\beta_0}. \tag{3.24}$$

The corresponding anomalous dimensions are known to three-loop accuracy [135, 136]. The scale dependence of the couplings λ_1^B and λ_T^Λ is the same to all orders, whereas for λ_2^B it differs starting from the second loop.

[38] For the nucleon the definitions in terms of chiral fields given in eqs. (3.21) are equivalent to the traditional definitions of λ_1^N and λ_2^N not involving chiral projections, as used in [48].

3.3. Moments

As we have seen in the previous section, distribution amplitudes are defined as matrix elements of nonlocal operators with quarks at light-like separations. A direct lattice calculation of such quantities in Euclidean spacetime is not possible. However, so-called moments of the DAs, e.g.,

$$V^B_{lmn} = \int [dx]\, x_1^l x_2^m x_3^n\, V^B(x_1, x_2, x_3)\,, \tag{3.25}$$

(and similarly for the other functions) are instead related to local operators, which we will be able to access in lattice QCD. To illustrate this connection let us look at an example. The DA $[V{-}A]^B$ is defined via the nonlocal matrix element previously shown in eq. (3.9a):

$$\begin{aligned}\langle 0|\big(f^{\uparrow T}(a_1 n) C \not{n} g^{\downarrow}(a_2 n)\big)\not{n} h^{\uparrow}(a_3 n)|B(p,\lambda)\rangle &= \\ = -\tfrac{1}{2}(p\cdot n)\not{n} u^{B\uparrow}(p,\lambda) \int [dx]\, e^{-ip\cdot n \sum_i a_i x_i}\, &[V{-}A]^B(x_1,x_2,x_3)\,,\end{aligned}$$

with arbitrary a_i. In particular, this implies for $a_i \to 0$ that

$$\langle 0|\big(f^{\uparrow T}(0) C \not{n} g^{\downarrow}(0)\big)\not{n} h^{\uparrow}(0)|B(p,\lambda)\rangle = -\tfrac{1}{2}(p\cdot n)\not{n} u^{B\uparrow}(p,\lambda)[V{-}A]^B_{000}\,, \tag{3.26}$$

i.e., the zeroth moment of the DA $[V{-}A]^B$ is related to the local operator on the left-hand side. Such relations enable lattice calculations of DAs in terms of their moments, a method which is well established [40–49]. A compilation of local operators suitable for lattice implementation will be given in section 4.2. In general, the calculation of an $(l+m+n)$-th moment will require operators with $l+m+n$ covariant derivatives. This constitutes an inherent limitation of the method, because calculations with a high number of derivatives cannot be realized in practice with sufficient precision. In practice, this usually means that we are limited to describing baryon DAs up to their second moments, although this is not a major drawback since these lowest contributions are indeed by far the most important ones.

An alternative to this moments method has been proposed in [140]. It revolves around the calculation of hadronic matrix elements of current-current correlators at purely space-like separations in position space. The connection to distribution amplitudes is then made in continuum perturbation theory. An advantage of this method would be that it could circumnavigate the complicated question of the renormalization behavior of local three-quark operators with derivatives which we will be discussing in this work. However, in order to be sensitive to anything but the value of the lowest moment, the position space method requires hadron sources with high momenta. Large momenta are also required in

other methods to calculate hadron properties in Euclidean space, such as [141]. Up until very recently this presented a grave problem spoiling any practical application since no satisfactory techniques for hadrons carrying high momenta on the lattice existed that could sufficiently suppress excited state contributions while maintaining acceptable signal-to-noise ratios. The situation has changed with the development of a novel momentum smearing technique [44, 142]. An early investigation of the position space method combined with momentum smearing indicates some promise [143] and should inspire further exploration to assess the potential as a complement to the established moments method.

In this thesis we focus on the traditional method. To this end we will express the shape parameters of the DAs Φ_+^B, Φ_-^B, and Π^B (as defined in eqs. (3.17)) in terms of moments of the standard DAs V^B, A^B, and T^B. The shape parameters φ_{nk}^B are related to n-th moments of $[V-A]^B$, while π_{nk}^B are related to n-th moments of T^B. These relations are instrumental both in extracting the quantities which we are interested in from the lattice correlators (section 4.2) as well as in deducing their renormalization matrices (section 3.5.4).

Leading twist – zeroth moments

By definition, the couplings of interest are related to the zeroth moments as follows:

$$f^{B\neq\Lambda} \equiv \varphi_{00}^B = [V-A]_{000}^B\,, \quad f^\Lambda \equiv \varphi_{00}^\Lambda = \sqrt{\tfrac{2}{3}}[V-A]_{000}^\Lambda\,, \quad f_T^{B\neq\Lambda} \equiv \pi_{00}^B = T_{000}^B\,, \quad \text{(3.27a–c)}$$

where $f_T^N = f^N$ due to isospin symmetry. Due to the symmetry relations (3.10), some zeroth moments of individual DAs vanish identically,

$$V_{000}^\Lambda = A_{000}^{B\neq\Lambda} = T_{000}^\Lambda = 0\,, \tag{3.28}$$

such that the above is equivalent to

$$\varphi_{00}^{B\neq\Lambda} = V_{000}^B\,, \qquad \varphi_{00}^\Lambda = -\sqrt{\tfrac{2}{3}}A_{000}^\Lambda\,, \qquad \pi_{00}^{B\neq\Lambda} = T_{000}^B\,. \qquad \text{(3.29a–c)}$$

Leading twist – first moments

The shape parameters defined in eqs. (3.17) can be expressed as linear combinations of V_{lmn}^B, A_{lmn}^B, and T_{lmn}^B via eqs. (3.12). For the N, Σ, and Ξ baryons,

$$\varphi_{00,(1)}^{B\neq\Lambda} = [V-A]_{100}^B + [V-A]_{010}^B + [V-A]_{001}^B\,, \tag{3.30a}$$

$$\pi_{00,(1)}^{B\neq\Lambda} = T_{100}^B + T_{010}^B + T_{001}^B\,, \tag{3.30b}$$

$$\varphi_{11}^{B\neq\Lambda} = \tfrac{1}{2}\big([V-A]_{100}^B - 2[V-A]_{010}^B + [V-A]_{001}^B\big)\,, \tag{3.30c}$$

$$\pi_{11}^{B\neq\Lambda} = \tfrac{1}{2}\big(T_{100}^B + T_{010}^B - 2T_{001}^B\big)\,, \tag{3.30d}$$

$$\varphi_{10}^{B\neq\Lambda} = \tfrac{1}{2}\big([V-A]_{100}^B - [V-A]_{001}^B\big)\,, \tag{3.30e}$$

where $\pi^N_{00,(1)} = \varphi^N_{00,(1)}$ and $\pi^N_{11} = \varphi^N_{11}$ due to isospin symmetry. For the Λ baryon the shape parameters are given by

$$\varphi^\Lambda_{00,(1)} = \sqrt{\tfrac{2}{3}}\big([V{-}A]^\Lambda_{100} + [V{-}A]^\Lambda_{010} + [V{-}A]^\Lambda_{001}\big)\,, \tag{3.31a}$$

$$\varphi^\Lambda_{11} = \tfrac{1}{\sqrt{6}}\big([V{-}A]^\Lambda_{100} - 2[V{-}A]^\Lambda_{010} + [V{-}A]^\Lambda_{001}\big)\,, \tag{3.31b}$$

$$\varphi^\Lambda_{10} = -\sqrt{\tfrac{3}{2}}\big([V{-}A]^\Lambda_{100} - [V{-}A]^\Lambda_{001}\big)\,, \tag{3.31c}$$

$$\pi^\Lambda_{10} = \sqrt{\tfrac{3}{2}}\big(T^\Lambda_{100} - T^\Lambda_{010}\big)\,. \tag{3.31d}$$

Leading twist – second moments

For the isospin-nonsinglet baryons we have 10 second order shape parameters:

$$\varphi^{B\neq\Lambda}_{00,(2)},\ \pi^{B\neq\Lambda}_{00,(2)},\ \varphi^{B\neq\Lambda}_{11,(2)},\ \pi^{B\neq\Lambda}_{11,(2)},\ \varphi^{B\neq\Lambda}_{20},\ \pi^{B\neq\Lambda}_{20},\ \varphi^{B\neq\Lambda}_{22},\ \pi^{B\neq\Lambda}_{22},\ \varphi^{B\neq\Lambda}_{10,(2)},\ \varphi^{B\neq\Lambda}_{21}\,. \tag{3.32}$$

Additionally we have a set of 8 parameters for the Λ baryon:

$$\varphi^\Lambda_{00,(2)},\ \varphi^\Lambda_{11,(2)},\ \varphi^\Lambda_{20},\ \varphi^\Lambda_{22},\ \varphi^\Lambda_{10,(2)},\ \pi^\Lambda_{10,(2)},\ \varphi^\Lambda_{21},\ \pi^\Lambda_{21}\,. \tag{3.33}$$

Their expression in terms of moments can be found in appendix D.1.

Leading twist – momentum sums

In the above we have defined additional objects that did not originally appear in the parametrizations (3.17). They are given the same names as the established shape parameters, but are distinguished by an extra subscript in parentheses, and correspond to expressing the same shape parameter using a different set of moments. For example, the leading twist normalization constant f^B can be written as a zeroth moment (φ^B_{00}), or as a sum of first moments ($\varphi^B_{00,(1)}$), a sum of second moments ($\varphi^B_{00,(2)}$), and so on. In the continuum all these expressions are equal, i.e., we have

$$\begin{aligned}
&\varphi^B_{00,(2)} = \varphi^B_{00,(1)} = \varphi^B_{00} \equiv f^B\,, && \pi^{B\neq\Lambda}_{00,(2)} = \pi^B_{00,(1)} = \pi^B_{00} \equiv f^B_T\,,\\
&\varphi^B_{11,(2)} = \varphi^B_{11}\,, && \pi^{B\neq\Lambda}_{11,(2)} = \pi^B_{11}\,,\\
&\varphi^B_{10,(2)} = \varphi^B_{10}\,, && \pi^\Lambda_{10,(2)} = \pi^\Lambda_{10}\,.
\end{aligned} \tag{3.34a–f}$$

This follows directly from the momentum conservation condition $x_1 + x_2 + x_3 = 1$, eq. (3.5).

In the language of operators this combination corresponds to rewriting a total derivative acting on a local three-quark operator as a sum of three operators with a covariant derivative acting on one of the quarks. However, the product rule for derivatives is violated

by discretization effects, meaning that the relations given above will be broken on the lattice. This also affects renormalization: The renormalization prescription for φ_{00}^B will differ from that for $\varphi_{00,(1)}^B$ and the latter will also include mixing with the other first moments, see section 3.5.4. Even so, we can still expect equations (3.34) to be restored for continuum extrapolated data renormalized in a scheme which respects the Lorentz symmetry, such as the $\overline{\text{MS}}$ scheme. In a lattice study one can use this as a consistency check, and we discuss and analyze it in more detail in section 4.4.1.

3.4. Operators

As stated in the previous section, moments of distribution amplitudes are related to local three-quark operators. In the following we will show how the latter can be assembled to form multiplets that transform under irreducible representations of both the spinorial hypercubic group $\overline{\text{H}(4)}$ and the permutation group $\mathcal{S}_3$, as these exhibit optimal transformation behavior for the task at hand.

3.4.1. Transformation behavior under $\overline{\text{H}(4)}$

Consider a generic local three-quark operator $\mathcal{O}$ containing n covariant derivatives,[39]

$$\mathcal{O} = T_{\alpha\beta\gamma,\mu_1\ldots\mu_n} f_\alpha g_\beta D_{\mu_1}\cdots D_{\mu_n} h_\gamma \,, \tag{3.35}$$

where T is an arbitrary coefficient tensor contracted with the Dirac indices of the quark fields and the Lorentz indices of the derivatives. For any group element $g \in \overline{\text{H}(4)}$ we define the g-transformed operator $g.\mathcal{O}$ as the operator where each part of the operator is individually transformed using the appropriate representation, i.e., the fundamental spinorial representation τ_1^4 for the quark fields and the fundamental representation τ_1^4 for the derivatives:

$$\begin{aligned} g.\mathcal{O} = {} & \big[\tau_1^4(g)\big]_{\alpha'\alpha}\big[\tau_1^4(g)\big]_{\beta'\beta}\big[\tau_1^4(g)\big]_{\mu_1'\mu_1}\cdots\big[\tau_1^4(g)\big]_{\mu_n'\mu_n}\big[\tau_1^4(g)\big]_{\gamma'\gamma} \\ & \times T_{\alpha\beta\gamma,\mu_1\ldots\mu_n} f_{\alpha'} g_{\beta'} D_{\mu_1'}\cdots D_{\mu_n'} h_{\gamma'} \,. \end{aligned} \tag{3.36}$$

From this, it becomes clear that the transformation behavior of operators with n derivatives is determined by the product of representations $\tau_1^4 \otimes \tau_1^4 \otimes \tau_1^4 \otimes \cdots \otimes \tau_1^4 \otimes \tau_1^4$, where the representation τ_1^4 appears n times.

[39] For the determination of the $\overline{\text{H}(4)}$ transformation behavior of the operators their flavor structure is not relevant and neither are the positions of derivatives. For notational purposes we will use three generic flavors, f, g, and h, and have all derivatives acting on the quark h.

Using eq. (2.61) one can decompose these products into sums of irreducible representations. To carry out this calculation explicitly, one needs to know the characters of all elements in the various representations of $\overline{\mathrm{H}(4)}$. This information can be found in the character table B.1 in appendix B. For the interesting cases of zero, one, or two derivatives we find:[40]

$$\tau_1^4 \otimes \tau_1^4 \otimes \tau_1^4 = 5\tau_1^4 \oplus \tau^8 \oplus 3\tau_1^{12}\,, \tag{3.37a}$$

$$\tau_1^4 \otimes \tau_1^4 \otimes \tau_1^4 \otimes \tau_1^4 = 8\tau_1^4 \oplus 4\tau^8 \oplus 12\tau_1^{12} \oplus 4\tau_2^{12}\,, \tag{3.37b}$$

$$\tau_1^4 \otimes \tau_1^4 \otimes \tau_1^4 \otimes \tau_1^4 \otimes \tau_1^4 = 20\tau_1^4 \oplus 4\tau_2^4 \oplus 20\tau^8 \oplus 40\tau_1^{12} \oplus 24\tau_2^{12}\,. \tag{3.37c}$$

On the right-hand sides of these equations we find only the spinorial representations (as expected, given that baryons are fermions), meaning that three-quark operators form 4-, 8-, or 12-dimensional multiplets transforming under the spinorial $\overline{\mathrm{H}(4)}$ representations τ_1^4, τ_2^4, τ^8, τ_1^{12}, and τ_2^{12}. E.g., the $4^3 = 64$ operators without derivatives will form five 4-dimensional, one 8-dim., and three 12-dim. multiplets.

We can construct these multiplets explicitly by using eq. (2.62). Let R be one of the spinorial representations and let d_R be its dimension. For a d_R-dimensional multiplet of operators $\mathcal{O}^{(i)}$, $i = 1, \ldots, d_R$ to transform under the representation R we have to demand[41]

$$g.\mathcal{O}^{(i)} = [R(g)]_{ji}\mathcal{O}^{(j)} \qquad \forall\, g \in \overline{\mathrm{H}(4)}\,. \tag{3.38}$$

This constitutes a system of linear equations whose solution will constrain the components of the coefficient tensors $T^{(i)}$, but will not fix them completely. It is already apparent from the structure of eq. (3.38) that the overall phase and normalization of a multiplet cannot be uniquely determined and remain as a choice of convention. Furthermore, in cases where multiple copies of the same representation appear on the right-hand side of the decompositions (3.37), the linear solution space will be multi-dimensional, e.g., in the case of operators without derivatives in the representation τ_1^{12} the solution space turns out to be three-dimensional, as predicted by eq. (3.37a). In principle, one could take any three linearly independent solutions and declare them the three multiplets in the representation τ_1^{12}. However, while all such choices would be equally valid mathematically, not all are equally smart from the physicist's point of view.

As a starting point we consider the three-quark operator multiplets (with zero, one, or two covariant derivatives) transforming irreducibly under $\overline{\mathrm{H}(4)}$ that have been worked out in [51].[42] We will not repeat all details of the construction here. Instead, we will

[40] The result for two derivatives, eq. (3.37c), is stated incorrectly in [50–52].

[41] When checking this property it is sufficient to do so only for the 6 generators of $\overline{\mathrm{H}(4)}$ since both the action, $(g_1 \circ g_2).\mathcal{O} = g_1.(g_2.\mathcal{O})$, and the representation, $R(g_1 \circ g_2) = R(g_1)R(g_2)$, respect the group structure.

[42] We have independently verified that all multiplets given therein really transform as advertised. See also the explicit expressions for the representation matrices collected in appendix B.2.

Table 3.1.: List of three-quark operator multiplets transforming irreducibly under $\overline{\mathrm{H}(4)}$, sorted by operator dimension and representation. For zero derivatives all operators are listed (leading twist: $\mathcal{O}_{6-9}$, higher twist: $\mathcal{O}_{1-5}$). For the operators with derivatives, only the leading twist multiplets are shown. Our knowledge of the decompositions (3.37) allows us to indicate the positions of the remaining higher twist operators by dots. The nomenclature follows [52].

	no derivatives dimension 9/2	1 derivative dimension 11/2	2 derivatives dimension 13/2
$\tau_1^{\frac{4}{}}$	$\mathcal{O}_1$, $\mathcal{O}_2$, $\mathcal{O}_3$, $\mathcal{O}_4$, $\mathcal{O}_5$	...	$\mathcal{O}_{DD1}$, $\mathcal{O}_{DD2}$, $\mathcal{O}_{DD3}$, ...
$\tau_2^{\frac{4}{}}$			$\mathcal{O}_{DD4}$, $\mathcal{O}_{DD5}$, $\mathcal{O}_{DD6}$, ...
$\tau^{\frac{8}{}}$	$\mathcal{O}_6$	$\mathcal{O}_{D1}$, ...	$\mathcal{O}_{DD7}$, $\mathcal{O}_{DD8}$, $\mathcal{O}_{DD9}$, ...
$\tau_1^{\frac{12}{}}$	$\mathcal{O}_7$, $\mathcal{O}_8$, $\mathcal{O}_9$	$\mathcal{O}_{D2}$, $\mathcal{O}_{D3}$, $\mathcal{O}_{D4}$, ...	$\mathcal{O}_{DD10}$, $\mathcal{O}_{DD11}$, $\mathcal{O}_{DD12}$, $\mathcal{O}_{DD13}$, ...
$\tau_2^{\frac{12}{}}$		$\mathcal{O}_{D5}$, $\mathcal{O}_{D6}$, $\mathcal{O}_{D7}$, $\mathcal{O}_{D8}$	$\mathcal{O}_{DD14}$, $\mathcal{O}_{DD15}$, $\mathcal{O}_{DD16}$, $\mathcal{O}_{DD17}$, $\mathcal{O}_{DD18}$, ...

discuss some of the properties of the resulting multiplets, analyze the structure of the $\overline{\mathrm{H}(4)}$ classification, and then proceed to improve upon it in the following sections.

In [51] all operators without derivatives are sorted into multiplets, but for the operators involving one or two covariant derivatives only multiplets of leading twist operators are constructed and named.[43] The resulting structure is summarized in table 3.1. The delineation of the leading twist operators is an important and useful property since, under renormalization, leading twist operators can only mix with other leading twist operators. We will therefore retain this property also in our improved operator multiplets.

Another property of the multiplets constructed in [51] concerns the quark chiralities. In the chiral Weyl representation the Dirac four-spinors consist of a pair of two-spinors corresponding to left- and right-handed quarks. The multiplets were constructed such that all operators contained have definite quark chiralities. In the example of $\tau_1^{\frac{12}{}}$ with no derivatives, the first multiplet, $\mathcal{O}_7$, is chosen such that all its operators are either RLL or LRR, while $\mathcal{O}_8$ has LRL/RLR, and $\mathcal{O}_9$ has LLR/RRL. We will call such operators chiral-odd. (The only chiral-even combination, LLL/RRR, simply does not appear here, but will do so in other cases, e.g., $\mathcal{O}_6$ in $\tau^{\frac{8}{}}$.) A comparison with eqs. (3.14) tells us that this classification corresponds to the DAs $[V{+}A]^B$, $[V{-}A]^B$, and T^B. While it is straightforward to select operator multiplets in this manner, it is not optimal in the context

[43] The absence of a classification for multiplets of higher twist operators with derivatives does not pose a problem since our lattice studies are not aiming to determine the higher moments of the higher twist DAs. Should the need arise, such multiplets could be constructed using eq. (3.38).

of SU(3) baryon distribution amplitudes where the DAs Φ_+^B, Φ_-^B, and Π^B provide a better basis instead. Therefore we will, over the course of the next two sections, incorporate the symmetry properties of SU(3) baryons into the operator construction.

Before that, however, it is worth taking a few minutes to figure out which of the many operator multiplets shown in table 3.1 are actually useful in the context of a lattice calculation of octet baryon distribution amplitudes. To narrow it down to the relevant operators we first classify the operators by number of derivatives, chirality and twist.[44] In the case of zero derivatives we have chiral-even higher twist operator multiplets $\mathcal{O}_{1-2}$, chiral-odd higher twist multiplets $\mathcal{O}_{3-5}$, a chiral-even leading twist multiplet $\mathcal{O}_6$, and chiral-even leading twist multiplets $\mathcal{O}_{7-9}$. In general, operators without derivatives are related to the zeroth moments, i.e., normalization constants. From the relevant definitions in eqs. (3.9) and (3.21)–(3.22) we can see that all leading twist DAs are related to three quarks in a chiral-odd combination and that we need both, chiral-odd and chiral-even operators, for the various higher twist normalization constants. The conclusion is therefore that $\mathcal{O}_{7-9}$ should be considered for f^B as well as $f_T^{B\neq\Lambda}$, while $\mathcal{O}_{3-5}$ should be considered for λ_1^B as well as λ_T^Λ, and $\mathcal{O}_{1-2}$ should be considered for λ_2^B. This leaves $\mathcal{O}_6$ as the odd man out. Chiral-even leading twist operators such as these are not relevant for octet baryon DAs, but they do couple to decuplet baryon DAs (which are not discussed in this work).

Among the operators with one derivative we find two chiral-even leading twist multiplets, $\mathcal{O}_{D1}$ and $\mathcal{O}_{D8}$, as well as two sets of chiral-odd leading twist multiplets, $\mathcal{O}_{D2-D4}$ in $\tau_1^{\frac{12}{}}$ and $\mathcal{O}_{D5-D7}$ in $\tau_2^{\frac{12}{}}$. The leading twist octet baryon DAs are chiral-odd, hence at first sight both $\mathcal{O}_{D2-D4}$ and $\mathcal{O}_{D5-D7}$ are candidates for the calculation of the first moments. To be able to answer the question whether we should use the operators from the representation $\tau_1^{\frac{12}{}}$ or $\tau_2^{\frac{12}{}}$ to calculate the first order shape parameters we should first examine which operators can mix under renormalization.

In principle, only operators with equal mass dimension and equal transformation behavior under $\overline{\mathrm{H}(4)}$ can mix. With respect to the presentation in table 3.1 this means that mixing is only allowed among operators grouped together in one and the same cell, but not between different columns or rows. In lattice QCD this condition is not as strict, because powers of the dimensionful regulator a can be used to adjust the mass dimension of operators. This effectively allows mixing within the same row, e.g., operators $a^{-1}\mathcal{O}_{7-9}$ could mix into $\mathcal{O}_{D2-D4}$.[45] The mixing of lower-dimensional operators into higher ones shown in this example is particularly troublesome because it involves negative powers of

[44] Chirality and twist of these operator multiplets can be read off from appendix A of [52].

[45] One might argue that the same could be said about the continuum, i.e., that the mixing should be allowed because one could just as well use a mass as the dimensionful quantitiy. However, since we are always working with mass-independent renormalization schemes, the continuum calculation is shielded from this additional complicacy.

the lattice spacing. In the end we are always interested in the continuum limit $a \to 0$, meaning that these contributions from lower-dimensional operators can become arbitrarily large. Still, the renormalized operators should give finite results, hence large cancelations are required. While one can try to take this mixing with lower-dimensional operators into account (see [51]), the precision achievable in a calculation that has to rely on the numerical cancelation of near infinities is of course expected to be much worse than in a calculation where this can be avoided.

Fortunately, we can indeed avoid these difficulties by working with the operators $\mathcal{O}_{D5-D7}$ instead of $\mathcal{O}_{D2-D4}$. They transform according to the irreducible representation τ_2^{12} of $\overline{\mathrm{H}(4)}$, where simply no operators without derivatives exist, such that this kind of mixing need not be considered. However, there does exist a fourth multiplet, $\mathcal{O}_{D8}$, in this representation which consists of operators with different chirality. In a continuum calculation with exact chiral symmetry there can be no mixing between these, but in most lattice actions (including the one we use, see section 4.3) chiral symmetry is broken [144] and we need to check whether mixing of $\mathcal{O}_{D8}$ into $\mathcal{O}_{D5-D7}$ could spoil the results. Since chiral symmetry is restored in the continuum limit, an admixture is a power-suppressed $\mathcal{O}(a)$ effect. Furthermore, in the continuum limit all octet-baryon-to-vacuum matrix elements of operators within $\mathcal{O}_{D8}$ vanish identically, even though the operators themselves are nonzero. We have also verified this property numerically on the lattice. In summary, the admixture of $\mathcal{O}_{D8}$ to $\mathcal{O}_{D5-D7}$ is completely negligible and can safely be ignored in our analysis.

Finally for the operators with two derivatives it should now be obvious (by looking at table 3.1 once again) that we will select the chiral-odd leading twist operator multiplets $\mathcal{O}_{DD4-DD6}$ from the representation τ_2^4 of $\overline{\mathrm{H}(4)}$ for the calculation of the second moments and ignore all other operators with two derivatives. Only for these operators there is no mixing with other operators containing one or no derivative. One can also see that there will be no easy way out if one were to consider operators with three derivatives: Since every row has an entry in at least one of the columns shown, calculations involving any operator with three derivatives will require that the mixing with lower-dimensional operators is fully taken into account, no matter what representation one would choose. This is of no practical relevance yet, as the present lattice methods suffer from increased noise with each additional derivative and currently going past two derivatives seems not feasible. Existing lattice results for the second moments of the nucleon already come with large relative errors of 200%–800% such that the values are compatible with zero [48].[46]

The opposite of the bothersome mixing described above is also possible. Higher-dimensional operators can mix into the renormalization of the lower ones (and by nature

[46] Still, such results are valuable because they provide general constraints for the magnitude of these quantities. This can at least exclude some nucleon DA models with very large values for the shape parameters.

this will affect each and every multiplet), e.g., operators $a\mathcal{O}_{D2-D4}$ can mix into $\mathcal{O}_{7-9}$. This behavior is a lot less dangerous though, because it is always suppressed by $\mathcal{O}(a)$. Its effects will safely vanish the continuum limit. Let us end this section with a summary of the operators which we will use:

- $\mathcal{O}_{7-9}$ from τ_1^{12} for the leading twist normalization constants
- $\mathcal{O}_{1-5}$ from τ_1^{4} for the higher twist normalization constants
- $\mathcal{O}_{D5-D7}$ from τ_2^{12} for the leading twist first moments
- $\mathcal{O}_{DD4-DD6}$ from τ_2^{4} for the leading twist second moments

3.4.2. The relation between SU(3) and $\mathcal{S}_3$

When constructing n-particle states from a set of N distinct single-particle basis states there is an interplay between irreducible representations of the symmetric group $\mathcal{S}_n$ and the dimensions of SU(N) representations or, in the language of particle physics, between symmetry properties and the dimensions of particle multiplets. To illustrate this connection we need to introduce some concepts from representation theory.

Each irreducible representation of $\mathcal{S}_n$ can be identified one-to-one with a Young diagram, that is a set of n boxes arranged in left-justified rows with each row being of shorter or equal length than the row above it.[47] In this manner, the Young diagrams are isomorphic to the partitions of the integer n. Since we are interested in baryons (three-particle states), let us take a look at $\mathcal{S}_3$. There are three irreducible representations (see section 2.2.2) and three admissible Young diagrams. The identification is as follows:[48]

T^a : 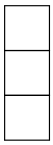 T^m : 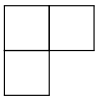 T^s : 

A standard Young tableau is created by arranging the integers $1, \ldots, n$ in the boxes of a Young diagram such that the entries in every row and in every column are in strictly increasing order. The number of standard Young tableaux that exist for a given Young diagram is equal to the dimension of the corresponding irreducible representation of $\mathcal{S}_n$. For $\mathcal{S}_3$ we have:

[47] Young diagrams and Young tableaux are powerful mathematical tools, used in representation theory, combinatorics, algebraic geometry, and other fields. A detailed treatment of their properties is beyond the scope of this thesis, we refer the reader to [145] for an overview.

[48] For any $\mathcal{S}_n$ the diagram with a single row/column corresponds to the trivial/signum representation, respectively.

T^a : $\begin{array}{|c|}\hline 1\\\hline 2\\\hline 3\\\hline\end{array}$ T^m : $\begin{array}{|c|c|}\hline 1&2\\\hline 3\\\cline{1-1}\end{array}$ $\begin{array}{|c|c|}\hline 1&3\\\hline 2\\\cline{1-1}\end{array}$ T^s : $\begin{array}{|c|c|c|}\hline 1&2&3\\\hline\end{array}$

This reconfirms that T^s and T^a are 1-dimensional and that T^m is 2-dimensional. In general, the number of standard Young tableaux can be calculated via the hook-length formula [146].

Each diagram is assigned a Young symmetrizer, an element of the group algebra that acts as a projection operator, by symmetrizing along all rows and antisymmetrizing along all columns. We define

$$Y^a = \frac{1}{6}\sum_{\pi\in\mathcal{S}_3}\operatorname{sgn}(\pi)\pi\,, \tag{3.39a}$$

$$Y^{ms} = \frac{1}{3}\big((123)+(213)\big)\circ\big((123)-(321)\big)\,, \tag{3.39b}$$

$$Y^{ma} = \frac{1}{3}\big((123)-(213)\big)\circ\big((123)+(321)\big)\,, \tag{3.39c}$$

$$Y^s = \frac{1}{6}\sum_{\pi\in\mathcal{S}_3}\pi\,. \tag{3.39d}$$

In this context, T^a is totally antisymmetric, T^m has mixed symmetry, and T^s is totally symmetric, justifying our naming conventions a posteriori. The Young symmetrizers are related to the construction of flavor wave functions. For example, the mixed-symmetric and mixed-antisymmetric flavor wave functions of the proton are given by

$$Y^{ms}|uud\rangle \propto 2|uud\rangle - |udu\rangle - |duu\rangle\,, \qquad Y^{ma}|uud\rangle \propto |udu\rangle - |duu\rangle\,. \tag{3.40a–b}$$

A collection of all relevant flavor wave functions can be found in appendix C.1.

The dimension of a SU(N) representation associated with a Young diagram of $\mathcal{S}_n$ is given by the number of so-called semistandard Young tableaux that can be built from a set of N allowed entries. A semistandard Young tableau is a filling of a Young diagram such that the entries in each row are weakly increasing while the entries in each column are strictly increasing. Given an integer N as well as the shape of a Young diagram, one can directly calculate the number of semistandard Young tableaux using the hook-content formula [147, Corollary 7.21.4], but for the case we are interested in it is both feasible and instructive to simply work out all the tableaux explicitly.

To understand SU(3) baryons we need to consider all semistandard Young tableaux that can be built by filling the Young diagrams of $\mathcal{S}_3$ from 3 allowed entries. The labels used for the filling are of no consequence; while mathematicians might prefer to use a canonically ordered set such as $\{1,2,3\}$, we will use $\{u,d,s\}$ with the implied ordering $u<d<s$

to hint at the connection to SU(3) flavor symmetry. The complete list of semistandard $\mathcal{S}_3$ Young tableaux with these entries is:

T^a :

u
d
s

T^m :

u	u
d	

d	d
s	

u	d
d	

u	s
s	

u	u
s	

d	s
s	

u	d
s	

u	s
d	

T^s :

u	u	u
u	d	s

u	u	d
d	d	s

u	d	d
u	s	s

d	d	d
d	s	s

u	u	s
s	s	s

From this we can read off the connection between particle multiplets and symmetry properties: The totally antisymmetric $\mathcal{S}_3$ representation T^a corresponds to a one-dimensional SU(3) representation (singlet), the mixed symmetry $\mathcal{S}_3$ representation T^m corresponds to an eight-dimensional SU(3) representation (octet), and the totally symmetric $\mathcal{S}_3$ representation T^s corresponds to a ten-dimensional SU(3) representation (decuplet). In a manner which is dual to this, the singlet and decuplet, both of which appear once in the decomposition of $3 \otimes 3 \otimes 3$, correspond to one-dimensional $\mathcal{S}_3$ representations, while the octet, appearing twice, corresponds to the only two-dimensional $\mathcal{S}_3$ representation.

3.4.3. Symmetry properties of baryons

According to the spin-statistics theorem [66], baryons are fermions. Their wave functions should be totally antisymmetric under the exchange of all properties (color, flavor, position, spin) of two constituent quarks. Let us consider the full wave function, a product of color, position, and spin-flavor wave functions, and analyze each part individually, starting with color.

Since baryons are color neutral, the three constituent quarks have to form a colorless SU(3) singlet state. The same reasoning as laid out for SU(3) flavor in section 3.4.2 also holds for SU(3) color and therefore the baryon color wave function has to be fully antisymmetric. This can be implemented using the Levi-Civita symbol ε^{abc} to contract the color indices. Moving on to the position part, we only consider ground state baryons with zero orbital angular momentum, thus requiring a totally symmetric spatial wave function.

This can be implemented by putting all three quarks at the same location (and without loss of generality we will usually take this location as the origin of our coordinate system). From this we can deduce that the remaining spin-flavor part has to be totally symmetric. Using our knowledge from section 3.4.2 we achieve this by taking a product of a totally (anti-)symmetric spinor structure with a totally (anti-)symmetric flavor structure for the (singlet) decuplet and by combining the two structures of mixed symmetry in case of the octet.

Putting these words into formulas, consider a three-quark operator,

$$SF^{f_1f_2f_3}_{\alpha_1\alpha_2\alpha_3,\bar\mu_1\bar\mu_2\bar\mu_3}\varepsilon^{a_1a_2a_3}[D^{\bar\mu_1}f_1]^{a_1}_{\alpha_1}(0)[D^{\bar\mu_2}f_2]^{a_2}_{\alpha_2}(0)[D^{\bar\mu_3}f_3]^{a_3}_{\alpha_3}(0)\,, \tag{3.41}$$

with a spin-flavor structure SF, color indices a_i, Lorentz multi-indices $\bar\mu_i$,[49] Dirac indices α_i, and quark flavors f_i. Together with the color structure, the product of three quark fields appearing in such an operator is completely invariant under any simultaneous exchange of Lorentz, Dirac, and flavor indices, e.g., $\bar\mu_1 \leftrightarrow \bar\mu_2$, $\alpha_1 \leftrightarrow \alpha_2$, and $f_1 \leftrightarrow f_2$ simultaneously. As expected, this implies that the only meaningful contributions from SF are those totally symmetric under any permutation of 1, 2, and 3, i.e., we shall only consider structures that fulfill

$$SF^{f_1f_2f_3}_{\alpha_1\alpha_2\alpha_3,\bar\mu_1\bar\mu_2\bar\mu_3} = SF^{f_{\pi_1}f_{\pi_2}f_{\pi_3}}_{\alpha_{\pi_1}\alpha_{\pi_2}\alpha_{\pi_3},\bar\mu_{\pi_1}\bar\mu_{\pi_2}\bar\mu_{\pi_3}} \qquad \forall\,\pi\in\mathcal{S}_3\,, \tag{3.42}$$

where π_i denote the appropriately permuted indices.

For the three SU(3) flavor multiplets we have

singlet ($\mathscr{S}$):
$$SF^{f_1f_2f_3}_{\alpha_1\alpha_2\alpha_3,\bar\mu_1\bar\mu_2\bar\mu_3} = S^{\mathscr{S}}_{\alpha_1\alpha_2\alpha_3,\bar\mu_1\bar\mu_2\bar\mu_3}F^{f_1f_2f_3}_{\mathscr{S}}\,, \tag{3.43a}$$

octet ($\mathscr{O}$):
$$SF^{f_1f_2f_3}_{\alpha_1\alpha_2\alpha_3,\bar\mu_1\bar\mu_2\bar\mu_3} = \sum_{t=1}^{2} S^{\mathscr{O},t}_{\alpha_1\alpha_2\alpha_3,\bar\mu_1\bar\mu_2\bar\mu_3}F^{f_1f_2f_3}_{\mathscr{O},t}\,, \tag{3.43b}$$

decuplet ($\mathscr{D}$):
$$SF^{f_1f_2f_3}_{\alpha_1\alpha_2\alpha_3,\bar\mu_1\bar\mu_2\bar\mu_3} = S^{\mathscr{D}}_{\alpha_1\alpha_2\alpha_3,\bar\mu_1\bar\mu_2\bar\mu_3}F^{f_1f_2f_3}_{\mathscr{D}}\,, \tag{3.43c}$$

where SF is guaranteed to respect eq. (3.42) by having the spin and the flavor structures individually transform according to the corresponding $\mathcal{S}_3$ representations (see sections 2.2 and 3.4.2):

$$S^{\mathscr{S}}_{\alpha_{\pi_1}\alpha_{\pi_2}\alpha_{\pi_3},\bar\mu_{\pi_1}\bar\mu_{\pi_2}\bar\mu_{\pi_3}} = T^a(\pi)S^{\mathscr{S}}_{\alpha_1\alpha_2\alpha_3,\bar\mu_1\bar\mu_2\bar\mu_3}\,, \tag{3.44a}$$

$$S^{\mathscr{O},t'}_{\alpha_{\pi_1}\alpha_{\pi_2}\alpha_{\pi_3},\bar\mu_{\pi_1}\bar\mu_{\pi_2}\bar\mu_{\pi_3}} = \sum_{t=1}^{2}[T^m(\pi)]_{tt'}S^{\mathscr{O},t}_{\alpha_1\alpha_2\alpha_3,\bar\mu_1\bar\mu_2\bar\mu_3}\,, \tag{3.44b}$$

$$S^{\mathscr{D}}_{\alpha_{\pi_1}\alpha_{\pi_2}\alpha_{\pi_3},\bar\mu_{\pi_1}\bar\mu_{\pi_2}\bar\mu_{\pi_3}} = T^s(\pi)S^{\mathscr{D}}_{\alpha_1\alpha_2\alpha_3,\bar\mu_1\bar\mu_2\bar\mu_3}\,, \tag{3.44c}$$

[49] In general, any given pair of contracted Lorentz multi-indices is to be understood as $S_{\bar\mu_i}D^{\bar\mu_i} = \sum_{m_i=0}^{\infty}S_{\mu_{i1}\ldots\mu_{im_i}}D^{\mu_{i1}}\cdots D^{\mu_{im_i}}$. In practice, we will only consider operators with zero, one, or two derivatives, i.e., the only nonvanishing contributions in these infinite sums will be those with either $m_1+m_2+m_3=0$, $m_1+m_2+m_3=1$, or $m_1+m_2+m_3=2$, respectively.

and

$$F_{\mathscr{S}}^{f_{\pi_1}f_{\pi_2}f_{\pi_3}} = T^a(\pi)F_{\mathscr{S}}^{f_1f_2f_3}\,, \tag{3.45a}$$

$$F_{\mathscr{O},t'}^{f_{\pi_1}f_{\pi_2}f_{\pi_3}} = \sum_{t=1}^{2}[T^m(\pi)]_{tt'}F_{\mathscr{O},t}^{f_1f_2f_3}\,, \tag{3.45b}$$

$$F_{\mathscr{D}}^{f_{\pi_1}f_{\pi_2}f_{\pi_3}} = T^s(\pi)F_{\mathscr{D}}^{f_1f_2f_3}\,. \tag{3.45c}$$

It is clear that these equations alone do not fix all components of S or F, but will provide some constraints.

Let us for the moment focus on F. Under the natural assumption that for each baryon only the correct flavor content can contribute to F (e.g., for the Λ baryon the only nonzero components of $F_{\mathscr{O},1}^{\Lambda}$ are $F_{\mathscr{O},1}^{\Lambda,uds}$ and permutations thereof) we can use the conditions (3.45) to fix all baryon flavor wave functions up to normalization and phase. The former is chosen in the canonical way, whereas the latter is a question of convention. Our conventions in that matter are laid out in appendix C.1, and the results for the flavor structures F can be read off from tables C.1–C.4, also contained in said appendix.

For the Dirac–Lorentz part S we will retain the useful transformation properties under $\overline{\mathrm{H}(4)}$ (see section 3.4.1) by only permitting linear combinations of operator multiplets (defined in [52]) from the same $\overline{\mathrm{H}(4)}$ representation. E.g., in the case of τ_1^{12} with no derivatives we consider linear combinations of $\mathcal{O}_7$, $\mathcal{O}_8$ and $\mathcal{O}_9$. The constraints (3.44) are fulfilled by an octet combination transforming under T^m,

$$t=1: \qquad \tfrac{1}{\sqrt{6}}(\mathcal{O}_7+\mathcal{O}_8-2\mathcal{O}_9)\,, \tag{3.46a}$$

$$t=2: \qquad \tfrac{1}{\sqrt{2}}(\mathcal{O}_7-\mathcal{O}_8)\,, \tag{3.46b}$$

and by a symmetric decuplet combination transforming under T^s,

$$\tfrac{1}{\sqrt{3}}(\mathcal{O}_7+\mathcal{O}_8+\mathcal{O}_9)\,. \tag{3.46c}$$

Using these constraints from $\mathcal{S}_3$ symmetry we can now proceed to find linear combinations of all operator multiplets, improved for the treatment of SU(3) baryons. As far as the operators without derivatives are concerned, the constraints (3.44) can be used to determine all singlet, octet, and decuplet operator multiplets (up to the prefactors that govern their normalization). They can be found in appendix C.2.1. For operators with derivatives the situation is more complicated. The $\mathcal{S}_3$ constraints do not fully fix the allowed linear combinations, leaving us with some remaining freedom. We will make good use of this by further optimizing the operators with the moments of distribution amplitudes in mind.

The shape parameters $\varphi^\star_{nk}$ are defined such that they do not mix under (one-loop) scale evolution and can therefore be assigned a one-loop anomalous dimension γ_{nk} (see eqs. (3.20)). Hence, we tune the linear combinations of our operators such that they are eigenoperators of the anomalous dimension matrices that will be calculated in section 3.5.1. By comparing the γ_{nk} of the shape parameters to the resulting eigenvalues one can identify the suitable operators for each shape parameter. With that, the remaining freedom is fully exhausted (once again, up to normalization) and these operators with one and two derivatives (corresponding to first and second order shape parameters) can be found in appendices C.2.2 and C.2.3.

Let us recapitulate what information is required to identify a specific operator. We will work with operators containing a certain number of derivatives which are grouped into multiplets transforming under irreducible representations of $\mathcal{S}_3$ and $\overline{\mathrm{H}(4)}$, therefore each operator is characterized by a $\mathcal{S}_3$ and a $\overline{\mathrm{H}(4)}$ representation, under which the multiplet it belongs to transforms. Since there can be several such multiplets for each representation pair, we will need an index to number these separate multiplets.[50] This classification of multiplets is shown in table 3.2. Furthermore, we will need yet another index if we wish to pick an individual operator from a multiplet[51] and we can specify a flavor structure as well. Given this wealth of indices, an example for the nomenclature is in order. Consider, e.g.,

$$\left(\mathscr{S}^{4}_{2,DD}\right)^{N,(3)}_{1} . \tag{3.47}$$

This specifies an operator with two derivatives (DD) that is part of a multiplet transforming under the $\overline{\mathrm{H}(4)}$ representation τ_2^4 (as indicated by the inner sub/superscript pair). The $\mathcal{S}_3$ transformation behavior of this multiplet is denoted by the script capital. In this case — $\mathscr{S}$ stands for the SU(3) singlet — it is governed by the totally antisymmetric $\mathcal{S}_3$ representation. (This part of the nomenclature is based on the associations made between SU(3) and $\mathcal{S}_3$ in the previous section 3.4.2.) Finally, the subscript selects the first such multiplet, while the integer superscript picks the third operator therefrom and the letter superscript specifies a flavor structure (here it is that of the nucleon). Admittedly, this crowd of indices may seem overwhelming, but it is necessary in case one wants to precisely identify a single operator. Fortunately, the full range of indices shown in this example will rarely be needed.

At this point some confusion might arise from the fact that we have just named a singlet operator for the proton, a particle which is certainly classified as an octet baryon. To clear this up, one should note that the classification of particle multiplets is, just as the study of the operator multiplet transformation behavior, based on the notion of SU(3) as

[50] The convention for the ordering is defined by appendix C.2.
[51] The convention for the ordering is defined by appendix A of [52].

Table 3.2.: Classification of the operator multiplets used in this work (analogous to table 3.1). Only the operators relevant in lattice studies of octet baryon distribution amplitudes are named. Other leading twist and higher twist operator multiplets are indicated by LT and HT, respectively. The nomenclature is explained in the main text and the operators are defined in appendix C.2.

	no derivatives dimension 9/2	1 derivative dimension 11/2	2 derivatives dimension 13/2
$\tau_1^{\underline{4}}$	$\left(\mathscr{S}_1^{\underline{4}}\right)_1$, $\left(\mathscr{O}_1^{\underline{4}}\right)_{1-2}$	HT	LT, HT
$\tau_2^{\underline{4}}$			$\left(\mathscr{S}_{2,DD}^{\underline{4}}\right)_{1-2}$, $\left(\mathscr{O}_{2,DD}^{\underline{4}}\right)_{1-6}$, $\left(\mathscr{D}_{2,DD}^{\underline{4}}\right)_{1-4}$, HT
$\tau^{\underline{8}}$	LT	LT, HT	LT, HT
$\tau_1^{\underline{12}}$	$\left(\mathscr{O}_1^{\underline{12}}\right)_1$, $\left(\mathscr{D}_1^{\underline{12}}\right)_1$	LT, HT	LT, HT
$\tau_2^{\underline{12}}$		$\left(\mathscr{S}_{2,D}^{\underline{12}}\right)_1$, $\left(\mathscr{O}_{2,D}^{\underline{12}}\right)_{1-4}$, $\left(\mathscr{D}_{2,D}^{\underline{12}}\right)_{1-3}$	LT, HT

an exact symmetry. In the real world however, SU(3) flavor symmetry is broken by the quark mass differences and hence operators whose transformation behavior is denoted as singlet or decuplet will indeed also be relevant for the renormalization of octet baryon distribution amplitudes carried out in section 3.5.4.

3.5. Renormalization of three-quark operators

In section 2.1.4 we have discussed the basics of renormalization concerning Green's functions built from simple fields and vertices stemming from the Lagrangian, using the quark propagator (a two-point function) as an example. Now we move on to a more advanced topic, namely the renormalization of composite operators. In particular, we are interested in local three-quark operators. The most generic form of such an operator is

$$\mathcal{O}(x) = SF^{f_1 f_2 f_3}_{\alpha_1\alpha_2\alpha_3,\bar{\mu}_1\bar{\mu}_2\bar{\mu}_3}\varepsilon^{a_1a_2a_3}[D^{\bar{\mu}_1}f_1]^{a_1}_{\alpha_1}(x)[D^{\bar{\mu}_2}f_2]^{a_2}_{\alpha_2}(x)[D^{\bar{\mu}_3}f_3]^{a_3}_{\alpha_3}(x)\,, \tag{3.48}$$

as introduced in eq. (3.41). Each individual operator is uniquely defined by its spin-flavor structure *SF*. Consider now a four-point function involving such an operator as well as three external quark legs of flavor g_i, each with the momentum p_i:

$$\begin{aligned}\Gamma(\mathcal{O}|p_1,p_2,p_3)^{g_1g_2g_3}_{\beta_1\beta_2\beta_3} = \varepsilon^{b_1b_2b_3}\int d^4x_1 d^4x_2 d^4x_3\, e^{i\sum_i p_i\cdot x_i} \\ \times\langle 0|\mathcal{O}(0)[\bar{g}_1]^{b_1}_{\beta_1}(x_1)[\bar{g}_2]^{b_2}_{\beta_2}(x_2)[\bar{g}_3]^{b_3}_{\beta_3}(x_3)|0\rangle\,.\end{aligned} \tag{3.49}$$

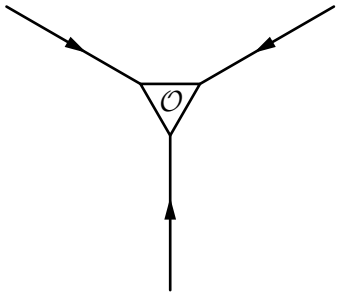

Figure 3.1.: Illustration of a tree-level contribution to the four-point function of an operator with no derivatives.

In the pictorial representation in figure 3.1 the local operator $\mathcal{O}$ appears similar to a three-quark "vertex," although we should keep in mind that there are no three-quark vertices in the QCD Lagrangian.

The calculation of perturbative corrections to this diagram will reveal new divergences that are specific to the operator $\mathcal{O}$ and cannot be canceled by the Lagrangian's counterterms alone. To obtain a finite result for any matrix element involving $\mathcal{O}$ one has to define a renormalization factor for this operator. Therefore, our next task is to calculate the vertex function in order to identify the divergences. As will become clear below, it is wise to define the amputated vertex function[52]

$$\Lambda(\mathcal{O}|p_1,p_2,p_3)^{g_1g_2g_3}_{\beta_1\beta_2\beta_3} = \Gamma(\mathcal{O}|p_1,p_2,p_3)^{g_1g_2g_3}_{\beta_1'\beta_2'\beta_3'}\big[S(-p_1)\big]^{-1}_{\beta_1'\beta_1}\big[S(-p_2)\big]^{-1}_{\beta_2'\beta_2}\big[S(-p_3)\big]^{-1}_{\beta_3'\beta_3}\,, \tag{3.50}$$

where each of the three external quark lines is multiplied by the inverse of a momentum space quark propagator,

$$S_{\alpha'\alpha}(-p) = \frac{\delta^{a'a}}{3}\int d^4x\, e^{i(-p)\cdot(0-x)}\, S^{a'a}_{\alpha'\alpha}(0-x)\,. \tag{3.51}$$

Before we turn to the calculation of Λ let us define a very useful object, namely the amputated flavor-independent four-point function

$$\begin{aligned} H^{\alpha_1\alpha_2\alpha_3,\bar\mu_1\bar\mu_2\bar\mu_3}_{\beta_1\beta_2\beta_3}(p_1,p_2,p_3) = \varepsilon^{a_1a_2a_3}\varepsilon^{b_1b_2b_3}\int d^4x_1 d^4x_2 d^4x_3\, e^{i\sum_i p_i\cdot x_i} \\ \times\,\langle 0|\prod_{j=1}^{3}[D^{\bar\mu_j}q_j]^{a_j}_{\alpha_j}(0)[\bar q_j]^{b_j}_{\beta_j'}(x_j)|0\rangle\prod_{k=1}^{3}\big[S(-p_k)\big]^{-1}_{\beta_k'\beta_k}\,. \end{aligned} \tag{3.52}$$

Some additional explanation might be required with respect to what we mean by flavor-independent. In H there appear three quark fields (q_1, q_2, and q_3) as well as three

[52] We don't need to assign any flavor labels to the propagators because the renormalization will be performed in the SU(3) symmetric limit where all quark masses are equal and the propagator is independent of flavor.

corresponding antiquark fields ($\bar{q}_1$, $\bar{q}_2$, and $\bar{q}_3$). First, in this formula there shall be no sum implied over any repeated flavor index q_i. Second, the three quark types are implied to be mutually distinct, i.e., in the calculation of this matrix element the quark q_1 can only be connected to the antiquark $\bar{q}_1$, but not to $\bar{q}_2$ or $\bar{q}_3$. Since all calculations are performed with massless quarks and since the strong interaction is flavor blind, the resulting H is independent of any specific choice of flavors.

After inserting the definition of $\mathcal{O}$ we can rewrite Λ in terms of H:

$$\begin{aligned}
\Lambda(\mathcal{O}|p_1,p_2,p_3)^{g_1g_2g_3}_{\beta_1\beta_2\beta_3} &= -SF^{f_1f_2f_3}_{\alpha_1\alpha_2\alpha_3,\bar{\mu}_1\bar{\mu}_2\bar{\mu}_3}\varepsilon^{a_1a_2a_3}\varepsilon^{b_1b_2b_3}\int d^4x_1 d^4x_2 d^4x_3\, e^{i\sum_i p_i\cdot x_i} \\
&\quad\times\langle 0|\prod_{i=1}^{3}[D^{\bar{\mu}_i}f_i]^{a_i}_{\alpha_i}(0)[\bar{g}_i]^{b_i}_{\beta'_i}(x_i)|0\rangle\prod_{j=1}^{3}\big[S(-p_j)\big]^{-1}_{\beta'_j\beta_j} \\
&= -\sum_{\pi\in\mathcal{S}_3} SF^{g_{\pi_1}g_{\pi_2}g_{\pi_3}}_{\alpha_1\alpha_2\alpha_3,\bar{\mu}_1\bar{\mu}_2\bar{\mu}_3}H^{\alpha_1\alpha_2\alpha_3,\bar{\mu}_1\bar{\mu}_2\bar{\mu}_3}_{\beta_{\pi_1}\beta_{\pi_2}\beta_{\pi_3}}(p_{\pi_1},p_{\pi_2},p_{\pi_3}) \\
&= -\sum_{\pi\in\mathcal{S}_3} SF^{g_{\pi_1}g_{\pi_2}g_{\pi_3}}_{\alpha_{\pi_1}\alpha_{\pi_2}\alpha_{\pi_3},\bar{\mu}_{\pi_1}\bar{\mu}_{\pi_2}\bar{\mu}_{\pi_3}}H^{\alpha_1\alpha_2\alpha_3,\bar{\mu}_1\bar{\mu}_2\bar{\mu}_3}_{\beta_1\beta_2\beta_3}(p_1,p_2,p_3) \\
&= -6SF^{g_1g_2g_3}_{\alpha_1\alpha_2\alpha_3,\bar{\mu}_1\bar{\mu}_2\bar{\mu}_3}H^{\alpha_1\alpha_2\alpha_3,\bar{\mu}_1\bar{\mu}_2\bar{\mu}_3}_{\beta_1\beta_2\beta_3}(p_1,p_2,p_3)\,. \qquad (3.53)
\end{aligned}$$

Unlike H, Λ has open flavor indices g_i. The quark field f_1 can, e.g., be connected to the antiquark field $\bar{g}_2$ if their flavor indices match (i.e., if $f_1 = g_2$). All these possible contractions are accounted for at the same time by introducing the sum over permutations π.[53] We further make use of the fact that H (by construction, cf. eq. (3.52)) is invariant under simultaneous permutation of all its indices and that also SF is totally symmetric (see eq. (3.42)).

In doing so we have shown that the flavor structure of the operator (contained in SF) can be disentangled from the four-point function, which is now flavor independent (H). This is a very useful insight as we therefore do not have to calculate the four-point function Λ individually for each operator. Instead, we should calculate the flavor-independent four-point function H just once, with open Dirac indices. The result can then be contracted with a spin-flavor structure to obtain Λ for any desired operator.

To handle all the operators we are interested in, we have to calculate contributions to H with zero, one, or two derivatives. Starting by thinking about one-loop corrections to the four-point matrix element of an operator with zero derivatives, cf. fig. 3.1, we find two types of diagrams. The first one, fig. 3.2(a), has a gluon connecting two quark legs of the operator, similar to a vertex correction diagram. Such diagrams are responsible for the appearance of new operator-specific divergences in the four-point function. The structure of

[53] In contrast to [51] this new approach does therefore not require an explicit calculation of the individual "crossed" diagrams.

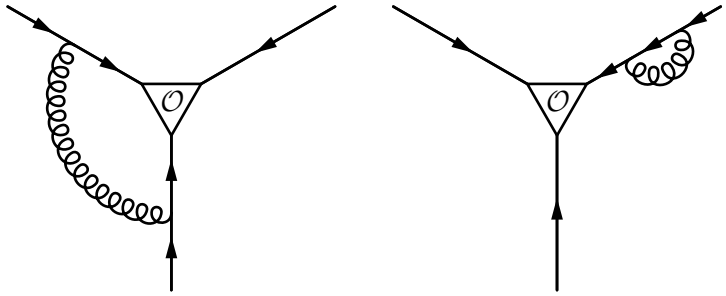

Figure 3.2.: One-loop contributions to the four-point matrix element for operators without derivatives. (The diagrams shown are representative of their respective classes, i.e., **(a)** stands for all diagrams where a gluon connects any two of the three quark legs and **(b)** stands for all diagrams where a self-energy bubble appears on one of the legs.)

these divergences will be discussed in section 3.5.1. The second diagram type on the other hand, shown in fig. 3.2(b), has both quark-gluon vertices appearing on the same quark leg. This diagram is one-particle-reducible, i.e., it could be separated into two independent pieces by "cutting" just one of the propagators. The two pieces are basically the tree-level diagram for the operator and the self-energy correction to the quark propagator. The loop corrections to the quark propagator are well known (see sections 2.1.3 and 2.1.4) and all information about the associated divergence is given by the renormalization factor Z_q. Therefore, diagrams of this type provide no new information regarding the operator $\mathcal{O}$. Having introduced the concept of an amputated vertex function above, we find that these extraneous self-energy diagrams appearing in the matrix element are neatly canceled by the inverse quark propagators and do not contribute to amputated vertex functions, so that henceforth we will no longer need to concern ourselves with self-energy diagrams.

Let us move on to the diagrams for operators with one covariant derivative, i.e., those that give contributions to $H^{\alpha_1\alpha_2\alpha_3,\bar{\mu}_1\bar{\mu}_2\bar{\mu}_3}_{\beta_1\beta_2\beta_3}$ with $m_1 + m_2 + m_3 = 1$. The single derivative can act on any of the three quarks, corresponding to $m_1 = 1$, $m_2 = 1$, or $m_3 = 1$. There is no conceptual difference between these three positions, therefore we will show only one set of diagrams in figure 3.3 below.

For operators without derivatives, all one-loop diagrams were built using two quark-gluon vertices, but when we start looking at operators with a derivative the situation becomes a bit more diverse. On the one hand, covariant derivatives appearing in the operator, $D_\mu = \partial_\mu - igt^A A^A_\mu$, consist of two parts. The first part is an ordinary derivative and is of $\mathcal{O}(1)$, while the second part contains a gluon field and is of $\mathcal{O}(g)$. On the other hand, quark-gluon vertices appearing in the perturbative expansion, $igt^A A^A_\mu \gamma^\mu$, are also of $\mathcal{O}(g)$.

One-loop order is $\mathcal{O}(\alpha_s)$, which is of course equivalent to $\mathcal{O}(g^2)$, and we now have two

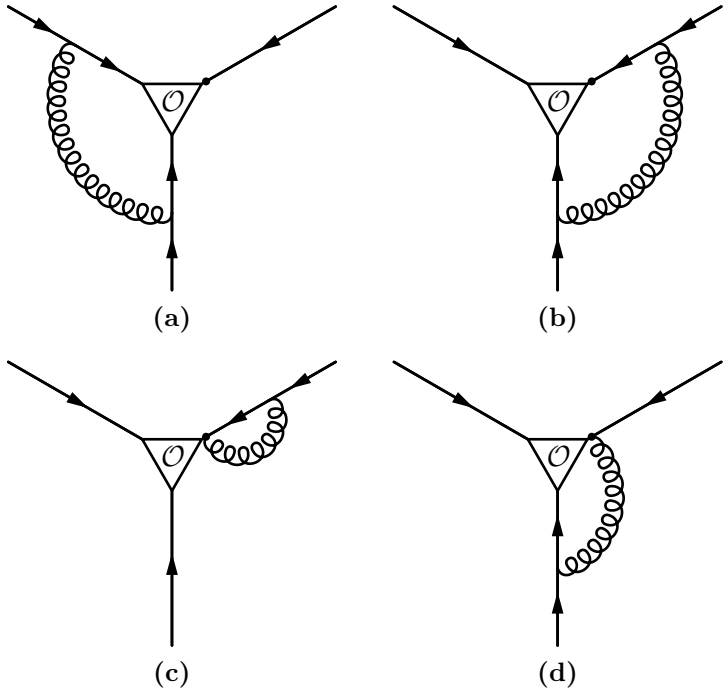

Figure 3.3.: One-loop contributions to the four-point function for operators with one derivative. Said derivative acting on one of the three quark fields in the operator is indicated by a dot.

ways to construct such diagrams. First, we can once again have two quark-gluon vertices, in which case the derivative part of the covariant derivative is needed and will simply lead to a factor proportional to the four-momentum associated with its quark line. The two vertices can either both appear on lines that do not feature the derivative, fig. 3.3(a), or one of the vertices can be on the derivative's quark line, fig. 3.3(b). Second, we can also have only one quark-gluon vertex connected to the gluon field from the covariant derivative. The single vertex can either be on the same line as the derivative, fig. 3.3(c), or not, fig. 3.3(d).

Finally, to understand the renormalization behavior of operators involving two covariant derivatives we will have to calculate all diagrams responsible for contributions to $H_{\beta_1\beta_2\beta_3}^{\alpha_1\alpha_2\alpha_3,\bar{\mu}_1\bar{\mu}_2\bar{\mu}_3}$ with $m_1 + m_2 + m_3 = 2$. Here we have to consider two unequal topologies: Either the two covariant derivatives can be attached to two different quark lines (corresponding to $m_1 = m_2 = 1$, $m_2 = m_3 = 1$, or $m_3 = m_1 = 1$), as exemplified in figure 3.4, or both derivatives are acting on the same quark (corresponding to $m_1 = 2$, $m_2 = 2$, or $m_3 = 2$), see figure 3.5. In any case, the rules for one-loop diagrams are still the same: Each diagram has exactly one gluon propagator that either connects two vertices to each other (subfigures (a) and (b)) or lies between a covariant derivative and a single quark-gluon vertex (remaining subfigures).

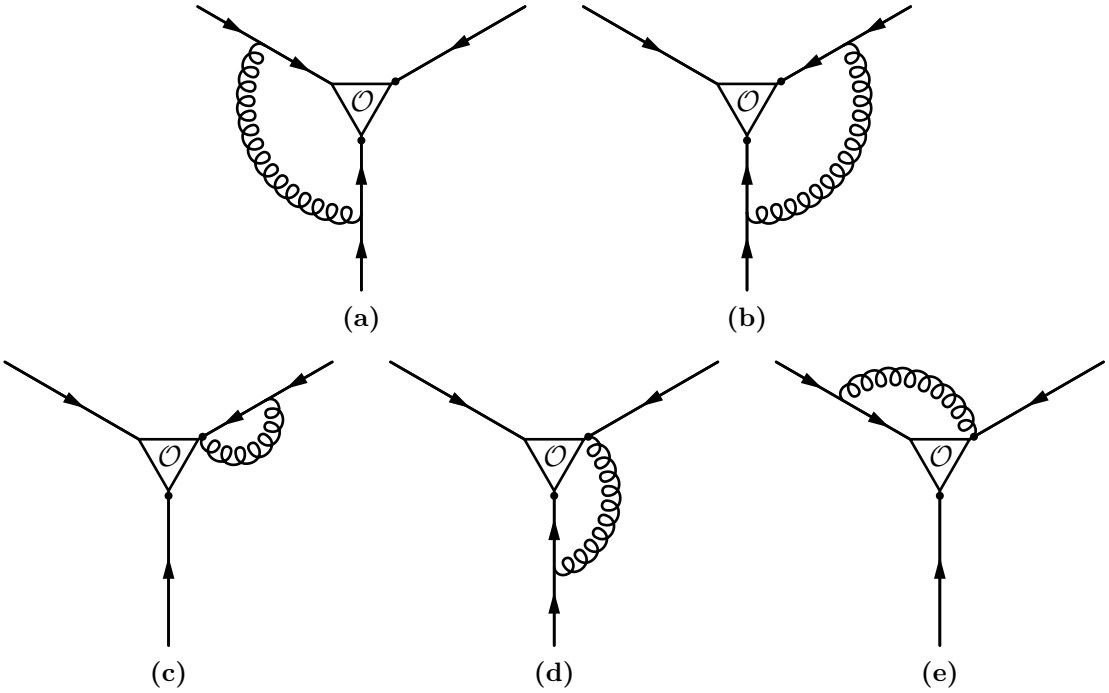

Figure 3.4.: One-loop contributions to the four-point function for operators with two derivatives, with the derivatives acting on two different quarks.

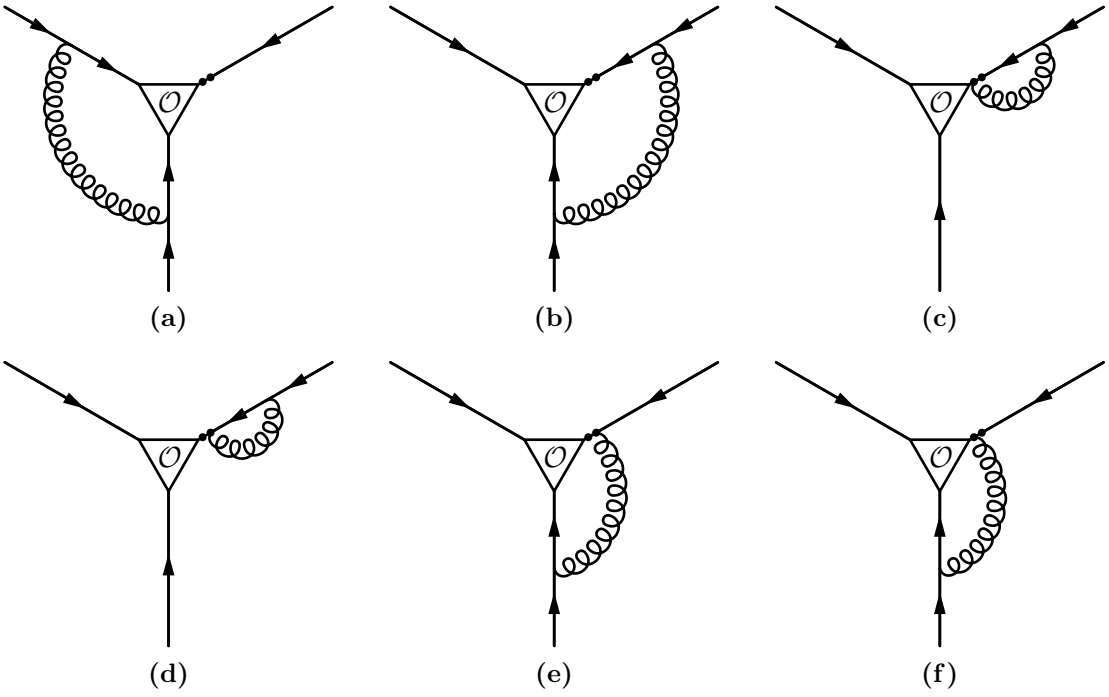

Figure 3.5.: One-loop contributions to the four-point function for operators with two derivatives, with both derivatives acting on the same quark.

Now that all diagram topologies for one-loop corrections to the vertex functions of operators with up to two covariant derivatives have been detailed, they have to be translated to formulas by use of the QCD Feynman rules. Since the RI′/SMOM renormalization condition is defined in the limit $m_q \to 0$ (see section 3.5.2), we shall work with massless quarks right from the start. We can then proceed with the actual calculation, a task that is straightforward, yet extensive. The diagrams give rise to a number of loop integrals, which are made finite by use of dimensional regularization, as introduced in section 2.1.3. The calculation of these various integrals can be tackled using a reduction algorithm [89] that is suitable for implementation on a computer. All individual contributions (each consisting not only of loop integrals but also of Dirac and color structures) to the flavor-independent four-point function H (with either zero, one, or two derivatives) have to be accounted for and added together. Finally, everything has to be expanded in the regulator ϵ such that the divergent parts can be identified. These computations have been performed in MATHEMATICA, a computer algebra system. An implementation of the reduction algorithm has been provided by N. Offen.

While obtaining H is one of the main achievements of this work, it would be both very impractical and extremely wasteful of paper to write down the result. Even for the simplest case without derivatives, H is an object with 4^6 components (due to having 6 open Dirac indices), with each component being given by a complicated analytical expression involving some special functions (polylogarithms or polygamma functions). Thankfully, the important quantities that can be extracted from H are much more compact and thus the reader will still be able to enjoy some tangible results, namely the $\overline{\text{MS}}$ Z-factors carrying all the information on the pole structure of H (in section 3.5.1) and the final results for the renormalization conversion factors (in section 3.5.3).

3.5.1. $\overline{\text{MS}}$ scheme for three-quark operators

The next goal should be to implement $\overline{\text{MS}}$ renormalization for H. However, for three-quark operators the procedure is not as straightforward as it was for the quark propagator (cf. eqs. (2.54)). We will illustrate the added subtleties by means of an example: Consider the individual contribution from a gluon connecting quark legs two and three, akin to figure 3.2(a). In Feynman gauge the result for this one-loop diagram is[54]

$$\frac{\alpha_s}{24\pi}\frac{1}{\epsilon}\mathbb{1}_4 \otimes \gamma^\mu\gamma^\nu \otimes \gamma_\mu\gamma_\nu + \text{finite terms}\,, \tag{3.54}$$

[54] We omit the open Dirac indices and instead use the notation $M_1 \otimes M_2 \otimes M_3$ to denote contributions of the type $(M_1)_{\alpha_1\beta_1}(M_2)_{\alpha_2\beta_2}(M_3)_{\alpha_3\beta_3}$ to $H^{\alpha_1\alpha_2\alpha_3}_{\beta_1\beta_2\beta_3}$. In this way the matrix M_1 stands for a Dirac structure on the leg of the first quark, and so on. We will also use $M^{\otimes 3} = M \otimes M \otimes M$.

which is written here already in a way that seems to have isolated the divergent part.[55] Remembering the typical one-loop $\overline{\text{MS}}$ combination $1/\bar{\epsilon}$ defined in eq. (2.53), one would therefore naively expect that the $\overline{\text{MS}}$ Z-factor would have to subtract the term

$$\frac{\alpha_s}{24\pi}\frac{1}{\bar{\epsilon}}\mathbb{1}_4 \otimes \gamma^\mu\gamma^\nu \otimes \gamma_\mu\gamma_\nu \,. \tag{3.55}$$

Now let us for the moment assume that at some time during the calculation we had decided to use the following identity for gamma matrices:

$$\gamma_\mu\gamma_\nu = \tfrac{1}{2}[\gamma_\mu,\gamma_\nu] + \tfrac{1}{2}\{\gamma_\mu,\gamma_\nu\} = \tfrac{1}{2}[\gamma_\mu,\gamma_\nu] + g_{\mu\nu}\,. \tag{3.56}$$

Since this is an exact identity, it cannot affect the value of the dimensionally regularized result, but it will affect its notation:

$$\begin{aligned}
&\frac{\alpha_s}{24\pi}\frac{1}{\epsilon}\mathbb{1}_4 \otimes \gamma^\mu\gamma^\nu \otimes \gamma_\mu\gamma_\nu + \text{finite terms} = \\
&\quad= \frac{\alpha_s}{24\pi}\frac{1}{\epsilon}\big(\mathbb{1}_4 \otimes \tfrac{1}{2}[\gamma^\mu,\gamma^\nu] \otimes \tfrac{1}{2}[\gamma_\mu,\gamma_\nu] + d\mathbb{1}_4^{\otimes 3}\big) + \text{finite terms} \\
&\quad= \frac{\alpha_s}{24\pi}\frac{1}{\epsilon}\big(\mathbb{1}_4 \otimes \tfrac{1}{2}[\gamma^\mu,\gamma^\nu] \otimes \tfrac{1}{2}[\gamma_\mu,\gamma_\nu] + 4\mathbb{1}_4^{\otimes 3}\big) - \frac{\alpha_s}{24\pi}2\mathbb{1}_4^{\otimes 3} + \text{finite terms} \\
&\quad= \frac{\alpha_s}{24\pi}\frac{1}{\epsilon}\big(\mathbb{1}_4 \otimes \tfrac{1}{2}[\gamma^\mu,\gamma^\nu] \otimes \tfrac{1}{2}[\gamma_\mu,\gamma_\nu] + 4\mathbb{1}_4^{\otimes 3}\big) + \text{finite terms}\,.
\end{aligned} \tag{3.57}$$

Presented with this form of the result, we might conclude that the $\overline{\text{MS}}$ Z-factor should subtract the term

$$\frac{\alpha_s}{24\pi}\frac{1}{\bar{\epsilon}}\big(\mathbb{1}_4 \otimes \tfrac{1}{2}[\gamma^\mu,\gamma^\nu] \otimes \tfrac{1}{2}[\gamma_\mu,\gamma_\nu] + 4\mathbb{1}_4^{\otimes 3}\big)\,. \tag{3.58}$$

Now we are faced with an ambiguity: Clearly the expressions (3.55) and (3.58) are not equal, as they differ by a finite term. And yet, both subtraction procedures are fit to completely remove the divergences from the diagram, all while adhering to the principle of $\overline{\text{MS}}$, which is to identify the structures multiplying the $1/\epsilon$ poles and then subtract only these structures multiplied by $1/\bar{\epsilon}$ (but not any other finite terms). The ambiguity arises from the fact that here we can freely rewrite the divergent structures in ways that generate additional finite terms, as seen in eq. (3.57). This is a new behavior that is inherent to the complex three-quark four-point function with open Dirac indices that we are working with. It does not occur in simpler quantities such as the quark propagator (which has just one quark line with a single Dirac structure).

[55] The full loop calculation leading to this result will not be presented here, but we can give some pointers as to why a divergent part of such form is not unexpected: There should be two Dirac matrices (one from a propagator, another from a vertex) on each quark leg taking part in the interaction as well as a trivial structure on the remaining (fully amputated) leg. Additionally, all Lorentz indices should be contracted among each other since the diagram has no open Lorentz indices and the divergent part may not depend on any external momentum vectors.

The two different approaches presented above are not the only ones. In fact, we can easily generate a whole family of different finite parts, e.g., by interpolating between the two cases with a continuous parameter. We might be tempted to ask which one of these prescriptions actually defines the $\overline{\text{MS}}$ scheme, but there is just no definitive answer to this question. For quantities like our three-quark operators the definition of *the* $\overline{\text{MS}}$ scheme is no longer unique, but there are many ways to define *an* $\overline{\text{MS}}$ scheme. To get a meaningful result one can choose any one of these schemes, as long as one takes care that a consistent scheme definition be maintained throughout all calculations. However, it is of equal importance to precisely specify which $\overline{\text{MS}}$ scheme is adopted, otherwise the result is effectively useless to anyone wishing to make exact comparisons or use it as an input value in another calculation.

We have some freedom of choice in selecting our scheme. Instead of simply picking an arbitrary scheme, we can carefully select one that allows us to reap some additional benefits. We will elect to utilize the scheme presented in [135], and the following discussion shall elucidate the motivation behind this. To begin, let us introduce the general definition of a fully antisymmetrized product of m gamma matrices:

$$\Gamma^{(m)}_{\mu_1\dots\mu_m} = \frac{1}{m!}\sum_{\pi\in\mathcal{S}_m} \operatorname{sgn}(\pi)\gamma_{\mu_{\pi_1}}\cdots\gamma_{\mu_{\pi_m}}\,. \tag{3.59}$$

Explicitly, the first few can be written as

$$\Gamma^{(0)} = \mathbb{1}_4\,, \qquad \Gamma^{(1)}_{\mu_1} = \gamma_{\mu_1}\,, \qquad \Gamma^{(2)}_{\mu_1\mu_2} = \tfrac{1}{2}[\gamma_{\mu_1},\gamma_{\mu_2}]\,. \tag{3.60a–c}$$

Another key definition is that of an evanescent operator, which means a (bare) operator that vanishes in $d = 4$ dimensions, but is in general nonzero for arbitrary d. The emergence of such operators has the same cause as the nonuniqueness of the $\overline{\text{MS}}$ scheme: In noninteger spacetime dimensions the Clifford algebra becomes infinite-dimensional.[56]

A typical example for an evanescent three-quark operator is given by[57]

$$\big(q^T C\Gamma^{\mu_1\cdots\mu_5}_{(5)} q\big)\gamma_5\Gamma^{(5)}_{\mu_1\dots\mu_5} q\,. \tag{3.61}$$

This operator is clearly evanescent, as no antisymmetrized product of more than 4 gamma matrices can exist in 4 dimensions, i.e.,

$$\Gamma^{(m)}_{\mu_1\dots\mu_m} \xrightarrow{d\to 4} 0 \qquad \forall\, m > 4\,. \tag{3.62}$$

[56] For integer d, any product of gamma matrices can be reduced to a linear combination of the 2^d basis matrices provided by $\Gamma^{(m)}_{\mu_1\dots\mu_m}$ with $0 \le m \le d$. For noninteger d, a basis consists of infinitely many elements, e.g., all $\Gamma^{(m)}_{\mu_1\dots\mu_m}$ (with no upper bound on m).

[57] Color, flavor, and position indices are of no relevance to this discussion and are therefore suppressed.

Notwithstanding that evanescent operators are unphysical (they vanish in the physical dimension $d = 4$), they can still affect other physical operators through the mixing under renormalization. As a reminder, the renormalization has to be performed in $d = 4 - 2\epsilon$ dimensions (where evanescent operators can exist). Only after the renormalization has been carried out and everything has been made finite can we return to 4 dimensions. Therefore, the existence of evanescent operators can affect the values of the renormalized vertex functions of physical operators. The other way round, the renormalized vertex functions of evanescent operators can become nonzero (through contributions from the mixing with the physical ones), even though the bare operators are zero. Furthermore, these operators may also mix under renormalization group scale evolution via the anomalous dimension matrix, meaning that even if we found a situation where matrix elements of evanescent operators turned out equal to zero at some scale, this need not hold after evolution to any other scale.

The concept of evanescent operators is not specific to our subject of baryon DAs. Their effects have been examined for quite some time, and methods to treat them properly have been found. A class of operators for an effective treatment of the electroweak interaction has been studied in [148], where an $\overline{\text{MS}}$ scheme in which renormalized evanescent operators vanish has been proposed. In this scheme the anomalous dimension matrix for physical and evanescent operators is upper block triangular, such that the Green's functions of evanescent operators can be kept at zero under evolution to any scale. Further research has shown that this construction is still not unique, as the upper block triangular structure can be kept intact under a change in the basis for the evanescent operators that induces changes in the physical part of the anomalous dimension matrix [149].

Specifically for three-quark operators, a new scheme was developed in [135]. It is designed for the calculation with open spinor indices performed in our work, and henceforth the label $\overline{\text{MS}}$ will always refer to this particular scheme. The definition is as follows: Vertex functions of three-quark operators are to be calculated with open indices. All structures multiplying $1/\epsilon$ poles are to be brought into a form consisting entirely of fully antisymmetrized Dirac matrices (as in our example, eq. (3.57)). Only these fully antisymmetrized structures (with the usual $\overline{\text{MS}}$ prefactor $1/\bar{\epsilon}$) are subtracted in order to obtain the renormalized result. For operators with a Dirac structure the renormalization is defined as the contraction of said Dirac structure and the renormalized operator with open indices. Since the renormalized three-quark operator is an object in 4 dimensions, the Dirac matrices can be taken to 4 dimensions as well, meaning that all renormalized evanescent operators automatically vanish in this scheme, e.g.,

$$\big[\big(q^T C\Gamma^{\mu_1\dots\mu_5}_{(5)} q\big)\gamma_5\Gamma^{(5)}_{\mu_1\dots\mu_5} q\big]^{\overline{\text{MS}}}_{\tau} = \big(C\Gamma^{\mu_1\dots\mu_5}_{(5)}\big)_{\alpha_1\alpha_2}\big(\gamma_5\Gamma^{(5)}_{\mu_1\dots\mu_5}\big)_{\tau\alpha_3}[q_{\alpha_1}q_{\alpha_2}q_{\alpha_3}]^{\overline{\text{MS}}} = 0\,. \quad (3.63)$$

Therefore, renormalized results in this $\overline{\text{MS}}$ scheme cannot be affected by evanescent operators and we will not have to involve any of them in our calculations. Furthermore, this approach also avoids any subtleties that can arise from the extension of the matrix γ_5 to $d \neq 4$ dimensions [150].

In [135] the $\overline{\text{MS}}$ Z-factor for three-quark operators without derivatives has been determined in Feynman gauge to two-loop order. To one-loop accuracy the result is

$$Z = \Gamma_{000} - \frac{\alpha_s}{24\pi}\frac{1}{\bar{\epsilon}}\big(\Gamma_{022} + \Gamma_{202} + \Gamma_{220} + 12\Gamma_{000}\big) + \mathcal{O}(\alpha_s^2)\,, \tag{3.64}$$

using the shorthands

$$\Gamma_{000} = \Gamma^{(0)} \otimes \Gamma^{(0)} \otimes \Gamma^{(0)} = \mathbb{1}_4^{\otimes 3}\,, \tag{3.65a}$$

$$\Gamma_{022} = \Gamma^{(0)} \otimes \Gamma^{\mu\nu}_{(2)} \otimes \Gamma^{(2)}_{\mu\nu} = \mathbb{1}_4 \otimes \tfrac{1}{2}[\gamma^\mu, \gamma^\nu] \otimes \tfrac{1}{2}[\gamma_\mu, \gamma_\nu]\,, \tag{3.65b}$$

and so on. We confirm that for operators without derivatives this Z-factor removes all divergences from the one-loop four-point function,

$$\big[H^{\alpha_1\alpha_2\alpha_3}_{\beta_1\beta_2\beta_3}(p_1,p_2,p_3)\big]^{\overline{\text{MS}}} = Z^{\alpha_1\alpha_2\alpha_3}_{\alpha_1'\alpha_2'\alpha_3'} H^{\alpha_1'\alpha_2'\alpha_3'}_{\beta_1\beta_2\beta_3}(p_1,p_2,p_3)\,, \tag{3.66}$$

and we also generalize the result from Feynman gauge ($\xi = 1$) to linear covariant gauge with arbitrary gauge parameter ξ:

$$Z = \Gamma_{000} - \xi\frac{\alpha_s}{2\pi}\frac{1}{\bar{\epsilon}}\Gamma_{000} - \frac{\alpha_s}{24\pi}\frac{1}{\bar{\epsilon}}\big(\Gamma_{022} + \Gamma_{202} + \Gamma_{220}\big) + \mathcal{O}(\alpha_s^2)\,. \tag{3.67}$$

The physical anomalous dimension matrix for operators without derivatives can be calculated as

$$\gamma = -\mu\left(\frac{d}{d\mu} Z\sqrt{Z_q}^3\right)\left(Z\sqrt{Z_q}^3\right)^{-1}. \tag{3.68}$$

In [136] it has been determined in our scheme, to three loops. The one-loop result,[58]

$$\gamma = -\frac{\alpha_s}{12\pi}\big(\Gamma_{022} + \Gamma_{202} + \Gamma_{220}\big) + \mathcal{O}(\alpha_s^2)\,, \tag{3.69}$$

is gauge and scheme independent. The one-loop anomalous dimensions for the leading twist and higher twist normalization factors, given by eq. (3.20a) and by the exponent in eq. (3.24), respectively, are equal to eigenvalues of this anomalous dimension matrix divided by $\alpha_s/(2\pi)$.

[58] To correctly reproduce this result starting from eqs. (3.67) and (3.68) one has to bear in mind that the QCD beta function, given in eq. (2.26) for 4 dimensions, comes with an additional contribution of $-\epsilon\alpha_s$ when evaluated in $4 - 2\epsilon$ dimensions, see, e.g., [151].

For operators including one derivative, the structure of the Z-factor is even more complicated. In addition to the $(4\times4)^{\otimes3}$ matrix structure (encoded in the Γ_{lmn}) that operates on the open Dirac indices, we now have an additional 3×3 matrix structure representing the mixing between operators that have the covariant derivative acting on the first, second, or third quark. For the flavorless amputated four-point functions with one derivative, the $\overline{\text{MS}}$ renormalization is given by[59]

$$\begin{pmatrix} H^{\alpha_1\alpha_2\alpha_3,\mu,-,-}_{\beta_1\beta_2\beta_3}(p_1,p_2,p_3) \\ H^{\alpha_1\alpha_2\alpha_3,-,\mu,-}_{\beta_1\beta_2\beta_3}(p_1,p_2,p_3) \\ H^{\alpha_1\alpha_2\alpha_3,-,-,\mu}_{\beta_1\beta_2\beta_3}(p_1,p_2,p_3) \end{pmatrix}^{\overline{\text{MS}}} = Z^{\alpha_1\alpha_2\alpha_3}_{\alpha'_1\alpha'_2\alpha'_3} \begin{pmatrix} H^{\alpha'_1\alpha'_2\alpha'_3,\mu,-,-}_{\beta_1\beta_2\beta_3}(p_1,p_2,p_3) \\ H^{\alpha'_1\alpha'_2\alpha'_3,-,\mu,-}_{\beta_1\beta_2\beta_3}(p_1,p_2,p_3) \\ H^{\alpha'_1\alpha'_2\alpha'_3,-,-,\mu}_{\beta_1\beta_2\beta_3}(p_1,p_2,p_3) \end{pmatrix}, \tag{3.70}$$

where

$$\begin{aligned} Z = {} & \mathbb{1}_3\otimes\Gamma_{000} - \xi\frac{\alpha_s}{2\pi}\frac{1}{\bar\epsilon}\mathbb{1}_3\otimes\Gamma_{000} + \frac{\alpha_s}{36\pi}\frac{1}{\bar\epsilon}\mathbb{1}_3\otimes\big(\Gamma_{022}+\Gamma_{202}+\Gamma_{220}\big) \\ & + \frac{\alpha_s}{72\pi}\frac{1}{\bar\epsilon}\begin{pmatrix}\Gamma_{022}&\Gamma_{220}&\Gamma_{202}\\ \Gamma_{220}&\Gamma_{202}&\Gamma_{022}\\ \Gamma_{202}&\Gamma_{022}&\Gamma_{220}\end{pmatrix} + \frac{2\alpha_s}{9\pi}\frac{1}{\bar\epsilon}\begin{pmatrix}2&-1&-1\\ -1&2&-1\\ -1&-1&2\end{pmatrix}\otimes\Gamma_{000} + \mathcal{O}(\alpha_s^2) \end{aligned} \tag{3.71}$$

is our one-loop result for the Z-factor. The one-loop anomalous dimension matrix is

$$\begin{aligned} \gamma = {} & \frac{\alpha_s}{18\pi}\mathbb{1}_3\otimes\big(\Gamma_{022}+\Gamma_{202}+\Gamma_{220}\big) \\ & + \frac{\alpha_s}{36\pi}\begin{pmatrix}\Gamma_{022}&\Gamma_{220}&\Gamma_{202}\\ \Gamma_{220}&\Gamma_{202}&\Gamma_{022}\\ \Gamma_{202}&\Gamma_{022}&\Gamma_{220}\end{pmatrix} + \frac{4\alpha_s}{9\pi}\begin{pmatrix}2&-1&-1\\ -1&2&-1\\ -1&-1&2\end{pmatrix}\otimes\Gamma_{000} + \mathcal{O}(\alpha_s^2)\,, \end{aligned} \tag{3.72}$$

and the anomalous dimensions for the leading twist DA shape parameters of up to first order given in eqs. (3.20a–c) are equal to eigenvalues of this matrix divided by $\alpha_s/(2\pi)$. For operators with two derivatives, the $\overline{\text{MS}}$ Z-factor can be found in appendix D.3.

3.5.2. RI′/SMOM scheme for three-quark operators

In addition to the destination $\overline{\text{MS}}$ scheme detailed above, we also need to specify the intermediate nonperturbative scheme that will be implemented on the lattice. In our case, we will be using an RI′/SMOM scheme, where RI′ refers to a regularization-invariant prescription as discussed in section 2.1.4 and SMOM denotes a symmetric choice for the renormalization point. The main motivation behind chosing this particular kind of scheme lies in the quest for smaller errors.

[59] In the most general case, the four-point function has three Lorentz multi-indices. For contributions with one derivative, only one of these does contain a single Lorentz index, while the other two are "empty." We visualize these empty multi-indices with underscores to clarify the position of the derivative.

A benchmark quantity for lattice renormalization and conversion to $\overline{\text{MS}}$ are the light quark masses, where the uncertainty due to renormalization (which was 9%) used to be the dominant one, amounting to half of the total error [152]. Through the development of new methods, such as these SMOM renormalization schemes, this uncertainty (especially the part due to the perturbative matching) could be greatly reduced. For lattice determinations of the $\overline{\text{MS}}$ light quark masses the renormalization procedure now gives a much smaller 2% error [153]. In the following we will apply such a modern SMOM scheme to the nonperturbative renormalization and perturbative matching for baryon DAs.

SMOM renormalization point

The definition of a renormalization point amounts to the specification of a momentum configuration that fixes all of the involved invariants by relating them to the renormalization scale μ. The four-point function of a three-quark operator, cf. eq. (3.49) and figure 3.1, depends on three external quark momenta, which we denote as p_1, p_2, and p_3. A typical MOM scheme might set all three external momenta to the same length, while keeping their sum, i.e., the total momentum flowing into the operator, at zero [136]:[60]

$$p_1^2 = p_2^2 = p_3^2 = \mu^2\,, \qquad \text{with } p_1 + p_2 + p_3 = 0\,. \tag{3.73}$$

Since we have a sum of momenta which vanishes, this is a so-called exceptional momentum configuration.

Adverse effects of such kinematics in lattice simulations have been discussed in [154], where it has been observed in a study of quark bilinear operators that the impact of low-energy behavior (in their case: chiral symmetry breaking) may not be sufficiently suppressed in the regime of very large momenta if the momentum configuration is exceptional, cf. also [155]. In a subsequent publication a new symmetric and nonexceptional momentum geometry has been used for the vertex functions of two-quark operators [156]. In this new scheme, which has been dubbed SMOM, the operator is no longer inserted at zero momentum. Instead, this momentum now has the same magnitude as the momenta of the external quarks.

It is argued that, compared to exceptional kinematics, SMOM has a better suppression of unwanted infrared contaminations [156]. A numerical test of this claim has been performed for the quark mass renormalization in [157]. In addition, nonexceptional momenta also exhibit a faster convergence behavior in the perturbative expansion of renormalization scheme conversion factors. In [158, 159] it has been found that the one- and two-loop

[60] The equation refers to Euclidean spacetime. In Minkowski space one would have to set the squares equal to $-\mu^2$ instead, i.e., the method is restricted to the deep Euclidean domain.

corrections for SMOM-to-$\overline{\text{MS}}$ conversion factors are significantly smaller than the respective terms in the perturbative expansion of MOM-to-$\overline{\text{MS}}$ factors. In fact, already the one-loop corrections for SMOM are smaller than even the third order terms for MOM. This points to a vastly improved convergence behavior that allows one to greatly reduce the systematic error attributed to the perturbative renormalization scheme matching. Further advantages of SMOM are that correlators evaluated with nonexceptional momenta have improved signal-to-noise ratio and that the mass dependence is very mild [96].

In light of these developments we will therefore also use such a nonexceptional, symmetric configuration for the renormalization of our three-quark operators, which is in contrast to previous work on the subject [52, 125]. The generalization of the SMOM concept from two to three quarks is not unique, as having more momenta opens up some additional degrees of freedom. For two momenta, merely imposing the condition that the geometry should be symmetric automatically fixes all three invariants and ensures a nonexceptional configuration. On the other hand, the geometry of three four-vectors is characterized by a total of six independent invariants (p_1^2, p_2^2, p_3^2, $p_1 \cdot p_2$, $p_1 \cdot p_3$, and $p_2 \cdot p_3$). Any symmetric setup for three momenta does require that the individual momenta on the external quark lines have the same magnitude as their sum,

$$p_1^2 = p_2^2 = p_3^2 = (p_1 + p_2 + p_3)^2 = \mu^2 \,, \tag{3.74}$$

which gives us only 4 conditions for these 6 quantities. Furthermore, this symmetry constraint alone does not guarantee a fully nonexceptional configuration, as variants with vanishing partial sums such as $p_1 + p_2 = 0$ are not yet excluded.

At this point we are again faced with a choice, because there are still many different nonexceptional configurations that we could select based on the conditions. From these equally valid but not equivalent options we pick

$$p_1^2 = p_2^2 = p_3^2 = (p_1 + p_2)^2 = (p_1 + p_3)^2 = (p_1 + p_2 + p_3)^2 = \mu^2 \tag{3.75}$$

as our SMOM setup (and from now on the label SMOM will always refer to this particular geometry). Of course we did not select a configuration at random, but rather decided on one that comes with some extra properties that will be useful to us. When evaluated on this momentum configuration, the tree-level vertex functions of our three-quark operator multiplets with derivatives are linearly independent, which is not necessarily true in general. We will make use of this quality in section 3.5.2. While an equation like (3.75) fixes the momentum geometry in an O(4)-invariant manner, an actual calculation will often require explicit expressions for the momentum components. Our SMOM configuration has the advantage that it can be neatly realized in the form of Euclidean four-vectors using only

small integers, for example as

$$p_1 = \tfrac{\mu}{2}\big(+1,+1,+1,+1\big)\,, \tag{3.76a}$$
$$p_2 = \tfrac{\mu}{2}\big(-1,-1,-1,+1\big)\,, \tag{3.76b}$$
$$p_3 = \tfrac{\mu}{2}\big(+1,-1,-1,-1\big)\,, \tag{3.76c}$$

which is what we have used whenever an explicit form of the momenta was needed.

RI′ renormalization condition

The second piece required for the definition of an RI′/SMOM scheme for three-quark operators is the formulation of a well-defined regularization-invariant renormalization condition. Such a construction will have to mimic the properties that we have observed from the RI′ condition for the quark propagator, eq. (2.55). I.e., the renormalized function is defined by enforcing a certain value for its projection onto the Born term. While the principle will be the same as we have seen before, there will be some key differences that we need to take into account. Instead of simple two-point functions we are now dealing with four-point functions with open flavor and Dirac indices as defined in eq. (3.50). Moreover, the renormalization condition will need to properly handle the possibility of operators mixing under renormalization.

Given a number of mixing three-quark operators one might naively try to impose the following condition for a pair of operators (let us call them $\mathcal{O}_m$ and $\mathcal{O}_n$):

$$\lim_{m_q\to 0}\big\langle \Lambda^{\mathrm{RI}}(\mathcal{O}_m), \Lambda^{\mathrm{Born}}(\mathcal{O}_n)\big\rangle\Big|_{\mathrm{SMOM}} \overset{!}{=} \lim_{m_q\to 0}\big\langle \Lambda^{\mathrm{Born}}(\mathcal{O}_m), \Lambda^{\mathrm{Born}}(\mathcal{O}_n)\big\rangle\Big|_{\mathrm{SMOM}}\,, \tag{3.77}$$

where Λ is the amputated vertex function (3.50), SMOM denotes the evaluation at the symmetric renormalization point defined in eq. (3.75) above, and

$$\big\langle M, N\big\rangle = \sum_{\substack{f_1,f_2,f_3\\ \alpha_1,\alpha_2,\alpha_3}} M^{f_1f_2f_3}_{\alpha_1\alpha_2\alpha_3}\big(N^{f_1f_2f_3}_{\alpha_1\alpha_2\alpha_3}\big)^* \tag{3.78}$$

constitutes a scalar product (on the space of the vertex functions) that contracts the flavor and Dirac indices.

However, such a definition of the renormalization condition is actually not very useful, as will become clear when we now examine the transformation behavior. In section 3.4.1 we have discussed three-quark operators that transform as multiplets under the irreducible spinorial representations of $\overline{\mathrm{H}(4)}$. Let $\mathcal{O}^{(i)}$ denote the i-th operator in a multiplet that transforms under the representation R (where R can be τ_1^4, τ_2^4, τ^8, τ_1^{12}, or τ_2^{12}, introduced

in section 2.2.3). From the transformation behavior of operators, spinors, and vectors we can deduce that the vertex function of $\mathcal{O}^{(i)}$ fulfills

$$\begin{aligned}\Lambda(\mathcal{O}^{(i)}|p_1,p_2,p_3)^{f_1f_2f_3}_{\alpha_1\alpha_2\alpha_3} &= [R(g)]_{i'i}\big[\tau_1^4(g)^\dagger\big]_{\alpha_1\alpha_1'}\big[\tau_1^4(g)^\dagger\big]_{\alpha_2\alpha_2'}\big[\tau_1^4(g)^\dagger\big]_{\alpha_3\alpha_3'}\\ &\quad\times\Lambda\big(\mathcal{O}^{(i')}\big|\tau_1^4(g)p_1,\tau_1^4(g)p_2,\tau_1^4(g)p_3\big)^{f_1f_2f_3}_{\alpha_1'\alpha_2'\alpha_3'},\end{aligned}\tag{3.79}$$

for all $g\in\overline{\mathrm{H}(4)}$. Therefore we have for the scalar product involving two of these four-point functions (where $\mathcal{O}_m^{(i)}$ shall denote the i-th operator in the multiplet $\mathcal{O}_m$):

$$\begin{aligned}\big\langle\Lambda(\mathcal{O}_m^{(i)}|p_1,p_2,p_3),\Lambda(\mathcal{O}_n^{(j)}|p_1,p_2,p_3)\big\rangle &= [R(g)]_{i'i}[R(g)^\dagger]_{jj'}\\ &\quad\times\big\langle\Lambda\big(\mathcal{O}_m^{(i')}\big|\tau_1^4(g)p_1,\tau_1^4(g)p_2,\tau_1^4(g)p_3\big),\Lambda\big(\mathcal{O}_n^{(j')}\big|\tau_1^4(g)p_1,\tau_1^4(g)p_2,\tau_1^4(g)p_3\big)\big\rangle\,.\end{aligned}\tag{3.80}$$

This equation exposes a flaw in the naive renormalization condition a la eq. (3.77): The construction is not $\overline{\mathrm{H}(4)}$ invariant. But it also shows us a way around: If we take the sum over all operators in the multiplets, then the representation matrices $R(g)$ drop out,[61]

$$\begin{aligned}\sum_i\big\langle\Lambda(\mathcal{O}_m^{(i)}|p_1,p_2,p_3),\Lambda(\mathcal{O}_n^{(i)}|p_1,p_2,p_3)\big\rangle &=\\ &=\sum_i\big\langle\Lambda\big(\mathcal{O}_m^{(i)}\big|\tau_1^4(g)p_1,\tau_1^4(g)p_2,\tau_1^4(g)p_3\big),\Lambda\big(\mathcal{O}_n^{(i)}\big|\tau_1^4(g)p_1,\tau_1^4(g)p_2,\tau_1^4(g)p_3\big)\big\rangle\,,\end{aligned}\tag{3.81}$$

leaving us with an object that is invariant under rotation of the three quark momenta.

Therefore, the multiplet-averaged Born overlap

$$\big(L^{\mathrm{S}}(\mathscr{R})\big)_{mn}=\lim_{m_q\to0}\sum_i\big\langle\Lambda^{\mathrm{S}}\big((\mathscr{R})_m^{B,(i)}\big),\Lambda^{\mathrm{Born}}\big((\mathscr{R})_n^{B,(i)}\big)\big\rangle\Big|_{\mathrm{SMOM}}\,,\tag{3.82}$$

which will be the foundation of our RI′/SMOM renormalization condition, is well defined: Since all SMOM configurations are isometric to each other, it takes the same value no matter what explicit directions we select for the momenta. Some further remarks on this definition are required: First, the letter $\mathscr{R}$ stands for a combined label indicating the transformation behavior with respect to $\overline{\mathrm{H}(4)}$ and $\mathcal{S}_3$ as well as the number of derivatives. The relevant values for $\mathscr{R}$ are $\mathscr{O}_1^{\underline{12}}$, $\mathscr{D}_1^{\underline{12}}$, $\mathscr{S}_1^{\underline{4}}$, $\mathscr{O}_1^{\underline{4}}$, $\mathscr{S}_{2,D}^{\underline{12}}$, $\mathscr{O}_{2,D}^{\underline{12}}$, $\mathscr{D}_{2,D}^{\underline{12}}$, $\mathscr{S}_{2,DD}^{\underline{4}}$, $\mathscr{O}_{2,DD}^{\underline{4}}$, and $\mathscr{D}_{2,DD}^{\underline{4}}$, shown in table 3.2 on page 73.[62] Second, the operators inserted in the vertex functions on the right-hand side depend on the baryon species and there is no sum implied over the repeated index B. Instead, the object L is independent of B by construction.[63] Third, the letter S

[61] In this equation the sums over repeated (i) run from 1 to the dimension of the representation R, which can be 4, 8, or 12.

[62] The corresponding operator multiplets $(\mathscr{R})_m^B$ are defined in appendix C.2.

[63] This can be seen by inserting explicit expressions for the vertex functions (equation (3.53)) and the flavor structures contained therein (tables C.1–C.4).

specifies which type of vertex function is to be taken. In our calculations, it can indicate the vertex function renormalized in a certain scheme ($\mathrm{S} = \overline{\mathrm{MS}}$ or $\mathrm{S} = \mathrm{RI}'$) as well as the noninteracting ($\mathrm{S} = \mathrm{Born}$) or lattice regularized one ($\mathrm{S} = \mathrm{lat}$).

With that, we can finally state the renormalization condition:

$$L^{\mathrm{RI}'}(\mathscr{R}) \stackrel{!}{=} L^{\mathrm{Born}}(\mathscr{R})\,. \tag{3.83}$$

This is, in general, an equation of matrices. The dimension of these square matrices is given by the number of multiplets that exist for the given $\mathscr{R}$, which can be read off from table 3.2. With our choice for the SMOM geometry, eq. (3.75), it turns out that the matrices L have full rank and are therefore invertible.

We will use this RI′/SMOM scheme for the nonperturbative renormalization of three-quark operators. From the condition given above, it should immediately be clear how to obtain the RI′/SMOM Z-factors. In particular, for the calculation on the lattice we have

$$Z^{\mathrm{lat,RI}'}(\mathscr{R}) = L^{\mathrm{Born}}(\mathscr{R})\big(L^{\mathrm{lat}}(\mathscr{R})\big)^{-1}\,. \tag{3.84}$$

In the lattice study accompanying this work the vertex functions required in the calculation of these renormalization factors have been determined on lattices of volume 32^4 with degenerate quark masses ($m_u = m_d = m_s$). From simulations with four different pseudoscalar meson masses in the range 232–605 MeV the results are extrapolated to $m_\pi^2 = m_K^2 = 0$, which corresponds to the limit $m_q \to 0$ required in the renormalization condition. The SMOM momenta (3.76) are set using twisted boundary conditions [160, 161] in the inversion of the Dirac operator. More information on the lattice setup will be provided in section 4.3.

3.5.3. Conversion to the $\overline{\mathrm{MS}}$ scheme

Up next is the determination of the conversion factors from the RI′/SMOM scheme to the $\overline{\mathrm{MS}}$ scheme. This part of the calculation will be performed in continuum perturbation theory. We are looking for matrices C that fulfill

$$L^{\overline{\mathrm{MS}}}(\mathscr{R}) = C(\mathscr{R})L^{\mathrm{RI}'}(\mathscr{R})\,. \tag{3.85}$$

In principle, one could obtain $C(\mathscr{R})$ as the product of an $\overline{\mathrm{MS}}$ Z-factor for $\mathscr{R}$ with the inverse of the corresponding RI′/SMOM Z-factor. However, from the RI′/SMOM renormalization condition, eq. (3.83), it follows that these conversion factors can also be obtained by evaluating

$$C(\mathscr{R}) = L^{\overline{\mathrm{MS}}}(\mathscr{R})\big(L^{\mathrm{Born}}(\mathscr{R})\big)^{-1}\,, \tag{3.86}$$

which is what we will be using. Similar to the determination of the conversion factor for the quark fields via eq. (2.58), using this method means that one does not have to carry out any continuum RI′/SMOM renormalization explicitly. Instead, knowledge of the $\overline{\text{MS}}$ renormalized vertex functions is sufficient.

Since we have already laid out both the perturbative calculation of the four-point functions and the $\overline{\text{MS}}$ renormalization procedure earlier in this chapter, we can directly proceed to giving the final results for the conversion factors. These results have been obtained in next-to-leading order perturbation theory and will be presented in Landau gauge, as this is the gauge that will be used in the determination of RI′/SMOM renormalization factors on the lattice.

For operators without derivatives, the multiplets in the $\overline{\text{H}(4)}$ representations τ_1^{12} and τ_1^4 are relevant for the renormalization of the octet baryon DA normalization constants of leading and higher twist, respectively. The RI′/SMOM-to-$\overline{\text{MS}}$ renormalization conversion factors for these multiplets are given by

$$C\big(\mathscr{O}_1^{12}\big) = C\big(\mathscr{D}_1^{12}\big)\,, \tag{3.87a}$$

$$C\big(\mathscr{D}_1^{12}\big) = 1 + \frac{\alpha_s}{4\pi}\Big(-\tfrac{5}{9} - \tfrac{5}{81}\pi^2 + \tfrac{10}{27}\ln(2) + \tfrac{4}{27}\psi_1\big(\tfrac{1}{3}\big) - \tfrac{1}{27}\psi_1\big(\tfrac{1}{4}\big)\Big)\,, \tag{3.87b}$$

and

$$C\big(\mathscr{S}_1^4\big) = 1 + \frac{\alpha_s}{4\pi}\Big(\tfrac{17}{3} + \tfrac{14}{27}\pi^2 + \tfrac{2}{9}\ln(2) - \tfrac{4}{9}\psi_1\big(\tfrac{1}{3}\big) - \tfrac{2}{9}\psi_1\big(\tfrac{1}{4}\big)\Big)\,, \tag{3.88a}$$

$$C\big(\mathscr{O}_1^4\big) = C\big(\mathscr{S}_1^4\big)\mathbb{1}_2\,, \tag{3.88b}$$

with the trigamma function

$$\psi_1(z) = \frac{d^2}{dz^2}\ln\big(\Gamma(z)\big) = \int_0^\infty dt\,\frac{te^{-tz}}{1-e^{-t}}\,, \qquad \begin{aligned}\psi_1\big(\tfrac{1}{3}\big) &\approx 10.0956\,,\\ \psi_1\big(\tfrac{1}{4}\big) &\approx 17.1973\,.\end{aligned} \tag{3.89a–c}$$

For the renormalization of first moments of DAs we consider operators with one derivative in the $\overline{\text{H}(4)}$ representation τ_2^{12}. The conversion factor for the singlet multiplet is given by

$$C\big(\mathscr{S}_{2,D}^{12}\big) = 1 + \frac{\alpha_s}{4\pi}\Big(-\tfrac{707}{162} - \tfrac{3625}{23328}\pi^2 + \tfrac{17}{54}\ln(2) + \tfrac{131}{486}\psi_1\big(\tfrac{1}{3}\big) - \tfrac{7}{288}\psi_1\big(\tfrac{1}{4}\big)\Big)\,. \tag{3.90a}$$

For the octet multiplets we have a 4×4 mixing matrix with the diagonal entries

$$C\big(\mathscr{O}_{2,D}^{12}\big)_{11} = 1 + \frac{\alpha_s}{4\pi}\Big(-\tfrac{53}{81} - \tfrac{149}{1458}\pi^2 + \tfrac{8}{27}\ln(2) + \tfrac{44}{243}\psi_1\big(\tfrac{1}{3}\big) - \tfrac{1}{54}\psi_1\big(\tfrac{1}{4}\big)\Big)\,, \tag{3.90b}$$

$$C\big(\mathscr{O}_{2,D}^{12}\big)_{22} = 1 + \frac{\alpha_s}{4\pi}\Big(-\tfrac{845}{162} - \tfrac{5413}{23328}\pi^2 + \tfrac{11}{54}\ln(2) + \tfrac{143}{486}\psi_1\big(\tfrac{1}{3}\big) + \tfrac{31}{864}\psi_1\big(\tfrac{1}{4}\big)\Big)\,, \tag{3.90c}$$

$$C\big(\mathscr{O}_{2,D}^{12}\big)_{33} = C\big(\mathscr{S}_{2,D}^{12}\big)\,, \tag{3.90d}$$

$$C\big(\mathscr{O}_{2,D}^{12}\big)_{44} = 1 + \frac{\alpha_s}{4\pi}\Big(-7 - \tfrac{115}{288}\pi^2 + \tfrac{4}{9}\ln(2) + \tfrac{1}{2}\psi_1\big(\tfrac{1}{3}\big) + \tfrac{19}{288}\psi_1\big(\tfrac{1}{4}\big)\Big)\,. \tag{3.90e}$$

As the only nonvanishing off-diagonal entries we find

$$C\big(\mathscr{O}^{\overline{12}}_{2,D}\big)_{21} = 4C\big(\mathscr{O}^{\overline{12}}_{2,D}\big)_{12} = \sqrt{2}\frac{\alpha_s}{4\pi}\Big(-\tfrac{4}{81} - \tfrac{95}{2916}\pi^2 - \tfrac{2}{27}\ln(2) - \tfrac{5}{243}\psi_1\big(\tfrac{1}{3}\big) + \tfrac{5}{108}\psi_1\big(\tfrac{1}{4}\big)\Big)\,. \tag{3.90f}$$

Similarly, we get a 3×3 mixing matrix for the decuplet multiplets, where the nonzero components are

$$C\big(\mathscr{D}^{\overline{12}}_{2,D}\big)_{mn} = C\big(\mathscr{O}^{\overline{12}}_{2,D}\big)_{mn} \qquad \forall\, m,n \in \{1,2\}\,, \tag{3.90g}$$

$$C\big(\mathscr{D}^{\overline{12}}_{2,D}\big)_{33} = 1 + \frac{\alpha_s}{4\pi}\Big(-\tfrac{11}{3} - \tfrac{19}{54}\pi^2 + \tfrac{4}{9}\ln(2) + \tfrac{4}{9}\psi_1\big(\tfrac{1}{3}\big) + \tfrac{1}{18}\psi_1\big(\tfrac{1}{4}\big)\Big)\,. \tag{3.90h}$$

Since the result for the conversion factors of operators with two derivatives are a bit unwieldy, they have been hidden from the casual reader's eyes and consigned to appendix D.4.

3.5.4. Renormalization of baryon distribution amplitudes

In the previous two sections we have discussed how operator multiplets transforming irreducibly under representations of $\overline{\mathrm{H}(4)}$ can be first renormalized in a RI′/SMOM scheme and then converted to the $\overline{\mathrm{MS}}$ scheme. Now it is time to combine this information and apply it to quantities that are relevant in practice, i.e., to baryon DAs.

From the discussion in section 3.4.1 we already know that the relevant operators for the renormalization of leading twist normalization constants, higher twist normalization constants, and first order shape parameters originate from the representations $\tau_1^{\overline{12}}$, $\tau_1^{\overline{4}}$, and $\tau_2^{\overline{12}}$, respectively. Therefore, we define the combined renormalization and conversion factors as

$$Z^{\mathscr{M}f} = \big(C_q Z_q^{\mathrm{lat,RI'}}\big)^{3/2} C\big(\mathscr{M}_1^{\overline{12}}\big) Z^{\mathrm{lat,RI'}}\big(\mathscr{M}_1^{\overline{12}}\big) \qquad \text{for } \mathscr{M} \in \{\mathscr{O}, \mathscr{D}\}\,, \tag{3.91a}$$

$$Z^{\mathscr{M}\lambda} = \big(C_q Z_q^{\mathrm{lat,RI'}}\big)^{3/2} C\big(\mathscr{M}_1^{\overline{4}}\big) Z^{\mathrm{lat,RI'}}\big(\mathscr{M}_1^{\overline{4}}\big) \qquad \text{for } \mathscr{M} \in \{\mathscr{S}, \mathscr{O}\}\,, \tag{3.91b}$$

$$Z^{\mathscr{M}\varphi_1} = \big(C_q Z_q^{\mathrm{lat,RI'}}\big)^{3/2} C\big(\mathscr{M}_{2,D}^{\overline{12}}\big) Z^{\mathrm{lat,RI'}}\big(\mathscr{M}_{2,D}^{\overline{12}}\big) \qquad \text{for } \mathscr{M} \in \{\mathscr{S}, \mathscr{O}, \mathscr{D}\}\,, \tag{3.91c}$$

including also the necessary quark field renormalization and conversion. As a whole, these products are always gauge invariant.

At the flavor symmetric point, the DAs are independent of the baryon species and we have one leading twist normalization constant ($f^\star$), two higher twist normalization constants ($\lambda_1^\star$, $\lambda_2^\star$), and three different first moments ($\varphi_{00,(1)}^\star$, $\varphi_{11}^\star$, $\varphi_{10}^\star$). The renormalization

of these quantites is governed by the (octet) factors defined above:[64]

$$f^\star = Z^{\mathscr{O}f}\, f^{\star,\mathrm{lat}}\,, \tag{3.92a}$$

$$\begin{pmatrix} \sqrt{6}\lambda_1^\star \\ \lambda_2^\star \end{pmatrix} = Z^{\mathscr{O}\lambda} \begin{pmatrix} \sqrt{6}\lambda_1^\star \\ \lambda_2^\star \end{pmatrix}^{\mathrm{lat}}, \tag{3.92b}$$

$$\begin{pmatrix} \varphi_{00,(1)}^\star \\ \sqrt{2}\varphi_{11}^\star \\ \sqrt{2}\varphi_{10}^\star \end{pmatrix} = Z^{\mathscr{O}\varphi_1} \begin{pmatrix} \varphi_{00,(1)}^\star \\ \sqrt{2}\varphi_{11}^\star \\ \sqrt{2}\varphi_{10}^\star \end{pmatrix}^{\mathrm{lat}}, \tag{3.92c}$$

where the superscript "lat" appearing on the right-hand sides indicates unrenormalized lattice data, while everything on the left-hand sides is now renormalized in the $\overline{\mathrm{MS}}$ scheme. The various square root factors result from an interplay between the normalization factors of operators and observables.

Away from the symmetric point the situation is not as straightforward. All DAs become baryon dependent and new normalization constants as well as new shape parameters belonging to the now independent DAs Π^B emerge. SU(3) flavor symmetry is broken and hence operators with the transformation behavior of singlet or decuplet now also have an impact on the renormalization of octet baryon DAs. The full renormalization patterns can be determined by expressing all normalization constants/shape parameters in terms of moments of standard DAs (cf. the definitions in sections 3.3 and 4.2), connecting these to linear combinations of the operators designed in this work (cf. the definitions and relations in appendix C.2), renormalizing each multiplet with the appropriate renormalization and conversion factors from the equations (3.91) above, and finally re-expressing everything in terms of normalization constants/shape parameters.

In the leading twist sector one has a second normalization constant $f_T^{B\neq\Lambda}$ for all isospin-nonsinglet baryons. The renormalization factors assigned to the transformation behavior of the octet and the decuplet need to be combined to obtain the renormalization matrix:

$$\begin{pmatrix} f^{B\neq\Lambda} \\ f_T^{B\neq\Lambda} \end{pmatrix} = \frac{1}{3} \begin{pmatrix} Z^{\mathscr{O}f} + 2Z^{\mathscr{D}f} & 2Z^{\mathscr{O}f} - 2Z^{\mathscr{D}f} \\ Z^{\mathscr{O}f} - Z^{\mathscr{D}f} & 2Z^{\mathscr{O}f} + Z^{\mathscr{D}f} \end{pmatrix} \begin{pmatrix} f^B \\ f_T^B \end{pmatrix}^{\mathrm{lat}}, \tag{3.93a}$$

$$f^\Lambda = Z^{\mathscr{O}f}\, f^{\Lambda,\mathrm{lat}}\,. \tag{3.93b}$$

If $f_T^{B\neq\Lambda} = f^B$ (as is the case for the nucleon and for the SU(3) symmetric limit), the first equation reduces to a multiplicative renormalization with one and the same factor $Z^{\mathscr{O}f}$. Thus the result at the flavor symmetric point given earlier is reproduced correctly.

[64] $Z^{\mathscr{O}\varphi_1}$ is a 4×4 matrix by definition because there are 4 leading twist operator multiplets in the representation τ_2^{12}. In eq. (3.92c) the symbol $Z^{\mathscr{O}\varphi_1}$ is implied to stand only for its upper left 3×3 block. The fourth row and column serve only to describe mixing related to the operator $\mathcal{O}_{D8}$, which is highly suppressed and therefore neglected, see section 3.4.1.

In the higher twist sector it is the Λ baryon which gains an additional normalization constant (λ_T^Λ) when going away from the symmetric point. For all other baryons, the leading twist normalization constants are still renormalized with the 2×2 octet matrix $Z^{\mathscr{O}\lambda}$, but for the Λ this matrix mingles with the singlet factor $Z^{\mathscr{S}\lambda}$ to describe the mixing of the three higher twist parameters:

$$\begin{pmatrix}\sqrt{6}\lambda_1^{B\neq\Lambda}\\ \lambda_2^{B\neq\Lambda}\end{pmatrix} = Z^{\mathscr{O}\lambda}\begin{pmatrix}\sqrt{6}\lambda_1^{B}\\ \lambda_2^{B}\end{pmatrix}^{\text{lat}}, \tag{3.94a}$$

$$\begin{pmatrix}\sqrt{6}\lambda_1^{\Lambda}\\ \sqrt{6}\lambda_T^{\Lambda}\\ \lambda_2^{\Lambda}\end{pmatrix} = \frac{1}{3}\begin{pmatrix} Z_{11}^{\mathscr{O}\lambda}+2Z^{\mathscr{S}\lambda} & 2Z_{11}^{\mathscr{O}\lambda}-2Z^{\mathscr{S}\lambda} & 3Z_{12}^{\mathscr{O}\lambda}\\ Z_{11}^{\mathscr{O}\lambda}-Z^{\mathscr{S}\lambda} & 2Z_{11}^{\mathscr{O}\lambda}+Z^{\mathscr{S}\lambda} & 3Z_{12}^{\mathscr{O}\lambda}\\ Z_{21}^{\mathscr{O}\lambda} & 2Z_{21}^{\mathscr{O}\lambda} & 3Z_{22}^{\mathscr{O}\lambda}\end{pmatrix}\begin{pmatrix}\sqrt{6}\lambda_1^{\Lambda}\\ \sqrt{6}\lambda_T^{\Lambda}\\ \lambda_2^{\Lambda}\end{pmatrix}^{\text{lat}}. \tag{3.94b}$$

Again, the larger mixing matrix reduces to $Z^{\mathscr{O}\lambda}$ at the symmetric point, where $\lambda_T^\Lambda = \lambda_1^\Lambda$.

In the case of the first moments of the leading twist DAs we work with the $\overline{\mathrm{H}(4)}$ representation τ_2^{12}. Here, operators transforming according to all three representations of $\mathcal{S}_3$ exist, cf. table 3.2. We have one singlet multiplet (renormalization factor $Z^{\mathscr{S}\varphi_1}$), four doublets of octet multiplets (renormalization matrix $Z^{\mathscr{O}\varphi_1}$), and three decuplet multiplets (renormalization matrix $Z^{\mathscr{D}\varphi_1}$). The DAs $\Pi^{B\neq\Lambda}$ are Φ_+-like and lead to two shape parameters ($\pi_{00,(1)}^{B\neq\Lambda}$, $\pi_{11}^{B\neq\Lambda}$) corresponding to symmetric polynomials, whereas the DA Π^Λ is Φ_--like and has a shape parameter ($\pi_{10,(1)}^{\Lambda}$) corresponding to an antisymmetric polynomial, cf. section 3.2.1. The renormalization pattern is

$$\begin{pmatrix}\varphi_{00,(1)}^{B\neq\Lambda}\\ \pi_{00,(1)}^{B\neq\Lambda}\\ \sqrt{2}\varphi_{11}^{B\neq\Lambda}\\ \sqrt{2}\pi_{11}^{B\neq\Lambda}\\ \sqrt{2}\varphi_{10}^{B\neq\Lambda}\end{pmatrix} = \frac{1}{3}\begin{pmatrix} \multicolumn{2}{|c|}{\multirow{2}{*}{$B_{11}^{\varphi_1}$}} & \multicolumn{2}{c|}{\multirow{2}{*}{$B_{12}^{\varphi_1}$}} & 3Z_{13}^{\mathscr{O}\varphi_1}\\ & & & & 3Z_{13}^{\mathscr{O}\varphi_1}\\ \multicolumn{2}{|c|}{\multirow{2}{*}{$B_{21}^{\varphi_1}$}} & \multicolumn{2}{c|}{\multirow{2}{*}{$B_{22}^{\varphi_1}$}} & 3Z_{23}^{\mathscr{O}\varphi_1}\\ & & & & 3Z_{23}^{\mathscr{O}\varphi_1}\\ Z_{31}^{\mathscr{O}\varphi_1} & 2Z_{31}^{\mathscr{O}\varphi_1} & Z_{32}^{\mathscr{O}\varphi_1} & 2Z_{32}^{\mathscr{O}\varphi_1} & 3Z_{33}^{\mathscr{O}\varphi_1}\end{pmatrix}\begin{pmatrix}\varphi_{00,(1)}^{B}\\ \pi_{00,(1)}^{B}\\ \sqrt{2}\varphi_{11}^{B}\\ \sqrt{2}\pi_{11}^{B}\\ \sqrt{2}\varphi_{10}^{B}\end{pmatrix}^{\text{lat}}, \tag{3.95a}$$

$$\begin{pmatrix}\varphi_{00,(1)}^{\Lambda}\\ \sqrt{2}\varphi_{11}^{\Lambda}\\ \sqrt{2}\varphi_{10}^{\Lambda}\\ \sqrt{2}\pi_{10}^{\Lambda}\end{pmatrix} = \frac{1}{3}\begin{pmatrix} 3Z_{11}^{\mathscr{O}\varphi_1} & 3Z_{12}^{\mathscr{O}\varphi_1} & Z_{13}^{\mathscr{O}\varphi_1} & 2Z_{13}^{\mathscr{O}\varphi_1}\\ 3Z_{21}^{\mathscr{O}\varphi_1} & 3Z_{22}^{\mathscr{O}\varphi_1} & Z_{23}^{\mathscr{O}\varphi_1} & 2Z_{23}^{\mathscr{O}\varphi_1}\\ 3Z_{31}^{\mathscr{O}\varphi_1} & 3Z_{32}^{\mathscr{O}\varphi_1} & \multicolumn{2}{c}{\multirow{2}{*}{$B_{33}^{\varphi_1}$}}\\ 3Z_{31}^{\mathscr{O}\varphi_1} & 3Z_{32}^{\mathscr{O}\varphi_1} & & \end{pmatrix}\begin{pmatrix}\varphi_{00,(1)}^{\Lambda}\\ \sqrt{2}\varphi_{11}^{\Lambda}\\ \sqrt{2}\varphi_{10}^{\Lambda}\\ \sqrt{2}\pi_{10}^{\Lambda}\end{pmatrix}^{\text{lat}}, \tag{3.95b}$$

where the interaction between renormalization factors corresponding to different $\mathcal{S}_3$ transformation behavior is encoded in the 2×2 blocks

$$B_{ij}^{\varphi_1} = \begin{cases}\begin{pmatrix} Z_{ij}^{\mathscr{O}\varphi_1}+2Z_{ij}^{\mathscr{D}\varphi_1} & 2Z_{ij}^{\mathscr{O}\varphi_1}-2Z_{ij}^{\mathscr{D}\varphi_1}\\ Z_{ij}^{\mathscr{O}\varphi_1}-Z_{ij}^{\mathscr{D}\varphi_1} & 2Z_{ij}^{\mathscr{O}\varphi_1}+Z_{ij}^{\mathscr{D}\varphi_1}\end{pmatrix} & \forall\, i,j\in\{1,2\}\,,\\ \begin{pmatrix} Z_{33}^{\mathscr{O}\varphi_1}+2Z^{\mathscr{S}\varphi_1} & 2Z_{33}^{\mathscr{O}\varphi_1}-2Z^{\mathscr{S}\varphi_1}\\ Z_{33}^{\mathscr{O}\varphi_1}-Z^{\mathscr{S}\varphi_1} & 2Z_{33}^{\mathscr{O}\varphi_1}+Z^{\mathscr{S}\varphi_1}\end{pmatrix} & \text{for } i=j=3\,.\end{cases} \tag{3.96}$$

In the SU(3) symmetric limit some of the shape parameters coincide ($\pi^{B\neq\Lambda}_{00,(1)} = \varphi^{B}_{00,(1)}$, $\pi^{B\neq\Lambda}_{11} = \varphi^{B}_{11}$, and $\pi^{\Lambda}_{10} = \varphi^{\Lambda}_{10}$), such that both equations become equivalent to eq. (3.92c). At the order of the second moments there will be up to 10 different shape parameters which mix under renormalization. The corresponding formulas can be found in the appendix, equations (D.10)–(D.13).

With the information given in this section we now know everything that is required for the renormalization of normalization constants and shape parameters. This therefore concludes our theoretical discussion regarding the renormalization of octet baryon distribution amplitudes. The next step will be to establish a lattice framework where these quantities can be measured.

Chapter 4

Application to lattice data

4.1. Overview

The development of the renormalization procedure in this work is embedded in an ongoing research effort aimed at providing precise results for the normalization constants and moments of baryon distribution amplitudes. It comprises the first lattice study of baryon DAs using $N_f = 2 + 1$ dynamical flavors, i.e., including the effects of strange quarks. The main selling point of simulations with a dynamical strange quark is that they will grant us a first look at hyperon DAs. The correlators designed to measure moments of SU(3) baryon DAs are given in section 4.2 below.

Our lattice simulations employ state-of-the-art methods, see section 4.3 for a few technical details on the lattice setup. As part of the coordinated lattice simulations (CLS) effort we will have access to a wide range of lattice ensembles including pion masses down to $m_\pi \approx m_\pi^{\text{phys}}$, lattice spacings down to $a \approx 0.04\,\text{fm}$ and lattice sizes up to $64^3 \times 192$. Utilizing their high statistics it will be possible in the future to obtain physical results for the desired quantities and to study sources of systematic errors. In [49] we have recently published early results using just 4 lattices at the single lattice spacing $a = 0.0857\,\text{fm}$. Via chiral perturbation theory the data have been extrapolated to the point of physical meson masses, cf. section 4.5. The results will be presented and discussed in section 4.6.

4.2. Lattice correlation functions

As mentioned in section 3.3, lattice QCD allows us to access moments of the DAs. They are related to matrix elements of local three-quark operators. Lattice calculations of baryon distribution amplitudes customarily [45–48] employ operators which are in the form of four-spinors, such as the one given in eq. (4.1) below. Regrettably, the relation

Table 4.1.: Definition of the Dirac matrix structures that appear in the local operators used in the lattice calculation, see eq. (4.1). Lorentz indices appearing in both $\Gamma_{\bar{r}}^{\mathcal{X}_{\bar{r}}}$ and $\tilde{\Gamma}^{\mathcal{X}_{\bar{r}}}$ are summed over implicitly.

$\mathcal{X}_{\bar{r}}$	$\mathcal{S}$	$\mathcal{P}$	$\mathcal{V}$	$\mathcal{A}$	$\mathcal{T}$	$\mathcal{V}_\rho$	$\mathcal{A}_\rho$	$\mathcal{T}_\rho$
$\Gamma_{\bar{r}}^{\mathcal{X}_{\bar{r}}}$	$\mathbb{1}_4$	γ_5	γ_η	$\gamma_\eta\gamma_5$	$\sigma_{\eta_1\eta_2}$	γ_ρ	$\gamma_\rho\gamma_5$	$i\sigma_{\rho\eta}$
$\tilde{\Gamma}^{\mathcal{X}_{\bar{r}}}$	γ_5	$\mathbb{1}_4$	$\gamma_\eta\gamma_5$	γ_η	$\sigma_{\eta_1\eta_2}\gamma_5$	γ_5	$\mathbb{1}_4$	$\gamma_\eta\gamma_5$

of these objects to the multiplets of operators transforming irreducibly under $\overline{\mathrm{H}(4)}$ is not immediately apparent. Nevertheless, the operators presented in the course of this section are indeed members of such multiplets and the relations are made explicit in appendix C.3.

For the construction of the lattice operators we start from the building block whose general form reads

$$\mathcal{X}^{B,lmn}_{\bar{r}\bar{l}\bar{m}\bar{n}} = \varepsilon^{abc}\Big(\big[i^l D_{\bar{l}} f^T(0)\big]^a C\Gamma_{\bar{r}}^{\mathcal{X}_{\bar{r}}}\big[i^m D_{\bar{m}} g(0)\big]^b\Big)\tilde{\Gamma}^{\mathcal{X}_{\bar{r}}}\big[i^n D_{\bar{n}} h(0)\big]^c\,. \tag{4.1}$$

Here we use a multi-index notation for Lorentz indices, in particular for the covariant derivatives, $D_{\bar{l}} \equiv D_{\lambda_1}\cdots D_{\lambda_l}$, with the integers l, m, and n specifying the number of derivatives acting on the first, second, and third quark, respectively. The quark flavors f, g, h are again set according to the convention for the baryon B specified in eq. (3.3). The Dirac structures that we consider, $\Gamma_{\bar{r}}^{\mathcal{X}_{\bar{r}}}$ and $\tilde{\Gamma}^{\mathcal{X}_{\bar{r}}}$, are listed in table 4.1. $\mathcal{X}_{\bar{r}} = \mathcal{S}, \mathcal{P}, \mathcal{V}, \mathcal{A}, \mathcal{T}$ are used for the higher twist normalization constants, while $\mathcal{X}_{\bar{r}} = \mathcal{V}_\rho, \mathcal{A}_\rho, \mathcal{T}_\rho$ correspond to leading twist.

Moments of baryon DAs can be extracted from the ground state contribution to the two-point correlation functions. Neglecting the exponentially suppressed excited states, the correlation functions can be written as

$$\langle \mathcal{O}_\tau(t,\mathbf{p})\bar{\mathcal{N}}^B_{\tau'}(0)\rangle = \frac{\sqrt{Z_B}}{2E_B}\sum_\lambda \langle 0|\mathcal{O}_\tau(0)|B(\mathbf{p},\lambda)\rangle\, \bar{u}^B_{\tau'}(\mathbf{p},\lambda)e^{-E_B t}\,, \tag{4.2}$$

with the ground state energy $E_B = E_B(\mathbf{p}) = \sqrt{m_B^2 + \mathbf{p}^2}$, where we assume the continuum dispersion relation. Here and in the following the source always sits at the origin, while the operator is projected onto the three-momentum $\mathbf{p}$. As sources for the baryon fields we have used the following interpolating currents (color antisymmetrization is implied):

$$\mathcal{N}^N = \big(u^T C\gamma_5 d\big)u\,, \tag{4.3a}$$
$$\mathcal{N}^\Sigma = \big(d^T C\gamma_5 s\big)d\,, \tag{4.3b}$$
$$\mathcal{N}^\Xi = \big(s^T C\gamma_5 u\big)s\,, \tag{4.3c}$$
$$\mathcal{N}^\Lambda = \tfrac{1}{\sqrt{6}}\big(2\big(u^T C\gamma_5 d\big)s + \big(u^T C\gamma_5 s\big)d + \big(s^T C\gamma_5 d\big)u\big)\,. \tag{4.3d}$$

The other baryons can then be obtained by means of isospin symmetry. In a lattice simulation a process called smearing (see the next section) will be applied to the quark sources in the interpolating currents. This introduces a momentum-dependent coupling $\sqrt{Z_B} = \sqrt{Z_B(\mathbf{p})}$ into the correlators, which describes the overlap between the smeared source operator and the physical baryon ground state. This quantity can be determined by measuring the smeared-smeared correlator

$$\langle \mathcal{N}^B_\tau(t,\mathbf{p})\bar{\mathcal{N}}^B_{\tau'}(0)(\gamma_+)_{\tau'\tau}\rangle = Z_B \frac{m_B + kE_B}{E_B} e^{-E_B t}\,, \tag{4.4}$$

where contracting with $\gamma_+ = (\mathbb{1} + k\gamma_4)/2$ using $k = m_{B^*}/E_{B^*}$ suppresses the leading negative parity contribution [48, 162].[65] The next step will be to define suitable operators and their corresponding lattice correlators that allow for the extraction of the moments X^B_{lmn} $(X = V, A, T)$.

4.2.1. Leading twist – normalization

In order to extract the leading twist normalization constants, the following linear combinations of operators are constructed such that their matrix elements do not contain any contributions of higher twist:

$$\mathcal{O}^{B,000}_{\mathcal{X},\mathfrak{A}} = -\gamma_1 \mathcal{X}^{B,000}_1 + \gamma_2 \mathcal{X}^{B,000}_2\,, \tag{4.5a}$$
$$\mathcal{O}^{B,000}_{\mathcal{X},\mathfrak{B}} = -\gamma_3 \mathcal{X}^{B,000}_3 + \gamma_4 \mathcal{X}^{B,000}_4\,, \tag{4.5b}$$
$$\mathcal{O}^{B,000}_{\mathcal{X},\mathfrak{C}} = -\gamma_1 \mathcal{X}^{B,000}_1 - \gamma_2 \mathcal{X}^{B,000}_2 + \gamma_3 \mathcal{X}^{B,000}_3 + \gamma_4 \mathcal{X}^{B,000}_4\,, \tag{4.5c}$$

where $\mathcal{X}$ can be $\mathcal{V}$, $\mathcal{A}$, or $\mathcal{T}$. For each $\mathcal{X}$, these three four-spinors of operators are related to a 12-dimensional operator multiplet belonging to the $\overline{\mathrm{H}(4)}$ representation τ_1^{12}, cf. eq. (C.18).

The leading twist baryon couplings can be determined from the following correlation functions:

$$\begin{aligned} C^{B,000}_{\mathcal{X},\mathfrak{A}}(t,\mathbf{p}) &= \left\langle \left(\gamma_4 \mathcal{O}^{B,000}_{\mathcal{X},\mathfrak{A}}(t,\mathbf{p})\right)_\tau \bar{\mathcal{N}}^B_{\tau'}(0)(\gamma_+)_{\tau'\tau}\right\rangle \\ &= c_X X^B_{000}\sqrt{Z_B}\frac{k(p_1^2 - p_2^2)}{E_B} e^{-E_B t}\,, \end{aligned} \tag{4.6a}$$
$$\begin{aligned} C^{B,000}_{\mathcal{X},\mathfrak{B}}(t,\mathbf{p}) &= \left\langle \left(\gamma_4 \mathcal{O}^{B,000}_{\mathcal{X},\mathfrak{B}}(t,\mathbf{p})\right)_\tau \bar{\mathcal{N}}^B_{\tau'}(0)(\gamma_+)_{\tau'\tau}\right\rangle \\ &= c_X X^B_{000}\sqrt{Z_B}\frac{E_B(m_B + kE_B) + kp_3^2}{E_B} e^{-E_B t}\,, \end{aligned} \tag{4.6b}$$
$$\begin{aligned} C^{B,000}_{\mathcal{X},\mathfrak{C}}(t,\mathbf{p}) &= \left\langle \left(\gamma_4 \mathcal{O}^{B,000}_{\mathcal{X},\mathfrak{C}}(t,\mathbf{p})\right)_\tau \bar{\mathcal{N}}^B_{\tau'}(0)(\gamma_+)_{\tau'\tau}\right\rangle \\ &= c_X X^B_{000}\sqrt{Z_B}\frac{E_B(m_B + kE_B) + k(p_1^2 + p_2^2 - p_3^2)}{E_B} e^{-E_B t}\,, \end{aligned} \tag{4.6c}$$

[65] B^* denotes the negative parity partner of the baryon B.

where $c_V = c_A = 1$ and $c_T = -2$. Again, $\mathcal{X}$ can be $\mathcal{V}$, $\mathcal{A}$, or $\mathcal{T}$. In practice we want to determine the coupling constants using zero-momentum correlators as they are less noisy and, therefore, can be measured with higher accuracy. For $C^{B,000}_{\mathcal{X},\mathfrak{A}}$ the ground state contribution vanishes for $\mathbf{p} = \mathbf{0}$, thus we consider only $C^{B,000}_{\mathcal{X},\mathfrak{B}}(t,\mathbf{0})$ and $C^{B,000}_{\mathcal{X},\mathfrak{C}}(t,\mathbf{0})$.

4.2.2. Leading twist – moments

First moments of DAs can be calculated utilizing operators containing one covariant derivative. For $l+m+n=1$ we define the leading twist combinations

$$\begin{aligned}
\mathcal{O}^{B,lmn}_{\mathcal{X},\mathfrak{A}} &= +\gamma_1\gamma_3\mathcal{X}^{B,lmn}_{\{13\}} + \gamma_1\gamma_4\mathcal{X}^{B,lmn}_{\{14\}} - \gamma_2\gamma_3\mathcal{X}^{B,lmn}_{\{23\}} - \gamma_2\gamma_4\mathcal{X}^{B,lmn}_{\{24\}} - 2\gamma_1\gamma_2\mathcal{X}^{B,lmn}_{\{12\}}\,,\\
\mathcal{O}^{B,lmn}_{\mathcal{X},\mathfrak{B}} &= +\gamma_1\gamma_3\mathcal{X}^{B,lmn}_{\{13\}} - \gamma_1\gamma_4\mathcal{X}^{B,lmn}_{\{14\}} + \gamma_2\gamma_3\mathcal{X}^{B,lmn}_{\{23\}} - \gamma_2\gamma_4\mathcal{X}^{B,lmn}_{\{24\}} + 2\gamma_3\gamma_4\mathcal{X}^{B,lmn}_{\{34\}}\,,\\
\mathcal{O}^{B,lmn}_{\mathcal{X},\mathfrak{C}} &= -\gamma_1\gamma_3\mathcal{X}^{B,lmn}_{\{13\}} + \gamma_1\gamma_4\mathcal{X}^{B,lmn}_{\{14\}} + \gamma_2\gamma_3\mathcal{X}^{B,lmn}_{\{23\}} - \gamma_2\gamma_4\mathcal{X}^{B,lmn}_{\{24\}}\,, \qquad \text{(4.7a–c)}
\end{aligned}$$

where the braces indicate symmetrization of indices including the appropriate factorial normalization factor. These operators are from the representation $\tau_2^{\frac{12}{2}}$, cf. eqs. (C.19).

For the calculation of the first moments of the leading twist DAs one can use the correlation functions ($l+m+n=1$)

$$\begin{aligned}
C^{B,lmn}_{\mathcal{X},\mathfrak{A},1}(t,\mathbf{p}) &= \left\langle \left(\gamma_4\gamma_1\mathcal{O}^{B,lmn}_{\mathcal{X},\mathfrak{A}}(t,\mathbf{p})\right)_\tau \bar{\mathcal{N}}^B_{\tau'}(0)(\gamma_+)_{\tau'\tau}\right\rangle\\
&= -c_X X^B_{lmn}\sqrt{Z_B}p_1\frac{E_B(m_B+kE_B)+k(2p_2^2-p_3^2)}{E_B}e^{-E_Bt}\,, \qquad \text{(4.8a)}\\
C^{B,lmn}_{\mathcal{X},\mathfrak{A},2}(t,\mathbf{p}) &= \left\langle \left(\gamma_4\gamma_2\mathcal{O}^{B,lmn}_{\mathcal{X},\mathfrak{A}}(t,\mathbf{p})\right)_\tau \bar{\mathcal{N}}^B_{\tau'}(0)(\gamma_+)_{\tau'\tau}\right\rangle\\
&= +c_X X^B_{lmn}\sqrt{Z_B}p_2\frac{E_B(m_B+kE_B)+k(2p_1^2-p_3^2)}{E_B}e^{-E_Bt}\,, \qquad \text{(4.8b)}\\
C^{B,lmn}_{\mathcal{X},\mathfrak{A},3}(t,\mathbf{p}) &= \left\langle \left(\gamma_4\gamma_3\mathcal{O}^{B,lmn}_{\mathcal{X},\mathfrak{A}}(t,\mathbf{p})\right)_\tau \bar{\mathcal{N}}^B_{\tau'}(0)(\gamma_+)_{\tau'\tau}\right\rangle\\
&= -c_X X^B_{lmn}\sqrt{Z_B}p_3\frac{k(p_1^2-p_2^2)}{E_B}e^{-E_Bt}\,, \qquad \text{(4.8c)}
\end{aligned}$$

$$\begin{aligned}
C^{B,lmn}_{\mathcal{X},\mathfrak{B},1}(t,\mathbf{p}) &= \left\langle \left(\gamma_4\gamma_1\mathcal{O}^{B,lmn}_{\mathcal{X},\mathfrak{B}}(t,\mathbf{p})\right)_\tau \bar{\mathcal{N}}^B_{\tau'}(0)(\gamma_+)_{\tau'\tau}\right\rangle\\
&= +c_X X^B_{lmn}\sqrt{Z_B}p_1\frac{E_B(m_B+kE_B)+kp_3^2}{E_B}e^{-E_Bt}\,, \qquad \text{(4.8d)}\\
C^{B,lmn}_{\mathcal{X},\mathfrak{B},2}(t,\mathbf{p}) &= \left\langle \left(\gamma_4\gamma_2\mathcal{O}^{B,lmn}_{\mathcal{X},\mathfrak{B}}(t,\mathbf{p})\right)_\tau \bar{\mathcal{N}}^B_{\tau'}(0)(\gamma_+)_{\tau'\tau}\right\rangle\\
&= +c_X X^B_{lmn}\sqrt{Z_B}p_2\frac{E_B(m_B+kE_B)+kp_3^2}{E_B}e^{-E_Bt}\,, \qquad \text{(4.8e)}\\
C^{B,lmn}_{\mathcal{X},\mathfrak{B},3}(t,\mathbf{p}) &= \left\langle \left(\gamma_4\gamma_3\mathcal{O}^{B,lmn}_{\mathcal{X},\mathfrak{B}}(t,\mathbf{p})\right)_\tau \bar{\mathcal{N}}^B_{\tau'}(0)(\gamma_+)_{\tau'\tau}\right\rangle\\
&= -c_X X^B_{lmn}\sqrt{Z_B}p_3\frac{2E_B(m_B+kE_B)+k(p_1^2+p_2^2)}{E_B}e^{-E_Bt}\,, \qquad \text{(4.8f)}
\end{aligned}$$

$$C^{B,lmn}_{\mathcal{X},\mathfrak{C},1}(t,\mathbf{p}) = \big\langle \big(\gamma_4\gamma_1 \mathcal{O}^{B,lmn}_{\mathcal{X},\mathfrak{C}}(t,\mathbf{p})\big)_\tau \bar{\mathcal{N}}^B_{\tau'}(0)(\gamma_+)_{\tau'\tau}\big\rangle$$
$$= -c_X X^B_{lmn}\sqrt{Z_B}p_1 \frac{E_B(m_B+kE_B)+kp_3^2}{E_B} e^{-E_B t}\,, \tag{4.8g}$$
$$C^{B,lmn}_{\mathcal{X},\mathfrak{C},2}(t,\mathbf{p}) = \big\langle \big(\gamma_4\gamma_2 \mathcal{O}^{B,lmn}_{\mathcal{X},\mathfrak{C}}(t,\mathbf{p})\big)_\tau \bar{\mathcal{N}}^B_{\tau'}(0)(\gamma_+)_{\tau'\tau}\big\rangle$$
$$= +c_X X^B_{lmn}\sqrt{Z_B}p_2 \frac{E_B(m_B+kE_B)+kp_3^2}{E_B} e^{-E_B t}\,, \tag{4.8h}$$
$$C^{B,lmn}_{\mathcal{X},\mathfrak{C},3}(t,\mathbf{p}) = \big\langle \big(\gamma_4\gamma_3 \mathcal{O}^{B,lmn}_{\mathcal{X},\mathfrak{C}}(t,\mathbf{p})\big)_\tau \bar{\mathcal{N}}^B_{\tau'}(0)(\gamma_+)_{\tau'\tau}\big\rangle$$
$$= +c_X X^B_{lmn}\sqrt{Z_B}p_3 \frac{k(p_1^2-p_2^2)}{E_B} e^{-E_B t}\,. \tag{4.8i}$$

One immediately notices that at least one nonzero component of spatial momentum is required to extract the first moments, as otherwise the right-hand sides will simply be equal to zero. We evaluate $C^{B,lmn}_{\mathcal{X},\mathfrak{A},1}$, $C^{B,lmn}_{\mathcal{X},\mathfrak{B},1}$, and $C^{B,lmn}_{\mathcal{X},\mathfrak{C},1}$ with momentum in x-direction, i.e., $\mathbf{p} = \frac{2\pi}{L}(\pm1,0,0)$, and evaluate $C^{B,lmn}_{\mathcal{X},\mathfrak{A},2}$, $C^{B,lmn}_{\mathcal{X},\mathfrak{B},2}$, and $C^{B,lmn}_{\mathcal{X},\mathfrak{C},2}$ with momentum in y-direction, i.e., $\mathbf{p} = \frac{2\pi}{L}(0,\pm1,0)$.[66] For momentum in z-direction ($\mathbf{p} = \frac{2\pi}{L}(0,0,\pm1)$), only the correlator $C^{B,lmn}_{\mathcal{X},\mathfrak{B},3}$ can be used. We do not consider the remaining two correlators as they require a higher number of nonvanishing momentum components, which would lead to larger statistical uncertainties. Finally, operators and correlators suitable for a lattice analysis of the second moments can be found in the appendix, eqs. (D.3)–(D.4).

Using the provided correlators one can determine all zeroth, first, and second moments of the standard leading twist DAs. By evaluating the linear combinations presented in section 3.3 one can thus obtain all leading twist normalization constants and shape parameters up to second order.

4.2.3. Higher twist

Higher twist normalization constants can be calculated from the correlation functions

$$\langle \mathcal{X}^{B,000}_\tau(t,\mathbf{p})\bar{\mathcal{N}}^B_{\tau'}(0)(\gamma_+)_{\tau'\tau}\rangle = \kappa^B_{\mathcal{X}} m_B \sqrt{Z_B}\frac{m_B+kE_B}{E_B} e^{-E_B t}\,, \tag{4.9}$$

where $\mathcal{X}$ can be $\mathcal{S}$, $\mathcal{P}$, $\mathcal{V}$, $\mathcal{A}$, or $\mathcal{T}$, cf. eq. (4.1) and table 4.1. The twist four couplings of interest defined in eqs. (3.21) and (3.22) are given by

$$\lambda_1^{B\neq\Lambda} = -\kappa^B_{\mathcal{V}}\,, \qquad \lambda_1^{\Lambda} = -\sqrt{6}\kappa^\Lambda_{\mathcal{A}}\,,$$
$$\lambda_2^{B\neq\Lambda} = \kappa^B_{\mathcal{T}}\,, \qquad \lambda_2^{\Lambda} = -2\sqrt{6}\big(\kappa^\Lambda_{\mathcal{S}}+\kappa^\Lambda_{\mathcal{P}}\big)\,,$$
$$\lambda_T^{\Lambda} = -\sqrt{6}\big(\kappa^\Lambda_{\mathcal{S}}-\kappa^\Lambda_{\mathcal{P}}\big)\,. \tag{4.10a–e}$$

[66] $L = N_s a$ is the spatial extent of the lattice, cf. table 4.2 on page 101

Due to symmetry properties of the associated operators it follows that

$$\kappa_{\mathcal{S}}^{B\neq\Lambda} = \kappa_{\mathcal{P}}^{B\neq\Lambda} = \kappa_{\mathcal{V}}^{\Lambda} = \kappa_{\mathcal{A}}^{B\neq\Lambda} = \kappa_{\mathcal{T}}^{\Lambda} = 0\,, \tag{4.11}$$

and the corresponding correlators vanish.

4.3. Lattice simulations

In the previous sections we have laid out the principles of how to obtain insight into distribution amplitudes from two-point correlation functions. In practice these correlators are evaluated using lattice QCD. Here we will give some information about our lattice study, but since the specifics of the lattice implementation are not the main focus of this work we will not go into all the minutiae and instead refer the interested reader to our publication [49].

In the analysis we have used lattice ensembles generated within the coordinated lattice simulations effort. These $N_f = 2 + 1$ simulations (i.e., 2 equal-mass light quark flavors and 1 heavier flavor) employ the nonperturbatively $\mathcal{O}(a)$ improved Wilson clover quark action [72, 163–165] and a tree-level Symanzik improved gauge action (Lüscher–Weisz action) [78, 166]. Wuppertal smearing [167] with APE smoothed gauge links [168] is applied to the baryon interpolators (4.3). This procedure generates spatially extended hadron sources that feature enhanced overlap with the desired ground state. The lattice ensembles are generated on supercomputers such as QPACE 2 [169] and analyzed using the Chroma software system [170] with various customizations and optimizations.

A list of the CLS ensembles used in this work is given in table 4.2 and is divided into two parts. The lattices in the first group are used to carry out the measurements of baryon distribution amplitudes from the correlators described in section 4.2, while the ones from the second set are used to produce the necessary RI′/SMOM renormalization factors as defined in section 3.5.2. Let us now address the properties of these lattices, highlighting the differences between the two groups.

First, one can see that the ensembles used for the determination of the observables have a larger volume, especially in time direction. This is desirable since the correlators, cf. eq. (4.2), are studied as functions of the Euclidean time (while the spatial directions are Fourier transformed in order to fix the three-momentum $\mathbf{p}$). On the other hand, the lattices used for renormalization have a shorter time extent, on par with the spatial directions. The vertex functions evaluated there, cf. eq. (3.52), require a Fourier transformation involving all spacetime directions and could not benefit from having one direction larger than the others.

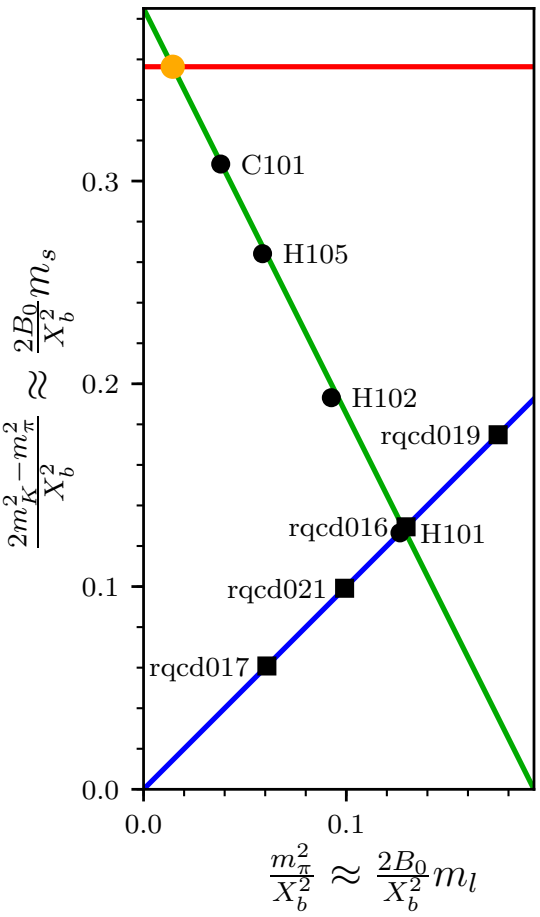

Figure 4.1.: Plot showing the meson masses of the lattice ensembles used in this study. All quantities are made dimensionless using the average octet baryon mass X_b, cf. eq. (4.16b). Along the flavor symmetric line (blue) the pseudoscalar mesons have equal mass ($m_K^2 = m_\pi^2$), which is equivalent to equal quark masses ($m_l = m_s$). The (green) line of physical normalized average quadratic meson mass ($(2m_K^2 + m_\pi^2)/X_b^2 = \text{phys.}$) corresponds to an approximately physical mean quark mass ($2m_l + m_s \approx \text{phys.}$). The red line is defined by $(2m_K^2 - m_\pi^2)/X_b^2 = \text{phys.}$ and indicates an approximately physical strange quark mass ($m_s \approx \text{phys.}$). The orange dot marks the physical point.

Table 4.2.: List of the ensembles used in this work, labeled by their CLS identifier. The lattice coupling $\beta = 3.40 \mathrel{\hat{=}} 6/g^2$ corresponds to the lattice spacing $a \approx 0.0857\,\text{fm}$. N_s and N_t give the number of lattice sites in spatial and temporal direction. The hopping parameters κ_l and κ_s govern the light and strange quark masses. Pion and kaon masses have been obtained from two-point functions. The last column gives the number of gauge field configurations used. An in-depth description of these lattices can be found in [171, 172].

id	β	N_s	N_t	κ_l	κ_s	m_π [MeV]	m_K [MeV]	conf.
C101	3.40	48	96	0.137030	0.136222041	222	474	1552
H105	3.40	32	96	0.136970	0.136340790	280	465	2833
H102	3.40	32	96	0.136865	0.136549339	355	440	1997
H101	3.40	32	96	0.13675962	0.13675962	420	420	2000
rqcd019	3.40	32	32	0.13660	0.13660	605	605	14
rqcd016	3.40	32	32	0.13675962	0.13675962	421	421	11
rqcd021	3.40	32	32	0.136813	0.136813	339	339	9
rqcd017	3.40	32	32	0.136865	0.136865	232	232	9

A related topic are the conditions imposed on the boundary of the finite volumes described by our lattice ensembles. On the longer lattices, open boundary conditions are used for the gauge links in time direction, while on the shorter ones we employ the more conventional periodic boundary conditions. The key point in favor of open boundaries is that they allow for simulations even at fine lattice spacings [173], where simulations using periodic boundaries run into the problem of increasingly large autocorrelation times (topological freezing) [174]. This will be of major importance when going to $a < 0.05\,\text{fm}$ in the future. Yet, at the comparatively larger lattice spacing studied in this work, periodic boundary conditions can still be used without problems [171].

A second difference lies in the masses. As schematically represented in figure 4.1, the ensembles where we calculate our observables are tuned such that the average quark mass reproduces (approximately) the physical value. At the flavor symmetric point (implemented on the H101 lattice), hadrons form SU(3) multiplets and their properties are related by symmetry. Notably, the distribution amplitudes have to be equal for all octet baryons, see eqs. (3.13). The real world is then approached in such a way that u and d quark masses decrease and simultaneously the s quark mass increases while their average is kept constant (the green line in figure 4.1). This course of action is ideal for studying the effects of SU(3) flavor symmetry breaking on DAs while extrapolating to the physical point. Also shown in figure 4.1 are the lattices used for renormalization, which lie on the blue line. Their simulation parameters are chosen such that the masses of all dynamical quark flavors are equal. This sets up a suitable environment for the calculation of the flavor-independent four-point function and the subsequent extrapolation to the chiral limit ($m_l = m_s \to 0$), where the renormalization scheme is defined.

The third and probably most striking difference that can be spotted from table 4.2 is in the number of configurations, which in the end translates to the statistical error achievable. The difference in the magnitude of these numbers is simply due to the fact that two very different calculations are to be performed on those two groups of lattices. In the determination of moments of baryon distribution amplitudes the statistical error has always constituted a major contribution to the total uncertainty. Averaging measurements from many gauge field configurations is absolutely essential in achieving a phenomenologically relevant precision for the final results. In contrast, the statistical error on the lattice renormalization factors just turns out to be very small, even when analyzing just $\mathcal{O}(10)$ configurations. It is completely negligible compared to other, systematic uncertainties inherent to the renormalization procedure.

To determine the moments of baryon distribution amplitudes on a lattice, the two-point functions (see section 4.2) are measured on each gauge field configuration. Suitable correlators are then averaged and a statistical analysis using a bootstrap method is

performed on the $\mathcal{O}(2000)$ configurations per ensemble. Finally, after fitting the expected ground state contributions (i.e., the right-hand sides of the correlator equations from section 4.2) to this data as functions of Euclidean time, we obtain the (unrenormalized) lattice results for the couplings and shape parameters.[67] This lattice analysis has been performed by F. Hutzler.

To renormalize these results we require the lattice RI′/SMOM renormalization factors, defined by eq. (3.84), which have been determined by A. Sternbeck and M. Göckeler. The key ingredient in this calculation are the flavor-independent four-point functions. Let us therefore spend a few words on how to calculate the required vertex functions on the lattice, as the necessary definitions given earlier in this work, eqs. (3.49)–(3.52), are written in the language of continuum QCD. The translation to lattice QCD is as follows: Instead of calculating vacuum expectation values in continuum perturbation theory one has to determine four-point correlation functions nonperturbatively by measuring them on gauge field ensembles. Spacetime integrals for the Fourier transformations are to be discretized by replacing them with sums over all lattice sites and instead of the translation-invariant continuum propagator $S(0-x)$ one has to use the lattice propagator $S(0,x)$.

With the information given here and in the previous sections we have the tools to determine not only the bare lattice results but also the nonperturbative lattice RI′/SMOM renormalization factors as well as the perturbative continuum RI′/SMOM-to-$\overline{\text{MS}}$ conversion factors. Putting all these parts together we can hence extract $\overline{\text{MS}}$ renormalized results for the DAs from each lattice.

4.4. Consistency checks

Now that we have these lattice data at our disposal we can immediately perform various consistency checks, which not only serve as a basic tool to spot possible mistakes but are also directly related to some interesting physics statements, e.g., with respect to renormalization or SU(3) breaking.

4.4.1. $\varphi^B_{00,(1)} = f^B$ and $\pi^{B\neq\Lambda}_{00,(1)} = f^B_T$

First, due to the momentum fraction conserving delta function $\delta(1-x_1-x_2-x_3)$ contained in the integration measure $[dx]$, cf. eq. (3.5), we can express any moment of a DA as a sum

[67] This is, of course, a gross oversimplification of the process. Many subtleties not discussed here have to be taken into account. To name a few, the open boundary conditions complicate averaging correlators with different source positions, the configurations have to be binned to reduce autocorrelations, and the fit ranges have to be optimized to exclude excited state contributions while maintaining good signal-to-noise ratio. See also our paper [49].

of even higher moments:

$$\begin{aligned}\mathrm{DA}_{lmn} &= \int [dx]\, x_1^l x_2^m x_3^n\, \mathrm{DA}(x_1,x_2,x_3) = \int [dx]\, (x_1+x_2+x_3) x_1^l x_2^m x_3^n\, \mathrm{DA}(x_1,x_2,x_3) \\ &= \mathrm{DA}_{(l+1)mn} + \mathrm{DA}_{l(m+1)n} + \mathrm{DA}_{lm(n+1)}\,. \end{aligned} \tag{4.12}$$

An application of this relation to the relevant DAs led to the equalities (3.34), repeated here for convenience:

$$\begin{aligned} &\varphi^B_{00,(2)} = \varphi^B_{00,(1)} = \varphi^B_{00} \equiv f^B\,, && \pi^{B\neq\Lambda}_{00,(2)} = \pi^B_{00,(1)} = \pi^B_{00} \equiv f^B_T\,, \\ &\varphi^B_{11,(2)} = \varphi^B_{11}\,, && \pi^{B\neq\Lambda}_{11,(2)} = \pi^B_{11}\,, \\ &\varphi^B_{10,(2)} = \varphi^B_{10}\,, && \pi^{\Lambda}_{10,(2)} = \pi^{\Lambda}_{10}\,. \end{aligned}$$

In the $\overline{\mathrm{MS}}$ continuum, eq. (4.12) and all equalities derived therefrom are (by definition) exact. Our operators are constructed as multiplets transforming under irreducible representations of $\overline{\mathrm{H}(4)}$ for optimal properties in simulations using hypercubically discretized spacetime. It is clear that such a construction does not reflect the symmetries of the O(4) Euclidean continuum. Furthermore, operators used for the determination of the shape parameters of different order are taken from different representations of $\overline{\mathrm{H}(4)}$. Therefore, we have no reason to expect that the unrenormalized lattice data should fulfill the equalities (3.34). This deviation must be cured by our lattice RI′/SMOM renormalization and continuum $\overline{\mathrm{MS}}$ conversion.

There is yet another issue we need to consider. A determination of higher moments requires additional derivatives in the operators used. In lattice QCD, the derivatives are generally realized as difference quotients [72] and therefore the derivatives will, at finite lattice spacing, always come with some discretization error. The sum rule (4.12) will be broken by these lattice spacing effects even after renormalization has been taken care of.

Having access to lattice data for the zeroth and first moments we can explicitly check $\varphi^B_{00,(1)} \stackrel{?}{=} f^B$ and $\pi^{B\neq\Lambda}_{00,(1)} \stackrel{?}{=} f^B_T$. To study the extent of possible deviations we have collected the values of the ratios $\varphi^B_{00,(1)}/f^B$ and $\pi^{B\neq\Lambda}_{00,(1)}/f^B_T$, both $\overline{\mathrm{MS}}$ renormalized and unrenormalized,[68] in table 4.3. As expected, the unrenormalized ratios differ strongly from unity, by more than 15%, demonstrating that the renormalization program is an essential component for precise lattice studies. In contrast, the $\overline{\mathrm{MS}}$ renormalized values lie much closer to one, deviating by less than 4%, serving as a check for the correctness of our renormalization. We attribute the remaining deviation to discretization errors caused by the derivatives in the three-quark operators, which should vanish in the continuum limit.

[68] Since chiral extrapolation is performed after renormalization these values are not taken from the physical point but from C101, the ensemble whose meson masses are closest to the physical ones, see table 4.2.

Table 4.3.: The normalizations of the leading twist DAs calculated from first moments divided by the same normalizations calculated as a zeroth moment. The values are obtained from the C101 lattice and given in the $\overline{\text{MS}}$ scheme (at 2 GeV) as well as unrenormalized (bare). Errors in parentheses are statistical.

	$\varphi^N_{00,(1)}/f^N$	$\varphi^\Sigma_{00,(1)}/f^\Sigma$	$\varphi^\Xi_{00,(1)}/f^\Xi$	$\varphi^\Lambda_{00,(1)}/f^\Lambda$	$\pi^\Sigma_{00,(1)}/f^\Sigma_T$	$\pi^\Xi_{00,(1)}/f^\Xi_T$
$\overline{\text{MS}}$	0.988(35)	0.971(17)	0.963(13)	0.971(23)	0.965(17)	0.967(13)
bare	0.842(30)	0.827(14)	0.820(11)	0.827(19)	0.822(14)	0.824(11)

Since our dataset consists of lattices of only one lattice spacing ($a = 0.0857\,\text{fm}$) we cannot currently substantiate our claim by performing this limit. Instead, we refer to [48], where in a study of nucleon distribution amplitudes (using a similar lattice action) comparable deviations have been observed. A continuum extrapolation from three lattices with different spacings has been shown to give a result in agreement with the value 1, indicating that discretization errors stemming from covariant derivatives in three-quark operators are under control.

4.4.2. $\lambda_2^{B\neq\Lambda} \approx -2\lambda_1^B$ and $\lambda_2^\Lambda \approx -2\lambda_T^\Lambda$

Next, let us look at relations involving the higher twist normalization constants. For the proton the approximate equality $\lambda_2^N \approx -2\lambda_1^N$ is well known [47, 162, 175]. It is a consequence of the associated local matrix element,

$$\langle 0|\big(u^T(0)Cd(0)\big)\gamma_5 u(0)|N(p,\lambda)\rangle = 8(\lambda_2^N + 2\lambda_1^N)m_N u^N(p,\lambda)\,, \tag{4.13}$$

vanishing in the nonrelativistic limit [162]. From our data it can be seen that the same holds analogously for the other isospin-nonsinglet baryons Σ and Ξ, but not for the Λ baryon. Instead, we find a new approximate equality $\lambda_2^\Lambda \approx -2\lambda_T^\Lambda$, corresponding to the similar matrix element

$$\langle 0|\big(u^T(0)Cd(0)\big)\gamma_5 s(0)|\Lambda(p,\lambda)\rangle = \tfrac{-1}{4\sqrt{6}}(\lambda_2^\Lambda + 2\lambda_T^\Lambda)m_\Lambda u^\Lambda(p,\lambda)\,. \tag{4.14}$$

To illustrate that these approximate equalities are fulfilled well by our results we present the data for the ratios $-2\lambda_1^{B\neq\Lambda}/\lambda_2^{B\neq\Lambda}$ and $-2\lambda_T^\Lambda/\lambda_2^\Lambda$ in table 4.4.

Looking at the situation from the perspective of renormalization one might naively expect that renormalization factors will cancel in the ratios, especially since all higher twist normalization constants are calculated using operators from the same $\overline{\text{H}(4)}$ representation τ_1^4. In reality this need not necessarily be true because all higher twist couplings can mix under renormalization. Having worked out the renormalization behavior explicitly we find that

Table 4.4.: Ratios of higher twist normalization constants (see section 4.4.2) and of leading twist normalization constants (see section 4.4.3). The values are obtained from the C101 lattice and given in the $\overline{\text{MS}}$ scheme (at 2 GeV) as well as unrenormalized (bare). Errors in parentheses are statistical.

	$-2\lambda_1^N/\lambda_2^N$	$-2\lambda_1^\Sigma/\lambda_2^\Sigma$	$-2\lambda_1^\Xi/\lambda_2^\Xi$	$-2\lambda_T^\Lambda/\lambda_2^\Lambda$	$\big(f^\Sigma + f^\Xi\big)\big/\big(f_T^\Sigma + f_T^\Xi\big)$
$\overline{\text{MS}}$	0.985(25)	1.031(14)	0.990(11)	1.012(16)	1.004(1)
bare	0.985(25)	1.027(14)	0.989(11)	1.011(16)	1.004(1)

the renormalized and unrenormalized values agree with each other (see table 4.4) and that indeed the naive expectation does come true due to the small off-diagonal elements in these renormalization factors.

4.4.3. $f^\Sigma + f^\Xi \approx f_T^\Sigma + f_T^\Xi$

There is yet another quantity we can examine. In our article [49] we have presented a new identity involving the distribution amplitudes of the Σ and Ξ baryons:

$$0 = \Phi_+^\Sigma(x_1,x_2,x_3) + \Phi_+^\Xi(x_1,x_2,x_3) - \Pi^\Sigma(x_1,x_2,x_3) - \Pi^\Xi(x_1,x_2,x_3) + \mathcal{O}(\delta m^2)\,, \quad (4.15)$$

where δm is a dimensionless parameter measuring the strength of SU(3) breaking [33, 49]:

$$\delta m = \frac{4(m_K^2 - m_\pi^2)}{3X_b^2}\,, \quad (4.16a)$$

$$X_b = (2m_N + 3m_\Sigma + 2m_\Xi + m_\Lambda)/8\,. \quad (4.16b)$$

This combination of DAs has been constructed such that the SU(3) breaking is minimal, i.e., all terms linear in δm cancel. Hence, it has the same theory status as the famous Gell-Mann–Okubo (GMO) sum rule for baryon masses [176, 177],

$$0 = 2m_N - m_\Sigma + 2m_\Xi - 3m_\Lambda + \mathcal{O}(\delta m^2)\,, \quad (4.17)$$

whose almost exact realization in nature (i.e., for the experimentally determined baryon masses available in [58]) is widely known:

$$\frac{2m_N + 2m_\Xi}{m_\Sigma + 3m_\Lambda} \approx 0.994\,. \quad (4.18)$$

The sum rule (4.15), while in principle valid for the full DAs (which are however unknown), also holds order by order in the moments. Let us therefore investigate the most relevant contribution, namely the normalizations. The corresponding GMO-like sum rule reads

$$0 = f^\Sigma + f^\Xi - f_T^\Sigma - f_T^\Xi + \mathcal{O}(\delta m^2)\,, \quad (4.19)$$

and it is fulfilled exceptionally well by our data, see table 4.4.

4.5. Chiral extrapolation

The lattice simulations for the DAs have been performed on four ensembles with four different — but always unphysical — mass parameters (see table 4.2 on page 101). In particular, we always have $m_\pi > m_\pi^{\text{phys}}$. Such simulations come with the advantage that they are less computer time intensive than runs with the true physical masses. But in the end, we are always interested in the DAs at the physical point, and therefore we will have to find a way to bridge the gap between the unphysical mass regime simulated in lattice QCD and the physical reality. The proper tools for this task at hand are provided by chiral perturbation theory [79].

This effective field theory technique approximates QCD via Lagrangians formulated not in terms of the basic degrees of freedom (quarks and gluons), but rather in terms of baryons and mesons (i.e., the relevant degrees of freedom in the nonperturbative low-energy regime of QCD). ChPT has many different applications [178], but we shall focus on its use alongside lattice simulations: Using ChPT one can determine the behavior of various observables as a function of the light pseudoscalar meson masses (which are in turn related to the quark masses). To get a physically relevant result one generates multiple lattices with different unphysical masses, fits the expected ChPT behavior to the data and then uses the fitted function to extrapolate to the physical point.

In [33] such extrapolation formulae have been derived for all octet baryon distribution amplitudes in the framework of covariant baryon chiral perturbation theory [179, 180] with three flavors in leading one-loop order. The lattice ensembles analysed in our study have all been tuned to have approximately physical average quark mass, i.e., they lie on the green line in figure 4.1. This particular choice allows one to parametrize the normalization constants and shape parameters as functions of the single variable δm, which has been defined in eq. (4.16a).

As an example, let us look at the ChPT formulas for the leading twist normalization constants (the formulas for the other quantities can be found in [33]):

$$f^B(\delta m) = g^B_{\Phi_+}(\delta m)\big(f^\star + \delta m\, \Delta f^B\big)\,, \tag{4.20a}$$

$$f_T^{B\neq\Lambda}(\delta m) = g^B_{\Pi}(\delta m)\big(f^\star + \delta m\, \Delta f_T^B\big)\,. \tag{4.20b}$$

(A fit of these functions to the renormalized lattice data will be shown in figure 4.2.) Using this ansatz, all our data points pertaining to the 6 observables f^N, f^Σ, f^Ξ, f^Λ, f_T^Σ, and f_T^Ξ are described by a set of 7 fit parameters. They are $f^\star$, which corresponds to the value at the symmetric point ($\delta m = 0$) and is therefore independent of the baryon species (cf. eq. (3.13a)), as well as Δf^N, Δf^Σ, Δf^Ξ, Δf^Λ, Δf_T^Σ, and Δf_T^Ξ, which are responsible for the splitting between different baryons away from the symmetric point. The curvature

of the extrapolation functions is governed by the prefactors g^B_{DA} that contain the chiral logarithms. They are functions of δm, normalized as $g^B_{\mathrm{DA}}(0) = 1$, and independent of the fit parameters.[69] The complete expressions for these prefactors will not be given here, as they can be read off from [33].

Using SU(3) ChPT one also finds that the symmetry breaking behavior in baryon DAs should, at leading chiral order, obey some additional constraints, i.e., not all amplitudes are independent [33]. In the leading twist sector, these constraints on the distribution amplitudes translate to the following relations between the fit parameters introduced above:

$$\Delta f^{\Xi} = -\Delta f^{\Sigma} - \Delta f^{N}\,, \tag{4.21a}$$

$$\Delta f_T^{\Sigma} = -\tfrac{3}{2}\Delta f^{\Lambda} - \tfrac{1}{2}\Delta f^{\Sigma}\,, \tag{4.21b}$$

$$\Delta f_T^{\Xi} = \tfrac{3}{2}\Delta f^{\Lambda} + \tfrac{1}{2}\Delta f^{\Sigma} - \Delta f^{N}\,. \tag{4.21c}$$

This would reduce the number of free parameters in a fit to the normalization constants from 7 to 4. However, SU(3) constraints such as these need only hold in the continuum and can in principle be broken by discretization effects on the lattice. Therefore, fits which simply enforce these relations might not be the best ansatz to describe results at a fixed nonzero lattice spacing. Indeed, we found that especially for the leading twist normalization constants these constraints are violated in our data. With our current dataset that is limited to just one spacing we are unable to examine the continuum limit, but in future studies it will be interesting to observe whether the breaking of SU(3) constraints decreases while advancing towards the continuum by analyzing data at various smaller lattice spacings. In the following, we will only show the analysis where all constraints on the DAs responsible for the SU(3) flavor symmetry breaking are ignored, as such fits are better suited for describing data at fixed nonzero a. For more information on the topic and for plots showing the fits including the SU(3) constraints see [49].

Figures 4.2–4.4 show the results of chiral fits (performed by P. Wein for our article [49]) to the full set of lattice data consisting of the leading twist normalization constants, the leading twist first order shape parameters, and the higher twist normalization constants. In all of these figures the red dotted line on the right side marks the physical point, while the leftmost data point corresponds to the symmetric point with approximately physical average quark mass (H101 lattice). The curves show the fitted mean value together with one-sigma error bands. Overall, one can see that the unconstrained leading one-loop order SU(3) ChPT formulae are suited to treat our lattice data, as most observables are described rather well by the fitted functions (χ^2 per degree of freedom is smaller than 1.5 in all fits).

[69] They do however depend on other ChPT parameters such as the ubiquitous pion decay constant or the axial low-energy constants, D and F, which are treated as fixed input values, see [33, 49].

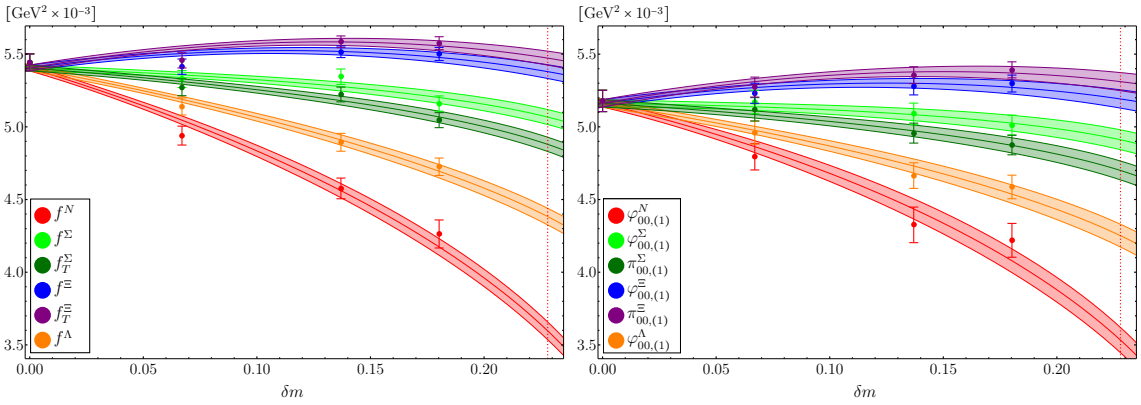

Figure 4.2.: Fit for the leading twist normalization constants f^B, $f_T^{B\neq\Lambda}$ (left) and the equivalent first moments $\varphi^B_{00,(1)}$, $\pi^{B\neq\Lambda}_{00,(1)}$ (right).

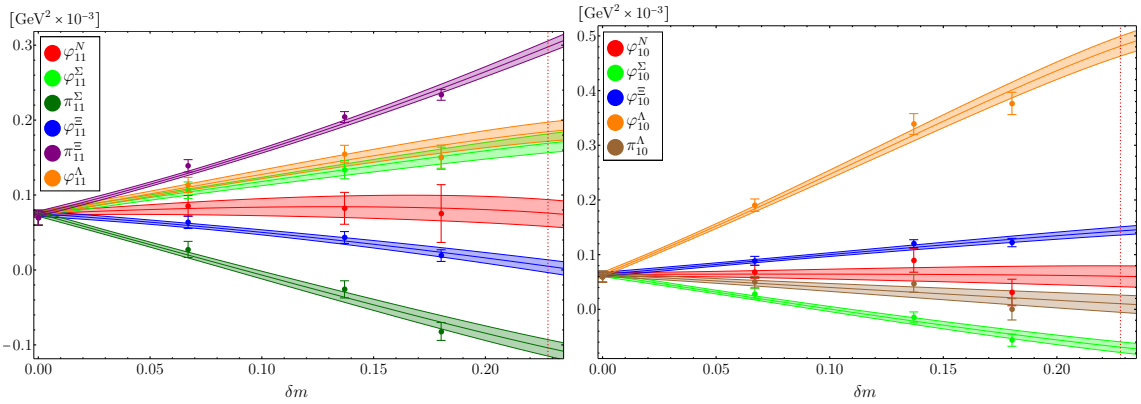

Figure 4.3.: Fit for the leading twist first moments φ^B_{11}, $\pi^{B\neq\Lambda}_{11}$ (left) and φ^B_{10}, π^Λ_{10} (right).

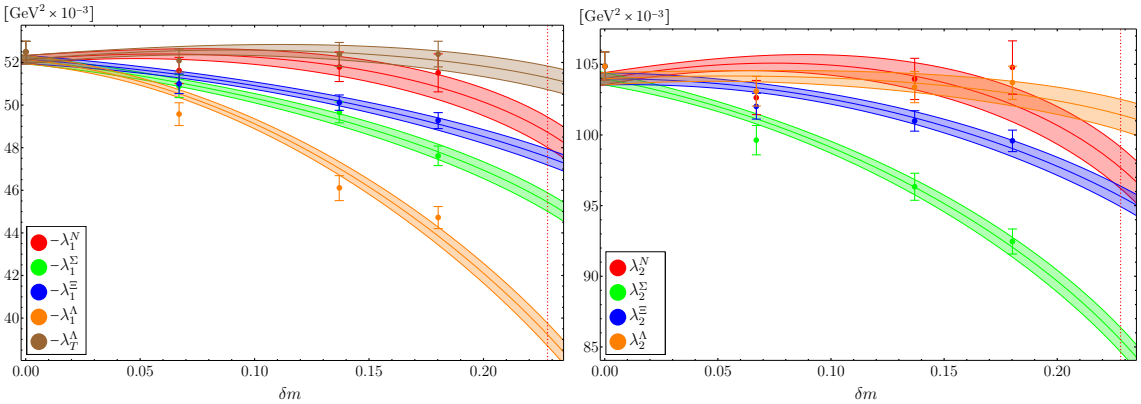

Figure 4.4.: Fit for the chiral-odd higher twist normalization constants λ_1^B, λ_T^Λ (left) and the chiral-even higher twist normalization constants λ_2^B (right).

We take the values obtained by extrapolating these fits to the physical point as our final results, which will be discussed in the next section.

4.6. Results

In table 4.5 we have collected the chirally extrapolated results for all quantities that have been examined in this study. The values are followed by two types of errors given in parentheses. The first ones are the statistical uncertainties obtained by propagating the error bars of the data points via the chiral fits presented in the previous section, while the second ones try to quantify the uncertainty in the renormalization factors. As mentioned previously, the statistical errors in the renormalization calculation are extremely small, therfore the goal shall be to gauge the systematics. To this effect, we perform the analysis including the chiral extrapolation a total of three times. First, with renormalization factors determined at $\mu^2 = 4\,\mathrm{GeV}^2$ (which we take as the central values). Second, with renormalization factors determined at $\mu^2 = 10\,\mathrm{GeV}^2$, followed by a perturbative renormalization group evolution back down to $\mu^2 = 4\,\mathrm{GeV}^2$ (to account for some uncertainty in setting the renormalization scale).[70] And third, neglecting the perturbative corrections in the conversion factors (to measure the extent of the loop effects). Then we take the difference between the first and second analysis as well as one half of the difference between the first and third (as the effect of higher loop corrections is expected to be smaller than the leading ones) and finally add these two quantities in quadrature to get an estimate for the error.

Let us now discuss our results in detail, starting with the normalization constants. To reiterate and illustrate what has been discussed in section 4.4.1, one can see by comparing the left and right panel in figure 4.2 that the extrapolated values for f^B, $f_T^{B\neq\Lambda}$ and $\varphi^B_{00,(1)}$, $\pi^{B\neq\Lambda}_{00,(1)}$ almost agree with each other, i.e., the sum rules (3.34) are broken only very mildly by the discretization effects in the derivatives. Comparing the size of the normalization constants of the nucleon to what has been obtained in the previous $N_f = 2$ study [48] our values are larger by 30% in case of f^N and by 20% for λ_1^N and λ_2^N. However, the final values quoted therein are taken after a continuum extrapolation has been performed. As one can see from their figure 7,[71] this amount corresponds to the effect of the continuum extrapolation and therefore our results at $a \approx 0.0857\,\mathrm{fm}$ are indeed compatible with what has been obtained at $a \approx 0.0813\,\mathrm{fm}$ in the older analysis. Conversely, this also means that we have to expect our result for f^N to be modified by about 30%

[70] The nonperturbative determination of the renormalization factors is performed for multiple sets of momenta of different magnitudes, and therefore different scales, by varying the twist parameter. The value at a certain target scale is then obtained by interpolating between these data points.

[71] Here we refer to the figure numbers in the journal version of [48], which differ from the `arXiv` preprint.

Table 4.5.: Couplings and shape parameters obtained from the unconstrained fits. All values are given in units of GeV^2 in the $\overline{\mathrm{MS}}$ scheme at a scale $\mu = 2\,\mathrm{GeV}$. The number in the first parentheses gives the statistical error after chiral extrapolation. The second one is an estimate of the systematic error due to the renormalization procedure.

B	N	Σ	Ξ	Λ
$f^B \times 10^3$	3.60(6)(2)	5.07(5)(2)	5.38(5)(2)	4.38(6)(2)
$f_T^B \times 10^3$	3.60(6)(2)	4.88(5)(2)	5.47(5)(2)	—
$\varphi^B_{00,(1)} \times 10^3$	3.53(9)(2)	4.91(7)(2)	5.19(6)(2)	4.25(8)(2)
$\pi^B_{00,(1)} \times 10^3$	3.53(9)(2)	4.70(6)(2)	5.31(6)(2)	—
$\varphi^B_{11} \times 10^3$	0.08(2)(1)	0.17(1)(2)	0.01(1)(2)	0.18(1)(1)
$\pi^B_{11} \times 10^3$	0.08(2)(1)	−0.10(1)(3)	0.30(1)(1)	—
$\varphi^B_{10} \times 10^3$	0.060(19)(3)	−0.069(10)(3)	0.14(1)(1)	0.48(2)(3)
$\pi^B_{10} \times 10^3$	—	—	—	0.010(16)(1)
$\lambda_1^B \times 10^3$	−49(1)(2)	−45.4(4)(21)	−47.6(4)(23)	−39(1)(2)
$\lambda_T^B \times 10^3$	—	—	—	−51(1)(2)
$\lambda_2^B \times 10^3$	98(1)(5)	86(1)(4)	96(1)(5)	101(1)(5)

once we are able to take the continuum limit, as our lattice action is similar to the one used in [48] and hence the discretization effects should be of comparable size.

As far as the size of f^N is concerned, lattice QCD and sum rule calculations have been known to be in disagreement for quite some time. The previous lattice studies [45–48] all favor values that are a bit smaller than what has been obtained in older leading order sum rule calculations [15, 38, 181]. This motivated an updated sum rule calculation at next-to-leading order [39], which showed that the first order radiative corrections are reasonably small. Therefore, it is very unlikely that the difference is only due to higher order perturbative effects. Our new lattice determination of f^N falls into the same range as the values obtained in the other lattice studies. While this shows parity among different lattice QCD simulations, it also means that, at present, the tension with QCD sum rules is not resolved. A comparison of some of the different results can be found in table 4.6.

Also for the first moments of the nucleon we find values that are in agreement with the previous lattice study,[72] but are significantly smaller than the older sum rule estimates. In case of the nucleon the approximate equality $\varphi^N_{10} \approx \varphi^N_{11}$ discussed in [48] is fulfilled by our results within errors. And while the absolute values for the first moments are small, we do observe enormous relative SU(3) breaking, e.g., $\pi^\Xi_{11} \gtrsim 3\varphi^N_{11}$ and $\varphi^\Lambda_{10} \gtrsim 7\varphi^N_{10}$. This is a

[72] Note that (unlike f^N) the moments have not been extrapolated to the continuum in [48], and that φ^N_{nk} in our notation corresponds to $f_N\varphi^N_{nk}$ in theirs.

Table 4.6.: Comparison of the central values of our $N_f = 2+1$ results (see table 4.5) with the $N_f = 2$ lattice study for the nucleon [48], the Chernyak–Ogloblin–Zhitnitsky (COZ) model [38] (which is based on leading order sum rules), and the next-to-leading order sum rule calculation [39]. All values are given in units of GeV^2. All quantities have been converted to the conventions established in this work and rescaled to $\mu = 2\,\mathrm{GeV}$, using the three-loop evolution equation for the couplings with the anomalous dimensions calculated in [136] and the one-loop equations (3.19) for the shape parameters. Note that f_Λ^T in [38] is proportional to the first moment π_{10}^Λ in our nomenclature.

B	work	method	$f^B\times10^3$	$f_T^B\times10^3$	$\varphi_{11}^B\times10^3$	$\pi_{11}^B\times10^3$	$\varphi_{10}^B\times10^3$	$\pi_{10}^B\times10^3$
N	ours	$N_f = 2+1$	3.60	3.60	0.08	0.08	0.06	—
	[48]	$N_f = 2$	2.84	2.84	0.085	0.085	0.082	—
	[38]	COZ	4.55	4.55	0.885	0.885	0.748	—
	[39]	NLO SR	4.65	4.65	—	—	—	—
Σ	ours	$N_f = 2+1$	5.07	4.88	0.17	−0.10	−0.069	—
	[38]	COZ	4.65	4.46	1.11	0.511	0.523	—
Ξ	ours	$N_f = 2+1$	5.38	5.47	0.01	0.30	0.14	—
	[38]	COZ	4.83	4.92	0.685	1.10	0.883	—
Λ	ours	$N_f = 2+1$	4.38	—	0.18	—	0.48	0.01
	[38]	COZ	4.69	—	1.05	—	1.39	1.32

remarkable new finding, as it is contrary to the case of the normalization constants, which differ by at most 50% between the various SU(3) octet baryons.

Our data shows furthermore that both of the first order shape parameters of the nucleon exhibit almost no δm dependence (see the red bands in figure 4.3), i.e., the light-cone momentum distribution in a nucleon is mostly invariant under a change of quark masses. The likely reason is that all valence quarks in a nucleon are light quarks and that there is no relative change in quark masses when going from the symmetric to the physical point. All other octet baryons contain at least one strange quark, and (as we will see from the discussion of figure 4.5 below) these heavier quarks have significant effects on the momentum distribution. In a sense, nucleons are therefore the real world baryons that are most similar to the theoretical concept of baryons at the symmetric point.

To best visualize distribution amplitudes one can make so-called barycentric plots [182], in which the support of the DAs ($0 \le x_1, x_2, x_3 \le 1$ with the constraint $x_1 + x_2 + x_3 = 1$) is mapped to an equilateral triangle. We shall do so for the standard DAs, $[V-A]^B$ and T^B (see section 3.2.1 for the relevant definitions), as these are the most convenient in phenomenological applications and also come with a straightforward physical interpretation:

The two DAs directly correspond to the two Fock states $f^\uparrow g^\downarrow h^\uparrow$ and $f^\uparrow g^\uparrow h^\downarrow$, respectively (cf. eqs. (3.14)), and the three variables x_i are interpreted as light-cone momentum fractions of the three constituent quarks. In figure 4.5 we show these plots, where for each DA the "boring" asymptotic part has been subtracted and the relevant overall normalization factor has been divided out, so that the interesting effects of the shape parameters are immediately visible and their relative strength can be compared across different DAs. The plots are realized as combined density and contour plots and are overlaid with red, blue, and green lines, which are lines of constant x_1, x_2, and x_3, respectively.

In case of the nucleon DA $[V-A]^B$ we observe an approximate symmetry under exchange of x_2 and x_3 (due to the previously mentioned relation $\varphi_{10}^N \approx \varphi_{11}^N$), which means that in the $u^\uparrow u^\downarrow d^\uparrow$ Fock state the second and third quark carry similar momentum fractions. Meanwhile, the leading $u^\uparrow$ quark, which has the same helicity as the nucleon state, carries the largest fraction of the light-cone momentum. These findings are in agreement with many earlier works [15, 38, 48]. It is worth mentioning however, that the approximate equality among the first order shape parameters is observed at a typical hadronic scale (here we have $\mu = 2\,\mathrm{GeV}$) and need not continue to hold when going to a scale of different magnitude, as the two first moments have different behavior under scale evolution, see eqs. (3.20).

In contrast, the symmetry that can be observed in the $u^\uparrow u^\uparrow d^\downarrow$ nucleon state (which is described by T^N) is universal and scale independent, as all amplitudes T^B have a definite symmetry property under exchange of x_1 and x_2, see eqs. (3.10). T^N, however, is not an independent DA. Taking into account the isospin relation (3.11), the spin-flavor structure of the nucleon light-cone wave function (3.14a) can be presented, schematically, as $[V-A]^N u^\uparrow(u^\downarrow d^\uparrow - d^\downarrow u^\uparrow)$. In this picture the symmetry under $x_2 \leftrightarrow x_3$ may be interpreted as an indication for these two valence quarks forming a dynamical scalar "diquark" [183]. This symmetry is assumed in many models, e.g., [184].

For the Σ hyperon we observe that the peak of both leading twist distribution amplitudes is shifted towards the single strange quark. In the $d^\uparrow d^\downarrow s^\uparrow$ Fock state this happens mostly at the expense of the $d^\downarrow$ quark, while in the $d^\uparrow d^\uparrow s^\downarrow$ state the s quark gathers additional momentum from both light quarks equally. The Ξ baryon contains two strange quarks which both carry more momentum than the single light quark. In the $s^\uparrow s^\downarrow u^\uparrow$ state the $s^\uparrow$ quark carries the largest fraction, while in the $s^\uparrow s^\uparrow u^\downarrow$ Fock state both s quarks contribute equally. As far as the size of these effects are concerned we find that for the Σ the magnitude is comparable to the nucleon, whereas the Ξ exhibits somewhat larger deviations from the asymptotic shape.

Overall, we find that the picture for the isospin-nonsinglet baryons can be described in terms of two competing patterns. First, the heavier strange quarks carry in general a

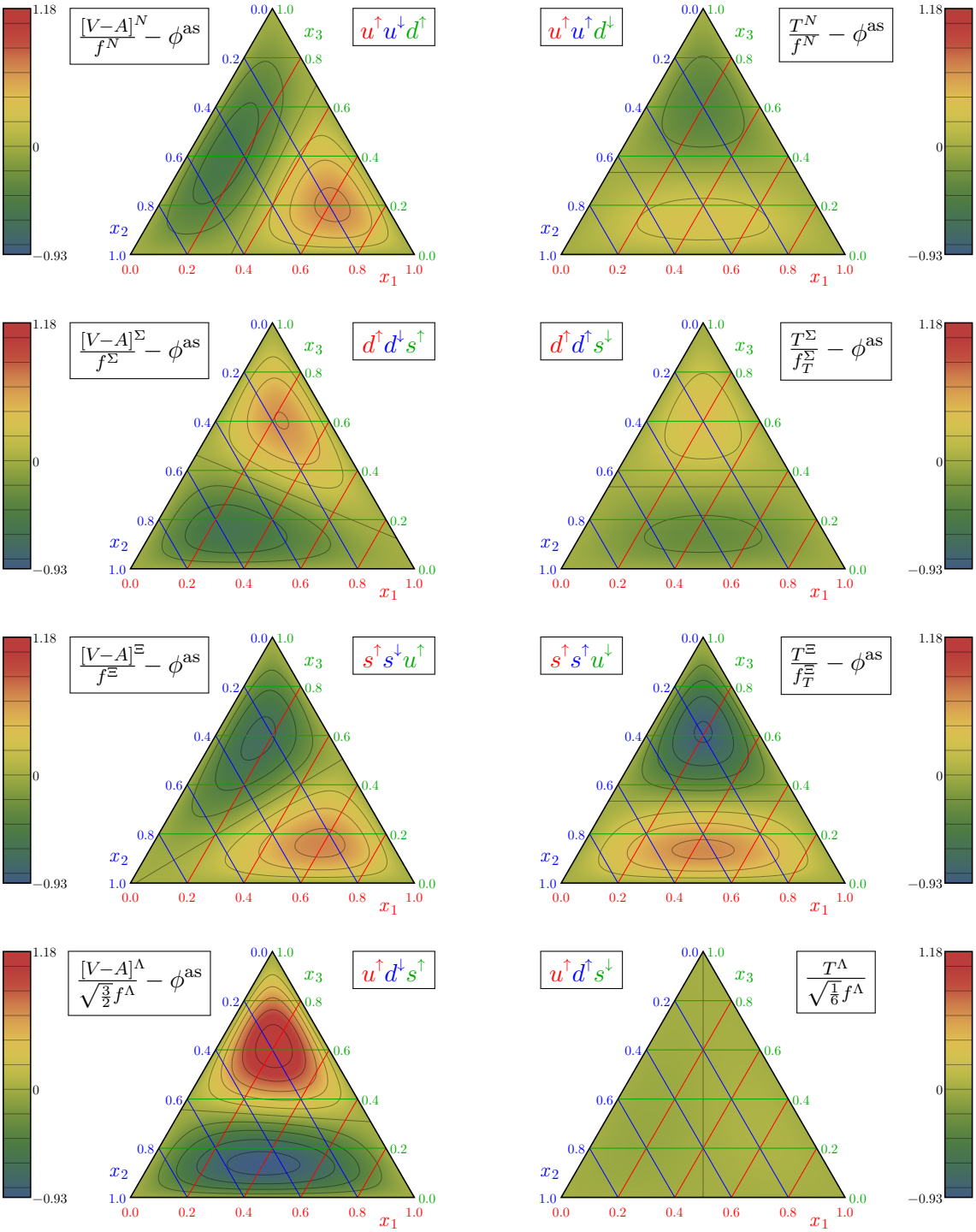

Figure 4.5.: Barycentric plots ($x_1+x_2+x_3 = 1$) showing the deviations of the DAs $[V-A]^B$ and T^B from the asymptotic shape $\phi^{\text{as}} \equiv 120x_1x_2x_3$. ($T^\Lambda$ vanishes in the asymptotic limit.) In this representation the coordinates x_i directly correspond to quarks of definite flavor and helicity.

larger fraction of the light-cone momentum than any light quarks. Second, the f quark is preferred over the g quark in the $f^\uparrow g^\downarrow h^\uparrow$ state, but both have to behave identically (by definition) in the DA corresponding to the $f^\uparrow g^\uparrow h^\downarrow$ state. This does not apply to the Λ baryon, since the symmetry properties of its DAs are reversed compared to the remaining members of the octet, cf. eqs. (3.10).

One can see that $[V{-}A]^\Lambda$ is clearly dominated by the strange quark. T^Λ on the other hand is a special case. This DA is antisymmetric under $x_1 \leftrightarrow x_2$, hence it has zero asymptotic contribution (this is by construction). Furthermore, its only first order shape parameter, π^Λ_{10}, is numerically very small (this is a new result). The conclusion is that the corresponding Fock state, $u^\uparrow d^\uparrow s^\downarrow$, should be expected to be strongly suppressed in the Λ baryon wave function, eq. (3.14b). This leads to a situation where — akin to the proton case, albeit for very different reasons — the leading twist sector can in very good approximation be described by just a single DA, in this case $[V{-}A]^\Lambda$.

In order to quantify this picture, we consider normalized first moments of $[V{-}A]^B$ and T^B,

$$\langle x_i\rangle^B = \frac{1}{\varphi^B_{00,(1)}}\int[dx]\,x_i\,[V{-}A]^B\,, \qquad \langle x_i\rangle_T^{B\neq\Lambda} = \frac{1}{\pi^B_{00,(1)}}\int[dx]\,x_i\,T^B\,, \tag{4.22a–b}$$

which are sometimes referred to as momentum fractions in the literature and interpreted as the portions of the hadron's total momentum carried by the individual valence quarks. This notion is somewhat imprecise since the averaging is done with a DA describing a single Fock state and not with the true wave function squared, and the interpretation as momentum fractions breaks down completely in case of T^Λ, which has no asymptotic part. That aside, these objects are nevertheless interesting because they provide a simple quantitative measure for the relative deviations of a DA from the asymptotic case $\langle x_1\rangle^{\text{as}} = \langle x_2\rangle^{\text{as}} = \langle x_3\rangle^{\text{as}} = 1/3$. To the first order, the $\langle x_i\rangle$ can be expressed in terms of the shape parameters as the following combinations:

$$\begin{aligned}
\langle x_1\rangle^{B\neq\Lambda} &= \frac{1}{3} + \frac{1}{3}\widehat{\varphi}^B_{11} + \widehat{\varphi}^B_{10}\,, & \langle x_1\rangle^{\Lambda} &= \frac{1}{3} + \frac{1}{3}\widehat{\varphi}^\Lambda_{11} - \frac{1}{3}\widehat{\varphi}^\Lambda_{10}\,, & \langle x_1\rangle_T^{B\neq\Lambda} &= \frac{1}{3} + \frac{1}{3}\widehat{\pi}^B_{11}\,,\\
\langle x_2\rangle^{B\neq\Lambda} &= \frac{1}{3} - \frac{2}{3}\widehat{\varphi}^B_{11}\,, & \langle x_2\rangle^{\Lambda} &= \frac{1}{3} - \frac{2}{3}\widehat{\varphi}^\Lambda_{11}\,, & \langle x_2\rangle_T^{B\neq\Lambda} &= \frac{1}{3} + \frac{1}{3}\widehat{\pi}^B_{11}\,,\\
\langle x_3\rangle^{B\neq\Lambda} &= \frac{1}{3} + \frac{1}{3}\widehat{\varphi}^B_{11} - \widehat{\varphi}^B_{10}\,, & \langle x_3\rangle^{\Lambda} &= \frac{1}{3} + \frac{1}{3}\widehat{\varphi}^\Lambda_{11} + \frac{1}{3}\widehat{\varphi}^\Lambda_{10}\,, & \langle x_3\rangle_T^{B\neq\Lambda} &= \frac{1}{3} - \frac{2}{3}\widehat{\pi}^B_{11}\,,
\end{aligned} \tag{4.23a–i}$$

with the normalized shape parameters

$$\widehat{\varphi}^B_{nk} = \frac{\varphi^B_{nk}}{\varphi^B_{00,(1)}}\,, \qquad\qquad \widehat{\pi}^{B\neq\Lambda}_{11} = \frac{\pi^B_{11}}{\pi^B_{00,(1)}}\,. \tag{4.24a–b}$$

Table 4.7.: Normalized first moments of the DAs $[V-A]^B$ and $T^{B\neq\Lambda}$ in the $\overline{\text{MS}}$ scheme at a scale $\mu = 2\,\text{GeV}$, obtained via eqs. (4.23).

B	N		Σ		Ξ		Λ	
$\langle x_1\rangle^B$	$u^\uparrow$	0.358	$d^\uparrow$	0.331	$s^\uparrow$	0.361	$u^\uparrow$	0.310
$\langle x_2\rangle^B$	$u^\downarrow$	0.319	$d^\downarrow$	0.310	$s^\downarrow$	0.333	$d^\downarrow$	0.304
$\langle x_3\rangle^B$	$d^\uparrow$	0.323	$s^\uparrow$	0.359	$u^\uparrow$	0.306	$s^\uparrow$	0.386
$\langle x_1\rangle_T^B$	$u^\uparrow$	0.340	$d^\uparrow$	0.326	$s^\uparrow$	0.352		—
$\langle x_2\rangle_T^B$	$u^\uparrow$	0.340	$d^\uparrow$	0.326	$s^\uparrow$	0.352		—
$\langle x_3\rangle_T^B$	$d^\downarrow$	0.319	$s^\downarrow$	0.348	$u^\downarrow$	0.296		—

The numerical results are summarized in table 4.7 and they fully support the qualitative picture suggested by the discussion of figure 4.5.

Chapter 5

Summary

In this work we have presented a new renormalization procedure for three-quark operators that enabled the first lattice study for the distribution amplitudes of the full baryon octet. We employed a convenient set of DAs defined for this purpose, which provides a unified description for the whole SU(3) octet (section 3.2). Unlike previous works on this subject, our approach allows for a simultaneous treatment of nucleons, Σ, Ξ, and Λ baryons as well as for a systematic study of SU(3) flavor breaking effects.

To provide the basis for a computational determination of distribution amplitudes we have defined suitable multiplets of local three-quark operators with covariant derivatives (section 3.4) which facilitate access to DAs in terms of their moments (section 3.3). Using our knowledge of the underlying symmetry groups (section 2.2) we were able to design these operators such that they reflect the multiplets of SU(3) flavor symmetry while simultaneously exhibiting optimal transformation behavior under the spinorial hypercubic group $\overline{\mathrm{H}(4)}$ (i.e., the relevant symmetry group for fermions on the lattice).

A major part of this work has been dedicated to working out the renormalization patterns for these operators (section 3.5). In this context, we employed two different renormalization schemes: A specifically crafted RI′/SMOM scheme fit for the nonperturbative renormalization of lattice data serves as an intermediate scheme, while the destination $\overline{\mathrm{MS}}$ scheme leads to results that can be used in other phenomenological studies. We connected these two schemes via conversion factors calculated in continuum perturbation theory.

As a first example of application, chapter 4 features our pioneering lattice study of baryon octet DAs using CLS ensembles at a single lattice spacing. To enable the numerical computation of moments of distribution amplitudes we had to find suitable two-point correlation functions (section 4.2), which have been implemented and measured in state-of-the-art lattice simulations (section 4.3). The resulting data were renormalized using

the procedure we developed and then extrapolated to the physical point using input from chiral perturbation theory (section 4.5).

Main results of this study are values for the normalization constants and first order shape parameters of the leading twist DAs of the baryon octet, as well as the higher twist normalization constants (section 4.6). Among our results certainly the most interesting finding concerns the shape parameters, where we record values which are an order of magnitude smaller than those from old QCD sum rule calculations. Simultaneously, we observe very strong relative SU(3) breaking effects. Our study was the first to tackle a lattice simulation of the DAs for the full baryon octet and these interesting discoveries undoubtedly warrant further research in this direction.

For the moment, the numerical values we present still have to be considered preliminary since they have been obtained from just four ensembles with the same lattice spacing and have not yet been extrapolated to the continuum. The plan for the future is to extend the analysis to the full set of CLS lattices, which also contains many ensembles with various smaller lattice constants. Using this wealth of data we will be able to perform a continuum limit extrapolation with high precision and provide final results for the distribution amplitudes of octet baryons.

Acknowledgments

First and foremost I would like to thank my colleagues from the Regensburg theory group with whom I have had the pleasure of collaborating on this project. I am indebted to A. Schäfer and V. M. Braun who provided scientific overview and theoretical guidance during my research. Credit for the development of the renormalization procedure goes to M. Göckeler, while the lattice study has been performed in close cooperation with F. Hutzler and P. Wein. The time that S. Bürger, F. Hutzler, P. Simeth, P. Wein, and F. Wutz have invested in proofreading this thesis is very much appreciated. I am also grateful to my former colleagues L. Greil, M. Knödlseder, D. Ostermeier, and B. Pirnay for many interesting discussions over the years. Last but not least I thank my parents for their neverending support.

Appendix A

Matrices

A.1. Pauli matrices

The Pauli matrices are defined as three traceless, Hermitian, and unitary (with $\det \sigma_i = -1$) matrices,

$$\sigma_1 = \begin{pmatrix} 0 & 1 \\ 1 & 0 \end{pmatrix}, \qquad \sigma_2 = \begin{pmatrix} 0 & -i \\ i & 0 \end{pmatrix}, \qquad \sigma_3 = \begin{pmatrix} 1 & 0 \\ 0 & -1 \end{pmatrix}, \tag{A.1a–c}$$

that (usually with an additional normalization factor of $\frac{1}{2}$) can serve as generators for SU(2). They are orthonormal with respect to the trace operation and, together with the identity matrix, form a basis of the complex vector space of 2×2 matrices, leading to a completeness relation:

$$\mathrm{tr}\{\sigma_i \sigma_j\} = 2\delta_{ij}\,, \tag{A.2a}$$

$$(\sigma_i)_{\alpha\beta}(\sigma_i)_{\gamma\delta} = 2\delta_{\alpha\delta}\delta_{\gamma\beta} - \delta_{\alpha\beta}\delta_{\gamma\delta}\,. \tag{A.2b}$$

The commutator and anticommutator of Pauli matrices take the simple forms

$$\big[\sigma_i, \sigma_j\big] = 2i\varepsilon_{ijk}\sigma_k\,, \tag{A.3a}$$

$$\big\{\sigma_i, \sigma_j\big\} = 2\delta_{ij}\mathbb{1}_2\,, \tag{A.3b}$$

where ε_{ijk} is the totally antisymmetric Levi-Civita symbol. There is one quadratic Casimir invariant,

$$\sigma_i \sigma_i = 3\mathbb{1}_2\,, \tag{A.4}$$

that commutes with all Pauli matrices and, in the context of SU(2) as (iso-)spin algebra, corresponds to the square of the total (iso-)spin operator.

A.2. Gell-Mann matrices

The t^A appearing, e.g., in covariant derivatives (2.2) or matrix parametrizations (2.64) are the generators of the Lie algebra of the special unitary group SU(3). In the fundamental representation they are 3×3 matrices related to the Gell-Mann matrices λ^A via

$$t^A = \frac{\lambda^A}{2}\,, \qquad A \in \{1, \ldots, 8\}\,. \tag{A.5}$$

These traceless Hermitian matrices are given by

$$\lambda^1 = \begin{pmatrix} 0 & 1 & 0 \\ 1 & 0 & 0 \\ 0 & 0 & 0 \end{pmatrix}, \qquad \lambda^2 = \begin{pmatrix} 0 & -i & 0 \\ i & 0 & 0 \\ 0 & 0 & 0 \end{pmatrix}, \qquad \lambda^3 = \begin{pmatrix} 1 & 0 & 0 \\ 0 & -1 & 0 \\ 0 & 0 & 0 \end{pmatrix},$$

$$\lambda^4 = \begin{pmatrix} 0 & 0 & 1 \\ 0 & 0 & 0 \\ 1 & 0 & 0 \end{pmatrix}, \qquad \lambda^5 = \begin{pmatrix} 0 & 0 & -i \\ 0 & 0 & 0 \\ i & 0 & 0 \end{pmatrix},$$

$$\lambda^6 = \begin{pmatrix} 0 & 0 & 0 \\ 0 & 0 & 1 \\ 0 & 1 & 0 \end{pmatrix}, \qquad \lambda^7 = \begin{pmatrix} 0 & 0 & 0 \\ 0 & 0 & -i \\ 0 & i & 0 \end{pmatrix}, \qquad \lambda^8 = \frac{1}{\sqrt{3}} \begin{pmatrix} 1 & 0 & 0 \\ 0 & 1 & 0 \\ 0 & 0 & -2 \end{pmatrix}. \tag{A.6a–h}$$

As an interesting sidenote we can immediately relate the form of the generators to some concepts of SU(3) flavor symmetry. The first three generators are obviously extended Pauli matrices, signaling that SU(3) has an SU(2) subalgebra.[73] This motivates SU(3) flavor symmetry as a generalization of its SU(2) isospin subgroup. Second, the generators of the Cartan subalgebra (which commute with each other and are represented by diagonal matrices), t^3 and t^8, are proportional to the two additive quantum numbers, isospin z-component and hypercharge (i.e., baryon number plus strangeness).

Moving on, we find that these generators are chosen such that their properties closely match those of the Pauli Matrices of SU(2) (see appendix A.1), being trace orthonormal and satisfying a Fierz-type relation ($a, b, c, d \in \{1, 2, 3\}$):

$$\mathrm{tr}\{t^A t^B\} = \frac{1}{2}\delta^{AB}\,, \tag{A.7a}$$

$$\left(t^A\right)^{ab}\left(t^A\right)^{cd} = \frac{1}{2}\delta^{ad}\delta^{cb} - \frac{1}{6}\delta^{ab}\delta^{cd}\,. \tag{A.7b}$$

The Lie bracket (i.e., the commutator) of two generators as well as their anticommutator

[73] Actually there are 3 overlapping SU(2) subalgebras: $\{t^1, t^2, t^3\}$, $\{t^4, t^5, \frac{1}{2}(\sqrt{3}t^8 + t^3)\}$, $\{t^6, t^7, \frac{1}{2}(\sqrt{3}t^8 - t^3)\}$. While the former one corresponds to isospin, the latter two are called V- and U-spin, cf. appendix C.1.

can be expressed as a linear combination of matrices:[74]

$$\big[t^A, t^B\big] = if^{ABC}t^C\,, \tag{A.8a}$$

$$\big\{t^A, t^B\big\} = \frac{1}{3}\delta^{AB}\mathbb{1}_3 + d^{ABC}t^C\,. \tag{A.8b}$$

The coefficients are the totally antisymmetric structure constants f^{ABC} and the totally symmetric constants d^{ABC}, which can be obtained from

$$if^{ABC} = 2\,\mathrm{tr}\big\{t^A\big[t^B, t^C\big]\big\}\,, \tag{A.9a}$$

$$d^{ABC} = 2\,\mathrm{tr}\big\{t^A\big\{t^B, t^C\big\}\big\}\,. \tag{A.9b}$$

These constants are real by construction and take the following values: (All index combinations not shown are either related to the ones below via permutation or are equal to zero.)

$$f^{123} = 1\,, \tag{A.10a}$$

$$f^{147} = -f^{156} = f^{246} = f^{257} = f^{345} = -f^{367} = \frac{1}{2}\,, \tag{A.10b}$$

$$f^{458} = f^{678} = \frac{\sqrt{3}}{2}\,, \tag{A.10c}$$

and

$$d^{118} = d^{228} = d^{338} = -d^{888} = \frac{1}{\sqrt{3}}\,, \tag{A.11a}$$

$$d^{146} = d^{157} = -d^{247} = d^{256} = d^{344} = d^{355} = -d^{366} = -d^{377} = \frac{1}{2}\,, \tag{A.11b}$$

$$d^{448} = d^{558} = d^{668} = d^{778} = -\frac{1}{2\sqrt{3}}\,. \tag{A.11c}$$

There is one quadratic and one cubic Casimir invariant:

$$t^A t^A = \frac{4}{3}\mathbb{1}_3\,, \tag{A.12a}$$

$$d^{ABC}t^A t^B t^C = \frac{10}{9}\mathbb{1}_3\,. \tag{A.12b}$$

Aside from the 3-dimensional fundamental representation we also have to consider the 8-dimensional adjoint representation, which is relevant for the transformation behavior of gluons as well as the ghost-gluon interaction, see eq. (2.12). In this representation, the generators are 8×8 matrices whose components are given directly by the structure constants,

$$\big(t^A\big)^{BC} = -if^{ABC}\,. \tag{A.13}$$

[74] While the first equation actually holds for the generators in all representations of SU(3), the second equation is specific to the fundamental representation, where the eight generators together with the identity matrix form a basis of the matrix space.

We use uppercase letters for the component indices to indicate that they run from 1 to 8 (as opposed to the indices in the fundamental representation running from 1 to 3). Employing the Jacobi identity,

$$0 = f^{ABZ} f^{ZCD} + f^{ACZ} f^{ZDB} + f^{ADZ} f^{ZBC} \,, \tag{A.14}$$

it is straightforward to show that the generators of the adjoint representation also fulfill the commutator equation (A.8a). Since the structure constants are real, the adjoint representation is a fully real matrix representation of SU(3).

A.3. Dirac matrices

The Dirac gamma matrices are a set of 4×4 matrices that generate the Clifford algebra. In Euclidean spacetime the gamma matrices have to obey the anticommutation relation

$$\{\gamma_\mu, \gamma_\nu\} = 2\delta_{\mu\nu} \mathbb{1}_4 \qquad \forall\, \mu, \nu \in \{1, \ldots, 4\} \,, \tag{A.15}$$

with the metric being the Kronecker delta symbol $\delta_{\mu\nu}$. For the relation to gamma matrices in Minkowski spacetime see appendix A.4. There are many explicit realizations for these matrices; for all calculations in Euclidean space we follow the convention of [47]:

$$\gamma_1 = \begin{pmatrix} 0 & 0 & 0 & i \\ 0 & 0 & i & 0 \\ 0 & -i & 0 & 0 \\ -i & 0 & 0 & 0 \end{pmatrix}, \qquad \gamma_2 = \begin{pmatrix} 0 & 0 & 0 & 1 \\ 0 & 0 & -1 & 0 \\ 0 & -1 & 0 & 0 \\ 1 & 0 & 0 & 0 \end{pmatrix},$$

$$\gamma_3 = \begin{pmatrix} 0 & 0 & i & 0 \\ 0 & 0 & 0 & -i \\ -i & 0 & 0 & 0 \\ 0 & i & 0 & 0 \end{pmatrix}, \qquad \gamma_4 = \begin{pmatrix} 0 & 0 & 1 & 0 \\ 0 & 0 & 0 & 1 \\ 1 & 0 & 0 & 0 \\ 0 & 1 & 0 & 0 \end{pmatrix}. \tag{A.16a–d}$$

It is helpful to define a fifth gamma matrix,

$$\gamma_5 = \gamma_1 \gamma_2 \gamma_3 \gamma_4 = \begin{pmatrix} -1 & 0 & 0 & 0 \\ 0 & -1 & 0 & 0 \\ 0 & 0 & 1 & 0 \\ 0 & 0 & 0 & 1 \end{pmatrix}, \tag{A.17}$$

that anticommutes with the other four matrices:

$$\{\gamma_\mu, \gamma_5\} = 0 \,. \tag{A.18}$$

This Weyl (chiral) representation can be related to the Pauli matrices as follows:

$$\gamma_\mu = \begin{pmatrix} 0 & \sigma_\mu^+ \\ \sigma_\mu^- & 0 \end{pmatrix}, \qquad \text{with } \sigma^\pm = (\pm i\boldsymbol{\sigma}, \mathbb{1}_2)\,. \tag{A.19}$$

The shape of γ_5 in this representation ensures that the chiral projectors $\gamma_{R/L} = \frac{1}{2}(\mathbb{1}_4 \pm \gamma_5)$ take a simple form, projecting out two-component right/left-handed spinors from a Dirac four-spinor.

Furthermore, we define

$$\sigma_{\mu\nu} = \frac{i}{2}[\gamma_\mu, \gamma_\nu]\,. \tag{A.20}$$

In our choice of representation all these matrices are Hermitian and self-inverse:

$$\gamma_\mu^\dagger = \gamma_\mu^{-1} = \gamma_\mu\,, \tag{A.21a}$$
$$\gamma_5^\dagger = \gamma_5^{-1} = \gamma_5\,, \tag{A.21b}$$
$$\sigma_{\mu\nu}^\dagger = \sigma_{\mu\nu}^{-1} = \sigma_{\mu\nu} \quad (\mu \neq \nu)\,. \tag{A.21c}$$

The 16 objects $\mathbb{1}_4$, γ_μ, γ_5, $\gamma_\mu\gamma_5$, and $\sigma_{\mu\nu}$ $(\mu < \nu)$ form a basis of the 16-dimensional complex vector space of 4×4 matrices with complex entries.

The charge conjugation matrix C can be used to transpose the gamma matrices:

$$\gamma_\mu^T = -C^{-1}\gamma_\mu C\,. \tag{A.22}$$

Our choice for its realization,

$$C = \gamma_2\gamma_4\,, \tag{A.23}$$

implies the additional properties

$$C^\dagger = C^{-1} = C^T = -C\,. \tag{A.24}$$

A.4. Minkowski and Euclidean space

Minkowski spacetime has $\mathrm{O}(1,3)$ symmetry that leaves invariant the spacetime interval $g^{\mu\nu}dx_\mu dx_\nu$ with the metric $g \equiv \mathrm{diag}(1,-1,-1,-1)$.[75] This type of spacetime appears in formulations of special relativity and therefore provides the mathematical foundation of the real world in regions where the spacetime can be considered flat.

[75] Alternatively, we could also work with $\mathrm{O}(3,1)$ symmetry without changing the relevant physics. For ways to possibly distinguish these two Lorentz groups see [124].

On the other hand, Euclidean spacetime has O(4) symmetry that leaves invariant the spacetime interval $\delta_{\mu\nu} dx_\mu dx_\nu$ with the metric $\delta \equiv \mathrm{diag}(1,1,1,1)$. Analytic continuation to Euclidean spacetime is used in lattice simulations because it allows for a probabilistic interpretation of the action in the QCD path integral.

When going from Minkowski to Euclidean spacetime one should perform the following replacements for four-vectors in position space,

$$x_M^0 \to -i x_4^E \,, \tag{A.25a}$$
$$x_M^j \to x_j^E \,, \tag{A.25b}$$

and for the corresponding covariant derivatives:

$$D_M^0 \to i D_4^E \,, \tag{A.26a}$$
$$D_M^j \to -D_j^E \,. \tag{A.26b}$$

(We use the super/subscripts E/M to indicate Euclidean/Minkowski space.) While not strictly necessary, it is convenient to define for the gamma matrices:

$$\gamma_M^0 = \gamma_4^E \,, \tag{A.27a}$$
$$\gamma_M^j = i\gamma_j^E \,, \tag{A.27b}$$
$$\gamma_M^5 = -\gamma_5^E \,. \tag{A.27c}$$

Both sets of matrices generate Clifford algebras with the appropriate metric,

$$\{\gamma_M^\mu, \gamma_M^\nu\} = 2g^{\mu\nu}\mathbb{1}_4 \,, \qquad \{\gamma_\mu^E, \gamma_\nu^E\} = 2\delta_{\mu\nu}\mathbb{1}_4 \,, \tag{A.28a–b}$$

and we find for the scalar products:

$$(x^\mu y_\mu)_M \to -(x_\mu y_\mu)^E \,, \tag{A.29a}$$
$$(x^\mu \gamma_\mu)_M \to -i(x_\mu \gamma_\mu)^E \,, \tag{A.29b}$$
$$(\gamma^\mu \otimes \gamma_\mu)_M = (\gamma_\mu \otimes \gamma_\mu)^E \,. \tag{A.29c}$$

Appendix B

The hypercubic group

B.1. Properties of the double-covering map

In section 2.2.3 we studied the hypercubic group H(4) and its double cover $\overline{\mathrm{H}(4)}$. We even postulated an explicit expression for the double covering map, but neglected to give a proof. In this appendix we will examine the properties of this map, which connects $\overline{\mathrm{H}(4)} \subset \mathrm{Pin}(4)$ to $\mathrm{H}(4) \subset \mathrm{O}(4)$ as defined in eq. (2.75):

$$\begin{aligned} c : \mathrm{Pin}(4) = \mathrm{SU}(2)^2 \rtimes Z_2 &\to \mathrm{O}(4)\,, \\ (U^+, U^-, \pm) &\mapsto R\,. \end{aligned}$$

To aid in the following calculations we give 4 different expressions for the matrix R,

$$\begin{aligned} R_{\mu\nu} \equiv [R(U^+, U^-, \pm)]_{\mu\nu} &= \tfrac{1}{2}\,\mathrm{tr}\big\{\sigma^+_\mu U^- \sigma^\mp_\nu U^{+\dagger}\big\} = \tfrac{1}{2}\,\mathrm{tr}\big\{\sigma^\pm_\mu U^\mp \sigma^-_\nu U^{\pm\dagger}\big\} \\ &= \tfrac{1}{2}\,\mathrm{tr}\big\{\sigma^-_\mu U^+ \sigma^\pm_\nu U^{-\dagger}\big\} = \tfrac{1}{2}\,\mathrm{tr}\big\{\sigma^\mp_\mu U^\pm \sigma^+_\nu U^{\mp\dagger}\big\}\,, \end{aligned} \tag{B.1}$$

which are all equal. (This is easy to see by using that the components of R, generated as traces of elements of SU(2), are guaranteed to be real.) To check the properties of the double-covering map we will also utilize some nice properties of the Pauli matrix vectors $\sigma^\pm = (\pm i\boldsymbol{\sigma}, \mathbb{1}_2)$:

$$\mathrm{tr}\big\{\sigma^-_\mu \sigma^+_\nu\big\} = 2\delta_{\mu\nu}\,, \tag{B.2a}$$

$$\mathrm{tr}\big\{\sigma^-_\mu \sigma^+_\nu \sigma^-_\rho \sigma^+_\lambda - \sigma^+_\mu \sigma^-_\nu \sigma^+_\rho \sigma^-_\lambda\big\} = 4\varepsilon_{\mu\nu\rho\lambda}\,, \tag{B.2b}$$

$$(\sigma^-_\mu)_{\alpha\alpha'}(\sigma^+_\mu)_{\beta\beta'} = 2\delta_{\alpha\beta'}\delta_{\beta\alpha'}\,. \tag{B.2c}$$

First, we confirm the group homomorphism property $R(g_1)R(g_2) = R(g_1 \circ g_2)$. Explicit calculation shows

$$\begin{aligned}
[R(U_1^+, U_1^-, \pm_1)]_{\mu\rho}[R(U_2^+, U_2^-, \pm_2)]_{\rho\nu} &= \tfrac{1}{4}\,\mathrm{tr}\big\{\sigma_\mu^{\pm_1} U_1^{\mp_1}\sigma_\rho^- U_1^{\pm_1\dagger}\big\}\,\mathrm{tr}\big\{\sigma_\rho^+ U_2^-\sigma_\nu^{\mp_2} U_2^{+\dagger}\big\} \\
&= \tfrac{1}{2}\,\mathrm{tr}\big\{\sigma_\mu^{\pm_1}(U_1^{\mp_1}U_2^-)\sigma_\nu^{\mp_2}(U_1^{\pm_1}U_2^+)^\dagger\big\} \\
&= \tfrac{1}{2}\,\mathrm{tr}\big\{\sigma_\mu^-(U_1^+U_2^{\pm_1})\sigma_\nu^{\pm_1\circ\pm_2}(U_1^-U_2^{\mp_1})^\dagger\big\} \\
&= [R(U_1^+U_2^{\pm_1}, U_1^-U_2^{\mp_1}, \pm_1\circ\pm_2)]_{\mu\nu} \\
&= \big[R\big((U_1^+, U_1^-, \pm_1)\circ(U_2^+, U_2^-, \pm_2)\big)\big]_{\mu\nu}\,, \qquad \text{(B.3)}
\end{aligned}$$

where, in the step from the second to the third line, we have modified all signs by $\mp_1$. The simultaneous change of all signs leaves the object invariant, see its definition (B.1).

Next, we test that R is actually in O(4), i.e., an orthogonal matrix with $RR^T = \mathbb{1}_4$:

$$\begin{aligned}
R_{\mu\rho}R_{\nu\rho} &= \tfrac{1}{4}\,\mathrm{tr}\big\{\sigma_\mu^\pm U^\mp\sigma_\rho^- U^{\pm\dagger}\big\}\,\mathrm{tr}\big\{\sigma_\nu^\mp U^\pm\sigma_\rho^+ U^{\mp\dagger}\big\} \\
&= \tfrac{1}{2}\,\mathrm{tr}\big\{\sigma_\mu^\pm U^\mp U^{\mp\dagger}\sigma_\nu^\mp U^\pm U^{\pm\dagger}\big\} = \tfrac{1}{2}\,\mathrm{tr}\big\{\sigma_\mu^\pm\sigma_\nu^\mp\big\} \\
&= \delta_{\mu\nu}\,. \qquad \text{(B.4)}
\end{aligned}$$

From this we already know that $|\det R(U^+, U^-, \pm)| = 1$. Still, it is instructive to look at the determinant in detail. We find that

$$\begin{aligned}
\det R(U^+, U^-, \pm) &= \varepsilon_{\mu\nu\rho\lambda}R_{\mu1}R_{\nu2}R_{\rho3}R_{\lambda4} \\
&= \tfrac{1}{4}\,\mathrm{tr}\big\{\sigma_\mu^-\sigma_\nu^+\sigma_\rho^-\sigma_\lambda^+ - \sigma_\mu^+\sigma_\nu^-\sigma_\rho^+\sigma_\lambda^-\big\}R_{\mu1}R_{\nu2}R_{\rho3}R_{\lambda4} \\
&= \tfrac{1}{4}\,\mathrm{tr}\big\{\sigma_1^\mp\sigma_2^\pm\sigma_3^\mp\sigma_4^\pm - \sigma_1^\pm\sigma_2^\mp\sigma_3^\pm\sigma_4^\mp\big\} = \pm\varepsilon_{1234} \\
&= \pm1\,, \qquad \text{(B.5)}
\end{aligned}$$

where we have used

$$\sigma_\mu^- R_{\mu\mu'} = U^-\sigma_{\mu'}^\mp U^{+\dagger}\,, \qquad\qquad \sigma_\mu^+ R_{\mu\mu'} = U^+\sigma_{\mu'}^\pm U^{-\dagger}\,, \qquad \text{(B.6a–b)}$$

which itself follows from the property (B.2c). This illustrates the fact that elements of the type $(U^+, U^-, +)$ are mapped to the subgroup of orientation preserving rotations, SO(4), while elements of the type $(U^+, U^-, -)$ are mapped to the orientation reversing complement, $\mathrm{O}(4) \setminus \mathrm{SO}(4)$.

B.2. Representations

Now that we have established a double cover $\overline{\mathrm{H}(4)} \to \mathrm{H}(4)$, we can immediately discuss some representations of $\overline{\mathrm{H}(4)}$. Two representations in particular are worth highlighting. Obviously, the double-covering map itself constitutes a 4-dimensional orthogonal representation.

Since this one descends from the fundamental representation of O(4), we will call it the fundamental representation of $\overline{\mathrm{H}(4)}$. It is denoted as τ_1^4 and defined by eqs. (2.75)–(2.76). Another important representation is a 4-dimensional unitary representation defined by the mapping

$$(U^+, U^-, +) \mapsto \begin{pmatrix} U^+ & 0 \\ 0 & U^- \end{pmatrix}^*, \qquad (U^+, U^-, -) \mapsto \begin{pmatrix} 0 & U^+ \\ U^- & 0 \end{pmatrix}^*. \tag{B.7a–b}$$

(It is straightforward to see that this is indeed a representation of $\overline{\mathrm{H}(4)}$ because it respects the group operation (2.74).) We call this one the fundamental spinorial representation, denoted as $\tau_1^{\frac{4}{}}$. Using the explicit matrices given below, the connection between these two representations can easily be checked: Deduce $(U^+, U^-, \pm)$ from $\tau_1^{\frac{4}{}}(g)$ via eqs.(B.7), apply the double covering map, and verify that the result is equal to $\tau_1^4(g)$.

As discussed in section 2.2.3 it is sufficient to write down the explicit forms of the 6 generators I_1, I_2, I_3, I_4, γ, and t. In the fundamental single-valued representation τ_1^4 they correspond to matrices of reflections and rotations. These matrices provide a four-dimensional representation for both H(4) and $\overline{\mathrm{H}(4)}$:

$$\tau_1^4(I_1) = \begin{pmatrix} -1 & 0 & 0 & 0 \\ 0 & 1 & 0 & 0 \\ 0 & 0 & 1 & 0 \\ 0 & 0 & 0 & 1 \end{pmatrix}, \quad \tau_1^4(I_2) = \begin{pmatrix} 1 & 0 & 0 & 0 \\ 0 & -1 & 0 & 0 \\ 0 & 0 & 1 & 0 \\ 0 & 0 & 0 & 1 \end{pmatrix}, \quad \tau_1^4(\gamma) = \begin{pmatrix} 0 & 0 & 1 & 0 \\ 0 & 1 & 0 & 0 \\ 1 & 0 & 0 & 0 \\ 0 & 0 & 0 & 1 \end{pmatrix},$$

$$\tau_1^4(I_3) = \begin{pmatrix} 1 & 0 & 0 & 0 \\ 0 & 1 & 0 & 0 \\ 0 & 0 & -1 & 0 \\ 0 & 0 & 0 & 1 \end{pmatrix}, \quad \tau_1^4(I_4) = \begin{pmatrix} 1 & 0 & 0 & 0 \\ 0 & 1 & 0 & 0 \\ 0 & 0 & 1 & 0 \\ 0 & 0 & 0 & -1 \end{pmatrix}, \quad \tau_1^4(t) = \begin{pmatrix} 1 & 0 & 0 & 0 \\ 0 & 0 & 1 & 0 \\ 0 & 0 & 0 & 1 \\ 0 & 1 & 0 & 0 \end{pmatrix}. \tag{B.8a–f}$$

To construct the matrices for the generators in the five spinorial representations, which are unique to $\overline{\mathrm{H}(4)}$, we follow [122] and define the building blocks

$$S_1 = \begin{pmatrix} 0 & 0 & 0 & i \\ 0 & 0 & i & 0 \\ 0 & i & 0 & 0 \\ i & 0 & 0 & 0 \end{pmatrix}, \quad S_2 = \begin{pmatrix} 0 & 0 & 0 & -1 \\ 0 & 0 & 1 & 0 \\ 0 & -1 & 0 & 0 \\ 1 & 0 & 0 & 0 \end{pmatrix}, \quad \Gamma = \frac{1}{\sqrt{2}} \begin{pmatrix} 0 & 0 & 1 & -1 \\ 0 & 0 & -1 & -1 \\ 1 & -1 & 0 & 0 \\ -1 & -1 & 0 & 0 \end{pmatrix},$$

$$S_3 = \begin{pmatrix} 0 & 0 & i & 0 \\ 0 & 0 & 0 & -i \\ i & 0 & 0 & 0 \\ 0 & -i & 0 & 0 \end{pmatrix}, \quad S_4 = \begin{pmatrix} 0 & 0 & -1 & 0 \\ 0 & 0 & 0 & -1 \\ 1 & 0 & 0 & 0 \\ 0 & 1 & 0 & 0 \end{pmatrix}, \quad T = \frac{1}{\sqrt{2}} \begin{pmatrix} 1 & -i & 0 & 0 \\ 1 & i & 0 & 0 \\ 0 & 0 & i & 1 \\ 0 & 0 & -i & 1 \end{pmatrix}. \tag{B.9a–f}$$

The four-, eight-, and twelve-dimensional irreducible spinorial representations of $\overline{\mathrm{H}(4)}$ are denoted as $\underline{4}_+$, $\underline{4}_-$, $\underline{8}$, $\underline{12}_+$, and $\underline{12}_-$ in [122], and they are constructed from these blocks as follows:

$$\underline{4}_+(I_i) = S_i \cdot 1\,, \qquad \underline{4}_+(\gamma) = \Gamma \cdot i\,, \qquad \underline{4}_+(t) = T \cdot e^{i\frac{7\pi}{4}}\,, \tag{B.10a–o}$$

$$\underline{4}_-(I_i) = S_i \cdot 1\,, \qquad \underline{4}_-(\gamma) = \Gamma \cdot (-i)\,, \qquad \underline{4}_-(t) = T \cdot e^{i\frac{7\pi}{4}}\,,$$

$$\underline{8}(I_i) = S_i \otimes \mathbb{1}_2\,, \qquad \underline{8}(\gamma) = \Gamma \otimes \begin{pmatrix} 0 & e^{i\frac{\pi}{3}} \\ e^{i\frac{2\pi}{3}} & 0 \end{pmatrix}, \qquad \underline{8}(t) = T \otimes \begin{pmatrix} e^{i\frac{5\pi}{12}} & 0 \\ 0 & e^{i\frac{13\pi}{12}} \end{pmatrix},$$

$$\underline{12}_+(I_i) = S_i \otimes \mathbb{1}_3\,, \quad \underline{12}_+(\gamma) = \Gamma \otimes \begin{pmatrix} 0 & 0 & -1 \\ 0 & i & 0 \\ 1 & 0 & 0 \end{pmatrix}, \quad \underline{12}_+(t) = T \otimes \begin{pmatrix} 0 & 0 & e^{i\frac{5\pi}{4}} \\ 1 & 0 & 0 \\ 0 & 1 & 0 \end{pmatrix},$$

$$\underline{12}_-(I_i) = S_i \otimes \mathbb{1}_3\,, \quad \underline{12}_-(\gamma) = \Gamma \otimes \begin{pmatrix} 0 & 0 & -1 \\ 0 & -i & 0 \\ 1 & 0 & 0 \end{pmatrix}, \quad \underline{12}_-(t) = T \otimes \begin{pmatrix} 0 & 0 & e^{i\frac{\pi}{4}} \\ 1 & 0 & 0 \\ 0 & -1 & 0 \end{pmatrix}.$$

As stated in section 2.2, the explicit form of representation matrices is never uniquely determined. By a change of basis in the representation space one can obtain different (but equivalent) matrices. If one were to scrutinize the $\overline{\mathrm{H}(4)}$ transfomation properties of the operator mutiplets using eq. (3.38), then one would see that it is not actually fulfilled for the multiplets from [52] together with the representation matrices in the basis of [122]. This can be rectified by a simple change of basis on the representation space. For that purpose we give the unitary matrices,

$$U_1^{\underline{4}} = \mathbb{1}_2 \otimes \mathbb{1}_2\,, \tag{B.11a}$$

$$U_2^{\underline{4}} = \begin{pmatrix} 0 & 1 \\ 1 & 0 \end{pmatrix} \otimes \begin{pmatrix} 0 & 1 \\ 1 & 0 \end{pmatrix}, \tag{B.11b}$$

$$U^{\underline{8}} = \mathbb{1}_2 \otimes \frac{1}{\sqrt{2}} \begin{pmatrix} 0 & 0 & i & e^{i\frac{2\pi}{3}} \\ 1 & e^{i\frac{7\pi}{6}} & 0 & 0 \\ 0 & 0 & -1 & e^{i\frac{\pi}{6}} \\ -i & e^{i\frac{5\pi}{3}} & 0 & 0 \end{pmatrix}, \tag{B.11c}$$

$$U_1^{\underline{12}} = \mathbb{1}_2 \otimes \frac{1}{\sqrt{2}} \begin{pmatrix} 0 & 0 & 0 & 1 & e^{i\frac{7\pi}{4}} & 0 \\ 0 & 0 & -\sqrt{2}i & 0 & 0 & 0 \\ 0 & 0 & 0 & -1 & e^{i\frac{7\pi}{4}} & 0 \\ 1 & e^{i\frac{3\pi}{4}} & 0 & 0 & 0 & 0 \\ 0 & 0 & 0 & 0 & 0 & \sqrt{2}i \\ -1 & e^{i\frac{3\pi}{4}} & 0 & 0 & 0 & 0 \end{pmatrix}, \tag{B.11d}$$

$$U_2^{\underline{12}} = \mathbb{1}_2 \otimes \frac{1}{\sqrt{2}} \begin{pmatrix} 1 & e^{i\frac{3\pi}{4}} & 0 & 0 & 0 & 0 \\ 0 & 0 & 0 & -1 & e^{i\frac{7\pi}{4}} & 0 \\ 1 & e^{i\frac{7\pi}{4}} & 0 & 0 & 0 & 0 \\ 0 & 0 & 0 & -1 & e^{i\frac{3\pi}{4}} & 0 \\ 0 & 0 & 0 & 0 & 0 & \sqrt{2}i \\ 0 & 0 & \sqrt{2}i & 0 & 0 & 0 \end{pmatrix}, \tag{B.11e}$$

and perform a change of basis:

$$\tau_1^{\underline{4}}(g) = U_1^{\underline{4}}\, \underline{4}_+(g) \left(U_1^{\underline{4}}\right)^\dagger, \tag{B.12a}$$

$$\tau_2^{\underline{4}}(g) = U_2^{\underline{4}}\, \underline{4}_-(g) \left(U_2^{\underline{4}}\right)^\dagger, \tag{B.12b}$$

$$\tau^{\underline{8}}(g) = U^{\underline{8}}\, \underline{8}(g) \left(U^{\underline{8}}\right)^\dagger, \tag{B.12c}$$

$$\tau_1^{\underline{12}}(g) = U_1^{\underline{12}}\, \underline{12}_+(g) \left(U_1^{\underline{12}}\right)^\dagger, \tag{B.12d}$$

$$\tau_2^{\underline{12}}(g) = U_2^{\underline{12}}\, \underline{12}_-(g) \left(U_2^{\underline{12}}\right)^\dagger. \tag{B.12e}$$

We denote the spinorial representations as $\tau_1^{\underline{4}}$, $\tau_2^{\underline{4}}$, $\tau^{\underline{8}}$, $\tau_1^{\underline{12}}$, and $\tau_2^{\underline{12}}$, following the notation of [52]. Using this form of the representation matrices one can verify that the operator multiplets that we take from there do transform under these irreducible representations of $\overline{\mathrm{H}(4)}$.

By construction, the transformation matrices given above exhibit a structure consisting of two blocks, each accounting for half of the representation's dimension. This is related to the way the multiplets are defined in [52]. Each multiplet is built such that the operators in the first half all have the same set of quark chiralities, while those in the second half have exactly the opposite chiralities.

B.3. Character table

Table B.1.: Character table of $\overline{\mathrm{H}(4)}$. For each conjugacy class C_h (where a superscript prime indicates a splitting class as discussed in section 2.2.3) we give its cardinality $|C_h|$ (the number of elements), the order n_h of its elements (the smallest integer for which $h^{n_h} = e$), a sample element h, and the character afforded by each representation. The superscript labels give the dimensions of the representations, while the subscripts enumerate different representations of the same dimension. Spinorial representations are marked by underlined superscripts. Most of the information presented here has been taken from [122].

C_h	$\lvert C_h\rvert$	n_h	h	τ_1^1	τ_3^1	τ_1^2	τ_1^3	τ_3^3	τ_2^1	τ_4^1	τ_2^2	τ_2^3	τ_4^3
1	1	1	$e = \gamma^4$	1	1	2	3	3	1	1	2	3	3
$1'$	1	2	$-e = \gamma^2$	1	1	2	3	3	1	1	2	3	3
2	8	4	I_1	1	1	2	3	3	−1	−1	−2	−3	−3
3	12	4	$I_2 I_1$	1	1	2	3	3	1	1	2	3	3
4	8	2	$I_3 I_2 I_1$	1	1	2	3	3	−1	−1	−2	−3	−3
5	2	2	$I_4 I_3 I_2 I_1$	1	1	2	3	3	1	1	2	3	3
6	24	4	γ	1	−1	0	1	−1	1	−1	0	1	−1
7	48	4	$I_2\gamma$	1	−1	0	1	−1	−1	1	0	−1	1
8	12	8	$I_3\gamma$	1	−1	0	1	−1	−1	1	0	−1	1
$8'$	12	8	$I_3\gamma^3$	1	−1	0	1	−1	−1	1	0	−1	1
9	24	2	$I_4 I_2\gamma$	1	−1	0	1	−1	1	−1	0	1	−1
10	48	8	$I_4 I_3\gamma$	1	−1	0	1	−1	1	−1	0	1	−1
11	24	8	$I_4 I_3 I_2\gamma$	1	−1	0	1	−1	−1	1	0	−1	1
12	24	4	$t\gamma t\gamma$	1	1	2	−1	−1	1	1	2	−1	−1
13	48	8	$I_1 t\gamma t\gamma$	1	1	2	−1	−1	−1	−1	−2	1	1
14	12	4	$I_2 I_1 t\gamma t\gamma$	1	1	2	−1	−1	1	1	2	−1	−1
$14'$	12	4	$I_2 I_1 t\gamma t\gamma^3$	1	1	2	−1	−1	1	1	2	−1	−1
15	32	6	t	1	1	−1	0	0	1	1	−1	0	0
$15'$	32	3	$\gamma^2 t$	1	1	−1	0	0	1	1	−1	0	0
16	64	12	$I_1 t$	1	1	−1	0	0	−1	−1	1	0	0
17	64	6	$I_2 t$	1	1	−1	0	0	−1	−1	1	0	0
18	64	6	$I_2 I_1 t$	1	1	−1	0	0	1	1	−1	0	0
19	96	8	$t\gamma$	1	−1	0	−1	1	1	−1	0	−1	1
20	48	8	$I_1 t\gamma$	1	−1	0	−1	1	−1	1	0	1	−1
$20'$	48	8	$I_1 t\gamma^3$	1	−1	0	−1	1	−1	1	0	1	−1

τ_1^4	τ_3^4	τ_1^8	τ_4^4	τ_2^4	τ_2^8	τ_3^6	τ_2^6	τ_4^6	τ_1^6	$\tau_1^{\underline{4}}$	$\tau_2^{\underline{4}}$	$\tau^{\underline{8}}$	$\tau_1^{\underline{12}}$	$\tau_2^{\underline{12}}$
4	4	8	4	4	8	6	6	6	6	4	4	8	12	12
4	4	8	4	4	8	6	6	6	6	−4	−4	−8	−12	−12
2	2	4	−2	−2	−4	0	0	0	0	0	0	0	0	0
0	0	0	0	0	0	−2	−2	−2	−2	0	0	0	0	0
−2	−2	−4	2	2	4	0	0	0	0	0	0	0	0	0
−4	−4	−8	−4	−4	−8	6	6	6	6	0	0	0	0	0
2	−2	0	2	−2	0	2	0	−2	0	0	0	0	0	0
0	0	0	0	0	0	0	2	0	−2	0	0	0	0	0
2	−2	0	−2	2	0	0	−2	0	2	$-2\sqrt{2}$	$2\sqrt{2}$	0	$-2\sqrt{2}$	$2\sqrt{2}$
2	−2	0	−2	2	0	0	−2	0	2	$2\sqrt{2}$	$-2\sqrt{2}$	0	$2\sqrt{2}$	$-2\sqrt{2}$
−2	2	0	−2	2	0	2	0	−2	0	0	0	0	0	0
0	0	0	0	0	0	−2	0	2	0	0	0	0	0	0
−2	2	0	2	−2	0	0	−2	0	2	0	0	0	0	0
0	0	0	0	0	0	2	−2	2	−2	0	0	0	0	0
0	0	0	0	0	0	0	0	0	0	0	0	0	0	0
0	0	0	0	0	0	−2	2	−2	2	2	2	4	−2	−2
0	0	0	0	0	0	−2	2	−2	2	−2	−2	−4	2	2
1	1	−1	1	1	−1	0	0	0	0	2	2	−2	0	0
1	1	−1	1	1	−1	0	0	0	0	−2	−2	2	0	0
−1	−1	1	1	1	−1	0	0	0	0	0	0	0	0	0
1	1	−1	−1	−1	1	0	0	0	0	0	0	0	0	0
−1	−1	1	−1	−1	1	0	0	0	0	0	0	0	0	0
0	0	0	0	0	0	0	0	0	0	0	0	0	0	0
0	0	0	0	0	0	0	0	0	0	$\sqrt{2}$	$-\sqrt{2}$	0	$-\sqrt{2}$	$\sqrt{2}$
0	0	0	0	0	0	0	0	0	0	$-\sqrt{2}$	$\sqrt{2}$	0	$\sqrt{2}$	$-\sqrt{2}$

Appendix C

Operators

C.1. Phase conventions and flavor wave functions

Starting with the standard representation for the quark triplet,

$$u = \begin{pmatrix} 1 \\ 0 \\ 0 \end{pmatrix}, \qquad d = \begin{pmatrix} 0 \\ 1 \\ 0 \end{pmatrix}, \qquad s = \begin{pmatrix} 0 \\ 0 \\ 1 \end{pmatrix}, \tag{C.1a–c}$$

we define the action of lowering operators $\hat{T}_-$, $\hat{U}_-$, and $\hat{V}_-$ for the isospin, U-spin, and V-spin, respectively, in this (fundamental) representation via the matrices (cf. app. A.2)

$$\begin{aligned} T_- &= \tfrac{1}{2}(\lambda^1 - i\lambda^2) & U_- &= \tfrac{1}{2}(\lambda^6 - i\lambda^7) & V_- &= \tfrac{1}{2}(\lambda^4 - i\lambda^5) \\ &= \begin{pmatrix} 0 & 0 & 0 \\ 1 & 0 & 0 \\ 0 & 0 & 0 \end{pmatrix}, & &= \begin{pmatrix} 0 & 0 & 0 \\ 0 & 0 & 0 \\ 0 & 1 & 0 \end{pmatrix}, & &= \begin{pmatrix} 0 & 0 & 0 \\ 0 & 0 & 0 \\ 1 & 0 & 0 \end{pmatrix}, \end{aligned} \tag{C.2a–c}$$

so that, as illustrated in figure C.1,

$$\hat{T}_- u = T_- u = d\,, \qquad \hat{U}_- d = U_- d = s\,, \qquad \hat{V}_- u = V_- u = s\,, \tag{C.3a–c}$$

while all other combinations result in zero.

The baryon octet can be presented as a traceless 3×3 matrix [185]

$$\begin{pmatrix} \frac{\Lambda}{\sqrt{6}} + \frac{\Sigma^0}{\sqrt{2}} & \Sigma^+ & p \\ \Sigma^- & \frac{\Lambda}{\sqrt{6}} - \frac{\Sigma^0}{\sqrt{2}} & n \\ \Xi^- & \Xi^0 & -2\frac{\Lambda}{\sqrt{6}} \end{pmatrix} = p\,\mathcal{K}_p + n\,\mathcal{K}_n + \cdots\,, \tag{C.4}$$

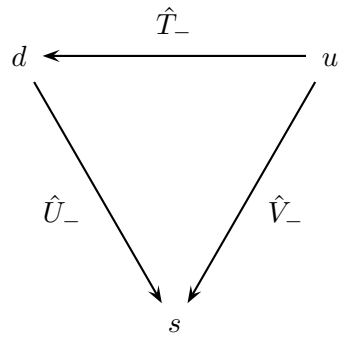

Figure C.1.: Action of isospin, U-spin, and V-spin lowering operators in the quark triplet.

where $\mathcal{K}_B$ are 3×3 matrices defined by this equation. We further define the application of the lowering operators $\hat{T}_-$, $\hat{U}_-$, and $\hat{V}_-$ to the octet by the usual expressions for the adjoint action,

$$\hat{T}_- \mathcal{K}_B = [T_-, \mathcal{K}_B]\,, \qquad \hat{U}_- \mathcal{K}_B = [U_-, \mathcal{K}_B]\,, \qquad \hat{V}_- \mathcal{K}_B = [V_-, \mathcal{K}_B]\,, \tag{C.5a–c}$$

without any additional phase factors.

The above choices specify our phase conventions. Starting from the proton state, the complete octet can be constructed by applying the following transformations as illustrated in figure C.2:

$$\hat{T}_- |p\rangle = |n\rangle\,, \tag{C.6a}$$
$$-\hat{U}_- |p\rangle = |\Sigma^+\rangle\,, \tag{C.6b}$$
$$\tfrac{1}{\sqrt{2}} \hat{T}_- \hat{U}_- |p\rangle = |\Sigma^0\rangle\,, \tag{C.6c}$$
$$\tfrac{1}{2} \hat{T}_- \hat{T}_- \hat{U}_- |p\rangle = |\Sigma^-\rangle\,, \tag{C.6d}$$
$$-\hat{V}_- \hat{U}_- |p\rangle = |\Xi^0\rangle\,, \tag{C.6e}$$
$$\hat{T}_- \hat{V}_- \hat{U}_- |p\rangle = |\Xi^-\rangle\,, \tag{C.6f}$$
$$\tfrac{-1}{\sqrt{6}} \big(\hat{V}_- + \hat{U}_- \hat{T}_-\big) |p\rangle = |\Lambda\rangle\,. \tag{C.6g}$$

Starting from the mixed-symmetric and mixed-antisymmetric flavor wave functions for the proton defined as (cf. eqs. (3.40))

$$|p_{\mathrm{MS}}\rangle = \frac{1}{\sqrt{6}}(2|uud\rangle - |udu\rangle - |duu\rangle)\,, \qquad |p_{\mathrm{MA}}\rangle = \frac{1}{\sqrt{2}}(|udu\rangle - |duu\rangle)\,, \tag{C.7a–b}$$

the wave functions of the octet can now be constructed by applying the transformations (C.6), see tables C.2 and C.3.

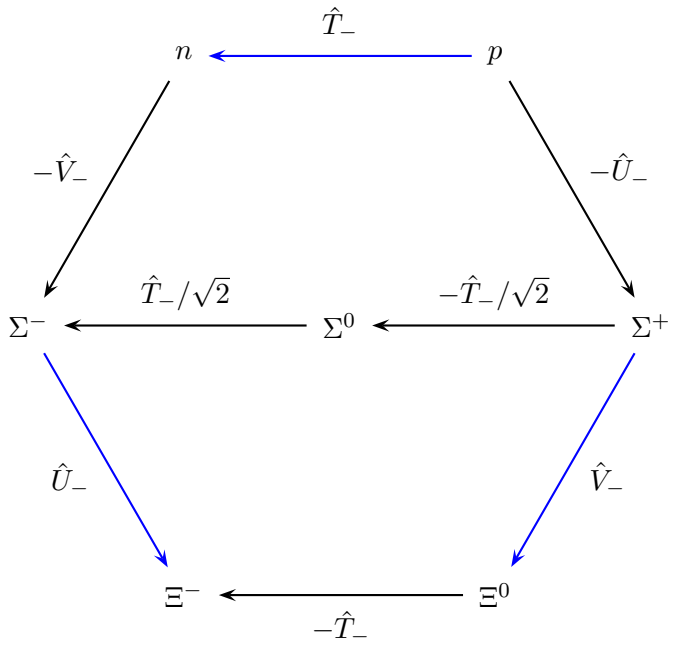

Figure C.2.: Illustration of our phase conventions. The Λ baryon is not shown since one needs a linear combination for its construction, cf. eq. (C.6g). Blue arrows indicate the cases where one has to apply a Fierz transformation to relate the distribution amplitudes at the symmetric point, see [126]. An explicit calculation shows that this always yields an additional minus sign that has to be taken into account in order to reproduce eqs. (C.9) and (3.13).

Together with the choice of flavor ordering in the matrix elements defining the DAs of the different baryons (cf. eqs. (3.3) and (3.4)),

$$\begin{aligned} p &\mathrel{\hat{=}} uud\,, & n &\mathrel{\hat{=}} ddu\,, & \Sigma^+ &\mathrel{\hat{=}} uus\,, & \Sigma^0 &\mathrel{\hat{=}} uds\,, \\ \Sigma^- &\mathrel{\hat{=}} dds\,, & \Xi^0 &\mathrel{\hat{=}} ssu\,, & \Xi^- &\mathrel{\hat{=}} ssd\,, & \Lambda &\mathrel{\hat{=}} uds\,, \end{aligned} \tag{C.8a–h}$$

our conventions also fix the relative signs of the octet baryon DAs. As shown in [33], this choice corresponds to the following identities for the DAs in the limit of exact isospin symmetry:

$$\mathrm{DA}^N \equiv \mathrm{DA}^p = -\mathrm{DA}^n\,, \tag{C.9a}$$

$$\mathrm{DA}^\Sigma \equiv \mathrm{DA}^{\Sigma^-} = \sqrt{2}\mathrm{DA}^{\Sigma^0} = -\mathrm{DA}^{\Sigma^+}\,, \tag{C.9b}$$

$$\mathrm{DA}^\Xi \equiv \mathrm{DA}^{\Xi^0} = -\mathrm{DA}^{\Xi^-}\,. \tag{C.9c}$$

This also fixes the relative phases at the flavor symmetric point in eqs. (3.13). All phases in the octet are now unambiguously determined up to a single unphysical global phase, which is commonly fixed by the condition that f^N has to be positive.

Table C.1.: Totally antisymmetric (A) flavor wave functions.

B	$\lvert B_{\mathrm{A}}\rangle = \sum_{f,g,h} F_{\mathscr{S}}^{B,fgh} \lvert fgh\rangle$
Λ	$(\lvert dus\rangle - \lvert uds\rangle + \lvert usd\rangle - \lvert dsu\rangle + \lvert sdu\rangle - \lvert sud\rangle)/\sqrt{6}$

Table C.2.: Mixed-symmetric (MS) flavor wave functions.

B	$\lvert B_{\mathrm{MS}}\rangle = \sum_{f,g,h} F_{\mathscr{O},1}^{B,fgh} \lvert fgh\rangle$
N	$(2\lvert uud\rangle - \lvert udu\rangle - \lvert duu\rangle)/\sqrt{6}$
Σ	$(2\lvert dds\rangle - \lvert dsd\rangle - \lvert sdd\rangle)/\sqrt{6}$
Ξ	$(2\lvert ssu\rangle - \lvert sus\rangle - \lvert uss\rangle)/\sqrt{6}$
Λ	$(\lvert dsu\rangle - \lvert usd\rangle + \lvert sdu\rangle - \lvert sud\rangle)/2$

Table C.3.: Mixed-antisymmetric (MA) flavor wave functions.

B	$\lvert B_{\mathrm{MA}}\rangle = \sum_{f,g,h} F_{\mathscr{O},2}^{B,fgh} \lvert fgh\rangle$
N	$(\lvert udu\rangle - \lvert duu\rangle)/\sqrt{2}$
Σ	$(\lvert dsd\rangle - \lvert sdd\rangle)/\sqrt{2}$
Ξ	$(\lvert sus\rangle - \lvert uss\rangle)/\sqrt{2}$
Λ	$(2\lvert dus\rangle - 2\lvert uds\rangle + \lvert dsu\rangle - \lvert usd\rangle + \lvert sud\rangle - \lvert sdu\rangle)/\sqrt{12}$

Table C.4.: Totally symmetric (S) flavor wave functions.

B	$\lvert B_{\mathrm{S}}\rangle = \sum_{f,g,h} F_{\mathscr{D}}^{B,fgh} \lvert fgh\rangle$
N	$(\lvert uud\rangle + \lvert udu\rangle + \lvert duu\rangle)/\sqrt{3}$
Σ	$(\lvert dds\rangle + \lvert dsd\rangle + \lvert sdd\rangle)/\sqrt{3}$
Ξ	$(\lvert ssu\rangle + \lvert sus\rangle + \lvert uss\rangle)/\sqrt{3}$

C.2. Optimal operator bases for renormalization

For the purpose of renormalization, it is convenient to employ operator multiplets that transform irreducibly not only with respect to the spinorial hypercubic group $\overline{\mathrm{H}(4)}$ but also with respect to the group $\mathcal{S}_3$ of permutations of the three quark flavors. The latter group has three inequivalent irreducible representations, which correspond to ground state particle multiplets in a SU(3) flavor symmetric world (see section 3.4.2). Therefore, we label multiplets of operators transforming under the one-dimensional trivial representation by $\mathscr{D}$, the one-dimensional totally antisymmetric representation by $\mathscr{S}$, and the two-dimensional representation by $\mathscr{O}$.

Furthermore, we want operators that have autonomous scale dependence under one-loop evolution, resulting in a direct correspondence between the operator multiplets and the

shape parameters in the SU(3) symmetric limit. The $\overline{\mathrm{H}(4)}$ and $\mathcal{S}_3$ constraints discussed above still leave enough freedom to be able to enforce this property as well.

As a starting point we use the operator multiplets defined in [52], which have been constructed to transform under irreducible representations of $\overline{\mathrm{H}(4)}$. We construct our new multiplets (with the desired additional properties) as linear combinations thereof. Since we will only combine multiplets from a single representation at a time, the $\overline{\mathrm{H}(4)}$ transformation properties will automatically carry over to our newly defined operator multiplets.

On the right-hand sides of the equations in the following sections we use the operator definitions and nomenclature of [52]. We use the subscripts f, g, and h to specify a derivative acting on the first, second, and third quark, respectively. E.g., $\mathcal{O}_{fg4}$ refers to the operator multiplet $\mathcal{O}_{DD4}$ with one derivative acting on the first quark and one derivative acting on the second. The operators in the next three subsections below are defined for generic flavors, i.e., not for any specific baryon B. To obtain the operators for particular baryons one has to adorn them with the respective flavor structures (which are defined by tables C.1–C.4):

$$\big(\mathscr{S}\mathcal{R}\big)^B_m = \sum_{f_1,f_2,f_3} F^{B,f_1f_2f_3}_{\mathscr{S}} \big(\mathscr{S}\mathcal{R}\big)_m \,, \tag{C.10a}$$

$$\big(\mathscr{O}\mathcal{R}\big)^B_m = \sum_{f_1,f_2,f_3} \sum_t F^{B,f_1f_2f_3}_{\mathscr{O},t} \big(\mathscr{O}\mathcal{R}\big)_{m,t} \,, \tag{C.10b}$$

$$\big(\mathscr{D}\mathcal{R}\big)^B_m = \sum_{f_1,f_2,f_3} F^{B,f_1f_2f_3}_{\mathscr{D}} \big(\mathscr{D}\mathcal{R}\big)_m \,, \tag{C.10c}$$

where $\mathcal{R}$ is a stand-in for any combined $\overline{\mathrm{H}(4)}$ representation and derivative label (such as $\frac{12}{2,D}$) and the quarks of generic flavor contained in the operators on the right-hand side are implied to be set to f_1, f_2, and f_3.

C.2.1. Zero derivatives

For operators without derivatives we consider all (leading twist and higher twist) operators. In the $\overline{\mathrm{H}(4)}$ representation $\tau_1^{\underline{12}}$ we have 1 doublet of octet multiplets[76] and 1 decuplet multiplet (leading twist):

$$\big(\mathscr{O}_1^{\underline{12}}\big)_{1,t} = \begin{cases} \frac{1}{\sqrt{6}}(\mathcal{O}_7 + \mathcal{O}_8 - 2\mathcal{O}_9) \,, \\ \frac{1}{\sqrt{2}}(\mathcal{O}_7 - \mathcal{O}_8) \,, \end{cases} \tag{C.11a}$$

$$\big(\mathscr{D}_1^{\underline{12}}\big)_1 = \tfrac{1}{\sqrt{3}}(\mathcal{O}_7 + \mathcal{O}_8 + \mathcal{O}_9) \,. \tag{C.11b}$$

[76] By "doublet of octet multiplets" we refer to two multiplets (which themselves are 12-, 8-, or 4-dimensional, as indicated by the underlined superscript) of operators transforming irreducibly under $\overline{\mathrm{H}(4)}$, where these two $\overline{\mathrm{H}(4)}$ multiplets together transform as a doublet under the two-dimensional representation of $\mathcal{S}_3$, which we associate with the SU(3) octet (cf. section 3.4.2). In our notation the first ($t = 1$) multiplet is always the mixed-symmetric one, while the second ($t = 2$) is mixed-antisymmetric.

In the $\overline{\mathrm{H}(4)}$ representation τ^8 we have 1 decuplet multiplet (leading twist):

$$\left(\mathscr{D}^8\right)_1 = \mathcal{O}_6\,. \tag{C.12}$$

In the $\overline{\mathrm{H}(4)}$ representation τ_1^4 we have 1 singlet multiplet and 2 doublets of octet multiplets (higher twist):[77]

$$\left(\mathscr{S}_1^4\right)_1 = \tfrac{1}{\sqrt{3}}(\mathcal{O}_3 - \mathcal{O}_4 - \mathcal{O}_5)\,, \tag{C.13a}$$

$$\left(\mathscr{O}_1^4\right)_{1,t} = \begin{cases} \tfrac{1}{\sqrt{2}}(\mathcal{O}_3 + \mathcal{O}_4)\,, \\ \tfrac{1}{\sqrt{6}}(-\mathcal{O}_3 + \mathcal{O}_4 - 2\mathcal{O}_5)\,, \end{cases} \tag{C.13b}$$

$$\left(\mathscr{O}_1^4\right)_{2,t} = \begin{cases} \mathcal{O}_2\,, \\ \tfrac{1}{\sqrt{3}}(2\mathcal{O}_1 + \mathcal{O}_2)\,. \end{cases} \tag{C.13c}$$

C.2.2. One derivative

For the case of one derivative we present all leading twist operators. In the $\overline{\mathrm{H}(4)}$ representation τ_2^{12} we have 1 singlet multiplet, 4 doublets of octet multiplets, and 3 decuplet multiplets:

$$\left(\mathscr{S}_{2,D}^{12}\right)_1 = \tfrac{1}{\sqrt{6}}\big[(\mathcal{O}_{g5} - \mathcal{O}_{h5}) + (\mathcal{O}_{h6} - \mathcal{O}_{f6}) + (\mathcal{O}_{f7} - \mathcal{O}_{g7})\big]\,,$$

$$\left(\mathscr{O}_{2,D}^{12}\right)_{1,t} = \begin{cases} \tfrac{1}{3\sqrt{2}}\big[(\mathcal{O}_{f5} + \mathcal{O}_{g5} + \mathcal{O}_{h5}) + (\mathcal{O}_{f6} + \mathcal{O}_{g6} + \mathcal{O}_{h6}) - 2(\mathcal{O}_{f7} + \mathcal{O}_{g7} + \mathcal{O}_{h7})\big]\,, \\ \tfrac{1}{\sqrt{6}}\big[(\mathcal{O}_{f5} + \mathcal{O}_{g5} + \mathcal{O}_{h5}) - (\mathcal{O}_{f6} + \mathcal{O}_{g6} + \mathcal{O}_{h6})\big]\,, \end{cases}$$

$$\left(\mathscr{O}_{2,D}^{12}\right)_{2,t} = \begin{cases} \tfrac{1}{6}\big[(-2\mathcal{O}_{f5} + \mathcal{O}_{g5} + \mathcal{O}_{h5}) + (\mathcal{O}_{f6} - 2\mathcal{O}_{g6} + \mathcal{O}_{h6}) - 2(\mathcal{O}_{f7} + \mathcal{O}_{g7} - 2\mathcal{O}_{h7})\big]\,, \\ \tfrac{1}{2\sqrt{3}}\big[(-2\mathcal{O}_{f5} + \mathcal{O}_{g5} + \mathcal{O}_{h5}) - (\mathcal{O}_{f6} - 2\mathcal{O}_{g6} + \mathcal{O}_{h6})\big]\,, \end{cases}$$

$$\left(\mathscr{O}_{2,D}^{12}\right)_{3,t} = \begin{cases} \tfrac{1}{2}\big[(\mathcal{O}_{g5} - \mathcal{O}_{h5}) - (\mathcal{O}_{h6} - \mathcal{O}_{f6})\big]\,, \\ -\tfrac{1}{2\sqrt{3}}\big[(\mathcal{O}_{g5} - \mathcal{O}_{h5}) + (\mathcal{O}_{h6} - \mathcal{O}_{f6}) - 2(\mathcal{O}_{f7} - \mathcal{O}_{g7})\big]\,, \end{cases}$$

$$\left(\mathscr{O}_{2,D}^{12}\right)_{4,t} = \begin{cases} \tfrac{1}{\sqrt{6}}(\mathcal{O}_{f8} + \mathcal{O}_{g8} - 2\mathcal{O}_{h8})\,, \\ \tfrac{1}{\sqrt{2}}(\mathcal{O}_{f8} - \mathcal{O}_{g8})\,, \end{cases}$$

$$\left(\mathscr{D}_{2,D}^{12}\right)_1 = \tfrac{1}{3}\big[(\mathcal{O}_{f5} + \mathcal{O}_{g5} + \mathcal{O}_{h5}) + (\mathcal{O}_{f6} + \mathcal{O}_{g6} + \mathcal{O}_{h6}) + (\mathcal{O}_{f7} + \mathcal{O}_{g7} + \mathcal{O}_{h7})\big]\,,$$

$$\left(\mathscr{D}_{2,D}^{12}\right)_2 = \tfrac{1}{3\sqrt{2}}\big[(-2\mathcal{O}_{f5} + \mathcal{O}_{g5} + \mathcal{O}_{h5}) + (\mathcal{O}_{f6} - 2\mathcal{O}_{g6} + \mathcal{O}_{h6}) + (\mathcal{O}_{f7} + \mathcal{O}_{g7} - 2\mathcal{O}_{h7})\big]\,,$$

$$\left(\mathscr{D}_{2,D}^{12}\right)_3 = \tfrac{1}{\sqrt{3}}(\mathcal{O}_{f8} + \mathcal{O}_{g8} + \mathcal{O}_{h8})\,. \tag{C.14a–h}$$

[77] The seemingly unorthodox construction and normalization of the operator (C.13c) can be traced back to the fact that the multiplets $\mathcal{O}_1$ and $\mathcal{O}_2$ were chosen in a suboptimal, nonorthogonal manner in [51].

For operators with one derivative in the $\overline{\mathrm{H}(4)}$ representation τ_1^{12} we have 1 singlet multiplet, 3 doublets of octet multiplets, and 2 decuplet multiplets:

$$
\begin{aligned}
\big(\mathscr{S}^{12}_{1,D}\big)_1 &= \tfrac{1}{\sqrt{6}}\big[(\mathcal{O}_{g2}-\mathcal{O}_{h2})+(\mathcal{O}_{h3}-\mathcal{O}_{f3})+(\mathcal{O}_{f4}-\mathcal{O}_{g4})\big]\,,\\
\big(\mathscr{O}^{12}_{1,D}\big)_{1,t} &= \begin{cases} \tfrac{1}{3\sqrt{2}}\big[(\mathcal{O}_{f2}+\mathcal{O}_{g2}+\mathcal{O}_{h2})+(\mathcal{O}_{f3}+\mathcal{O}_{g3}+\mathcal{O}_{h3})-2(\mathcal{O}_{f4}+\mathcal{O}_{g4}+\mathcal{O}_{h4})\big]\,,\\ \tfrac{1}{\sqrt{6}}\big[(\mathcal{O}_{f2}+\mathcal{O}_{g2}+\mathcal{O}_{h2})-(\mathcal{O}_{f3}+\mathcal{O}_{g3}+\mathcal{O}_{h3})\big]\,, \end{cases}\\
\big(\mathscr{O}^{12}_{1,D}\big)_{2,t} &= \begin{cases} \tfrac{1}{6}\big[(-2\mathcal{O}_{f2}+\mathcal{O}_{g2}+\mathcal{O}_{h2})+(\mathcal{O}_{f3}-2\mathcal{O}_{g3}+\mathcal{O}_{h3})-2(\mathcal{O}_{f4}+\mathcal{O}_{g4}-2\mathcal{O}_{h4})\big]\,,\\ \tfrac{1}{2\sqrt{3}}\big[(-2\mathcal{O}_{f2}+\mathcal{O}_{g2}+\mathcal{O}_{h2})-(\mathcal{O}_{f3}-2\mathcal{O}_{g3}+\mathcal{O}_{h3})\big]\,, \end{cases}\\
\big(\mathscr{O}^{12}_{1,D}\big)_{3,t} &= \begin{cases} \tfrac{1}{2}\big[(\mathcal{O}_{g2}-\mathcal{O}_{h2})-(\mathcal{O}_{h3}-\mathcal{O}_{f3})\big]\,,\\ -\tfrac{1}{2\sqrt{3}}\big[(\mathcal{O}_{g2}-\mathcal{O}_{h2})+(\mathcal{O}_{h3}-\mathcal{O}_{f3})-2(\mathcal{O}_{f4}-\mathcal{O}_{g4})\big]\,, \end{cases}\\
\big(\mathscr{D}^{12}_{1,D}\big)_1 &= \tfrac{1}{3}\big[(\mathcal{O}_{f2}+\mathcal{O}_{g2}+\mathcal{O}_{h2})+(\mathcal{O}_{f3}+\mathcal{O}_{g3}+\mathcal{O}_{h3})+(\mathcal{O}_{f4}+\mathcal{O}_{g4}+\mathcal{O}_{h4})\big]\,,\\
\big(\mathscr{D}^{12}_{1,D}\big)_2 &= \tfrac{1}{3\sqrt{2}}\big[(-2\mathcal{O}_{f2}+\mathcal{O}_{g2}+\mathcal{O}_{h2})+(\mathcal{O}_{f3}-2\mathcal{O}_{g3}+\mathcal{O}_{h3})+(\mathcal{O}_{f4}+\mathcal{O}_{g4}-2\mathcal{O}_{h4})\big]\,.
\end{aligned}
\tag{C.15a–f}
$$

For operators with one derivative in the $\overline{\mathrm{H}(4)}$ representation τ^8 we have 1 doublet of octet multiplets and 1 decuplet multiplet:

$$
\big(\mathscr{O}^{8}_{D}\big)_{1,t} = \begin{cases} \tfrac{1}{\sqrt{6}}(\mathcal{O}_{f1}+\mathcal{O}_{g1}-2\mathcal{O}_{h1})\,,\\ \tfrac{1}{\sqrt{2}}(\mathcal{O}_{f1}-\mathcal{O}_{g1})\,, \end{cases} \tag{C.16a}
$$

$$
\big(\mathscr{D}^{8}_{D}\big)_1 = \tfrac{1}{\sqrt{3}}(\mathcal{O}_{f1}+\mathcal{O}_{g1}+\mathcal{O}_{h1})\,. \tag{C.16b}
$$

C.2.3. Two derivatives

Due to the enormous amount of possible three-quark operators with two derivatives we focus on those leading twist operators that are relevant in practice. They are the operator multiplets transforming according to the $\overline{\mathrm{H}(4)}$ representation τ_2^4. In this representation we have 2 singlet multiplets, 6 doublets of octet multiplets, and 4 decuplet multiplets:

$$
\begin{aligned}
\big(\mathscr{S}^{4}_{2,DD}\big)_1 = \tfrac{1}{2\sqrt{3}}\big[&(\mathcal{O}_{fg4}-\mathcal{O}_{fh4}+\mathcal{O}_{gg4}-\mathcal{O}_{hh4})\\
&+(-\mathcal{O}_{ff5}-\mathcal{O}_{fg5}+\mathcal{O}_{gh5}+\mathcal{O}_{hh5})\\
&+(\mathcal{O}_{ff6}+\mathcal{O}_{fh6}-\mathcal{O}_{gg6}-\mathcal{O}_{gh6})\big]\,,
\end{aligned}
\tag{C.17a}
$$

$$
\begin{aligned}
\big(\mathscr{S}^{4}_{2,DD}\big)_2 = \tfrac{1}{2\sqrt{15}}\big[&(-3\mathcal{O}_{fg4}+3\mathcal{O}_{fh4}+\mathcal{O}_{gg4}-\mathcal{O}_{hh4})\\
&+(-\mathcal{O}_{ff5}+3\mathcal{O}_{fg5}-3\mathcal{O}_{gh5}+\mathcal{O}_{hh5})\\
&+(\mathcal{O}_{ff6}-3\mathcal{O}_{fh6}-\mathcal{O}_{gg6}+3\mathcal{O}_{gh6})\big]\,,
\end{aligned}
\tag{C.17b}
$$

$$\left(\mathscr{O}^4_{2,DD}\right)_{1,t} = \begin{cases} \frac{1}{3\sqrt{10}}\big[(\mathcal{O}_{ff4} + 2\mathcal{O}_{fg4} + 2\mathcal{O}_{fh4} + \mathcal{O}_{gg4} + 2\mathcal{O}_{gh4} + \mathcal{O}_{hh4}) \\ \quad + (\mathcal{O}_{ff5} + 2\mathcal{O}_{fg5} + 2\mathcal{O}_{fh5} + \mathcal{O}_{gg5} + 2\mathcal{O}_{gh5} + \mathcal{O}_{hh5}) \\ \quad - 2(\mathcal{O}_{ff6} + 2\mathcal{O}_{fg6} + 2\mathcal{O}_{fh6} + \mathcal{O}_{gg6} + 2\mathcal{O}_{gh6} + \mathcal{O}_{hh6})\big], \\ \frac{1}{\sqrt{30}}\big[(\mathcal{O}_{ff4} + 2\mathcal{O}_{fg4} + 2\mathcal{O}_{fh4} + \mathcal{O}_{gg4} + 2\mathcal{O}_{gh4} + \mathcal{O}_{hh4}) \\ \quad - (\mathcal{O}_{ff5} + 2\mathcal{O}_{fg5} + 2\mathcal{O}_{fh5} + \mathcal{O}_{gg5} + 2\mathcal{O}_{gh5} + \mathcal{O}_{hh5})\big], \end{cases} \tag{C.17c}$$

$$\left(\mathscr{O}^4_{2,DD}\right)_{2,t} = \begin{cases} \frac{1}{6\sqrt{2}}\big[(-2\mathcal{O}_{ff4} - \mathcal{O}_{fg4} - \mathcal{O}_{fh4} + \mathcal{O}_{gg4} + 2\mathcal{O}_{gh4} + \mathcal{O}_{hh4}) \\ \quad + (\mathcal{O}_{ff5} - \mathcal{O}_{fg5} + 2\mathcal{O}_{fh5} - 2\mathcal{O}_{gg5} - \mathcal{O}_{gh5} + \mathcal{O}_{hh5}) \\ \quad - 2(\mathcal{O}_{ff6} + 2\mathcal{O}_{fg6} - \mathcal{O}_{fh6} + \mathcal{O}_{gg6} - \mathcal{O}_{gh6} - 2\mathcal{O}_{hh6})\big], \\ \frac{1}{2\sqrt{6}}\big[(-2\mathcal{O}_{ff4} - \mathcal{O}_{fg4} - \mathcal{O}_{fh4} + \mathcal{O}_{gg4} + 2\mathcal{O}_{gh4} + \mathcal{O}_{hh4}) \\ \quad - (\mathcal{O}_{ff5} - \mathcal{O}_{fg5} + 2\mathcal{O}_{fh5} - 2\mathcal{O}_{gg5} - \mathcal{O}_{gh5} + \mathcal{O}_{hh5})\big], \end{cases} \tag{C.17d}$$

$$\left(\mathscr{O}^4_{2,DD}\right)_{3,t} = \begin{cases} \frac{1}{2\sqrt{114}}\big[(2\mathcal{O}_{ff4} - 3\mathcal{O}_{fg4} - 3\mathcal{O}_{fh4} + 3\mathcal{O}_{gg4} - 6\mathcal{O}_{gh4} + 3\mathcal{O}_{hh4}) \\ \quad + (3\mathcal{O}_{ff5} - 3\mathcal{O}_{fg5} - 6\mathcal{O}_{fh5} + 2\mathcal{O}_{gg5} - 3\mathcal{O}_{gh5} + 3\mathcal{O}_{hh5}) \\ \quad - 2(3\mathcal{O}_{ff6} - 6\mathcal{O}_{fg6} - 3\mathcal{O}_{fh6} + 3\mathcal{O}_{gg6} - 3\mathcal{O}_{gh6} + 2\mathcal{O}_{hh6})\big], \\ \frac{1}{2\sqrt{38}}\big[(2\mathcal{O}_{ff4} - 3\mathcal{O}_{fg4} - 3\mathcal{O}_{fh4} + 3\mathcal{O}_{gg4} - 6\mathcal{O}_{gh4} + 3\mathcal{O}_{hh4}) \\ \quad - (3\mathcal{O}_{ff5} - 3\mathcal{O}_{fg5} - 6\mathcal{O}_{fh5} + 2\mathcal{O}_{gg5} - 3\mathcal{O}_{gh5} + 3\mathcal{O}_{hh5})\big], \end{cases} \tag{C.17e}$$

$$\left(\mathscr{O}^4_{2,DD}\right)_{4,t} = \begin{cases} \frac{1}{4\sqrt{129}}\big[(-6\mathcal{O}_{ff4} + 9\mathcal{O}_{fg4} + 9\mathcal{O}_{fh4} + \mathcal{O}_{gg4} - 12\mathcal{O}_{gh4} + \mathcal{O}_{hh4}) \\ \quad + (\mathcal{O}_{ff5} + 9\mathcal{O}_{fg5} - 12\mathcal{O}_{fh5} - 6\mathcal{O}_{gg5} + 9\mathcal{O}_{gh5} + \mathcal{O}_{hh5}) \\ \quad - 2(\mathcal{O}_{ff6} - 12\mathcal{O}_{fg6} + 9\mathcal{O}_{fh6} + \mathcal{O}_{gg6} + 9\mathcal{O}_{gh6} - 6\mathcal{O}_{hh6})\big], \\ \frac{1}{4\sqrt{43}}\big[(-6\mathcal{O}_{ff4} + 9\mathcal{O}_{fg4} + 9\mathcal{O}_{fh4} + \mathcal{O}_{gg4} - 12\mathcal{O}_{gh4} + \mathcal{O}_{hh4}) \\ \quad - (\mathcal{O}_{ff5} + 9\mathcal{O}_{fg5} - 12\mathcal{O}_{fh5} - 6\mathcal{O}_{gg5} + 9\mathcal{O}_{gh5} + \mathcal{O}_{hh5})\big], \end{cases} \tag{C.17f}$$

$$\left(\mathscr{O}^4_{2,DD}\right)_{5,t} = \begin{cases} \frac{1}{2\sqrt{2}}\big[(\mathcal{O}_{fg4} - \mathcal{O}_{fh4} + \mathcal{O}_{gg4} - \mathcal{O}_{hh4}) \\ \quad - (-\mathcal{O}_{ff5} - \mathcal{O}_{fg5} + \mathcal{O}_{gh5} + \mathcal{O}_{hh5})\big], \\ -\frac{1}{2\sqrt{6}}\big[(\mathcal{O}_{fg4} - \mathcal{O}_{fh4} + \mathcal{O}_{gg4} - \mathcal{O}_{hh4}) \\ \quad + (-\mathcal{O}_{ff5} - \mathcal{O}_{fg5} + \mathcal{O}_{gh5} + \mathcal{O}_{hh5}) \\ \quad - 2(\mathcal{O}_{ff6} + \mathcal{O}_{fh6} - \mathcal{O}_{gg6} - \mathcal{O}_{gh6})\big], \end{cases} \tag{C.17g}$$

$$\left(\mathscr{O}^4_{2,DD}\right)_{6,t} = \begin{cases} \frac{1}{2\sqrt{10}}\big[(-3\mathcal{O}_{fg4} + 3\mathcal{O}_{fh4} + \mathcal{O}_{gg4} - \mathcal{O}_{hh4}) \\ \quad - (-\mathcal{O}_{ff5} + 3\mathcal{O}_{fg5} - 3\mathcal{O}_{gh5} + \mathcal{O}_{hh5})\big], \\ -\frac{1}{2\sqrt{30}}\big[(-3\mathcal{O}_{fg4} + 3\mathcal{O}_{fh4} + \mathcal{O}_{gg4} - \mathcal{O}_{hh4}) \\ \quad + (-\mathcal{O}_{ff5} + 3\mathcal{O}_{fg5} - 3\mathcal{O}_{gh5} + \mathcal{O}_{hh5}) \\ \quad - 2(\mathcal{O}_{ff6} - 3\mathcal{O}_{fh6} - \mathcal{O}_{gg6} + 3\mathcal{O}_{gh6})\big], \end{cases} \tag{C.17h}$$

$$\begin{aligned}
\left(\mathscr{D}^4_{2,DD}\right)_1 = \tfrac{1}{3\sqrt{5}}\big[&(\mathcal{O}_{ff4} + 2\mathcal{O}_{fg4} + 2\mathcal{O}_{fh4} + \mathcal{O}_{gg4} + 2\mathcal{O}_{gh4} + \mathcal{O}_{hh4}) \\
&+ (\mathcal{O}_{ff5} + 2\mathcal{O}_{fg5} + 2\mathcal{O}_{fh5} + \mathcal{O}_{gg5} + 2\mathcal{O}_{gh5} + \mathcal{O}_{hh5}) \\
&+ (\mathcal{O}_{ff6} + 2\mathcal{O}_{fg6} + 2\mathcal{O}_{fh6} + \mathcal{O}_{gg6} + 2\mathcal{O}_{gh6} + \mathcal{O}_{hh6})\big]\,, \qquad \text{(C.17i)} \\
\left(\mathscr{D}^4_{2,DD}\right)_2 = \tfrac{1}{6}\big[&(-2\mathcal{O}_{ff4} - \mathcal{O}_{fg4} - \mathcal{O}_{fh4} + \mathcal{O}_{gg4} + 2\mathcal{O}_{gh4} + \mathcal{O}_{hh4}) \\
&+ (\mathcal{O}_{ff5} - \mathcal{O}_{fg5} + 2\mathcal{O}_{fh5} - 2\mathcal{O}_{gg5} - \mathcal{O}_{gh5} + \mathcal{O}_{hh5}) \\
&+ (\mathcal{O}_{ff6} + 2\mathcal{O}_{fg6} - \mathcal{O}_{fh6} + \mathcal{O}_{gg6} - \mathcal{O}_{gh6} - 2\mathcal{O}_{hh6})\big]\,, \qquad \text{(C.17j)} \\
\left(\mathscr{D}^4_{2,DD}\right)_3 = \tfrac{1}{2\sqrt{57}}\big[&(2\mathcal{O}_{ff4} - 3\mathcal{O}_{fg4} - 3\mathcal{O}_{fh4} + 3\mathcal{O}_{gg4} - 6\mathcal{O}_{gh4} + 3\mathcal{O}_{hh4}) \\
&+ (3\mathcal{O}_{ff5} - 3\mathcal{O}_{fg5} - 6\mathcal{O}_{fh5} + 2\mathcal{O}_{gg5} - 3\mathcal{O}_{gh5} + 3\mathcal{O}_{hh5}) \\
&+ (3\mathcal{O}_{ff6} - 6\mathcal{O}_{fg6} - 3\mathcal{O}_{fh6} + 3\mathcal{O}_{gg6} - 3\mathcal{O}_{gh6} + 2\mathcal{O}_{hh6})\big]\,, \qquad \text{(C.17k)} \\
\left(\mathscr{D}^4_{2,DD}\right)_4 = \tfrac{1}{2\sqrt{258}}\big[&(-6\mathcal{O}_{ff4} + 9\mathcal{O}_{fg4} + 9\mathcal{O}_{fh4} + \mathcal{O}_{gg4} - 12\mathcal{O}_{gh4} + \mathcal{O}_{hh4}) \\
&+ (\mathcal{O}_{ff5} + 9\mathcal{O}_{fg5} - 12\mathcal{O}_{fh5} - 6\mathcal{O}_{gg5} + 9\mathcal{O}_{gh5} + \mathcal{O}_{hh5}) \\
&+ (\mathcal{O}_{ff6} - 12\mathcal{O}_{fg6} + 9\mathcal{O}_{fh6} + \mathcal{O}_{gg6} + 9\mathcal{O}_{gh6} - 6\mathcal{O}_{hh6})\big]\,. \qquad \text{(C.17l)}
\end{aligned}$$

C.3. Relation of lattice operators to $\overline{\text{H(4)}}$ operators

In the following we will relate the lattice operators defined in eqs. (4.5), (4.7), and (D.3) to those of [52]. It is implied that within the generic operators appearing on the right-hand sides of these equations the quark flavors are chosen such that they agree with the conventions (3.3) for the baryon B. For the operators without derivatives in the $\overline{\text{H}(4)}$ representation τ_1^{12} we have

$$\mathcal{O}^{B,000}_{\mathcal{T},\mathfrak{A}} = 4\begin{pmatrix} -\mathcal{O}_9^{(6)} \\ +\mathcal{O}_9^{(1)} \\ -\mathcal{O}_9^{(12)} \\ +\mathcal{O}_9^{(7)} \end{pmatrix}, \quad \mathcal{O}^{B,000}_{\mathcal{T},\mathfrak{B}} = 4\begin{pmatrix} -\mathcal{O}_9^{(4)} \\ +\mathcal{O}_9^{(3)} \\ -\mathcal{O}_9^{(10)} \\ +\mathcal{O}_9^{(9)} \end{pmatrix}, \quad \mathcal{O}^{B,000}_{\mathcal{T},\mathfrak{C}} = 4\sqrt{2}\begin{pmatrix} +\mathcal{O}_9^{(2)} \\ -\mathcal{O}_9^{(5)} \\ +\mathcal{O}_9^{(8)} \\ -\mathcal{O}_9^{(11)} \end{pmatrix}, \quad \text{(C.18a–c)}$$

where the operators for the structure $\mathcal{V}{+}\mathcal{A}$ (or $\mathcal{V}{-}\mathcal{A}$) can be obtained by replacing $\mathcal{O}_9$ by $\mathcal{O}_7$ (or $\mathcal{O}_8$). For the operators with derivatives it is additionally implied that on the right-hand side the position of the derivative is set as mandated by the superscripts lmn (with $l+m+n=1$). In the $\overline{\text{H}(4)}$ representation τ_2^{12}:

$$\mathcal{O}^{B,lmn}_{\mathcal{T},\mathfrak{A}} = 4\sqrt{2}\begin{pmatrix} +\mathcal{O}_{D7}^{(1)} \\ -\mathcal{O}_{D7}^{(2)} \\ -\mathcal{O}_{D7}^{(7)} \\ +\mathcal{O}_{D7}^{(8)} \end{pmatrix}, \quad \mathcal{O}^{B,lmn}_{\mathcal{T},\mathfrak{B}} = 4\sqrt{2}\begin{pmatrix} +\mathcal{O}_{D7}^{(3)} \\ -\mathcal{O}_{D7}^{(4)} \\ -\mathcal{O}_{D7}^{(9)} \\ +\mathcal{O}_{D7}^{(10)} \end{pmatrix}, \quad \mathcal{O}^{B,lmn}_{\mathcal{T},\mathfrak{C}} = 4\begin{pmatrix} +\mathcal{O}_{D7}^{(6)} \\ +\mathcal{O}_{D7}^{(5)} \\ -\mathcal{O}_{D7}^{(12)} \\ -\mathcal{O}_{D7}^{(11)} \end{pmatrix}, \quad \text{(C.19a–c)}$$

where the operators for the structure $\mathcal{V}+\mathcal{A}$ (or $\mathcal{V}-\mathcal{A}$) can be obtained by replacing $\mathcal{O}_{D7}$ by $\mathcal{O}_{D5}$ (or $\mathcal{O}_{D6}$). For operators with two derivatives ($l+m+n=2$) we use the multiplets from the $\overline{\mathrm{H}(4)}$ representation τ_2^4:

$$\mathcal{O}_{\mathcal{T}}^{B,lmn} = -\frac{8}{\sqrt{3}} \begin{pmatrix} \mathcal{O}_{DD6}^{(4)} \\ \mathcal{O}_{DD6}^{(3)} \\ \mathcal{O}_{DD6}^{(2)} \\ \mathcal{O}_{DD6}^{(1)} \end{pmatrix}, \tag{C.20}$$

where the operators for the structure $\mathcal{V}+\mathcal{A}$ (or $\mathcal{V}-\mathcal{A}$) can be obtained by replacing $\mathcal{O}_{DD6}$ by $\mathcal{O}_{DD4}$ (or $\mathcal{O}_{DD5}$).

Similarly, the operators which are relevant for higher twist normalization constants (see section 4.2.3) can be expressed in terms of $\mathcal{O}_{1-5}$ belonging to the $\overline{\mathrm{H}(4)}$ representation τ_1^4. In the chiral-odd sector we have

$$(\mathcal{V}+\mathcal{A})^{B,000} = -4\sqrt{2} \begin{pmatrix} \mathcal{O}_3^{(1)} \\ \mathcal{O}_3^{(2)} \\ \mathcal{O}_3^{(3)} \\ \mathcal{O}_3^{(4)} \end{pmatrix}, \qquad (\mathcal{V}-\mathcal{A})^{B,000} = -4\sqrt{2} \begin{pmatrix} \mathcal{O}_4^{(1)} \\ \mathcal{O}_4^{(2)} \\ \mathcal{O}_4^{(3)} \\ \mathcal{O}_4^{(4)} \end{pmatrix}, \tag{C.21a–b}$$

relevant for λ_1^B, and

$$(\mathcal{S}-\mathcal{P})^{B,000} = -2\sqrt{2} \begin{pmatrix} \mathcal{O}_5^{(1)} \\ \mathcal{O}_5^{(2)} \\ \mathcal{O}_5^{(3)} \\ \mathcal{O}_5^{(4)} \end{pmatrix}, \tag{C.21c}$$

relevant for λ_T^Λ. In the chiral-even sector (λ_2^B) we obtain:

$$(\mathcal{S}+\mathcal{P})^{B,000} = 2\sqrt{\frac{2}{3}} \begin{pmatrix} 2\mathcal{O}_1^{(1)} + \mathcal{O}_2^{(1)} \\ 2\mathcal{O}_1^{(2)} + \mathcal{O}_2^{(2)} \\ 2\mathcal{O}_1^{(3)} + \mathcal{O}_2^{(3)} \\ 2\mathcal{O}_1^{(4)} + \mathcal{O}_2^{(4)} \end{pmatrix}, \qquad \mathcal{T}^{B,000} = 4\sqrt{6} \begin{pmatrix} \mathcal{O}_2^{(1)} \\ \mathcal{O}_2^{(2)} \\ \mathcal{O}_2^{(3)} \\ \mathcal{O}_2^{(4)} \end{pmatrix}. \tag{C.21d–e}$$

Appendix D

Second order shape parameters and their renormalization

Over the course of this work we have so far omitted most equations concerning the renormalization of second order shape parameters in order not to overcrowd the main text with long formulas. Instead, they are collected in this appendix.

D.1. Expression as second moments of standard DAs

Analogous to what has been shown for the lower orders in section 3.3, the second order shape parameters of the baryons can be calculated as linear combinations of second moments. For $B\neq\Lambda$ we find

$$\begin{aligned}
\varphi_{00,(2)}^{B\neq\Lambda} &= [V{-}A]_{200}^{B} + [V{-}A]_{020}^{B} + [V{-}A]_{002}^{B} \\
&\quad + 2[V{-}A]_{011}^{B} + 2[V{-}A]_{101}^{B} + 2[V{-}A]_{110}^{B}\,, && \text{(D.1a)}\\
\pi_{00,(2)}^{B\neq\Lambda} &= T_{200}^{B} + T_{020}^{B} + T_{002}^{B} + 2T_{011}^{B} + 2T_{101}^{B} + 2T_{110}^{B}\,, && \text{(D.1b)}\\
\varphi_{11,(2)}^{B\neq\Lambda} &= \tfrac{1}{2}\big([V{-}A]_{200}^{B} - 2[V{-}A]_{020}^{B} + [V{-}A]_{002}^{B} \\
&\quad - [V{-}A]_{011}^{B} + 2[V{-}A]_{101}^{B} - [V{-}A]_{110}^{B}\big)\,, && \text{(D.1c)}\\
\pi_{11,(2)}^{B\neq\Lambda} &= \tfrac{1}{2}\big(T_{200}^{B} + T_{020}^{B} - 2T_{002}^{B} - T_{011}^{B} - T_{101}^{B} + 2T_{110}^{B}\big)\,, && \text{(D.1d)}\\
\varphi_{20}^{B\neq\Lambda} &= 3[V{-}A]_{200}^{B} + 2[V{-}A]_{020}^{B} + 3[V{-}A]_{002}^{B} \\
&\quad - 3[V{-}A]_{011}^{B} - 6[V{-}A]_{101}^{B} - 3[V{-}A]_{110}^{B}\,, && \text{(D.1e)}\\
\pi_{20}^{B\neq\Lambda} &= 3T_{200}^{B} + 3T_{020}^{B} + 2T_{002}^{B} - 3T_{011}^{B} - 3T_{101}^{B} - 6T_{110}^{B}\,, && \text{(D.1f)}\\
\varphi_{22}^{B\neq\Lambda} &= [V{-}A]_{200}^{B} - 6[V{-}A]_{020}^{B} + [V{-}A]_{002}^{B} \\
&\quad + 9[V{-}A]_{011}^{B} - 12[V{-}A]_{101}^{B} + 9[V{-}A]_{110}^{B}\,, && \text{(D.1g)}
\end{aligned}$$

$$\pi_{22}^{B\neq\Lambda} = T_{200}^{B} + T_{020}^{B} - 6T_{002}^{B} + 9T_{011}^{B} + 9T_{101}^{B} - 12T_{110}^{B}\,, \tag{D.1h}$$

$$\varphi_{10,(2)}^{B\neq\Lambda} = \tfrac{1}{2}\big([V{-}A]_{200}^{B} - [V{-}A]_{002}^{B} - [V{-}A]_{011}^{B} + [V{-}A]_{110}^{B}\big)\,, \tag{D.1i}$$

$$\varphi_{21}^{B\neq\Lambda} = [V{-}A]_{200}^{B} - [V{-}A]_{002}^{B} + 3[V{-}A]_{011}^{B} - 3[V{-}A]_{110}^{B}\,, \tag{D.1j}$$

whereas the Λ once again has a different set of moments, namely

$$\begin{aligned}\varphi_{00,(2)}^{\Lambda} = \sqrt{\tfrac{2}{3}}\big([V{-}A]_{200}^{\Lambda} + [V{-}A]_{020}^{\Lambda} + [V{-}A]_{002}^{\Lambda} \\ + 2[V{-}A]_{011}^{\Lambda} + 2[V{-}A]_{101}^{\Lambda} + 2[V{-}A]_{110}^{\Lambda}\big)\,,\end{aligned} \tag{D.2a}$$

$$\begin{aligned}\varphi_{11,(2)}^{\Lambda} = \tfrac{1}{\sqrt{6}}\big([V{-}A]_{200}^{\Lambda} - 2[V{-}A]_{020}^{\Lambda} + [V{-}A]_{002}^{\Lambda} \\ - [V{-}A]_{011}^{\Lambda} + 2[V{-}A]_{101}^{\Lambda} - [V{-}A]_{110}^{\Lambda}\big)\,,\end{aligned} \tag{D.2b}$$

$$\begin{aligned}\varphi_{20}^{\Lambda} = \sqrt{\tfrac{2}{3}}\big(3[V{-}A]_{200}^{\Lambda} + 2[V{-}A]_{020}^{\Lambda} + 3[V{-}A]_{002}^{\Lambda} \\ - 3[V{-}A]_{011}^{\Lambda} - 6[V{-}A]_{101}^{\Lambda} - 3[V{-}A]_{110}^{\Lambda}\big)\,,\end{aligned} \tag{D.2c}$$

$$\begin{aligned}\varphi_{22}^{\Lambda} = \sqrt{\tfrac{2}{3}}\big([V{-}A]_{200}^{\Lambda} - 6[V{-}A]_{020}^{\Lambda} + [V{-}A]_{002}^{\Lambda} \\ + 9[V{-}A]_{011}^{\Lambda} - 12[V{-}A]_{101}^{\Lambda} + 9[V{-}A]_{110}^{\Lambda}\big)\,,\end{aligned} \tag{D.2d}$$

$$\varphi_{10,(2)}^{\Lambda} = -\sqrt{\tfrac{3}{2}}\big([V{-}A]_{200}^{\Lambda} - [V{-}A]_{002}^{\Lambda} - [V{-}A]_{011}^{\Lambda} + [V{-}A]_{110}^{\Lambda}\big)\,, \tag{D.2e}$$

$$\pi_{10,(2)}^{\Lambda} = \sqrt{\tfrac{3}{2}}\big(T_{200}^{\Lambda} - T_{020}^{\Lambda} - T_{011}^{\Lambda} + T_{101}^{\Lambda}\big)\,, \tag{D.2f}$$

$$\varphi_{21}^{\Lambda} = -\sqrt{6}\big([V{-}A]_{200}^{\Lambda} - [V{-}A]_{002}^{\Lambda} + 3[V{-}A]_{011}^{\Lambda} - 3[V{-}A]_{110}^{\Lambda}\big)\,, \tag{D.2g}$$

$$\pi_{21}^{\Lambda} = \sqrt{6}\big(T_{200}^{\Lambda} - T_{020}^{\Lambda} + 3T_{011}^{\Lambda} - 3T_{101}^{\Lambda}\big)\,. \tag{D.2h}$$

D.2. Lattice correlation functions

To be able to access the second moments on the lattice we define the following leading twist combination of operators with two derivatives ($l+m+n=2$):

$$\mathcal{O}_{\mathcal{X}}^{B,lmn} = -\gamma_1\gamma_2\gamma_3\mathcal{X}_{\{123\}}^{B,lmn} + \gamma_1\gamma_2\gamma_4\mathcal{X}_{\{124\}}^{B,lmn} - \gamma_1\gamma_3\gamma_4\mathcal{X}_{\{134\}}^{B,lmn} + \gamma_2\gamma_3\gamma_4\mathcal{X}_{\{234\}}^{B,lmn}\,. \tag{D.3}$$

The general builing block $\mathcal{X}_{\bar{r}\bar{l}\bar{m}\bar{n}}^{B,lmn}$ is defined in eq. (4.1), and $\mathcal{X}$ can be $\mathcal{V}$, $\mathcal{A}$, or $\mathcal{T}$.

In this case we have one four-spinor of operators, in accordance with the fact that we want to use operators from the four-dimensional $\overline{\mathrm{H}(4)}$ representation τ_2^4, cf. eq. (C.20). As a reminder: We chose this representation because its operators with two derivatives are immune to the undesirable mixing with operators of lower dimension, see table 3.1 on page 64 and the related discussion in section 3.4.1. A consequence of having 4- instead of 12-dimensional multiplets is that there are fewer independent correlation functions than in

the case of one derivative. For lattice calculations of the second moments ($l+m+n=2$) we suggest to evaluate the following set:

$$\begin{aligned} C^{B,lmn}_{\mathcal{X},1}(t,\mathbf{p}) &= \left\langle \left(\gamma_4\gamma_2\gamma_3 \mathcal{O}^{B,lmn}_{\mathcal{X}}(t,\mathbf{p})\right)_\tau \bar{\mathcal{N}}^B_{\tau'}(0)(\gamma_+)_{\tau'\tau}\right\rangle \\ &= -c_X X^B_{lmn}\sqrt{Z_B}p_2p_3\frac{E_B(m_B+kE_B)+kp_1^2}{E_B}e^{-E_Bt}\,, \qquad \text{(D.4a)} \\ C^{B,lmn}_{\mathcal{X},2}(t,\mathbf{p}) &= \left\langle \left(\gamma_4\gamma_1\gamma_3 \mathcal{O}^{B,lmn}_{\mathcal{X}}(t,\mathbf{p})\right)_\tau \bar{\mathcal{N}}^B_{\tau'}(0)(\gamma_+)_{\tau'\tau}\right\rangle \\ &= +c_X X^B_{lmn}\sqrt{Z_B}p_1p_3\frac{E_B(m_B+kE_B)+kp_2^2}{E_B}e^{-E_Bt}\,, \qquad \text{(D.4b)} \\ C^{B,lmn}_{\mathcal{X},3}(t,\mathbf{p}) &= \left\langle \left(\gamma_4\gamma_1\gamma_2 \mathcal{O}^{B,lmn}_{\mathcal{X}}(t,\mathbf{p})\right)_\tau \bar{\mathcal{N}}^B_{\tau'}(0)(\gamma_+)_{\tau'\tau}\right\rangle \\ &= -c_X X^B_{lmn}\sqrt{Z_B}p_1p_2\frac{E_B(m_B+kE_B)+kp_3^2}{E_B}e^{-E_Bt}\,. \qquad \text{(D.4c)} \end{aligned}$$

At least two nonvanishing components of $\mathbf{p}$ are required in order to obtain nonzero values for the correlation functions involving the operators with two derivatives. Naturally, one should evaluate $C^{B,lmn}_{\mathcal{X},1}$ with $\mathbf{p}=\frac{2\pi}{L}(0,\pm1,\pm1)$ and $\mathbf{p}=\frac{2\pi}{L}(0,\pm1,\mp1)$, evaluate $C^{B,lmn}_{\mathcal{X},2}$ with $\mathbf{p}=\frac{2\pi}{L}(\pm1,0,\pm1)$ and $\mathbf{p}=\frac{2\pi}{L}(\pm1,0,\mp1)$ as well as $C^{B,lmn}_{\mathcal{X},3}$ with $\mathbf{p}=\frac{2\pi}{L}(\pm1,\pm1,0)$ and $\mathbf{p}=\frac{2\pi}{L}(\pm1,\mp1,0)$.

By calculating the correlators defined above on the lattice and then fitting the results to the respective expected expressions on the right-hand sides one can extract lattice values for the moments X^B_{lmn} of the standard DAs $X=V,A,T$, and therefore, by virtue of the equations given in the previous section, also for the second order shape parameters.

D.3. $\overline{\text{MS}}$ Z-factor

In section 3.5.1 we gave results for the Z-factors of three-quark operators with less than two derivatives. Here we will now present the result for the remaining, most complicated case. Given two derivatives, there are a total of 6 possibilities for their positions: 3 with both derivatives acting on the same quark and 3 with derivatives on two different quarks. The Z-factor has a 6×6 matrix structure intermixing the vertex functions with the various derivative positions:

$$\begin{pmatrix} H^{\alpha_1\alpha_2\alpha_3,\mu\nu,-,-}_{\beta_1\beta_2\beta_3}(p_1,p_2,p_3) \\ H^{\alpha_1\alpha_2\alpha_3,-,\mu\nu,-}_{\beta_1\beta_2\beta_3}(p_1,p_2,p_3) \\ H^{\alpha_1\alpha_2\alpha_3,-,-,\mu\nu}_{\beta_1\beta_2\beta_3}(p_1,p_2,p_3) \\ H^{\alpha_1\alpha_2\alpha_3,-,\mu,\nu}_{\beta_1\beta_2\beta_3}(p_1,p_2,p_3) \\ H^{\alpha_1\alpha_2\alpha_3,\mu,-,\nu}_{\beta_1\beta_2\beta_3}(p_1,p_2,p_3) \\ H^{\alpha_1\alpha_2\alpha_3,\mu,\nu,-}_{\beta_1\beta_2\beta_3}(p_1,p_2,p_3) \end{pmatrix}^{\overline{\text{MS}}} = Z^{\alpha_1\alpha_2\alpha_3}_{\alpha'_1\alpha'_2\alpha'_3} \begin{pmatrix} H^{\alpha'_1\alpha'_2\alpha'_3,\mu\nu,-,-}_{\beta_1\beta_2\beta_3}(p_1,p_2,p_3) \\ H^{\alpha'_1\alpha'_2\alpha'_3,-,\mu\nu,-}_{\beta_1\beta_2\beta_3}(p_1,p_2,p_3) \\ H^{\alpha'_1\alpha'_2\alpha'_3,-,-,\mu\nu}_{\beta_1\beta_2\beta_3}(p_1,p_2,p_3) \\ H^{\alpha'_1\alpha'_2\alpha'_3,-,\mu,\nu}_{\beta_1\beta_2\beta_3}(p_1,p_2,p_3) \\ H^{\alpha'_1\alpha'_2\alpha'_3,\mu,-,\nu}_{\beta_1\beta_2\beta_3}(p_1,p_2,p_3) \\ H^{\alpha'_1\alpha'_2\alpha'_3,\mu,\nu,-}_{\beta_1\beta_2\beta_3}(p_1,p_2,p_3) \end{pmatrix}. \qquad \text{(D.5)}$$

Our one-loop result for this Z-factor is

$$Z = \mathbb{1}_6 \otimes \Gamma_{000} - \xi \frac{\alpha_s}{2\pi} \frac{1}{\bar{\epsilon}} \mathbb{1}_6 \otimes \Gamma_{000} + \begin{pmatrix} Z_{ss} & Z_{sd} \\ Z_{ds} & Z_{dd} \end{pmatrix} + \mathcal{O}(\alpha_s^2)\,, \tag{D.6}$$

where, for better readability, we have partitioned the nontrivial parts into 3×3 blocks responsible for two derivatives on the same quark, derivatives on two different quarks, or the mixing between those sectors:[78]

$$\begin{aligned} Z_{ss} &= \frac{\alpha_s}{48\pi} \frac{1}{\bar{\epsilon}} \mathbb{1}_3 \otimes \left(\Gamma_{022} + \Gamma_{202} + \Gamma_{220}\right) \\ &\quad + \frac{\alpha_s}{144\pi} \frac{1}{\bar{\epsilon}} \begin{pmatrix} 3\Gamma_{022} & \Gamma_{220} & \Gamma_{202} \\ \Gamma_{220} & 3\Gamma_{202} & \Gamma_{022} \\ \Gamma_{202} & \Gamma_{022} & 3\Gamma_{220} \end{pmatrix} + \frac{\alpha_s}{36\pi} \frac{1}{\bar{\epsilon}} \begin{pmatrix} 26 & -3 & -3 \\ -3 & 26 & -3 \\ -3 & -3 & 26 \end{pmatrix} \otimes \Gamma_{000}\,, \end{aligned} \tag{D.7a}$$

$$\begin{aligned} Z_{dd} &= \frac{\alpha_s}{36\pi} \frac{1}{\bar{\epsilon}} \mathbb{1}_3 \otimes \left(\Gamma_{022} + \Gamma_{202} + \Gamma_{220}\right) \\ &\quad + \frac{\alpha_s}{144\pi} \frac{1}{\bar{\epsilon}} \begin{pmatrix} -\Gamma_{022} & 2\Gamma_{220} & 2\Gamma_{202} \\ 2\Gamma_{220} & -\Gamma_{202} & 2\Gamma_{022} \\ 2\Gamma_{202} & 2\Gamma_{022} & -\Gamma_{220} \end{pmatrix} + \frac{\alpha_s}{36\pi} \frac{1}{\bar{\epsilon}} \begin{pmatrix} 31 & -8 & -8 \\ -8 & 31 & -8 \\ -8 & -8 & 31 \end{pmatrix} \otimes \Gamma_{000}\,, \end{aligned} \tag{D.7b}$$

$$Z_{sd} = 3Z_{ds}^T = \frac{\alpha_s}{48\pi} \frac{1}{\bar{\epsilon}} \begin{pmatrix} 0 & \Gamma_{202} & \Gamma_{220} \\ \Gamma_{022} & 0 & \Gamma_{220} \\ \Gamma_{022} & \Gamma_{202} & 0 \end{pmatrix} + \frac{5\alpha_s}{12\pi} \frac{1}{\bar{\epsilon}} \begin{pmatrix} 0 & -1 & -1 \\ -1 & 0 & -1 \\ -1 & -1 & 0 \end{pmatrix} \otimes \Gamma_{000}\,. \tag{D.7c}$$

As far as the anomalous dimension matrix is concerned, we will refrain from writing down the full expression. Instead, we will point out that in the cases of zero and one derivatives a relation between the Z-factors (eqs. (3.67) and (3.71)) and the anomalous dimension matrices (eqs. (3.69) and (3.72)) can be observed: The one-loop anomalous dimension can be obtained by taking the gauge-independent part of the one-loop contribution to the Z-factor and multiplying it by $2\bar{\epsilon}$. The same also holds for the anomalous dimension matrix for operators with two derivatives. All of the anomalous dimensions of the shape parameters given in eqs. (3.20) are related to eigenvalues of this matrix by a factor of $\alpha_s/(2\pi)$.

D.4. Conversion factors

The calculation of the RI′/SMOM-to-$\overline{\text{MS}}$ conversion factors for the second moments proceeds analogous to section 3.5.3. This time we are working with operators with two derivatives from the representation τ_2^4. The 2×2 mixing matrix $C\big(\mathscr{S}_{2,DD}^4\big)$ for the singlet multiplets

[78] The transpose operation in the last line applies to the 3×3 matrix structure.

is given by

$$
\begin{aligned}
C\big(\mathscr{S}^4_{2,DD}\big)_{11} &= 1+\frac{\alpha_s}{4\pi}\Big(-\tfrac{11317}{2592}-\tfrac{7393}{46656}\pi^2+\tfrac{11}{30}\ln(2)+\tfrac{3419}{9720}\psi_1\big(\tfrac{1}{3}\big)-\tfrac{73}{960}\psi_1\big(\tfrac{1}{4}\big)\Big)\,,\\
C\big(\mathscr{S}^4_{2,DD}\big)_{22} &= 1+\frac{\alpha_s}{4\pi}\Big(-\tfrac{35171}{4320}-\tfrac{1061}{4320}\pi^2+\tfrac{127}{360}\psi_1\big(\tfrac{1}{3}\big)+\tfrac{1}{96}\psi_1\big(\tfrac{1}{4}\big)\Big)\,,\\
C\big(\mathscr{S}^4_{2,DD}\big)_{21} &= \sqrt{5}\frac{\alpha_s}{4\pi}\Big(-\tfrac{2171}{7200}-\tfrac{5129}{64800}\pi^2-\tfrac{2}{15}\ln(2)-\tfrac{17}{5400}\psi_1\big(\tfrac{1}{3}\big)+\tfrac{13}{160}\psi_1\big(\tfrac{1}{4}\big)\Big)\,,\\
C\big(\mathscr{S}^4_{2,DD}\big)_{12} &= \sqrt{5}\frac{\alpha_s}{4\pi}\Big(-\tfrac{79}{2592}-\tfrac{1003}{46656}\pi^2-\tfrac{1}{10}\ln(2)-\tfrac{127}{9720}\psi_1\big(\tfrac{1}{3}\big)+\tfrac{29}{960}\psi_1\big(\tfrac{1}{4}\big)\Big)\,. \qquad \text{(D.8a–d)}
\end{aligned}
$$

In the octet sector we have a 6×6 conversion matrix $C\big(\mathscr{O}^4_{2,DD}\big)$, which is block diagonal. The nonzero entries are

$$
C\big(\mathscr{O}^4_{2,DD}\big)_{mn} = \begin{cases} C\big(\mathscr{D}^4_{2,DD}\big)_{mn} & \forall\, m,n\in\{1,2,3,4\}\,,\\ C\big(\mathscr{S}^4_{2,DD}\big)_{m-4,n-4} & \forall\, m,n\in\{5,6\}\,. \end{cases} \qquad \text{(D.8e)}
$$

Finally, there are 4 decuplet multiplets and a corresponding matrix $C\big(\mathscr{D}^4_{2,DD}\big)$ specified by the components

$$
\begin{aligned}
C\big(\mathscr{D}^4_{2,DD}\big)_{11} &= 1+\frac{\alpha_s}{4\pi}\Big(-\tfrac{107}{135}-\tfrac{176}{1215}\pi^2+\tfrac{34}{105}\ln(2)+\tfrac{724}{2835}\psi_1\big(\tfrac{1}{3}\big)-\tfrac{8}{315}\psi_1\big(\tfrac{1}{4}\big)\Big)\,,\\
C\big(\mathscr{D}^4_{2,DD}\big)_{22} &= 1+\frac{\alpha_s}{4\pi}\Big(-\tfrac{4667}{864}-\tfrac{167}{576}\pi^2+\tfrac{7}{120}\ln(2)+\tfrac{41}{120}\psi_1\big(\tfrac{1}{3}\big)+\tfrac{179}{2880}\psi_1\big(\tfrac{1}{4}\big)\Big)\,,\\
C\big(\mathscr{D}^4_{2,DD}\big)_{33} &= 1+\frac{\alpha_s}{4\pi}\Big(-\tfrac{50837}{7200}-\tfrac{60523}{388800}\pi^2+\tfrac{113}{200}\ln(2)+\tfrac{5023}{16200}\psi_1\big(\tfrac{1}{3}\big)-\tfrac{49}{960}\psi_1\big(\tfrac{1}{4}\big)\Big)\,,\\
C\big(\mathscr{D}^4_{2,DD}\big)_{44} &= 1+\frac{\alpha_s}{4\pi}\Big(-\tfrac{2537}{300}-\tfrac{11983}{43200}\pi^2-\tfrac{17}{6300}\ln(2)+\tfrac{2063}{6300}\psi_1\big(\tfrac{1}{3}\big)+\tfrac{397}{6720}\psi_1\big(\tfrac{1}{4}\big)\Big)\,,\\
C\big(\mathscr{D}^4_{2,DD}\big)_{21} &= \sqrt{5}\frac{\alpha_s}{4\pi}\Big(\tfrac{10}{189}-\tfrac{1009}{34020}\pi^2-\tfrac{8}{105}\ln(2)-\tfrac{22}{405}\psi_1\big(\tfrac{1}{3}\big)+\tfrac{83}{1260}\psi_1\big(\tfrac{1}{4}\big)\Big)\,,\\
C\big(\mathscr{D}^4_{2,DD}\big)_{12} &= \sqrt{5}\frac{\alpha_s}{4\pi}\Big(\tfrac{73}{2700}-\tfrac{149}{97200}\pi^2-\tfrac{43}{4050}\psi_1\big(\tfrac{1}{3}\big)+\tfrac{31}{3600}\psi_1\big(\tfrac{1}{4}\big)\Big)\,,\\
C\big(\mathscr{D}^4_{2,DD}\big)_{31} &= \sqrt{\tfrac{19}{15}}\frac{\alpha_s}{4\pi}\Big(-\tfrac{818}{3591}+\tfrac{1193}{6804}\pi^2+\tfrac{556}{399}\ln(2)+\tfrac{1166}{10773}\psi_1\big(\tfrac{1}{3}\big)-\tfrac{395}{1596}\psi_1\big(\tfrac{1}{4}\big)\Big)\,,\\
C\big(\mathscr{D}^4_{2,DD}\big)_{13} &= \sqrt{\tfrac{19}{15}}\frac{\alpha_s}{4\pi}\Big(-\tfrac{1}{60}-\tfrac{1}{6480}\pi^2+\tfrac{4}{75}\ln(2)+\tfrac{29}{1350}\psi_1\big(\tfrac{1}{3}\big)-\tfrac{17}{1200}\psi_1\big(\tfrac{1}{4}\big)\Big)\,,\\
C\big(\mathscr{D}^4_{2,DD}\big)_{32} &= \sqrt{\tfrac{19}{3}}\frac{\alpha_s}{4\pi}\Big(-\tfrac{25711}{82080}-\tfrac{125923}{1477440}\pi^2-\tfrac{613}{2280}\ln(2)-\tfrac{1217}{61560}\psi_1\big(\tfrac{1}{3}\big)+\tfrac{359}{3648}\psi_1\big(\tfrac{1}{4}\big)\Big)\,,\\
C\big(\mathscr{D}^4_{2,DD}\big)_{23} &= \sqrt{\tfrac{19}{3}}\frac{\alpha_s}{4\pi}\Big(-\tfrac{193}{4320}-\tfrac{7019}{388800}\pi^2-\tfrac{7}{120}\ln(2)-\tfrac{103}{16200}\psi_1\big(\tfrac{1}{3}\big)+\tfrac{107}{4800}\psi_1\big(\tfrac{1}{4}\big)\Big)\,,\\
C\big(\mathscr{D}^4_{2,DD}\big)_{41} &= \sqrt{\tfrac{43}{30}}\frac{\alpha_s}{4\pi}\Big(-\tfrac{464}{3483}-\tfrac{7189}{125388}\pi^2-\tfrac{1184}{2709}\ln(2)+\tfrac{1886}{73143}\psi_1\big(\tfrac{1}{3}\big)+\tfrac{145}{3612}\psi_1\big(\tfrac{1}{4}\big)\Big)\,,\\
C\big(\mathscr{D}^4_{2,DD}\big)_{14} &= \sqrt{\tfrac{43}{30}}\frac{\alpha_s}{4\pi}\Big(\tfrac{1}{45}+\tfrac{7}{1620}\pi^2-\tfrac{8}{525}\ln(2)-\tfrac{34}{4725}\psi_1\big(\tfrac{1}{3}\big)+\tfrac{1}{2100}\psi_1\big(\tfrac{1}{4}\big)\Big)\,,\\
C\big(\mathscr{D}^4_{2,DD}\big)_{42} &= \sqrt{\tfrac{43}{6}}\frac{\alpha_s}{4\pi}\Big(-\tfrac{45319}{139320}-\tfrac{1103741}{20062080}\pi^2-\tfrac{2443}{15480}\ln(2)+\tfrac{13723}{417960}\psi_1\big(\tfrac{1}{3}\big)+\tfrac{547}{16512}\psi_1\big(\tfrac{1}{4}\big)\Big)\,,\\
C\big(\mathscr{D}^4_{2,DD}\big)_{24} &= \sqrt{\tfrac{43}{6}}\frac{\alpha_s}{4\pi}\Big(-\tfrac{151}{7560}-\tfrac{4253}{680400}\pi^2-\tfrac{13}{210}\ln(2)+\tfrac{17}{4050}\psi_1\big(\tfrac{1}{3}\big)+\tfrac{29}{8400}\psi_1\big(\tfrac{1}{4}\big)\Big)\,,
\end{aligned}
$$

$$C\big(\mathscr{D}^4_{2,DD}\big)_{43} = \sqrt{\tfrac{43}{38}}\frac{\alpha_s}{4\pi}\Big(-\tfrac{41401}{696600} - \tfrac{2129159}{100310400}\pi^2 - \tfrac{4883}{25800}\ln(2) + \tfrac{87457}{2089800}\psi_1\big(\tfrac{1}{3}\big) - \tfrac{551}{82560}\psi_1\big(\tfrac{1}{4}\big)\Big)\,,$$
$$C\big(\mathscr{D}^4_{2,DD}\big)_{34} = \sqrt{\tfrac{43}{38}}\frac{\alpha_s}{4\pi}\Big(\tfrac{1007}{4200} + \tfrac{8353}{226800}\pi^2 - \tfrac{47}{1050}\ln(2) + \tfrac{347}{9450}\psi_1\big(\tfrac{1}{3}\big) - \tfrac{103}{1680}\psi_1\big(\tfrac{1}{4}\big)\Big)\,. \quad \text{(D.8f–u)}$$

D.5. Renormalization

The combined renormalization and conversion factors for the second order shape parameters are calculated using operators with two derivatives from the $\overline{\mathrm{H}(4)}$ representation τ_2^4 and are defined as

$$Z^{\mathscr{M}\varphi_2} = \big(C_q Z_q^{\mathrm{lat,RI'}}\big)^{3/2} C\big(\mathscr{M}^4_{2,DD}\big) Z^{\mathrm{lat,RI'}}\big(\mathscr{M}^4_{2,DD}\big) \qquad \text{for } \mathscr{M} \in \{\mathscr{S},\mathscr{O},\mathscr{D}\}\,. \quad \text{(D.9)}$$

At the flavor symmetric point there is only one independent leading twist DA, namely $\Phi^\star_+ + \Phi^\star_-$, which is, at second order in the conformal expansion, fully characterized by the 6 parameters $\varphi^\star_{00,(2)}$, $\varphi^\star_{11,(2)}$, $\varphi^\star_{20}$, $\varphi^\star_{22}$, $\varphi^\star_{10,(2)}$, and $\varphi^\star_{21}$, cf. eqs. (3.17a–b). Their renormalization is described by the octet matrix $Z^{\mathscr{O}\varphi_2}$:

$$\begin{pmatrix} \varphi^\star_{00,(2)} \\ \sqrt{5}\varphi^\star_{11,(2)} \\ \sqrt{\frac{15}{76}}\varphi^\star_{20} \\ \sqrt{\frac{15}{344}}\varphi^\star_{22} \\ \sqrt{5}\varphi^\star_{10,(2)} \\ \frac{1}{2}\varphi^\star_{21} \end{pmatrix} = Z^{\mathscr{O}\varphi_2} \begin{pmatrix} \varphi^\star_{00,(2)} \\ \sqrt{5}\varphi^\star_{11,(2)} \\ \sqrt{\frac{15}{76}}\varphi^\star_{20} \\ \sqrt{\frac{15}{344}}\varphi^\star_{22} \\ \sqrt{5}\varphi^\star_{10,(2)} \\ \frac{1}{2}\varphi^\star_{21} \end{pmatrix}^{\mathrm{lat}}. \quad \text{(D.10)}$$

In the real world, where SU(3) flavor symmetry is broken, the distribution amplitudes Π^B lead to additional independent parameters. For the N, Σ, and Ξ baryons the moments of $\Phi_+^{B\neq\Lambda}$ have siblings in $\Pi^{B\neq\Lambda}$, called $\pi^{B\neq\Lambda}_{00,(2)}$, $\pi^{B\neq\Lambda}_{11,(2)}$, $\pi^{B\neq\Lambda}_{20}$, and $\pi^{B\neq\Lambda}_{22}$, while for the Λ baryon the DA Π^Λ contains partners $\pi^\Lambda_{10,(2)}$ and π^Λ_{21} of the moments of Φ^Λ_-, leading to a total of 10 or 8 parameters, respectively. The renormalization pattern is given by

$$\begin{pmatrix} \varphi^{B\neq\Lambda}_{00,(2)} \\ \pi^{B\neq\Lambda}_{00,(2)} \\ \sqrt{5}\varphi^{B\neq\Lambda}_{11,(2)} \\ \sqrt{5}\pi^{B\neq\Lambda}_{11,(2)} \\ \sqrt{\frac{15}{76}}\varphi^{B\neq\Lambda}_{20} \\ \sqrt{\frac{15}{76}}\pi^{B\neq\Lambda}_{20} \\ \sqrt{\frac{15}{344}}\varphi^{B\neq\Lambda}_{22} \\ \sqrt{\frac{15}{344}}\pi^{B\neq\Lambda}_{22} \\ \sqrt{5}\varphi^{B\neq\Lambda}_{10,(2)} \\ \frac{1}{2}\varphi^{B\neq\Lambda}_{21} \end{pmatrix} = Z^{\varphi_2,B} \begin{pmatrix} \varphi^{B}_{00,(2)} \\ \pi^{B}_{00,(2)} \\ \sqrt{5}\varphi^{B}_{11,(2)} \\ \sqrt{5}\pi^{B}_{11,(2)} \\ \sqrt{\frac{15}{76}}\varphi^{B}_{20} \\ \sqrt{\frac{15}{76}}\pi^{B}_{20} \\ \sqrt{\frac{15}{344}}\varphi^{B}_{22} \\ \sqrt{\frac{15}{344}}\pi^{B}_{22} \\ \sqrt{5}\varphi^{B}_{10,(2)} \\ \frac{1}{2}\varphi^{B}_{21} \end{pmatrix}^{\mathrm{lat}}, \qquad \begin{pmatrix} \varphi^{\Lambda}_{00,(2)} \\ \sqrt{5}\varphi^{\Lambda}_{11,(2)} \\ \sqrt{\frac{15}{76}}\varphi^{\Lambda}_{20} \\ \sqrt{\frac{15}{344}}\varphi^{\Lambda}_{22} \\ \sqrt{5}\varphi^{\Lambda}_{10,(2)} \\ \sqrt{5}\pi^{\Lambda}_{10,(2)} \\ \frac{1}{2}\varphi^{\Lambda}_{21} \\ \frac{1}{2}\pi^{\Lambda}_{21} \end{pmatrix} = Z^{\varphi_2,\Lambda} \begin{pmatrix} \varphi^{\Lambda}_{00,(2)} \\ \sqrt{5}\varphi^{\Lambda}_{11,(2)} \\ \sqrt{\frac{15}{76}}\varphi^{\Lambda}_{20} \\ \sqrt{\frac{15}{344}}\varphi^{\Lambda}_{22} \\ \sqrt{5}\varphi^{\Lambda}_{10,(2)} \\ \sqrt{5}\pi^{\Lambda}_{10,(2)} \\ \frac{1}{2}\varphi^{\Lambda}_{21} \\ \frac{1}{2}\pi^{\Lambda}_{21} \end{pmatrix}^{\mathrm{lat}}, \quad \text{(D.11a–b)}$$

with the matrices

$$Z^{\varphi_2,B\neq\Lambda} = \frac{1}{3}\begin{pmatrix} \begin{array}{|c|c|c|c|} \hline B_{11}^{\varphi_2} & B_{12}^{\varphi_2} & B_{13}^{\varphi_2} & B_{14}^{\varphi_2} \\ \hline B_{21}^{\varphi_2} & B_{22}^{\varphi_2} & B_{23}^{\varphi_2} & B_{24}^{\varphi_2} \\ \hline B_{31}^{\varphi_2} & B_{32}^{\varphi_2} & B_{33}^{\varphi_2} & B_{34}^{\varphi_2} \\ \hline B_{41}^{\varphi_2} & B_{42}^{\varphi_2} & B_{43}^{\varphi_2} & B_{44}^{\varphi_2} \\ \hline \end{array} & \begin{matrix} 3Z_{15}^{\mathscr{O}\varphi_2} & 3Z_{16}^{\mathscr{O}\varphi_2} \\ 3Z_{15}^{\mathscr{O}\varphi_2} & 3Z_{16}^{\mathscr{O}\varphi_2} \\ 3Z_{25}^{\mathscr{O}\varphi_2} & 3Z_{26}^{\mathscr{O}\varphi_2} \\ 3Z_{25}^{\mathscr{O}\varphi_2} & 3Z_{26}^{\mathscr{O}\varphi_2} \\ 3Z_{35}^{\mathscr{O}\varphi_2} & 3Z_{36}^{\mathscr{O}\varphi_2} \\ 3Z_{35}^{\mathscr{O}\varphi_2} & 3Z_{36}^{\mathscr{O}\varphi_2} \\ 3Z_{45}^{\mathscr{O}\varphi_2} & 3Z_{46}^{\mathscr{O}\varphi_2} \\ 3Z_{45}^{\mathscr{O}\varphi_2} & 3Z_{46}^{\mathscr{O}\varphi_2} \end{matrix} \\ \begin{matrix} Z_{51}^{\mathscr{O}\varphi_2} & 2Z_{51}^{\mathscr{O}\varphi_2} & Z_{52}^{\mathscr{O}\varphi_2} & 2Z_{52}^{\mathscr{O}\varphi_2} & Z_{53}^{\mathscr{O}\varphi_2} & 2Z_{53}^{\mathscr{O}\varphi_2} & Z_{54}^{\mathscr{O}\varphi_2} & 2Z_{54}^{\mathscr{O}\varphi_2} \\ Z_{61}^{\mathscr{O}\varphi_2} & 2Z_{61}^{\mathscr{O}\varphi_2} & Z_{62}^{\mathscr{O}\varphi_2} & 2Z_{62}^{\mathscr{O}\varphi_2} & Z_{63}^{\mathscr{O}\varphi_2} & 2Z_{63}^{\mathscr{O}\varphi_2} & Z_{64}^{\mathscr{O}\varphi_2} & 2Z_{64}^{\mathscr{O}\varphi_2} \end{matrix} & \begin{matrix} 3Z_{55}^{\mathscr{O}\varphi_2} & 3Z_{56}^{\mathscr{O}\varphi_2} \\ 3Z_{65}^{\mathscr{O}\varphi_2} & 3Z_{66}^{\mathscr{O}\varphi_2} \end{matrix} \end{pmatrix},$$

$$Z^{\varphi_2,\Lambda} = \frac{1}{3}\begin{pmatrix} \begin{matrix} 3Z_{11}^{\mathscr{O}\varphi_2} & 3Z_{12}^{\mathscr{O}\varphi_2} & 3Z_{13}^{\mathscr{O}\varphi_2} & 3Z_{14}^{\mathscr{O}\varphi_2} & Z_{15}^{\mathscr{O}\varphi_2} & 2Z_{15}^{\mathscr{O}\varphi_2} & Z_{16}^{\mathscr{O}\varphi_2} & 2Z_{16}^{\mathscr{O}\varphi_2} \\ 3Z_{21}^{\mathscr{O}\varphi_2} & 3Z_{22}^{\mathscr{O}\varphi_2} & 3Z_{23}^{\mathscr{O}\varphi_2} & 3Z_{24}^{\mathscr{O}\varphi_2} & Z_{25}^{\mathscr{O}\varphi_2} & 2Z_{25}^{\mathscr{O}\varphi_2} & Z_{26}^{\mathscr{O}\varphi_2} & 2Z_{26}^{\mathscr{O}\varphi_2} \\ 3Z_{31}^{\mathscr{O}\varphi_2} & 3Z_{32}^{\mathscr{O}\varphi_2} & 3Z_{33}^{\mathscr{O}\varphi_2} & 3Z_{34}^{\mathscr{O}\varphi_2} & Z_{35}^{\mathscr{O}\varphi_2} & 2Z_{35}^{\mathscr{O}\varphi_2} & Z_{36}^{\mathscr{O}\varphi_2} & 2Z_{36}^{\mathscr{O}\varphi_2} \\ 3Z_{41}^{\mathscr{O}\varphi_2} & 3Z_{42}^{\mathscr{O}\varphi_2} & 3Z_{43}^{\mathscr{O}\varphi_2} & 3Z_{44}^{\mathscr{O}\varphi_2} & Z_{45}^{\mathscr{O}\varphi_2} & 2Z_{45}^{\mathscr{O}\varphi_2} & Z_{46}^{\mathscr{O}\varphi_2} & 2Z_{46}^{\mathscr{O}\varphi_2} \\ 3Z_{51}^{\mathscr{O}\varphi_2} & 3Z_{52}^{\mathscr{O}\varphi_2} & 3Z_{53}^{\mathscr{O}\varphi_2} & 3Z_{54}^{\mathscr{O}\varphi_2} & \multicolumn{4}{c}{\multirow{2}{*}{$\begin{array}{|c|c|} \hline B_{55}^{\varphi_2} & B_{56}^{\varphi_2} \\ \hline B_{65}^{\varphi_2} & B_{66}^{\varphi_2} \\ \hline \end{array}$}} \\ 3Z_{51}^{\mathscr{O}\varphi_2} & 3Z_{52}^{\mathscr{O}\varphi_2} & 3Z_{53}^{\mathscr{O}\varphi_2} & 3Z_{54}^{\mathscr{O}\varphi_2} & \multicolumn{4}{c}{} \\ 3Z_{61}^{\mathscr{O}\varphi_2} & 3Z_{62}^{\mathscr{O}\varphi_2} & 3Z_{63}^{\mathscr{O}\varphi_2} & 3Z_{64}^{\mathscr{O}\varphi_2} & \multicolumn{4}{c}{} \\ 3Z_{61}^{\mathscr{O}\varphi_2} & 3Z_{62}^{\mathscr{O}\varphi_2} & 3Z_{63}^{\mathscr{O}\varphi_2} & 3Z_{64}^{\mathscr{O}\varphi_2} & \multicolumn{4}{c}{} \end{matrix} \end{pmatrix}. \tag{D.12a–b}$$

Similar to the situation in case of the first order shape parameters (compare section 3.5.4), the incorporation of the moments of $\Pi^{B\neq\Lambda}$ requires additional information from the renormalization matrix of operators with the symmetry of the decuplet ($Z^{\mathscr{D}\varphi_2}$), while the renormalization behavior of the moments of Π^{Λ} is affected by the singlet sector ($Z^{\mathscr{S}\varphi_2}$). This nontrivial behavior is manifest in the 2×2 submatrices

$$B_{ij}^{\varphi_2} = \begin{cases} \begin{pmatrix} Z_{ij}^{\mathscr{O}\varphi_2} + 2Z_{ij}^{\mathscr{D}\varphi_2} & 2Z_{ij}^{\mathscr{O}\varphi_2} - 2Z_{ij}^{\mathscr{D}\varphi_2} \\ Z_{ij}^{\mathscr{O}\varphi_2} - Z_{ij}^{\mathscr{D}\varphi_2} & 2Z_{ij}^{\mathscr{O}\varphi_2} + Z_{ij}^{\mathscr{D}\varphi_2} \end{pmatrix} & \forall\, i,j \in \{1,2,3,4\}\,, \\ \begin{pmatrix} Z_{ij}^{\mathscr{O}\varphi_2} + 2Z_{i-4,j-4}^{\mathscr{S}\varphi_2} & 2Z_{ij}^{\mathscr{O}\varphi_2} - 2Z_{i-4,j-4}^{\mathscr{S}\varphi_2} \\ Z_{ij}^{\mathscr{O}\varphi_2} - Z_{i-4,j-4}^{\mathscr{S}\varphi_2} & 2Z_{ij}^{\mathscr{O}\varphi_2} + Z_{i-4,j-4}^{\mathscr{S}\varphi_2} \end{pmatrix} & \forall\, i,j \in \{5,6\}\,. \end{cases} \tag{D.13}$$

Bibliography

[1] **ATLAS** Collaboration, G. Aad *et al.*, "Observation of a new particle in the search for the Standard Model Higgs boson with the ATLAS detector at the LHC," *Phys. Lett.* **B716** (2012) 1, arXiv:1207.7214 [hep-ex].

[2] **CMS** Collaboration, S. Chatrchyan *et al.*, "Observation of a new boson at a mass of 125 GeV with the CMS experiment at the LHC," *Phys. Lett.* **B716** (2012) 30, arXiv:1207.7235 [hep-ex].

[3] P. W. Higgs, "Broken Symmetries and the Masses of Gauge Bosons," *Phys. Rev. Lett.* **13** (1964) 508.

[4] F. Englert and R. Brout, "Broken Symmetry and the Mass of Gauge Vector Mesons," *Phys. Rev. Lett.* **13** (1964) 321.

[5] H. Fritzsch, M. Gell-Mann, and H. Leutwyler, "Advantages of the color octet gluon picture," *Phys. Lett.* **47B** (1973) 365.

[6] D. J. Gross and F. Wilczek, "Ultraviolet Behavior of Non-Abelian Gauge Theories," *Phys. Rev. Lett.* **30** (1973) 1343.

[7] H. D. Politzer, "Reliable Perturbative Results for Strong Interactions?," *Phys. Rev. Lett.* **30** (1973) 1346.

[8] S. Weinberg, "Non-Abelian Gauge Theories of the Strong Interactions," *Phys. Rev. Lett.* **31** (1973) 494.

[9] H. Fritzsch, M. Gell-Mann, and P. Minkowski, "Vectorlike weak currents and new elementary fermions," *Phys. Lett.* **59B** (1975) 256.

[10] R. W. McAllister and R. Hofstadter, "Elastic Scattering of 188 MeV Electrons from the Proton and the Alpha Particle," *Phys. Rev.* **102** (1956) 851.

[11] V. M. Braun, A. Lenz, and M. Wittmann, "Nucleon form factors in QCD," *Phys. Rev.* **D73** (2006) 094019, arXiv:hep-ph/0604050.

[12] J. C. Collins, D. E. Soper, and G. Sterman, "Factorization of Hard Processes in QCD," *Adv. Ser. Direct. High Energy Phys.* **5** (1989) 1, arXiv:hep-ph/0409313.

[13] G. P. Lepage and S. J. Brodsky, "Exclusive processes in perturbative quantum chromodynamics," *Phys. Rev.* **D22** (1980) 2157.

[14] G. P. Lepage and S. J. Brodsky, "Exclusive Processes in Quantum Chromodynamics: The Form Factors of Baryons at Large Momentum Transfer," *Phys. Rev. Lett.* **43** (1979) 545. [Erratum: *ibid.* **43** (1979) 1625].

[15] V. L. Chernyak and I. R. Zhitnitsky, "Nucleon wave function and nucleon form factors in QCD," *Nucl. Phys.* **B246** (1984) 52.

[16] M. Knödlseder, *Nucleon Electromagnetic Form Factors in perturbative QCD*. PhD thesis, Universität Regensburg, 2015. `urn:nbn:de:bvb:355-epub-322462`.

[17] **NNPDF** Collaboration, R. D. Ball *et al.*, "Parton distributions from high-precision collider data," *Eur. Phys. J.* **C** (2017) to be published, `arXiv:1706.00428 [hep-ph]`.

[18] Yu. L. Dokshitser, "Calculation of structure functions of deep-inelastic scattering and e^+e^- annihilation by perturbation theory in quantum chromodynamics," *Sov. Phys. JETP* **46** (1977) 641. [Russian: *Zh. Eksp. Teor. Fiz.* **73** (1977) 1216].

[19] V. N. Gribov and L. N. Lipatov, "Deep inelastic *ep* scattering in perturbation theory," *Sov. J. Nucl. Phys.* **15** (1972) 438. [Russian: *Yad. Fiz.* **15** (1972) 781].

[20] G. Altarelli and G. Parisi, "Asymptotic freedom in parton language," *Nucl. Phys.* **B126** (1977) 298.

[21] **BaBar** Collaboration, B. Aubert *et al.*, "Measurement of the $\gamma\gamma^* \to \pi^0$ transition form factor," *Phys. Rev.* **D80** (2009) 052002, `arXiv:0905.4778 [hep-ex]`.

[22] **Belle** Collaboration, S. Uehara *et al.*, "Measurement of $\gamma\gamma^* \to \pi^0$ transition form factor at Belle," *Phys. Rev.* **D86** (2012) 092007, `arXiv:1205.3249 [hep-ex]`.

[23] S. S. Agaev, V. M. Braun, N. Offen, and F. A. Porkert, "Belle data on the $\pi^0\gamma^*\gamma$ form factor: A game changer?," *Phys. Rev.* **D86** (2012) 077504, `arXiv:1206.3968 [hep-ph]`.

[24] V. M. Braun, A. Lenz, N. Mahnke, and E. Stein, "Light-cone sum rules for the nucleon form factors," *Phys. Rev.* **D65** (2002) 074011, `arXiv:hep-ph/0112085`.

[25] I. V. Anikin, V. M. Braun, and N. Offen, "Nucleon form factors and distribution amplitudes in QCD," *Phys. Rev.* **D88** (2013) 114021, `arXiv:1310.1375 [hep-ph]`.

[26] E. Cisbani, "Overview of nucleon form factor experiments with 12 GeV at Jefferson Lab," *EPJ Web Conf.* **73** (2014) 01008.

[27] I. V. Anikin, V. M. Braun, and N. Offen, "Electroproduction of the $N^*(1535)$ nucleon resonance in QCD," *Phys. Rev.* **D92** (2015) 014018, `arXiv:1505.05759 [hep-ph]`.

[28] I. G. Aznauryan *et al.*, "Studies of Nucleon Resonance Structure in Exclusive Meson Electroproduction," *Int. J. Mod. Phys.* **E22** (2013) 1330015, arXiv:1212.4891 [nucl-th].

[29] S. Dobbs, A. Tomaradze, T. Xiao, K. K. Seth, and G. Bonvicini, "First measurements of timelike form factors of the hyperons, Λ^0, Σ^0, Σ^+, Ξ^0, Ξ^-, and Ω^-, and evidence of diquark correlations," *Phys. Lett.* **B739** (2014) 90, arXiv:1410.8356 [hep-ex].

[30] **$\overline{\text{P}}$ANDA** Collaboration, W. Erni *et al.*, "Physics Performance Report for $\overline{\text{P}}$ANDA: Strong Interaction Studies with Antiprotons," arXiv:0903.3905 [hep-ex].

[31] Y.-L. Liu and M.-Q. Huang, "Distribution amplitudes of Σ and Λ and their electromagnetic form factors," *Nucl. Phys.* **A821** (2009) 80, arXiv:0811.1812 [hep-ph].

[32] Y.-L. Liu and M.-Q. Huang, "Light-cone distribution amplitudes of Ξ and their applications," *Phys. Rev.* **D80** (2009) 055015, arXiv:0909.0372 [hep-ph].

[33] P. Wein and A. Schäfer, "Model-independent calculation of $\text{SU}(3)_f$ violation in baryon octet light-cone distribution amplitudes," *JHEP* **05** (2015) 073, arXiv:1501.07218 [hep-ph].

[34] P. Wein, *Chiral perturbation theory for generalized parton distributions and baryon distribution amplitudes.* PhD thesis, Universität Regensburg, 2016. urn:nbn:de:bvb:355-epub-347744.

[35] M. Kobayashi, J. Haba, T. Homma, H. Kawai, K. Miyake, T. S. Nakamura, N. Sasao, and Y. Sugimoto, "New Measurement of the Asymmetry Parameter for the $\Sigma^+ \to p\gamma$ Decay," *Phys. Rev. Lett.* **59** (1987) 868.

[36] **E761** Collaboration, M. Foucher *et al.*, "Measurement of the Asymmetry Parameter in the Hyperon Radiative Decay $\Sigma^+ \to p\gamma$," *Phys. Rev. Lett.* **68** (1992) 3004.

[37] Y. Hara, "Nonleptonic Decays of Baryons and the Eightfold Way," *Phys. Rev. Lett.* **12** (1964) 378.

[38] V. L. Chernyak, A. A. Ogloblin, and I. R. Zhitnitsky, "Wave functions of octet baryons," *Z. Phys.* **C42** (1989) 569. [Russian: *Yad. Fiz.* **48** (1988) 1410].

[39] M. Gruber, "The nucleon wave function at the origin," *Phys. Lett.* **B699** (2011) 169, arXiv:1011.0758 [hep-ph].

[40] G. Martinelli and C. T. Sachrajda, "A lattice calculation of the second moment of the pion's distribution amplitude," *Phys. Lett.* **B190** (1987) 151.

[41] **QCDSF and UKQCD** Collaborations, V. M. Braun, M. Göckeler, R. Horsley, H. Perlt, D. Pleiter, P. E. L. Rakow, G. Schierholz, A. Schiller, W. Schroers, H. Stüben, and J. M. Zanotti, "Moments of pseudoscalar meson distribution amplitudes from the lattice," *Phys. Rev.* **D74** (2006) 074501, arXiv:hep-lat/0606012.

[42] **RBC and UKQCD** Collaborations, R. Arthur, P. A. Boyle, D. Brömmel, M. A. Donnellan, J. M. Flynn, A. Jüttner, T. D. Rae, and C. T. C. Sachrajda, "Lattice results for low moments of light meson distribution amplitudes," *Phys. Rev.* **D83** (2011) 074505, arXiv:1011.5906 [hep-lat].

[43] V. M. Braun, S. Collins, M. Göckeler, P. Pérez-Rubio, A. Schäfer, R. W. Schiel, and A. Sternbeck, "Second moment of the pion light-cone distribution amplitude from lattice QCD," *Phys. Rev.* **D92** (2015) 014504, arXiv:1503.03656 [hep-lat].

[44] **RQCD** Collaboration, G. S. Bali, V. M. Braun, M. Göckeler, M. Gruber, F. Hutzler, P. Korcyl, B. Lang, and A. Schäfer, "Second moment of the pion distribution amplitude with the momentum smearing technique," *Phys. Lett.* **B774** (2017) 91, arXiv:1705.10236 [hep-lat].

[45] G. Martinelli and C. T. Sachrajda, "The quark distribution amplitude of the proton: A lattice computation of the lowest two moments," *Phys. Lett.* **B217** (1989) 319.

[46] **QCDSF** Collaboration, M. Göckeler, R. Horsley, T. Kaltenbrunner, Y. Nakamura, D. Pleiter, P. E. L. Rakow, A. Schäfer, G. Schierholz, H. Stüben, N. Warkentin, and J. M. Zanotti, "Nucleon Distribution Amplitudes from Lattice QCD," *Phys. Rev. Lett.* **101** (2008) 112002, arXiv:0804.1877 [hep-lat].

[47] **QCDSF** Collaboration, V. M. Braun, M. Göckeler, R. Horsley, T. Kaltenbrunner, Y. Nakamura, D. Pleiter, P. E. L. Rakow, A. Schäfer, G. Schierholz, H. Stüben, N. Warkentin, and J. M. Zanotti, "Nucleon distribution amplitudes and proton decay matrix elements on the lattice," *Phys. Rev.* **D79** (2009) 034504, arXiv:0811.2712 [hep-lat].

[48] V. M. Braun, S. Collins, B. Gläßle, M. Göckeler, A. Schäfer, R. W. Schiel, W. Söldner, A. Sternbeck, and P. Wein, "Light-cone distribution amplitudes of the nucleon and negative parity nucleon resonances from lattice QCD," *Phys. Rev.* **D89** (2014) 094511, arXiv:1403.4189 [hep-lat].

[49] G. S. Bali, V. M. Braun, M. Göckeler, M. Gruber, F. Hutzler, A. Schäfer, R. W. Schiel, J. Simeth, W. Söldner, A. Sternbeck, and P. Wein, "Light-cone distribution amplitudes of the baryon octet," *JHEP* **02** (2016) 070, arXiv:1512.02050 [hep-lat].

[50] T. Kaltenbrunner, *Gitter-Operatoren für Baryon-Wellenfunktionen.* Diploma thesis, Universität Regensburg, 2006.

[51] T. Kaltenbrunner, *Renormalization of Three-Quark Operators for the Nucleon Distribution Amplitude.* PhD thesis, Universität Regensburg, 2008. urn:nbn:de:bvb:355-opus-11093.

[52] T. Kaltenbrunner, M. Göckeler, and A. Schäfer, "Irreducible multiplets of three-quark operators on the lattice: Controlling mixing under renormalization," *Eur. Phys. J.* **C55** (2008) 387, arXiv:0801.3932 [hep-lat].

[53] C. Itzykson and J.-B. Zuber, *Quantum Field Theory*. McGraw–Hill (New York, USA), 1980. [Republished by Dover Publications (Mineola, USA), 2005].

[54] M. E. Peskin and D. V. Schroeder, *An Introduction to Quantum Field Theory*. Perseus Books (Reading, USA), 1995.

[55] **DØ** Collaboration, S. Abachi *et al.*, "Search for High Mass Top Quark Production in $p\bar{p}$ Collisions at $\sqrt{s} = 1.8\,\text{TeV}$," *Phys. Rev. Lett.* **74** (1995) 2422, arXiv:hep-ex/9411001.

[56] **CDF** Collaboration, F. Abe *et al.*, "Observation of Top Quark Production in $\bar{p}p$ Collisions with the Collider Detector at Fermilab," *Phys. Rev. Lett.* **74** (1995) 2626, arXiv:hep-ex/9503002.

[57] O. Eberhardt, G. Herbert, H. Lacker, A. Lenz, A. Menzel, U. Nierste, and M. Wiebusch, "Impact of a Higgs Boson at a Mass of 126 GeV on the Standard Model with Three and Four Fermion Generations," *Phys. Rev. Lett.* **109** (2012) 241802, arXiv:1209.1101 [hep-ph].

[58] **Particle Data Group** Collaboration, C. Patrignani *et al.*, "Review of Particle Physics," *Chin. Phys.* **C40** (2016) 100001.

[59] C. N. Yang and R. L. Mills, "Conservation of Isotopic Spin and Isotopic Gauge Invariance," *Phys. Rev.* **96** (1954) 191.

[60] C. G. Callan, Jr., R. F. Dashen, and D. J. Gross, "The structure of the gauge theory vacuum," *Phys. Lett.* **63B** (1976) 334.

[61] J. H. Christenson, J. W. Cronin, V. L. Fitch, and R. Turlay, "Evidence for the 2π Decay of the K_2^0 Meson," *Phys. Rev. Lett.* **13** (1964) 138.

[62] A. D. Sakharov, "Violation of *CP* Invariance, *C* Asymmetry, and Baryon Asymmetry of the Universe," *JETP Lett.* **5** (1967) 24. [Erratum: *ibid.* **5** (1967) 109], [Russian: *Pis'ma v ZhETF* **5** (1967) 32].

[63] M. Pospelov and A. Ritz, "Theta vacua, QCD sum rules, and the neutron electric dipole moment," *Nucl. Phys.* **B573** (2000) 177, arXiv:hep-ph/9908508.

[64] R. D. Peccei, "The Strong *CP* Problem," *Adv. Ser. Direct. High Energy Phys.* **3** (1989) 503.

[65] L. D. Faddeev and V. N. Popov, "Feynman diagrams for the Yang–Mills field," *Phys. Lett.* **25B** (1967) 29.

[66] W. Pauli, "The Connection Between Spin and Statistics," *Phys. Rev.* **58** (1940) 716.

[67] C. Becchi, A. Rouet, and R. Stora, "Renormalization of Gauge Theories," *Annals Phys.* **98** (1976) 287.

[68] I. V. Tyutin, "Gauge Invariance in Field Theory and Statistical Physics in Operator Formalism," *LEBEDEV-75-39* (1975), arXiv:0812.0580 [hep-th].

[69] J. Collins, *Foundations of perturbative QCD*. Cambridge University Press (Cambridge, UK), 2011.

[70] G. C. Wick, "The Evaluation of the Collision Matrix," *Phys. Rev.* **80** (1950) 268.

[71] P. A. Baikov, K. G. Chetyrkin, and J. H. Kühn, "Five-Loop Running of the QCD Coupling Constant," *Phys. Rev. Lett.* **118** (2017) 082002, `arXiv:1606.08659 [hep-ph]`.

[72] K. G. Wilson, "Confinement of quarks," *Phys. Rev.* **D10** (1974) 2445.

[73] S. Dürr, Z. Fodor, J. Frison, C. Hoelbling, R. Hoffmann, S. D. Katz, S. Krieg, T. Kurth, L. Lellouch, T. Lippert, K. K. Szabo, and G. Vulvert, "Ab Initio Determination of Light Hadron Masses," *Science* **322** (2008) 1224, `arXiv:0906.3599 [hep-lat]`.

[74] C. Gattringer and C. B. Lang, *Quantum Chromodynamics on the Lattice*. Springer (Berlin, Germany), 2010.

[75] S. Duane, A. D. Kennedy, B. J. Pendleton, and D. Roweth, "Hybrid Monte Carlo," *Phys. Lett.* **B195** (1987) 216.

[76] K. Osterwalder and R. Schrader, "Axioms for Euclidean Green's Functions," *Commun. Math. Phys.* **31** (1973) 83.

[77] M. Lüscher, "Construction of a Selfadjoint, Strictly Positive Transfer Matrix for Euclidean Lattice Gauge Theories," *Commun. Math. Phys.* **54** (1977) 283.

[78] M. Lüscher and P. Weisz, "On-shell Improved Lattice Gauge Theories," *Commun. Math. Phys.* **97** (1985) 59. [Erratum: *ibid.* **98** (1985) 433].

[79] S. Weinberg, "Phenomenological Lagrangians," *Physica* **96A** (1979) 327.

[80] A. Cucchieri, T. Mendes, and E. M. da S. Santos, "Simulating linear covariant gauges on the lattice: a new approach," *PoS* **QCD-TNT09** (2009) 009, `arXiv:1001.2002 [hep-lat]`.

[81] A. Cucchieri, T. Mendes, G. M. Nakamura, and E. M. S. Santos, "Feynman Gauge on the Lattice: New Results and Perspectives," *AIP Conf. Proc.* **1354** (2011) 45, `arXiv:1101.5080 [hep-lat]`.

[82] V. N. Gribov, "Quantization of non-Abelian gauge theories," *Nucl. Phys.* **B139** (1978) 1.

[83] H. Neuberger, "Nonperturbative BRS invariance and the Gribov problem," *Phys. Lett.* **B183** (1987) 337.

[84] I. L. Bogolubsky, E.-M. Ilgenfritz, M. Müller-Preussker, and A. Sternbeck, "Lattice gluodynamics computation of Landau-gauge Green's functions in the deep infrared," *Phys. Lett.* **B676** (2009) 69, `arXiv:0901.0736 [hep-lat]`.

[85] O. Oliveira, A. Kızılersü, P. J. Silva, J.-I. Skullerud, A. Sternbeck, and A. G. Williams, "Lattice Landau Gauge Quark Propagator and the Quark-Gluon Vertex," *Acta Phys. Polon. B Proc. Suppl.* **9** (2016) 363, arXiv:1605.09632 [hep-lat].

[86] C. G. Bollini and J. J. Giambiagi, "Dimensional Renormalization: The Number of Dimensions as a Regularizing Parameter," *Nuovo Cim.* **12B** (1972) 20.

[87] G. 't Hooft and M. Veltman, "Regularization and renormalization of gauge fields," *Nucl. Phys.* **B44** (1972) 189.

[88] G. Passarino and M. Veltman, "One-loop corrections for e^+e^- annihilation into $\mu^+\mu^-$ in the Weinberg model," *Nucl. Phys.* **B160** (1979) 151.

[89] G. Duplančić and B. Nižić, "Reduction method for dimensionally regulated one-loop N-point Feynman integrals," *Eur. Phys. J.* **C35** (2004) 105, arXiv:hep-ph/0303184.

[90] G. 't Hooft, "Dimensional regularization and the renormalization group," *Nucl. Phys.* **B61** (1973) 455.

[91] W. A. Bardeen, A. J. Buras, D. W. Duke, and T. Muta, "Deep-inelastic scattering beyond the leading order in asymptotically free gauge theories," *Phys. Rev.* **D18** (1978) 3998.

[92] G. Martinelli, C. Pittori, C. T. Sachrajda, M. Testa, and A. Vladikas, "A general method for non-perturbative renormalization of lattice operators," *Nucl. Phys.* **B445** (1995) 81, arXiv:hep-lat/9411010.

[93] M. A. Shifman, A. I. Vainshtein, and V. I. Zakharov, "QCD and resonance physics. Theoretical foundations," *Nucl. Phys.* **B147** (1979) 385.

[94] P. Ball, V. M. Braun, and H. G. Dosch, "Form factors of semileptonic D decays from QCD sum rules," *Phys. Rev.* **D44** (1991) 3567.

[95] T. M. Aliev and M. Savcı, "Octet negative parity to octet positive parity electromagnetic transitions in light cone QCD," *J. Phys.* **G41** (2014) 075007, arXiv:1403.0096 [hep-ph].

[96] Y. Aoki, "Non-perturbative renormalization in lattice QCD," *PoS* **LAT2009** (2009) 012, arXiv:1005.2339 [hep-lat].

[97] J. A. Gracey, "Three loop anomalous dimension of non-singlet quark currents in the RI′ scheme," *Nucl. Phys.* **B662** (2003) 247, arXiv:hep-ph/0304113.

[98] M. Constantinou, M. Costa, M. Göckeler, R. Horsley, H. Panagopoulos, H. Perlt, P. E. L. Rakow, G. Schierholz, and A. Schiller, "Perturbatively improving regularization-invariant momentum scheme renormalization constants," *Phys. Rev.* **D87** (2013) 096019, arXiv:1303.6776 [hep-lat].

[99] **QCDSF and UKQCD** Collaborations, M. Göckeler, R. Horsley, Y. Nakamura, H. Perlt, D. Pleiter, P. E. L. Rakow, A. Schäfer, G. Schierholz, A. Schiller, H. Stüben, and J. M. Zanotti, "Perturbative and nonperturbative renormalization in lattice QCD," *Phys. Rev.* **D82** (2010) 114511, `arXiv:1003.5756 [hep-lat]`. [Erratum: *ibid.* **D86** (2012) 099903(E)].

[100] P. Korcyl, "Alleviating the window problem in large volume renormalization schemes," (2017), `arXiv:1705.06119 [hep-lat]`.

[101] J. J. Rotman, *An Introduction to the Theory of Groups*. Springer (New York, USA), 4th ed., 1995.

[102] H. Georgi, *Lie Algebras in Particle Physics*. Westview Press (Boulder, USA), 2nd ed., 1999.

[103] W. Fulton and J. Harris, *Representation Theory: A First Course*. Springer (New York, USA), 2004.

[104] V. Dabbaghian-Abdoly, "An algorithm for constructing representations of finite groups," *J. Symbolic Comput.* **39** (2005) 671.

[105] Y. Ne'eman, "The Symmetry Approach to Particle Physics," *Proc. Intern. Conf. Nucleon Structure* (1963) 172. Reprinted in [106].

[106] M. Gell-Mann and Y. Ne'eman, *The Eightfold Way: A Review – With A Collection of Reprints*. W. A. Benjamin (New York, USA), 1964. [Republished by Westview Press (Boulder, USA), 2000].

[107] M. Gell-Mann, "Strange Particle Physics. Strong Interactions," *Proc. Intern. Conf. High Energy Phys.* (1962) 805. Reprinted in [106].

[108] V. E. Barnes *et al.*, "Observation of a Hyperon with Strangeness Minus Three," *Phys. Rev. Lett.* **12** (1964) 204. Reprinted in [106].

[109] M. Gell-Mann, "A schematic model of baryons and mesons," *Phys. Lett.* **8** (1964) 214. Reprinted in [106].

[110] G. Zweig, "An SU(3) model for strong interaction symmetry and its breaking. II.," *CERN 8419/TH.412* (1964).

[111] G. D. Rochester and C. C. Butler, "Evidence for the Existence of New Unstable Elementary Particles," *Nature* **160** (1947) 855.

[112] M. Gell-Mann, "The Interpretation of the New Particles as Displaced Charge Multiplets," *Suppl. del Nuovo Cim.* **4** (1956) 848.

[113] B. V. Struminsky, "Magnetic moments of baryons in the quark model," *JINR P-1939* (1965), `arXiv:0904.0343 [physics.hist-ph]`.

[114] O. W. Greenberg, "Spin and Unitary-Spin Independence in a Paraquark Model of Baryons and Mesons," *Phys. Rev. Lett.* **13** (1964) 598.

[115] M. Y. Han and Y. Nambu, "Three-Triplet Model with Double SU(3) Symmetry," *Phys. Rev.* **139** (1965) B1006.

[116] R. Alkofer and J. Greensite, "Quark confinement: the hard problem of hadron physics," *J. Phys.* **G34** (2007) S3, arXiv:hep-ph/0610365.

[117] G. S. Bali, "QCD forces and heavy quark bound states," *Phys. Rept.* **343** (2001) 1, arXiv:hep-ph/0001312.

[118] B. E. Sagan, *The Symmetric Group – Representations, Combinatorial Algorithms, and Symmetric Functions*. Springer (New York, USA), 2nd ed., 2001.

[119] J. Dai and X.-C. Song, "Structure and representation theory of double group of four-dimensional cubic group," (2000), arXiv:hep-lat/0010024.

[120] M. Baake, B. Gemünden, and R. Oedingen, "Structure and representations of the symmetry group of the four-dimensional cube," *J. Math. Phys.* **23** (1982) 944. [Erratum: *ibid.* **23** (1982) 2595].

[121] J. E. Mandula, G. Zweig, and J. Govaerts, "Representations of the rotation reflection symmetry group of the four-dimensional cubic lattice," *Nucl. Phys.* **B228** (1983) 91.

[122] J. Dai and X.-C. Song, "Structure and representation theory for the double group of the four-dimensional cubic group," *J. Math. Phys.* **42** (2001) 2213, arXiv:hep-lat/0102001.

[123] H. B. Lawson, Jr. and M.-L. Michelsohn, *Spin Geometry*. Princeton University Press (Princeton, USA), 1989.

[124] M. Berg, C. DeWitt-Morette, S. Gwo, and E. Kramer, "The Pin Groups in Physics: C, P, and T," *Rev. Math. Phys.* **13** (2001) 953, arXiv:math-ph/0012006.

[125] **QCDSF and UKQCD** Collaborations, M. Göckeler, R. Horsley, T. Kaltenbrunner, Y. Nakamura, D. Pleiter, P. E. L. Rakow, A. Schäfer, G. Schierholz, H. Stüben, N. Warkentin, and J. M. Zanotti, "Non-perturbative renormalization of three-quark operators," *Nucl. Phys.* **B812** (2009) 205, arXiv:0810.3762 [hep-lat].

[126] V. Braun, R. J. Fries, N. Mahnke, and E. Stein, "Higher twist distribution amplitudes of the nucleon in QCD," *Nucl. Phys.* **B589** (2000) 381, arXiv:hep-ph/0007279. [Erratum: *ibid.* **B607** (2001) 433].

[127] K. G. Wilson, "Non-Lagrangian Models of Current Algebra," *Phys. Rev.* **179** (1969) 1499.

[128] D. J. Gross and S. B. Treiman, "Light-Cone Structure of Current Commutators in the Gluon-Quark Model," *Phys. Rev.* **D4** (1971) 1059.

[129] V. M. Braun, G. P. Korchemsky, and D. Müller, "The Uses of Conformal Symmetry in QCD," *Prog. Part. Nucl. Phys.* **51** (2003) 311, arXiv:hep-ph/0306057.

[130] V. L. Chernyak and A. R. Zhitnitsky, "Asymptotic behaviour of exclusive processes in QCD," *Phys. Rept.* **112** (1984) 173.

[131] X. Ji, J.-P. Ma, and F. Yuan, "Three-quark light-cone amplitudes of the proton and quark orbital-motion-dependent observables," *Nucl. Phys.* **B652** (2003) 383, arXiv:hep-ph/0210430.

[132] A. V. Belitsky and A. V. Radyushkin, "Unraveling hadron structure with generalized parton distributions," *Phys. Rept.* **418** (2005) 1, arXiv:hep-ph/0504030.

[133] E. E. Salpeter and H. A. Bethe, "A Relativistic Equation for Bound-State Problems," *Phys. Rev.* **84** (1951) 1232.

[134] V. M. Braun, A. N. Manashov, and J. Rohrwild, "Baryon operators of higher twist in QCD and nucleon distribution amplitudes," *Nucl. Phys.* **B807** (2009) 89, arXiv:0806.2531 [hep-ph].

[135] S. Kränkl and A. Manashov, "Two-loop renormalization of three-quark operators in QCD," *Phys. Lett.* **B703** (2011) 519, arXiv:1107.3718 [hep-ph].

[136] J. A. Gracey, "Three loop renormalization of 3-quark operators in QCD," *JHEP* **09** (2012) 052, arXiv:1208.5619 [hep-ph].

[137] M. Claudson, M. B. Wise, and L. J. Hall, "Chiral lagrangian for deep mine physics," *Nucl. Phys.* **B195** (1982) 297.

[138] V. M. Belyaev and B. L. Ioffe, "Determination of the baryon mass and baryon resonances from the quantum-chromodynamics sum rule. Strange baryons," *Sov. Phys. JETP* **57** (1983) 716. [Russian: *Zh. Eksp. Teor. Fiz.* **84** (1983) 1236].

[139] B. L. Ioffe and A. V. Smilga, "Hyperon magnetic moments in QCD," *Phys. Lett.* **133B** (1983) 436.

[140] V. M. Braun and D. Müller, "Exclusive processes in position space and the pion distribution amplitude," *Eur. Phys. J.* **C55** (2008) 349, arXiv:0709.1348 [hep-ph].

[141] X. Ji, "Parton Physics on a Euclidean Lattice," *Phys. Rev. Lett.* **110** (2013) 262002, arXiv:1305.1539 [hep-ph].

[142] **RQCD** Collaboration, G. S. Bali, B. Lang, B. U. Musch, and A. Schäfer, "Novel quark smearing for hadrons with high momenta in lattice QCD," *Phys. Rev.* **D93** (2016) 094515, arXiv:1602.05525 [hep-lat].

[143] G. S. Bali, V. M. Braun, M. Göckeler, M. Gruber, F. Hutzler, P. Korcyl, B. Lang, A. Schäfer, P. Wein, and J.-H. Zhang, "Pion distribution amplitude from Euclidean correlation functions," (2017), arXiv:1709.04325 [hep-lat].

[144] H. B. Nielsen and M. Ninomiya, "A no-go theorem for regularizing chiral fermions," *Phys. Lett.* **105B** (1981) 219.

[145] W. Fulton, *Young Tableaux*. Cambridge University Press (Cambridge, UK), 1997.

[146] J. S. Frame, G. de B. Robinson, and R. M. Thrall, "The hook graphs of the symmetric group," *Canad. J. Math.* **6** (1954) 316.

[147] R. P. Stanley, *Enumerative Combinatorics*, vol. 2. Cambridge University Press (Cambridge, UK), 1999.

[148] M. J. Dugan and B. Grinstein, "On the vanishing of evanescent operators," *Phys. Lett.* **B256** (1991) 239.

[149] S. Herrlich and U. Nierste, "Evanescent operators, scheme dependences and double insertions," *Nucl. Phys.* **B455** (1995) 39, arXiv:hep-ph/9412375.

[150] F. Jegerlehner, "Facts of life with γ_5," *Eur. Phys. J.* **C18** (2001) 673, arXiv:hep-th/0005255.

[151] T. Luthe, A. Maier, P. Marquard, and Y. Schröder, "Towards the five-loop Beta function for a general gauge group," *JHEP* **07** (2016) 127, arXiv:1606.08662 [hep-ph].

[152] **RBC and UKQCD** Collaborations, C. Allton *et al.*, "Physical results from $2+1$ flavor domain wall QCD and SU(2) chiral perturbation theory," *Phys. Rev.* **D78** (2008) 114509, arXiv:0804.0473 [hep-lat].

[153] **RBC and UKQCD** Collaborations, Y. Aoki *et al.*, "Continuum limit physics from $2+1$ flavor domain wall QCD," *Phys. Rev.* **D83** (2011) 074508, arXiv:1011.0892 [hep-lat].

[154] **RBC and UKQCD** Collaborations, Y. Aoki *et al.*, "Nonperturbative renormalization of quark bilinear operators and B_K using domain wall fermions," *Phys. Rev.* **D78** (2008) 054510, arXiv:0712.1061 [hep-lat].

[155] S. Weinberg, "High-Energy Behavior in Quantum Field Theory," *Phys. Rev.* **118** (1960) 838.

[156] **RBC and UKQCD** Collaborations, C. Sturm, Y. Aoki, N. H. Christ, T. Izubuchi, C. T. C. Sachrajda, and A. Soni, "Renormalization of quark bilinear operators in a momentum-subtraction scheme with a nonexceptional subtraction point," *Phys. Rev.* **D80** (2009) 014501, arXiv:0901.2599 [hep-ph].

[157] **RBC and UKQCD** Collaborations, Y. Aoki, "Quark mass renormalization with non-exceptional momenta," *PoS* **LATTICE 2008** (2009) 222, arXiv:0901.2595 [hep-lat].

[158] L. G. Almeida and C. Sturm, "Two-loop matching factors for light quark masses and three-loop mass anomalous dimensions in the regularization invariant symmetric momentum-subtraction schemes," *Phys. Rev.* **D82** (2010) 054017, arXiv:1004.4613 [hep-ph].

[159] M. Gorbahn and S. Jäger, "Precise $\overline{\text{MS}}$ light-quark masses from lattice QCD in the regularization invariant symmetric momentum-subtraction scheme," *Phys. Rev.* **D82** (2010) 114001, arXiv:1004.3997 [hep-ph].

[160] P. F. Bedaque, "Aharonov–Bohm effect and nucleon-nucleon phase shifts on the lattice," *Phys. Lett.* **B593** (2004) 82, arXiv:nucl-th/0402051.

[161] C. T. Sachrajda and G. Villadoro, "Twisted boundary conditions in lattice simulations," *Phys. Lett.* **B609** (2005) 73, arXiv:hep-lat/0411033.

[162] D. B. Leinweber, W. Melnitchouk, D. G. Richards, A. G. Williams, and J. M. Zanotti, "Baryon Spectroscopy in Lattice QCD," *Lect. Notes Phys.* **663** (2005) 71, arXiv:nucl-th/0406032.

[163] M. Lüscher, S. Sint, R. Sommer, and P. Weisz, "Chiral symmetry and $\mathcal{O}(a)$ improvement in lattice QCD," *Nucl. Phys.* **B478** (1996) 365, arXiv:hep-lat/9605038.

[164] J. Bulava and S. Schaefer, "Improvement of $N_f = 3$ lattice QCD with Wilson fermions and tree-level improved gauge action," *Nucl. Phys.* **B874** (2013) 188, arXiv:1304.7093 [hep-lat].

[165] B. Sheikholeslami and R. Wohlert, "Improved continuum limit lattice action for QCD with Wilson fermions," *Nucl. Phys.* **B259** (1985) 572.

[166] K. Symanzik, "Continuum limit and improved action in lattice theories (I). Principles and ϕ^4 theory," *Nucl. Phys.* **B226** (1983) 187.

[167] S. Güsken, "A study of smearing techniques for hadron correlation functions," *Nucl. Phys. B (Proc. Suppl.)* **17** (1990) 361.

[168] M. Falcioni, M. L. Paciello, G. Parisi, and B. Taglienti, "Again on SU(3) glueball mass," *Nucl. Phys.* **B251** (1985) 624.

[169] P. Arts *et al.*, "QPACE 2 and Domain Decomposition on the Intel Xeon Phi," *PoS* **LATTICE2014** (2015) 021, arXiv:1502.04025 [cs.DC].

[170] **SciDAC, LHPC, and UKQCD** Collaborations, R. G. Edwards and B. Joó, "The Chroma Software System for Lattice QCD," *Nucl. Phys. B (Proc. Suppl.)* **140** (2005) 832, arXiv:hep-lat/0409003.

[171] M. Bruno *et al.*, "Simulation of QCD with $N_f = 2 + 1$ flavors of non-perturbatively improved Wilson fermions," *JHEP* **02** (2015) 043, arXiv:1411.3982 [hep-lat].

[172] **RQCD** Collaboration, G. S. Bali, E. E. Scholz, J. Simeth, and W. Söldner, "Lattice simulations with $N_f = 2 + 1$ improved Wilson fermions at a fixed strange quark mass," *Phys. Rev.* **D94** (2016) 074501, arXiv:1606.09039 [hep-lat].

[173] M. Lüscher and S. Schaefer, "Lattice QCD without topology barriers," *JHEP* **07** (2011) 036, arXiv:1105.4749 [hep-lat].

[174] **ALPHA** Collaboration, M. Bruno, S. Schaefer, and R. Sommer, "Topological susceptibility and the sampling of field space in $N_f = 2$ lattice QCD simulations," *JHEP* **08** (2014) 150, arXiv:1406.5363 [hep-lat].

[175] **RBC and UKQCD** Collaborations, Y. Aoki, P. Boyle, P. Cooney, L. Del Debbio, R. Kenway, C. M. Maynard, A. Soni, and R. Tweedie, "Proton lifetime bounds from chirally symmetric lattice QCD," *Phys. Rev.* **D78** (2008) 054505, arXiv:0806.1031 [hep-lat].

[176] M. Gell-Mann, "The Eightfold Way: A Theory of Strong Interaction Symmetry," *CTSL-20* (1961). Reprinted in [106].

[177] S. Okubo, "Note on Unitary Symmetry in Strong Interactions," *Prog. Theor. Phys.* **27** (1962) 949.

[178] S. Scherer and M. R. Schindler, *A Primer for Chiral Perturbation Theory*. Springer (Berlin, Germany), 2012.

[179] J. Gasser, M. E. Sainio, and A. Švarc, "Nucleons with chiral loops," *Nucl. Phys.* **B307** (1988) 779.

[180] T. Becher and H. Leutwyler, "Baryon chiral perturbation theory in manifestly Lorentz invariant form," *Eur. Phys. J.* **C9** (1999) 643, arXiv:hep-ph/9901384.

[181] I. D. King and C. T. Sachrajda, "Nucleon wave functions and QCD sum rules," *Nucl. Phys.* **B279** (1987) 785.

[182] A. F. Möbius, *Der barycentrische Calcul*. Verlag von Johann Ambrosius Barth (Leipzig, Germany), 1827. urn:nbn:de:bvb:12-bsb10082429-2.

[183] F. Wilczek, "Diquarks as Inspiration and as Objects," in *From Fields to Strings: Circumnavigating Theoretical Physics*. World Scientific Publishing (Singapore), 2004. arXiv:hep-ph/0409168.

[184] J. Bolz and P. Kroll, "Modelling the nucleon wave function from soft and hard processes," *Z. Phys.* **A356** (1996) 327, arXiv:hep-ph/9603289.

[185] H. Georgi, *Weak Interactions and Modern Particle Theory*. Benjamin Cummings (Menlo Park, USA), 1984. [Updated online version: http://www.people.fas.harvard.edu/~hgeorgi/weak.pdf].